A study of the clinical characteristics and immunopathology of SARS-CoV-2 associated diseases in children

Harsita Patel

A thesis submitted for the degree of Doctor of Philosophy

Section of Paediatric Infectious Disease, Department of Infectious Disease, Imperial College London, United Kingdom

October 2023

Declaration of Originality

I, Harsita Patel, declare that the work presented in this thesis is my own. This project was supervised by Professor Michael Levin and Dr Vanessa Sancho Shimizu. The thesis is submitted in fulfilment of the requirements for the degree of Doctor of Philosophy. The work described in this thesis has not been previously submitted and approved for the award of a degree by this or any other university. I certify any work performed by anyone other than myself, has been identified and appropriately acknowledged in the text below.

Chapter 4:

I developed the study design, analysis plan, identified the cohorts and assembled the samples for antibody testing. I worked with Dr Samuel Nichols, Mr Oliver Powell, Ms Giselle D'Souza, Ms Leire Estramiana Elorrieta, Ms Sobia Mustafa, and Mrs Sarah Darnell to process the samples collected for antibody testing from the Diagnosis and Management of Febrile Illness using RNA Personalised Molecular Signature Diagnosis Study (DIAMONDS) and the Delirium and Population Health Informatics Cohort (DELPHIC) study. The samples from the remaining cohorts had been previously collected and processed by researchers in each respective study and biobanked. I identified appropriate samples from the biobank and led the organisation and aliquoting of samples for antibody testing at the Francis Crick Institute, with the help of Dr Ivvone Pena Paz, Mr Oliver Powell, Dr Ivana Pennisi, Dr Shea Hamilton and Dr Diego Estrada-Rivadeneyra. At the beginning of the pandemic, when commercial kits for SARS-CoV-2 antibody testing were not readily available and due to the need to provide rapid answers, we collaborated with Dr George Kassiotis and his team who had optimised a fluorescence-activated cell sorting (FACS) based coronavirus antibody assay which allowed high-throughput sampling. Due to the restrictions placed during the Coronavirus Disease 2019 (COVID-19) pandemic, I was unable to attend the Francis Crick Institute to perform the antibody assays and therefore the experiments were completed by members of the Kassiotis group. I performed all the analyses with the exception of the severity analysis on the adult COVID-19 cohort, which was performed by Dr Claire Broderick and included for comparison and sake of completeness. The Multisystem Inflammatory Syndrome in Children (MIS-C) severity score used in this chapter was designed by myself and Dr Clare Wilson.

Chapter 5:

I designed the study and performed all the analyses presented in this chapter. I worked together with Ms Sobia Mustafa and Mrs Sarah Darnell to recruit study participants and process samples collected at St Mary's Hospital as part of DIAMONDS. Local clinical research teams at each of the other DIAMONDS sites were responsible for recruiting study participants and collecting and processing samples. Coronavirus antibody testing was carried out using a FACS-based assay at the Francis Crick Institute in collaboration with Dr George Kassiotis and his team. The samples collected in 2022 were unable to undergo antibody testing at the Francis Crick Institute, therefore, Dr Diego Estrada-Rivadeneyra and Dr Shea Hamilton performed Mesoscale Discovery (MSD) SARS-CoV-2 antibody assays on these samples.

Chapter 6:

Professor Michael Levin is the Chief Investigator of the Best Available Treatment Study (BATS) and led the set-up of the study. I am a co-investigator for BATS and led the ethics and UK clinical and regulatory management. This involved writing the clinical study protocol, obtaining ethical approval, and registering the study on the International Standard Randomised Controlled Trial Number (ISRCTN) registry. Together with the BATS working group, I helped design the case report form and contributed to the data entry for patients with MIS-C admitted to St Mary's Hospital, London. The BATS working group comprised of: Dr Claire Broderick, Dr Samuel Channon-Wells, Dr Aubrey Cunnington, Dr Tisham De, Ms Giselle D'Souza, Dr Jethro Herberg, Dr Myrsini Kaforou, Ms Ilana Keren, Dr Andrew McArdle, Dr Ruud Nijman, Dr Eleanor Seaby, Dr Priyen Shah, Ms Ortensia Vito and Dr Elizabeth Whittaker. The data entry was carried out by a team of healthcare professionals at each site. The data cleaning and quality checks were led by Dr Andrew McArdle and Dr Samuel Channon-Wells with support from the BATS working group. I conducted all the data analysis presented in this chapter, with the exception of the physiological score calculations, which were performed by Dr Clare Wilson; and the design of the severity categories which I did in collaboration with Dr Clare Wilson.

Chapter 7:

I recruited patients with MIS-C and healthy COVID-19 vaccinated adults as part of the DIAMONDS project (MIS-C: n = 5; healthy COVID-19 vaccinated adults: n = 10) and collected and processed their serum samples. I optimised and performed the immunohistochemistry (IHC) and enzyme-linked immunosorbent assay (ELISA) experiments and completed the data analysis. Dr Michael Carter

recruited and collected samples from patients with MIS-C admitted to the Evelina Children's Hospital Paediatric Intensive Care Unit (PICU) (n=5). Vaccine myocarditis, adult myocarditis/inflammatory cardiomyopathy, healthy pre-pandemic paediatric controls and healthy cardiac tissue donors were recruited and had samples collected and processed by researchers in each respective study. Ms Amalia Sintou prepared microscope slides with cryosections of the cardiac tissue in preparation for IHC. The ELISA positive controls serum samples were from adult myocarditis patients who had previous high readings in similar assays performed by Dr Alma Octavia.

Chapter 8:

I recruited and collected samples from children with MIS-C, febrile paediatric controls and healthy paediatric controls attending St Mary's Hospital, London as well as healthy adult controls as part of DIAMONDS for the SARS-CoV-2 QuantiFERON assay. Dr Michael Carter and Mr Paul Wellman recruited and collected samples from children with MIS-C, febrile paediatric controls and healthy paediatric controls attending the Evelina Children's Hospital, London. Mr Oliver Powell organised the laboratory set up for the SARS-CoV-2 QuantiFERON assay and completed the biological risk assessment for this work. I worked together with Mr Oliver Powell, Dr Samuel Nichols, Ms Giselle D'Souza and Ms Leire Estramiana Elorrieta to process the SARS-CoV-2 QuantiFERON samples. I optimised and carried out the multiplex assays and performed all the analyses for this dataset.

I performed the mass cytometry experiment and the downstream analysis for samples from the SARS-CoV-2 QuantiFERON assay. Dr Michael Carter optimised the protocol, carried out the mass cytometry experiments on whole blood samples from the same individuals and prepared the barcoding and antibody mastermixes - these were custom conjugated to metal tags at the National Institute for Health Research (NIHR) Biomedical Research Centre (BRC) at Guy's and St Thomas' NHS Foundation Trust. The frozen stained samples were thawed and prepared for data acquisition by Dr Michael Carter. The mass cytometry was performed at the NIHR BRC Flow Core Facility by the flow facility staff. The initial de-barcoding, quality check control of the data and cell gating was carried out by the cytometry specialist bioinformatics team at King's College London: Dr Filomena Spada, Dr Nedyalko Petrov and Ms Manuela Terranova Barberio, and was overseen by Dr Michael Carter.

The clinical research teams at each respective site recruited and collected samples for RNA sequencing (RNA-seq) as part of DIAMONDS. Ms Giselle D'Souza, Dr Samuel Nichols, Mr Oliver Powell and Dr Victoria Wright performed the laboratory work. The samples were sequenced at The Wellcome Centre for Human Genetics in Oxford, UK. Dr Dominic Habgood-Coote processed the raw RNA-seq data,

generating gene counts. Dr Heather Jackson performed the quality control checks and normalised the data. I identified the genes of interest and performed the gene expression analysis.

Harsita Patel

October 2023

Copyright Declaration

Dedication

To my family.

Acknowledgements

First and foremost, I would like to thank my supervisor Professor Michael Levin for his support, inspirational guidance, and invaluable insights. Thank you for giving me the incredible opportunities which have been instrumental in shaping me both as a scientist and as an individual. I would like to thank my co-supervisor Dr Vanessa Sancho Shimizu for her guidance and feedback.

I am grateful to all the collaborators and colleagues who have helped me throughout my PhD including:

The Levin laboratory group, particularly Mr Oliver Powell, Dr Victoria Wright, Dr Samuel Nichols, Dr Shea Hamilton, and Dr Diego Estrada-Rivadeneyra as well as Dr George Kassiotis and his team at the Francis Crick Institute for their invaluable contributions to the antibody work.

I am thankful to Professor Sian Harding and Dr Susanne Sattler for their expert guidance with the immunohistochemistry work and to Professor Jane Burns and her team at the University of California San Diego for generously sharing the samples from COVID-19 vaccine-induced myocarditis patients. I would like to thank Ms Amalia Sintou for supervising me in the laboratory and for always being kind and patient. I am grateful to Dr Alma Octavia for sharing the positive control myocarditis patient samples with me and for our chats in the lab!

I would like to thank all the members of the BATS team and especially Dr Andrew McArdle for skilfully leading such a fantastic piece of work and Dr Clare Wilson for a wonderful collaboration on the severity work.

I am grateful for the collaborative efforts of Mr Oliver Powell, Dr Michael Carter and Dr Heather Jackson, whose dedication and expertise were crucial in making the QuantiFERON/mass cytometry work possible.

Special thanks to the St Mary's DIAMONDS clinical research team, including Dr Jethro Herberg, Dr Priyen Shah, Ms Sobia Mustafa and Mrs Sarah Darnell, as well as Dr Tisham De for managing the DIAMONDS database and helping with any database related queries.

I would like to extend my gratitude to everyone in the section of Paediatric Infectious Disease for your help and support, with special thanks to Dr Camilla Gladstone, Dr Claire Dunican, Dr Fadil Bidmos, Dr Ortensia Vito, Dr Stephanie Hodeib and Dr Helen Payne.

I am grateful to members of the DIAMONDS and BATS consortia, as well as all the other collaborative studies, for their collective contributions. My deepest appreciation goes to the patients and families who have generously participated in this research, making these findings possible.

I would also like to thank my mentors Dr Robert Boyle, Dr Jayanta Banerjee, and Dr Elizabeth Whittaker – your guidance during this time has been invaluable, thank you all so much.

A massive thank you to all my friends, for celebrating the wins with me and listening to me and being there during the challenging times. Special thanks to Eleni, Rich, Andrew, Amanda, Kat, Kristina, Jacinta, Marnie, Qiong, Ishani and Priya.

Finally, I would like to thank my family. Thank you for believing in me and for your unwavering love, support, and encouragement – this would not have been possible without you.

To each and every one of you, thank you for being an essential part of this incredible journey.

Abstract

The Coronavirus Disease 2019 (COVID-19) pandemic presented a remarkable epidemiological trend, with low rates of severe paediatric cases and an age-dependent increase in disease severity, raising questions about underlying mechanisms. A small proportion of children developed a severe inflammatory illness several weeks after Severe Acute Respiratory Syndrome Coronavirus 2 (SARS-CoV-2) infection. This syndrome, now called Multisystem Inflammatory Syndrome in Children (MIS-C) is characterised by fever, rash, and conjunctivitis, and can rapidly progress to shock and multiorgan failure. The overlapping features of MIS-C with other conditions, including Kawasaki Disease and sepsis, posed additional challenges. Following the introduction of COVID-19 vaccines there were reports of increased rates of myocarditis in young adults. The evolving diseases associated with SARS-CoV-2 raised many questions regarding the immunopathogenesis of these diverse syndromes, diagnostic approaches, and treatment strategies.

I aimed to explore and understand the clinical characteristics and immunopathology of SARS-CoV-2 associated diseases in children by using a multidisciplinary approach including: descriptive analyses of large clinical datasets, development of diagnostic and severity scores, antibody profiling and mechanistic studies investigating the role of antibodies and T cells.

Key findings include:

- Age-related differences in COVID-19 severity are not driven by antibody dependent enhancement.
- A clinical diagnostic score can accurately differentiate MIS-C from other conditions.
- Utility of SARS-CoV-2 serology testing for MIS-C diagnosis diminishes over time.
- A clinical and laboratory marker-based severity score can identify MIS-C patients at risk of severe disease.
- The cardiac pathology in MIS-C and COVID-19 vaccine-induced myocarditis is unlikely to be antibody driven.
- Acute MIS-C exhibit reduced T cell response to antigen stimulation, suggesting transient T cell exhaustion.

My research contributes to the understanding of the clinical and immunological aspects of SARS-COV-2 associated diseases in children and the findings have significant implications for vaccine development, clinical management and provide critical insights that can guide further research.

Table of contents

List of figures

List of tables

Abbreviations

&	And
=	Equals
<	Less than
≤	Less than or equal to
>	Greater than
-	Minus
%	Percentage
a.u.	Absorbance units
ab	Antibody
ACE-2	Angiotensin converting enzyme 2
ADCC	Antibody dependent cell mediated cytotoxicity
ADE	Antibody dependent enhancement
ag1	SARS-CoV-2 antigen 1
AHA	American Heart Association
ALT	Alanine transferase
APCs	Antigen presenting cells
APC	Allophycocyanin
APTT	Activated partial thromboplastin time
ARDS	Acute respiratory distress syndrome
AU/ml	Arbitrary units per millilitres
AUC	Area under the curve
AVPU	Alert, verbal, pain, unresponsive
BATS	Best Available Treatment Study
BAU/ml	Binding antibody units per millilitres
BH	Benjamini Hochberg
BD	Becton, Dickinson and company
BNP	Brain natriuretic peptide
BCG	Bacillus Calmette–Guérin
BRC	Biomedical research centre
BSA	Bovine Serum Albumin
CAA	Coronary artery aneurysm
CASP8	Cysteine-aspartic acid protease eight
CD	Cluster of differentiation

CDC	Centers for Disease Control and Prevention
CI	Confidence interval
CL2	Containment level two
CMRI	Cardiac magnetic resonance imaging
COVID-19	Coronavirus Disease 2019
CRF	Case record form
CRP	C-reactive protein
CRT	Capillary refill time
CT	Computed tomography
CTLA4	Cytotoxic T-lymphocyte antigen 4
CXCL9	Chemokine ligand nine
Cy-TOF	Cytometry at time-of-flight
CYBB	Cytochrome b-245 beta chain
cDNA	Complementary deoxyribonucleic acid
DAPI	4',6-diamidino-2-phenylindole
DB	Definite bacterial
DCs	Dendritic cells
DELPHIC	Delirium and Population Health Informatics Cohort
DIAMONDS	Diagnosis and Management of Febrile Illness using RNA Personalised Molecular Signature Diagnosis Study
DNA	Deoxyribonucleic acid
DNI	Delta neutrophil index
DV	Definite viral
E	Envelope protein
ECG	Electrocardiogram
ECHO	Echocardiogram
ECMO	Extracorporeal membrane oxygenation
EDTA	Ethylenediaminetetraacetic acid
ELISA	Enzyme-Linked Immunosorbent assay
EU	European Union
EUCLIDS	European Union Childhood Life-threatening Infectious Disease Study
FACS	Fluorescence-activated cell sorting
FADD	Fas associated via death domain
FAS	Fas cell surface death receptor

FASL	Fas cell surface death receptor ligand
FCS	Forward scatter
FITC	Fluorescein isothiocyanate
FN	False negative
FP	False positive
γδT cells	Gamma delta T cells
g/L	Grams per Litre
GCFP	Grating-coupled fluorescence plasmonic
GI	Gastrointestinal
G-CSF	Granulocyte colony stimulating factor
GM-CSF	Granulocyte macrophage colony stimulating factor
HVA	Healthy vaccinated adults
HAC	Healthy adult controls
Hb	Haemoglobin
HCoV-229E	Human coronavirus 229E
HCoV-HKU1	Human coronavirus HKU1
HCoV-NL63	Human coronavirus NL63
HCoV-OC43	Human coronavirus OC43
HEK293T cells	Human embryonic kidney 293T cells
HLA	Human leucocyte antigen
HPC	Healthy paediatric controls
HR	Heart rate
HRP	Horseradish peroxidase
HTS	High throughput sampler
IDEA	IGRA in Diagnostic Evaluation of Active TB
IFNAR2	Interferon alpha receptor 2 gene
IFNs	Interferons
IFNα	Interferon alpha
IFNα2	Interferon alpha 2
IFNβ	Interferon beta
IFNγ	Interferon gamma
IFNγR1	Interferon gamma receptor 1
IFNγR2	Interferon gamma receptor 2
IFNλ1	Interferon lambda 1

IFNλ2/3,	Interferon lambda 2/3
Ig	Immunoglobulin
IgA	Immunoglobulin A
IgG	Immunoglobulin G
IgM	Immunoglobulin M
IGRA	Interferon Gamma Release Assay
IHC	Immunohistochemistry
IHKB	Imperial Health Knowledge Bank
IL1	Interleukin 1
IL10	Interleukin 10
IL12	Interleukin 12
IL12p70	Interleukin 12p70
IL13	Interleukin 13
IL17	Interleukin 17
IL1β	Interleukin 1 beta
IL2	Interleukin 2
IL2RA	Interleukin 2 receptor alpha subunit
IL2RB	Interleukin 2 receptor beta subunit
IL2RG	Interleukin 2 receptor gamma subunit
IL6	Interleukin 6
IL7	Interleukin 7
IL8	Interleukin 8
INF	Inflammatory disease
INR	International normalised ratio
IP10	Interferon gamma induced protein 10
IQR	Interquartile range
IRFs	Interferon regulatory factors
ISRCTN	International Standard Randomised Controlled Trial Number
IU/L	International units per litre
IVIG	Intravenous immunoglobulin
KD	Kawasaki Disease
L	Litres
LAG3	Lymphocyte activating gene 3
LAMP	Loop-mediated isothermal amplification

LASSO	Least Absolute Shrinkage and Selection Operator
LDH	Lactate dehydrogenase
Log2	Logarithm base 2
LOR	Log odds ratio
LVD	Left ventricular dysfunction
M	Membrane protein
M-CSF	Macrophage colony stimulating factor
Mab	Monoclonal antibodies
MAS	Macrophage activation syndrome
MBL	Mannose binding lectin
MCP1	Monocyte chemoattractant protein one
MDT	Multidisciplinary team
MERS	Middle Eastern respiratory syndrome
MERS-CoV	Middle East respiratory syndrome coronavirus
µg/L	Microgram per litre
mg	Milligram
mg/L	Milligram per litre
MHC	Major histocompatibility complex
MHC II	Major histocompatibility complex class II
MIP1α	Macrophage inflammatory protein 1-alpha
MIS-A	Multisystem Inflammatory Syndrome in Adults
MIS-C	Multisystem Inflammatory Syndrome in Children
MISTIC	Multisystem Inflammatory Syndrome Therapies in Children
mit	Mitogen
µl	Microlitres
ml	Millilitres
µmol/L	Micromole per litre
mmol/L	Millimole per litre
mRNA	Messenger ribonucleic acid
MSC	Microbiological safety cabinet
MSD	Mesoscale discovery
nm	Nanometres
N	Nucleocapsid protein
n	Number (count)

NETs	Neutrophil extracellular traps
NF$\boldsymbol{\kappa B}$	Nuclear factor kappa-light-chain enhancer of B cells
ng/L	Nanogram per litre
ng/ml	Nanogram per millilitre
NHS	National Health Service
NK	Natural killer
NLR	Nucleotide-binding oligomerization domain (NOD)-like receptors
NLRP3	Nucleotide-Binding Domain Leucine-Rich–Containing Family, Pyrin Domain–Containing-3
NOD	Nucleotide-binding oligomerization domain
NPV	Negative predictive value
OAS	2'-5'-oligoadenylate synthetase
OR	Odds ratio
PAMPs	Pathogen associated molecular patterns
PBs	Plasmablasts
PBS	Phosphate buffered saline
PC	Principal component
PCA	Principal component analysis
PCD	Programmed cell death
PCR	Polymerase chain reaction
PCT	Procalcitonin
PD-1	Programmed cell death protein 1
PDL1	Programmed cell death ligand 1
PDL2	Programmed cell death ligand 2
PE	Phycoerythrin
PERFORM	Personalised Risk assessment in Febrile illness to Optimise Real-life Management
PHA	Phytohemagglutinin
PICU	Paediatric Intensive Care Unit
PIMS-TS	Paediatric Inflammatory Multisystem Syndrome Temporally associated with SARS-CoV-2
PL	Parameter logistics
PMT	Photomultiplier tube
PPRs	Pattern recognition receptors

PPV	Positive predictive value
PreVAIL kIds	Predicting Viral Associated Inflammatory Disease Severity in Children with Laboratory Diagnostics and Artificial Intelligence
QC	Quality control
RCF	Relative Centrifugal Force
RCPCH	Royal College of Paediatrics and Child Health
RCT	Randomised Control Trial
RECOVERY	Randomised Evaluation of COVID-19 Therapy
REDCap	Research Electronic Data Capture
RIG-I	Retinoic acid-inducible gene I
RLR	Retinoic acid-inducible gene I (RIG-I) Like Receptors
RNA	Ribonucleic acid
RNA-seq	Ribonucleic acid sequencing
RNase L	Ribonuclease L
ROC	Receiving operator curve
rpm	Revolutions per minute
RR	Respiratory rate
rRNA	Ribosomal ribonucleic acid
RRT	Renal replacement therapy
RT	Room temperature
qRT-PCR	Quantitative reverse transcription-polymerase chain reaction
RT-PCR	Reverse transcription polymerase chain reaction
s	Seconds
S	Spike protein
S0-S8	Standard 0 – Standard 8
SA-PE	Streptavidin phycoerythrin
SARS	Severe acute respiratory syndrome
SARS-CoV	Severe acute respiratory syndrome coronavirus
SARS-CoV-2	Severe acute respiratory syndrome coronavirus 2
SBI	Severe bacterial illness
SBP	Systolic blood pressure
SCS	Side scatter
SLE	Systemic lupus erythematosus
SOCS1	Suppressor Of Cytokine Signalling 1

SOP	Standard Operating Procedure
sTREM-1	Soluble Triggering Receptor Expressed on Myeloid Cells-1
SVI	Severe viral illness
Tbet	T-box transcription factor
TCR	T cell receptor
Tfh	T follicular helper
Th	T helper
TLR	Toll like receptor
TMB	3,3',5,5'-Tetramethylbenzidine
TMPRSS2	Transmembrane protease serine protease 2
TN	True negative
TNFα	Tumour necrosis factor alpha
TP	True positive
TP1	Timepoint one
TP2	Timepoint two
TP3	Timepoint three
Tregs	Regulatory T cells
TSS	Toxic shock syndrome
UK	United Kingdom
US	United States
vs	Versus
WBC	White blood cells
WGA	Wheat Germ Agglutinin
WHO	World Health Organisation
XIAP	X-linked inhibitor of apoptosis protein

Publications

Publications arising from the work described in this thesis at the time of submission:

1) Patel, H. *et al.* Evaluation of Autoantibody Binding to Cardiac Tissue in Multisystem Inflammatory Syndrome in Children and COVID-19 Vaccination–Induced Myocarditis. *JAMA Network Open* 6, e2314291 (2023).

Manuscripts under review from the work described in this thesis at the time of submission:

1) Patel, H. *et al.* Immunology of severe febrile illness in children in the COVID-19 era, under review at *Nature Communications*, September 2023

Publications arising from the work that is not described in this thesis but was performed in the duration of this PhD:

1) Patel, H., Burgner, D. & Whittaker, E. Multisystem inflammatory syndrome in children: a longitudinal perspective on risk factors and future directions. *Pediatr Res* 1–3 (2023)
2) Channon-Wells, S. *et al.* Immunoglobulin, glucocorticoid, or combination therapy for multisystem inflammatory syndrome in children: a propensity-weighted cohort study. *The Lancet Rheumatology* 5, e184–e199 (2023).
3) Patel, H., McArdle, A., Seaby, E., Levin, M. & Whittaker, E. The immunopathogenesis of SARS-CoV-2 infection in children: diagnostics, treatment and prevention. *Clinical & Translational Immunology* 11, e1405 (2022).
4) McArdle, A. J. *et al.* Treatment of Multisystem Inflammatory Syndrome in Children. *New England Journal of Medicine* 385, 11–22 (2021).
5) Deakin, C. T. *et al.* Favorable antibody responses to human coronaviruses in children and adolescents with autoimmune rheumatic diseases. *Med (N Y)* 2, 1093-1109.e6 (2021).

Foreword

Completing my PhD on SARS-CoV-2 associated diseases in children during the global COVID-19 pandemic has been a remarkable journey, defined by both unique opportunities and difficult challenges. The pandemic brought about an unprecedented global crisis which has had a significant impact on our lives, communities, and the field of research.

In the last few years, there has been an extraordinary focus on COVID-19, leading to significant redirection of research efforts towards understanding SARS-CoV-2 and its associated complications. The fast-changing nature of the pandemic, together with the immense urgency to generate knowledge and find solutions, greatly impacted my research journey. Some of the research questions I had initially addressed in my PhD were also being investigated and subsequently reported by others. Consequently, the introduction of my thesis has an unconventional structure, beginning with a brief overview of the topic, followed by a description of the knowledge gaps that were prevalent at the time which guided my research and subsequently an up-to-date literature review.

Working within a dynamic and rapidly evolving research landscape, also required me to adapt and reframe the focus and scope of my own research. For example, following the emergence of MIS-C and COVID-19 vaccine-induced myocarditis, I promptly shifted my focus to investigating these important new conditions. Undertaking research during the COVID-19 pandemic posed additional challenges including workplace restrictions, limited access to research facilities and difficulties in learning novel laboratory techniques requiring supervision due to social distancing rules.

Despite the challenges, the pandemic also presented unique opportunities, including fostering a strong research community focussed on mitigating the impact of a new virus. I consider myself fortunate to have been part of this community, where knowledge sharing and collaboration were prioritised. Additionally, I had the privilege of being part of an exceptional team that steered the multi-national Best Available Treatment Study. I was also able to leverage the existing infrastructure of the multi-country DIAMONDS consortium, led by my supervisor Professor Michael Levin, to rapidly collect valuable data and samples from individuals with SARS-CoV-2 associated disease. Contributing to such a critical research endeavour during my PhD has been a challenging yet immensely rewarding experience.

Chapter 1: Introduction

Coronavirus disease 2019 (COVID-19) is a highly contagious infectious disease, caused by severe acute respiratory syndrome coronavirus 2 (SARS-CoV-2), which was declared as a global pandemic by the World Health Organisation (WHO) in March 2020. Following the emergence and rapid spread of SARS-CoV-2, there was an urgent need to understand the new virus, its associated disease, and the intricate host-virus interactions. This understanding was vital for effectively mitigating the impact of COVID-19 through the development of diagnostics, therapeutics, vaccines, and public health measures. It became quickly apparent that there were age-related differences in the host-immune response to SARS-CoV-2, and the emergence of SARS-CoV-2 associated paediatric conditions, such as Multisystem Inflammatory Syndrome in Children (MIS-C) and COVID-19 vaccine-induced myocarditis, introduced further complexities to this ongoing health emergency. Understanding these complexities and the diverse effects of SARS-CoV-2 associated diseases is essential for optimising patient care and outcomes across all age groups.

This chapter provides essential background knowledge about coronaviruses, SARS-CoV-2 and its associated diseases. Each research topic addressed in my PhD is introduced, followed by a summary of the knowledge gaps that existed at the commencement of my research. Subsequently, a comprehensive up-to-date literature review is provided.

1.1 Viruses

1.1.1 Common characteristics of viruses

Viruses are obligate intracellular parasites, which means they lack the components for independent reproduction and require the internal machinery of a host cell for replication and production of new virus particles[1–3]. They are small in size ranging from approximately 20 nanometres (nm) to 100nm in diameter. The instructions for viral replication and protein synthesis are contained within genetic material composed of deoxyribonucleic acid (DNA) or ribonucleic acid (RNA)[1–3]. The genetic material is enclosed within a protein capsid for protection and some viruses have an additional lipid membrane envelope. The envelope is acquired from the host cell membrane and can aid viral entry into host cells as well as help evade the host immune system[1–3]. Many viruses have viral attachment proteins e.g., glycoproteins, which mediate the attachment of the virus particle to the host cell by interacting with specific receptors[1–3]. In some viruses, additional matrix proteins can be found which connect the envelope with the capsid, which serve multiple functions including providing structural support or facilitating viral assembly and budding[1,2]. These structures influence the virus' ability to infect a host cell and cause disease, and can vary in size, shape and complexity depending on the virus.

1.1.2 Viral replication and life cycle

Figure 1-1 displays the various stages of a generic viral life cycle. The first stage includes **attachment** of the viral attachment proteins to specific receptors on the surface of host cells[4]. Next, viral **entry** into the host cell occurs either via fusion of the viral envelope to the cell membrane or through endocytosis[4]. The viral genetic material is released from the capsid/envelope through **uncoating**, for **replication** and **transcription** using the host cell machinery[4]. The viral proteins are **translated**, followed by **assembly** into new virus particles (virions)[4]. Finally, the virions are **released** from the cell, either through **budding**, which allows the virus to acquire the host cell membrane upon exit, or through **cell lysis**[4].

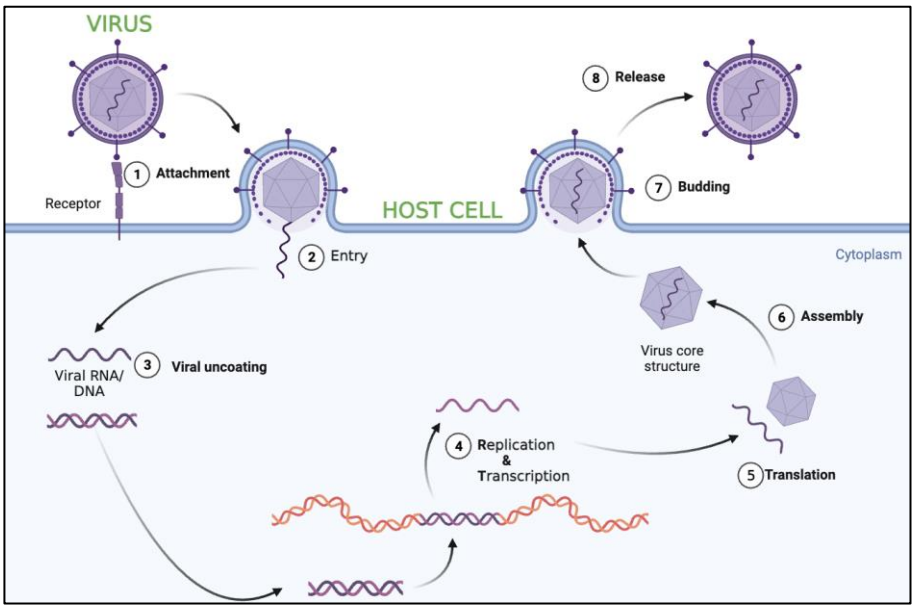

Figure 1-1 Stages of a generic virus life cycle.

This figure was made using Biorender.

1.1.3 Host response to viral infection

Virus entry into host cells results in a complex interaction between the host immune system and the invading virus. An effective host immune response is critical for virus clearance, infection control and prevention of reinfection. Detection of viral pathogens by the host immune system triggers several responses including the early innate immune response and the subsequent adaptive immune response[5]. Understanding the host-virus interaction and the delicate balance between viral clearance and immunopathology is vital for developing effective infection prevention, diagnostics, and management strategies.

1.1.4 Innate immune response

The innate immune response comprises physical, chemical, and cellular components. The initial defences against viral entry and access to target tissues include mechanical barriers such as the skin and mucosal surfaces, and chemical defences as provided by the acidic environment in the stomach[5]. However, if a virus manages to evade these barriers and enter host cells, the host immune response relies on cellular sensors termed pattern recognition receptors (PRRs) to identify pathogen-associated molecular patterns (PAMPs), which have been conserved among most pathogens[6,7].

Activation of PRRs triggers several signalling cascades resulting in the activation of nuclear factor kappa-light-chain enhancer of B cells (NFκB) and interferon regulatory factors (IRFs)[8–10]. NFκB activation upregulates genes encoding proinflammatory cytokines such as interleukin one (IL1), interleukin six (IL6) and tumour necrosis factor alpha (TNFα)[11,12], while activation of IRFs increases expression of interferons (IFNs), which are important for mounting an anti-viral immune response[13–15]. Type I IFNs (IFNα, IFNβ) and Type III IFN (IFNλ) inhibit virus replication and promote downstream anti-viral immunity while Type II IFN (IFNγ) activates immune cells and enhances antigen presentation[13–15].

Type I IFNs also activate natural killer (NK) cells which provide defence against viruses by eliminating virus infected cells, and modulate the immune response through production of pro-inflammatory cytokines and interaction with dendritic cells (DCs), which are antigen presenting cells (APCs) that play an essential role in the adaptive immune response[16,17]. The innate immune response also involves other cell types such as macrophages, neutrophils, and gamma delta T cells ($\gamma\delta$T cells), as well as host proteins such as natural antibodies and complement[5,18]. Cytokines and chemokines are necessary for coordinating the immune response and recruiting macrophages, neutrophils, DCs, and NK cells to sites of infection[5,18]. The coordinated actions of the innate immune response components aim to control viral replication, eliminate infected cells, and activate the adaptive immune response.

1.1.5 Adaptive immune response

The adaptive immune response is targeted and specific to the virus and is necessary for virus clearance and establishing long-term immunity. It can be divided into two components, the B cell lymphocyte mediated humoral response and the T cell lymphocyte mediated cellular response[5,18]. The early innate immune response activates APCs such as DCs and macrophages, which migrate to the lymphoid tissue for interaction with and activation of lymphocytes[5,18].

1.1.5.1 B cell response

B cell activation leads to clonal expansion of B cells and generation of virus specific antibody-producing short-lived plasma cells, along with long-lived plasma cells and memory B cells which provide long-term immunity[5,18]. Antibodies have numerous functions including 1) neutralising free viral particles to prevent further infection of host cells, 2) coating viruses to promote elimination by phagocytic cells such as macrophages and neutrophils, 3) binding viral proteins on the surface of infected cells to

trigger the complement cascade and antibody dependent cell mediated cytotoxicity (ADCC) to eliminate infected cells, and 4) preventing reinfection especially at mucosal surfaces, facilitated by immunoglobulin A (IgA) and immunoglobulin G (IgG)[5,18].

1.1.5.2 T cell response

T cells can be divided into two main subtypes depending on their cell surface markers, Cluster of Differentiation (CD) 4^+ T cells and $CD8^+$ T cells. $CD4^+$ T cells recognise viral antigens presented on the Major Histocompatibility Complex (MHC) class II molecules by APCs[5,18]. Following activation, $CD4^+$ T cells differentiate into different subsets. Some of the major subsets include T helper (Th) 1, Th2, Th17, T follicular helper (Tfh) cells and T regulatory cells (Tregs)[19]. Generally, Th1 cells augment cell-mediated immune responses, Th2 cells stimulate B cell activation and antibody production, Th17 cells aid recruitment of immune cells to sites of infections, Tfh cells support the B cell antibody response, and Tregs maintain immune tolerance and prevent an excessive immune response[19].

$CD8^+$ T cells are activated following recognition of viral antigens presented on MHC class I molecules by APCs. This leads to $CD8^+$ T cells clonal expansion and differentiation into effector cytotoxic $CD8^+$ T cells. Cytotoxic $CD8^+$ T cells directly recognise and eliminate virus-infected cells by inducing programmed cell death (apoptosis) in the infected cells or through the release of cytotoxic molecules such as perforins and granzymes which cause cell lysis[5,20]. Following resolution of acute infection, a portion of activated T cells differentiate into memory T cells to provide long-term immunity against the specific virus. Memory T cells can respond quicker to future exposure to the same virus, leading to a faster and stronger immune response[5].

1.1.5.3 Vaccination

Vaccination harnesses the long-term memory of adaptive immunity to protect against infectious diseases. Vaccines contain components of pathogens (e.g. genetic material or weakened/inactivated forms of the pathogen), which are recognised by the immune system as “non-self”, triggering the activation of the adaptive immune response and generation of memory B and T cells[5,18,21]. By priming the immune system to recognise and remember pathogens, vaccines lead to a more effective and longer-lasting protection, while reducing the risk of severe illness, disease transmission and the burden on healthcare systems, compared to acquiring natural immunity through infection[22].

1.1.6 Immunopathology

There is a delicate balance between the host mounting a robust immune response for viral clearance and preventing immunopathology and tissue damage (Figure 1-2). Once the host immune response detects viral infection, it triggers the recruitment and migration of immune cells to sites of infection to control the infection. However, if there is excessive accumulation and activation of immune cells, it can lead to host tissue damage, contributing to the progression of the disease[23]. In some situations, viral infections can trigger autoimmune diseases, whereby virus-specific antibodies or antibodies against self that are produced following cell damage due to infection can mistakenly target healthy tissue, leading to tissue destruction and disease (e.g. Guillain-Barré syndrome)[23]. A dysregulated complement response also contributes to immunopathology by causing excessive inflammation leading to tissue damage. In severe infections, the production of pro-inflammatory cytokines can become uncontrolled, leading to a cytokine storm[24] (Figure 1-2). This cytokine storm can cause tissue damage, systemic inflammation and organ dysfunction[24]. Finally, post-viral inflammatory conditions can also occur after the acute infection has resolved. These conditions are characterised by a dysregulated immune response causing persistent or recurrent inflammation even after the virus has been cleared from the body[25].

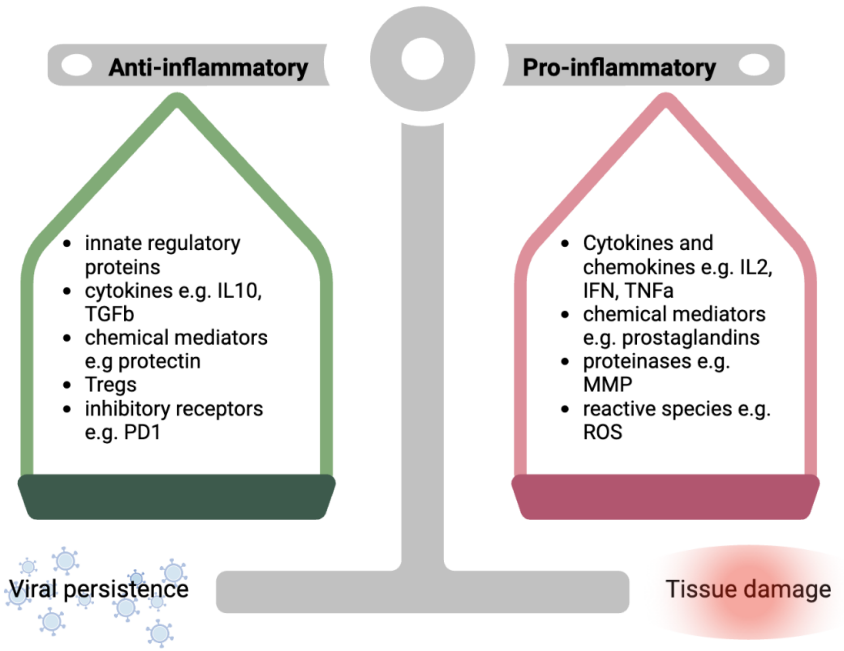

Figure 1-2 Host immune response: balancing inflammation and immunity during viral infection.

IL10 = interleukin ten, TGFb = transforming growth factor beta, Tregs = T regulatory cells, PD1 = programmed cell death protein 1, IL2 = interleukin two, IFN = interferon, TNFa = tumour necrosis factor alpha, MMP = matrix metalloproteinase, ROS = reactive oxygen species. This figure was made using Biorender.

1.2 Coronaviruses

Coronaviruses are enveloped, single-stranded RNA viruses that can infect mammals and birds. They belong to the *Coronaviridae* family and are named for their crown-like (corona in Greek) appearance under an electron microscope[26]. In humans, they cause respiratory tract infections of varying severity; from mild common cold-like illness to severe life-threatening disease[26].

1.2.1 Seasonal coronaviruses

The four commonly detected seasonal coronaviruses include: Human Coronavirus NL63 (HCoV-NL63), Human Coronavirus 229E (HCoV-229E), Human Coronavirus OC43 (HCoV-OC43) and Human Coronavirus HKU1 (HCoV-HKU1)[27]. Seasonal coronaviruses are distributed across the globe and have been detected across all age groups[27]. They typically cause mild, self-limiting respiratory illness[28] in both adults and children and account for 15-30% of all recorded respiratory tract infections[29].

1.2.2 Previous coronavirus outbreaks

Coronaviruses can also cause severe and sometimes fatal infections in humans. One of the most highly pathogenic strains of coronaviruses is Severe Acute Respiratory Syndrome Coronavirus (SARS-CoV), which resulted in the 2002-2004 Severe Acute Respiratory Syndrome (SARS) epidemic[30,31]. SARS-CoV emerged in China and spread to other countries resulting in a global epidemic[30,31]. The origin of the virus remains elusive, but studies have suggested transmission from bats through an intermediate host[32,33]. Patients with SARS typically presented with fever, cough and dyspnoea and the disease had a high mortality rate, particularly in older adults, of approximately 10%[34]. Over 8000 cases of SARS were reported, with 774 deaths[35]. The exact number of children affected by SARS is unknown; however, it is estimated that children under the age of 18 years only accounted for approximately 5% of the cases. Moreover, children were noted to have a milder form of the disease compared to adults, with no fatalities reported in the paediatric cohort[36].

Middle East Respiratory Syndrome-related Coronavirus (MERS-CoV) is another coronavirus strain that can cause severe disease in humans, and led to the 2012 Middle East Respiratory Syndrome (MERS) outbreak[37,38]. MERS-CoV was first identified in Saudi Arabia in 2012[37,38]. The first outbreak primarily affected people in countries in the Middle East, where approximately half of the cases were attributed to primary transmission of MERS-CoV from camels to humans, while the other half were thought to

be due to secondary human-human transmission[39,40]. A second outbreak in South Korea occurred in 2015, which was the largest outside of the Middle East[39]. The index case was a returning traveller from the Middle East and the epidemic was associated with human-to-human transmission within healthcare settings[39,41]. The clinical features of MERS were similar to that of SARS with an even higher mortality rate of approximately 35%[37,39]. Over 2600 cases and 936 deaths have been reported to date[42]. MERS primarily affected the adult population, and paediatric cases were reported to have a milder disease course, accounting for approximately 2% of all cases[36].

The SARS outbreak was ultimately controlled using rigorous public health measures; however, sporadic cases of MERS continue to be reported[42].

1.2.3 SARS-CoV-2

1.2.3.1 Structural biology and viral entry

SARS-CoV-2, the virus responsible for the COVID-19 pandemic, was first identified in a cluster of patients with pneumonia in late 2019 in Wuhan, China[43,44]. SARS-CoV-2 shares 79% sequence similarity with SARS-CoV45. It has a diameter of 100 – 200 nm and contains four structural and 16 non-structural proteins[46]. The structural proteins consist of the Nucleocapsid protein (N), which contains the RNA genome, and the Spike (S), Envelope (E) and Membrane (M) proteins, which are components of the lipid envelope[46] (Figure 1-3). The SARS-CoV-2 S protein consists of two subunits, the S1 subunit, which binds to the host cell surface receptor, Angiotensin Converting Enzyme 2 (ACE-2), and the S2 subunit which facilitates membrane fusion[47]. Efficient viral entry into host cells also requires the cleavage and activation of the S proteins by the host proteases including transmembrane protease serine 2 (TMPRSS2) and furin[47–50]. The ACE-2 receptor is likely to be the primary mode of entry, however, alternative routes involving endosomes and other co-receptors have been proposed[47,50].

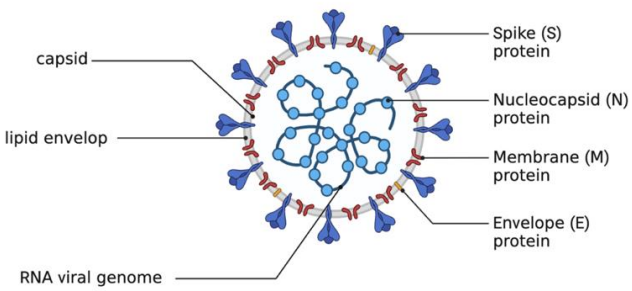

Figure 1-3 Structure of severe acute respiratory syndrome coronavirus 2 (SARS-CoV-2).

This figure was made using Biorender.

1.2.3.2 SARS-CoV-2 transmission and global spread

The origin of SARS-CoV-2 is believed to be through zoonotic spillover and the early cases were linked to the Huanan Seafood Wholesale Market in Wuhan, China[45], but the exact source and pathway of transmission remains under investigation. Subsequently, efficient human-to-human transmission of SARS-CoV-2 contributed to the rapid spread of the virus across the globe, and along with the severity of the disease led to the WHO declaring COVID-19 as a global pandemic in March 2020[51]. SARS-CoV-2 is primarily transmitted through close contact with infected secretions or respiratory droplets expelled from symptomatic or asymptomatic infected individuals, e.g. either directly by coughing or sneezing or indirectly from contaminated objects[52,53]. In certain situations, airborne transmission has also been described, for instance during aerosol generating medical procedures or during choir practice in a crowded indoor space[52]. As of 28 June 2023, there have been 767,518,723 confirmed cases of COVID-19, including 6,947,192 deaths, reported to the WHO[54], the distribution of these cases is shown in Figure 1-4.

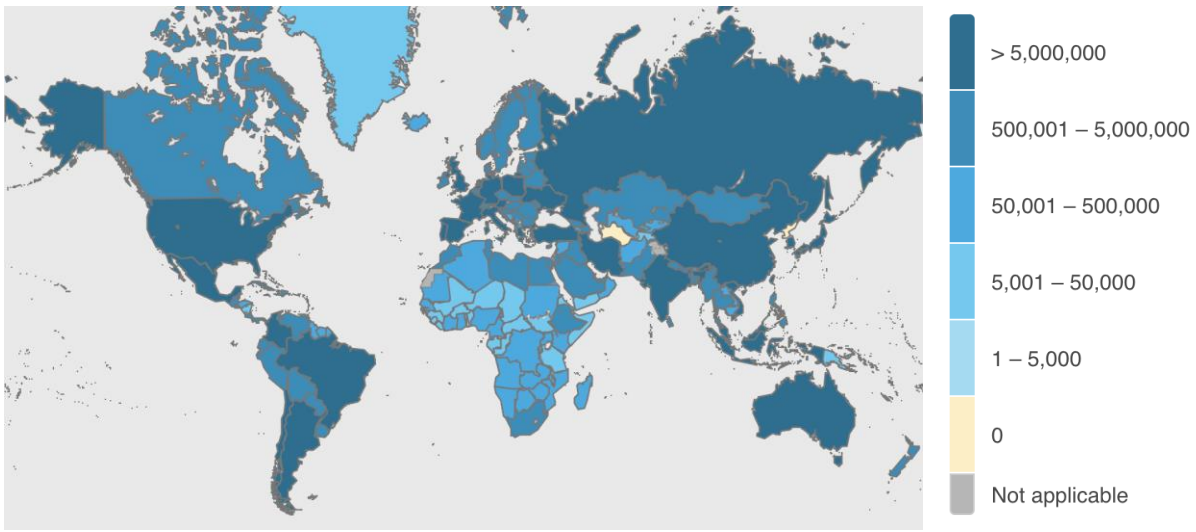

Figure 1-4 Global map illustrating the recorded cases of COVID-19 as of 28/06/2023 from the WHO COVID-19 Dashboard[54].

1.2.3.3 Host immune response to SARS-CoV-2

Innate immune response to SARS-CoV-2

The innate immune response provides the first line of defence against SARS-CoV-2 and research is ongoing to provide a comprehensive understanding of underlying mechanisms. PAMPs in SARS-CoV-2 proteins and RNA are recognised by PRR, including toll-like receptors (TLR) and retinoic acid-inducible gene (RIG-I) like receptors (RLR)[55], triggering intracellular signalling cascades resulting in activation of NFκB and IRF pathways[55]. This leads to the production of proinflammatory cytokines and IFNs, which help inhibit SARS-CoV-2 replication[55]. Another category of PRR is the nucleotide-binding oligomerization domain (NOD)-like receptors (NLRs). NLR, specifically, Nucleotide-Binding Domain Leucine-Rich–Containing Family, Pyrin Domain–Containing-3 (NLRP3) forms inflammasome complexes, which result in the production of pro-inflammatory cytokines upon activation by viral components[55]. Mannose binding lectin (MBL), a component of the complement system, acts as a soluble PRR and binds to SARS-CoV-2, resulting in activation of the complement system, inducing inflammation, and enhancing phagocytosis[56]. In addition, the cellular components of the innate immune response such as NK cells, macrophages, neutrophils, and DCs also play crucial roles in controlling SARS-CoV-2 infection and activating the adaptive immune response[56].

SARS-CoV-2 has developed various evasion strategies against the innate immune system, including downregulating or delaying IFN responses, inducing MHC II downregulation on APCs, NK cell apoptosis, and impairing neutrophil and DC function[55,57–60]. These evasion strategies can delay or downregulate the innate immune response, leading to suboptimal priming and subsequent dysregulation of the adaptive immune response. This can impede effective viral clearance and cause increased inflammation, contributing to the development of severe disease[61–63].

Adaptive immune response to SARS-CoV-2

The B cell response against SARS-CoV-2 appears to be typical of other viral infections. Levels of IgM peak at 2-4 weeks and decline to background levels thereafter and levels of IgG have been shown to persist at high levels at 3 months[56,64,65]. The majority of individuals with mild or moderate infection mount a robust humoral response, with adequate levels of neutralising antibodies against SARS-CoV-2. However, critically unwell individuals have been reported to exhibit higher levels of anti-SARS-CoV-2 antibodies[66–69]. Moreover, patients with severe disease were found to have changes in their B cell subpopulations with transiently increased proliferating plasmablasts (PBs) and reduced memory B

cells during acute illness[70–72]. However, these changes in B cell subpopulations were not associated with levels of neutralising antibodies[70], suggesting that the increase in PBs are not solely due to production of antibodies against the SARS-CoV-2 Spike protein, which is the primary neutralising antibody. This implies that patients with severe COVID-19 mount a broader range of B cell responses, targeting antigens other than the Spike protein.

One of the characteristic features of severe COVID-19 is profound lymphopenia[73–77]. Several mechanisms for reduced $CD4^+$ and $CD8^+$ T cells have been proposed including suboptimal activation of the adaptive immune response due to impaired innate immunity[62], infection[78] or apoptosis of T lymphocytes[79,80], damage to lymphatic tissue[81,82] and lymphocyte sequestration[83]. In addition to reduced T cell counts observed in severe COVID-19, there is reduced expression of activation markers and increased expression of exhaustion markers on T cells, indicating reduced T cell function[60]. Moreover, there are increased proportions of activated Tregs and reduced proportions of naïve Tregs, suggesting an effort to modulate the immune response[60]. These changes suggest complex alterations in T cell responses during severe COVID-19, involving both pro-inflammatory and immune-regulatory mechanisms.

<u>COVID-19 hyperinflammation</u>

There appear to be two overlapping phases of the immune response to SARS-CoV-2 (Figure 1-5). The first phase is a protective immune response aimed at eliminating the virus, some patients progress on to a second phase of illness, occurring around day 10-14[84]. The second phase is characterised by an over-activated or dysregulated host response and hyperinflammation[84]. Several factors including viral load, rate of viral replication, host genetics, patient age and pre-existing comorbidities have been postulated to influence COVID-19 hyperinflammation[62,85], however the specific mechanisms underlying this dysregulated response are still being investigated. It is important to note that COVID-19 hyperinflammation in acute infection is characteristic of adult disease and is very rare in paediatric cases[86].

COVID-19 hyperinflammation is characterised by excessive recruitment and activation of innate and adaptive immune cells, coupled with ineffective modulation of the immune response. As such, elevated circulating levels of the proinflammatory cytokines are seen, including IFNγ, macrophage-colony stimulating factor (M-CSF), granulocyte-colony stimulating factor (G-CSF), granulocyte-macrophage-colony stimulating factor (GM-CSF), IFNγ induced protein-10 (IP10), monocyte chemoattractant protein-1 (MCP1), macrophage inflammatory protein 1-alpha (MIP1α), interleukin

one beta (IL1β), interleukin two (IL2), IL6, interleukin seven (IL7), interleukin ten (IL10), interleukin twelve (IL12), interleukin thirteen (IL13) and interleukin seventeen (IL17)[73,74,76,87]. The resultant cytokine storm contributes to the tissue damage and overwhelming systemic inflammation seen in severe COVID-19[24,85,88–90].

The complement system acts as a bridge between the innate and adaptive immune responses, however unregulated complement activity contributes to hyperinflammation[91], endothelial cell dysfunction, and subsequent coagulopathy observed in severe COVID-19[92]. Endothelial cell injury can occur through direct SARS-CoV-2 infection of endothelial cells as well as indirect effects of a systemic inflammatory state. This results in increased vascular permeability, promotion of neutrophil infiltration and formation of neutrophil extracellular traps (NETs), activation of coagulation and suppressed anticoagulation mechanisms. Ultimately, contributing to systemic thrombosis and disseminated intravascular coagulation[93,94].

Clinical features of cytokine storm in COVID-19 include overwhelming persistent fevers, hypotension and deranged coagulation, which can progress to multiorgan failure and death[85]. Elevated levels of cytokines, such as IL6[76,95–98], IL10[76] and TNFα[76,98] have been associated with poorer prognosis and mortality. Targeting these cytokines and their signalling pathways has been an active area of research and a focal point for clinical interventions[99–101]. IL6 inhibitors such as tocilizumab, have shown promise in improving outcomes in severe COVID-19[102]. Similarly, other immunomodulatory treatments such as corticosteroids have become the mainstay of treatment in severe disease[100].

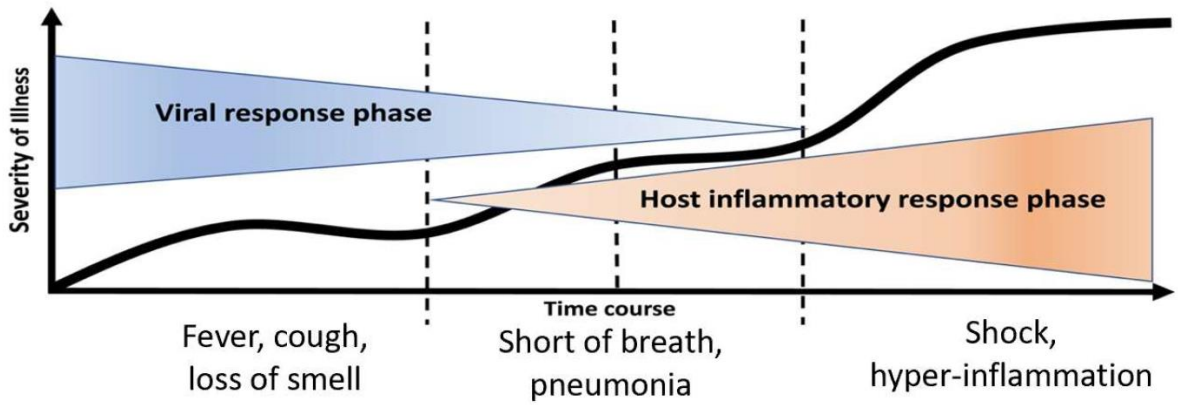

Figure 1-5 Progression of disease in adults following SARS-CoV-2 infection.

Adapted from Siddiqi & Mehra 2020[84].

1.3 COVID-19

1.3.1 Clinical characterisation

The clinical manifestations of COVID-19 vary widely, ranging from asymptomatic infections to severe life-threatening disease with an estimated mortality rate of between 1-5%[103–105]. Most infected individuals develop symptoms 4-5 days[106–108] following exposure; however, the incubation period can extend up to 14 days[106–108]. It is also estimated that nearly one-third of infected adults and around half of infected children never become symptomatic[109–112], which along with a relatively long incubation period adds to the challenges of controlling disease transmission.

Symptomatic adults typically present with fever, cough, dyspnoea, fatigue and loss of taste and smell[45,74,76,113,114]. Indeed, while the respiratory system is primarily affected, the impact of SARS-CoV-2 extends beyond respiratory symptoms. Additional clinical manifestations relating to the gastrointestinal (GI), renal, central nervous and cardiovascular systems have been reported[45,74,76,114,115]. These effects are either through direct SARS-CoV-2 infection or secondary to hyperinflammation. Amongst symptomatic patients, severity ranges from a mild common cold-like illness (40%), moderate pneumonia with no oxygen requirement (40%), to severe pneumonia (15%), acute respiratory distress syndrome (ARDS) with multi-organ failure and death (5%)[116].

The most common presenting symptoms in children with COVID-19 are fever and cough; with rhinorrhoea, dyspnoea and GI symptoms being less frequently present[103,104,112,117]. Most children are either asymptomatic or develop a mild to moderate disease with recovery within 14 days[103,118,119]. Severe COVID-19 (~2%) and mortality (less than (<) 0.1%) have been reported in a relatively small percentage of paediatric cases[103,118,119].

1.3.2 Risk factors

Several risk factors influence the severity of COVID-19 in adults and children. In adults, male sex, increasing age, Black, Asian or Hispanic ethnicity, pre-existing comorbidities (e.g. diabetes, cardiovascular disease, obesity, immunosuppression), smoking, and COVID-19 unvaccinated status have been identified as significant risk factors for severe disease[120–125]. In children, age less than one year, Black, Asian or Hispanic ethnicity, underlying medical conditions (e.g. prematurity, asthma, obesity, neurological conditions and cardiovascular disease) have been reported to increase risk of

severe disease[126–128]. Additionally, socioeconomic factors, including access to healthcare and living conditions, can contribute to increased vulnerability and severe COVID-19 outcomes[124].

Genetic factors influencing disease susceptibility and severity in COVID-19 have been investigated. Studies have identified genetic susceptibility loci related to histo-blood group ABO system transferase (ABO) and ACE-2[129]. Additionally, severity loci including TMPRSS2, Human leucocyte antigen (HLA), TLR7, and interferon alpha receptor 2 (IFNAR2) have been implicated[129]. Rare inborn errors of mutations have also been reported, including in the Chromosome X gene, which may explain the observed sex differences, and loss of function mutation in TLR7 with subsequent impaired type I interferon response[129].

1.3.3 Diagnosis of COVID-19

The WHO[130] and the Centers for Disease Control and Prevention (CDC)[131] have developed case definitions for COVID-19. COVID-19 should be considered in individuals presenting with fever and/or respiratory symptoms, in the absence of another obvious cause. Microbiological testing must be performed in suspected cases to confirm SARS-CoV-2 infection. The preferred method of testing is reverse transcription-polymerase chain reaction (RT-PCR) to detect SARS-CoV-2 RNA in respiratory samples, such as nasopharyngeal or oropharyngeal swabs[130,131]. Other diagnostic methods, such as antigen tests or loop-mediated isothermal amplification (LAMP) tests, can be used[130,131].

1.3.4 Clinical investigations findings in COVID-19

Laboratory investigations in COVID-19 hospitalised patients reveal elevated neutrophil counts, inflammatory markers (c-reactive protein (CRP), ferritin), lactate dehydrogenase (LDH), D-dimers, creatine kinase and significantly decreased lymphocyte counts[76,104,114,132]. There is evidence of deranged coagulation (raised prothrombin time), altered liver function (raised alanine transferase (ALT)) and poor renal function (raised urea and creatinine)[76,104,114,132]. Chest imaging can aid clinical diagnosis and can help identify any pulmonary complications[116]. Chest x-rays may show consolidation, which indicates areas of lung tissue filled with fluid, inflammatory cells and debris, or pleural effusion, which is an accumulation of fluid in the pleural space[133]. The most common findings on chest CT are ground-glass opacities associated with consolidation[133].

1.3.5 Management of COVID-19 hospitalised patients

The management of COVID-19 involves infection prevention, supportive care, and specific medical interventions. Early in the pandemic, treatment options were limited, therefore experimental drugs were trialled and drugs repurposed. Since then, evidence of efficacy has emerged for various treatment options, including both repurposed and novel drugs. Among them are antiviral drugs (e.g. remdesivir[134]), anti-SARS-CoV-2 monoclonal antibodies (e.g. sotrovimab[135]), anti-inflammatory drugs (e.g. corticosteroids[136]), and immunomodulatory agents (e.g. tocilizumab (anti-IL6)[102]). Treatment choice is now guided by the severity of the illness and individual risk factors[137].

1.3.6 COVID-19 vaccination

In December 2020, the first COVID-19 vaccines were authorised for emergency use. Since then, vaccination has been the mainstay of controlling the COVID-19 pandemic. Several vaccines using different technologies have been approved for administration, including the viral vector and messenger RNA (mRNA) vaccines, which have been the most widely used[138]. The viral vector vaccines use a modified version of a different virus (e.g. non-replicating adenoviral strain) as a vector to deliver genes that encode SARS-CoV-2 antigens into host cells, prompting them to produce viral antigens[138]. Examples of viral vector COVID-19 vaccines include the Oxford-AstraZeneca vaccine[139] and the Johnson & Johnson vaccine[140]. The mRNA vaccines contain synthetic mRNA that encodes the instructions for producing SARS-CoV-2 S protein, which, following entry into host cells, directs them to make the SARS-CoV-2 S protein[138]. The mRNA vaccines include BNT162b2 mRNA (Pfizer-BioNTech) and mRNA-1273 (Moderna)[141,142]. Both types of vaccines induce immunological memory and provide protection against COVID-19[138].

1.3.7 Long-term outcomes in COVID-19

The outcomes of COVID-19 can vary depending on age, pre-existing comorbidities, vaccination status and the severity of the illness. While most individuals experience a mild to moderate disease course and recover without complications[143,144], long-term sequelae, such as fatigue, respiratory impairment, cardiac complications, and mental health issues, have been reported. These will be described in the “Long COVID” section below[145].

1.4 The role of antibodies in COVID-19 disease severity and age-related differences

Antibodies are essential components of the immune response which can confer protection but can also contribute to immunopathology. There is evidence which suggests that antibodies play a role in the intense inflammatory process underlying severe COVID-19 disease in adults. Studies have demonstrated that deterioration in disease occurs 9-17 days into the illness course[146], when viral titres are decreasing[147] and SARS-CoV-2 IgM and IgG are being detected in the circulation[148]. Moreover, there are several reports of higher antibody levels in patients with severe COVID-19 compared to those with a milder disease course[66,67,69].

One intriguing aspect of COVID-19 is the variation in disease severity among different age groups. Adults, particularly those with underlying health conditions, are more susceptible to severe disease and complications. In contrast, children typically experience milder symptoms or remain asymptomatic[149]. The age-related differences in COVID-19 differ from the trends observed in most other respiratory viruses, where there are two peaks of disease susceptibility - in the very young and the elderly[150]. The infant peak is explained by absence of acquired immunity, while the elderly peak is attributed to waning of acquired immunity[151]. COVID-19[152,153], SARS[34] and MERS[154] appear to deviate from this pattern, primarily affecting adults, suggesting that different mechanisms are responsible for the increased disease severity and mortality in this specific group.

1.4.1 Knowledge gaps in the role of antibodies in COVID-19 disease severity and age-related differences at the beginning of this PhD

When I embarked on my PhD, there were significant gaps in the understanding of the role of antibodies in both the dysregulated immune response to SARS-CoV-2 and the observed variations in disease severity among different age groups. There was limited information on the immune response to SARS-CoV-2 in children, implications of pre-existing comorbidities, the influence of genetics as well as role of environmental and social factors. Within this broader context, I chose to investigate the role of antibodies in COVID-19 disease severity, focusing on studying the concept of antibody dependent enhancement (ADE) as a potential explanation for the age-related differences observed in outcomes of SARS-CoV-2 infection.

ADE is a mechanism by which antibodies can contribute to disease severity. There are several mechanisms by which ADE induces immunopathology. These include non-neutralising antibodies increasing the uptake of the virus into Fc gamma receptor expressing phagocytic cells leading to increased viral replication, modulation of the immune response through excessive Fc-mediated effector function and immune complex formation and complement activation[155]. There is compelling evidence of disease severity following ADE from other infections, including influenza, dengue and SARS[156]. Studies on SARS have shown higher titres and increased rates of production of SARS-CoV Spike antibodies in deceased patients compared with recovered patients, suggesting their involvement in disease severity[157]. Furthermore, SARS-CoV Spike antibodies have been shown to promote acute lung injury through increased recruitment and accumulation of neutrophils and pro-inflammatory macrophages in animal models[158].

Although ADE has been observed in other viral infections, its potential involvement in COVID-19 and its role in age-related differences was undetermined. My research, therefore, sought to explore the role of cross-reactive antibodies from seasonal coronaviruses and their potential for either providing protection or causing damage through ADE. It is plausible that adults, over their lifetime, have accumulated antibodies to various seasonal coronaviruses, which can potentially lead to ADE and more severe COVID-19. Investigating the role of ADE in COVID-19 severity is crucial in understanding the underlying mechanisms of age-related differences in disease outcomes and has significant implications for vaccination development and delivery strategies.

1.4.2 Current understanding of the role of antibodies in COVID-19 disease severity and age-related differences

As my PhD progressed, new studies were published that have shed light on factors contributing to age-related differences in COVID-19 severity including the role of antibodies.

1.4.2.1 Role of antibodies in COVID-19 disease severity

The role of antibodies in COVID-19 disease outcomes has been studied in both adults and children. Several studies have reported findings in line with the earlier studies showing higher titres[69,157,159,160], breadth[161,162] and fc mediated effector function[163,164] of SARS-CoV-2 IgG antibodies in adults with severe COVID-19 compared to those with moderate or mild disease. Furthermore, Pierce et al. reported that the high antibody titres detected in adult patients with severe COVID-19 were functionally effective in terms of neutralising capacity and ability to induce phagocytosis[163].

Conversely, Takita et al. showed lower antibody levels were found in deceased patients, compared to those who survived[165]. Moreover, other groups have shown that adults with severe COVID-19 have a delayed humoral response[166–168] and decreased antibody binding strength[159], suggesting a suboptimal antibody response. Several studies in adults have also demonstrated a positive correlation between age and SARS-CoV-2 antibody titres[163,169,170], suggesting that age-related factors may influence the antibody response and potentially contribute to disease severity.

There are very few studies which have investigated the antibody response in paediatric COVID-19. Sananez et al. showed progressively rising SARS-CoV-2 IgG titres with asymptomatic, mild and moderate disease, however, children with severe COVID-19 were not able to mount a detectable antibody response during acute illness[171]. Intriguingly, no significant difference was observed across the disease severity groups in the neutralising ability of antibodies tested in convalescent samples[171]. Similarly, Anderson et al. also showed undetectable SARS-CoV-2 IgG levels in the majority of severe paediatric COVID-19 cases, with variable levels of IgG titres in asymptomatic and mild disease[172].

Some studies have made comparisons between the antibody response in adults and children with SARS-CoV-2 infection. It is important to note that the children included in these studies were predominantly mild cases while the adults had more severe disease. Adults generally exhibited higher antibody titres and stronger neutralising capacity compared to children[159,162,163,173], and a significant positive correlation was noted between age and neutralising activity[163]. Adults with symptomatic disease had significantly higher antibody titres compared to adults with asymptomatic disease, however, the same trend was not observed in the paediatric cohort – contrary to the findings by Sananez et al. discussed above[174]. Additionally, Weisberg et al. showed that children with COVID-19 were found to have a narrower breadth of anti-SARS-CoV-2 antibodies, primarily targeting the S protein, compared to adult cases[162]. While Hachim et al. report a stronger antibody response in children directed to accessory proteins such as non-structural protein 1[173].

Research in this field is ongoing and the findings so far collectively suggest that adults and children mount distinct antibody responses to SARS-CoV-2, which likely contribute to the disease outcomes. Adults generally exhibit higher and more robust antibody responses compared to children. It can be postulated that a less effective immune response in adults results in delayed viral clearance and severe disease. However, it is important to note that the antibody response is just one aspect of the immune response, and other mechanisms also play a role in determining disease severity and outcome.

1.4.2.2 Cross-reactive antibodies and ADE

The presence of cross-reactive antibodies and their potential protective and harmful impact on disease outcome in COVID-19 has been investigated. Several studies have reported that antibody titres of seasonal coronaviruses and pre-existing cross-reactive humoral immunity did not differ by age[163,175,176]. Lv et al. reported that cross-reactivity between SARS-CoV-2 and SARS-CoV is common in adults, however, these antibodies do not have neutralising capacity[177]. Gua et al. demonstrated that higher titres of cross-reactive HCoV-OC43 S IgG were associated with COVID-19 disease severity[178]. While Sagar et al. suggested that prior infection with seasonal coronaviruses may in fact provide protection, as it was associated with less severe COVID-19[179]. Additionally, Ng et al. demonstrated that levels of cross-reactive antibodies were higher in children compared to adults, and that these antibodies had neutralising effects against SARS-CoV-2[180] *in vitro*. It appears that cross-reactive antibodies in COVID-19 may have both protective and potentially deleterious effects which require further exploration.

While some researchers have investigated the potential role of ADE in COVID-19, the evidence remains limited. Hoepel et al. demonstrated *in vitro* that immune complexes formed from anti-SARS-CoV-2 antibodies and SARS-CoV-2 S protein could induce macrophage hyperinflammation, suggesting a potential mechanism for ADE[181]. Others have reported that severe COVID-19 patients had increased levels of SARS-CoV-2 IgG afucosylation, compared to patients with mild disease[182,183]. Afucosylated IgG antibodies, which lack the sugar molecule fucose in their Fc region, have been associated with enhanced antibody-dependent cellular cytotoxicity (ADCC) due to increased affinity to Fc receptors[184]. While these studies provide insights into possible mechanisms for ADE in COVID-19, further research is needed to fully understand its role in COVID-19 pathogenesis. However, the fact that numerous trials of convalescent plasma therapy have been undertaken safely, and that no worsening of disease has been reported with repeated infections, suggests that ADE is unlikely to play a role in COVID-19[185–188].

1.4.2.3 Additional factors contributing to age-related differences

In addition to humoral immunity, multiple other factors are being investigated to explain the age-related differences seen in COVID-19 severity. Children are likely to mount a stronger innate immune response, including a stronger type I IFN response[62,163,189], and may have pre-existing cross-reactive T cell immunity[190], which could contribute to better control of infection and milder symptoms.

Moreover, differences in endothelial function and clotting may also play a role, as children have less pre-damaged endothelium[191]. Variations in ACE-2 and TMPRSS2 receptor expression[191], presence of autoantibodies[192], impact of comorbidities, along with genetic[193] and environmental factors[191], are also being investigated.

1.5 SARS-COV-2 associated inflammatory conditions in children

Although the majority of children are less susceptible to SARS-CoV-2 infection and severe disease compared to adults, a small proportion of children experience serious complications following exposure to SARS-CoV-2 antigens. These include Paediatric Inflammatory Multisystem Syndrome Temporally associated with SARS-CoV-2 (PIMS-TS), also known as Multisystem Inflammatory Syndrome in Children (MIS-C), and COVID-19 vaccine-induced myocarditis. Although these conditions are rare, they can have significant impact on affected individuals and therefore have become an important area of research focus in recent years.

1.5.1 MIS-C

In May 2020, paediatricians in the UK raised an alert and published a case definition for a new childhood inflammatory condition associated with SARS-CoV-2, following reports of previously healthy children presenting to hospital with persistent fever, multi-system inflammation and cardiogenic shock[194]. Subsequently, similar clusters of cases were reported across Europe, Israel and the US, with notably fewer cases reported from Asia[195]. The condition was initially termed Paediatric Inflammatory Multisystem Syndrome Temporally associated with SARS-CoV-2 (PIMS-TS) in the UK and later went on to be named Multisystem Inflammatory Syndrome in Children (MIS-C), which is now commonly used worldwide. The term MIS-C will be used for this thesis.

MIS-C is characterised by widespread inflammation affecting multiple organ systems, including the heart, lungs, GI tract, and skin[196–200]. The exact underlying mechanisms of MIS-C are still being investigated, but it is believed to be a post-infectious inflammatory syndrome which occurs following exposure to SARS-CoV-2[201]. The syndrome has overlapping features with other infectious and inflammatory conditions, including COVID-19 hyperinflammation, bacterial sepsis, Kawasaki Disease (KD), Toxic Shock Syndrome (TSS) and Macrophage Activation Syndrome (MAS)[196,202].

The emergence of MIS-C presented diagnostic uncertainty for healthcare professionals, as little was initially known about this novel condition, and the similarities between MIS-C and other conditions posed additional challenges. To aid identification and diagnosis, as well as facilitate effective surveillance and research efforts, the Royal College of Paediatrics and Child Health (RCPCH) in the UK[194], CDC[203], and WHO[204] developed case definitions for MIS-C. The case definitions are consistent in their core features with subtle differences, primarily the absence of a requirement for evidence of SARS-CoV-2 exposure in the UK definition (Appendix 1, Table A1-1). The UK case definition includes

any child (< 18 years of age) who presents with persistent fever, inflammation, and evidence of single or multi-organ failure, where a microbial cause has been excluded and SARS-CoV-2 polymerase chain reaction (PCR) test may be positive or negative[194]. The differences in the case definitions arose because the RCPCH definition was designed to determine the existence of a link between MIS-C and SARS-CoV-2, leading to the exclusion of evidence of SARS-CoV-2 infection within the case definition.

The estimated incidence of MIS-C is 1 in 3-4000 in individuals under 21 years of age infected with SARS-CoV-2[205,206]. However, this estimate may not capture the full extent of MIS-C cases, as children with milder forms of illness that do not require hospitalisation may go unnoticed. Additionally, the true denominator of MIS-C cases remains unknown due to the lack of widespread SARS-CoV-2 testing in children. The temporal association of MIS-C and SARS-CoV-2 has been demonstrated by the peak of MIS-C cases following 2-8 weeks after the peak in COVID-19 cases[197,198,207,208] (Figure 1-6). The median age of affected children is 8-9 years, with a slight male preponderance and over representation of Black, South Asian and Hispanic ethnicities[196–200,209,210]. Around 20-30% of patients have underlying comorbidities, with obesity, asthma and diabetes being most frequently cited[199,209,210].

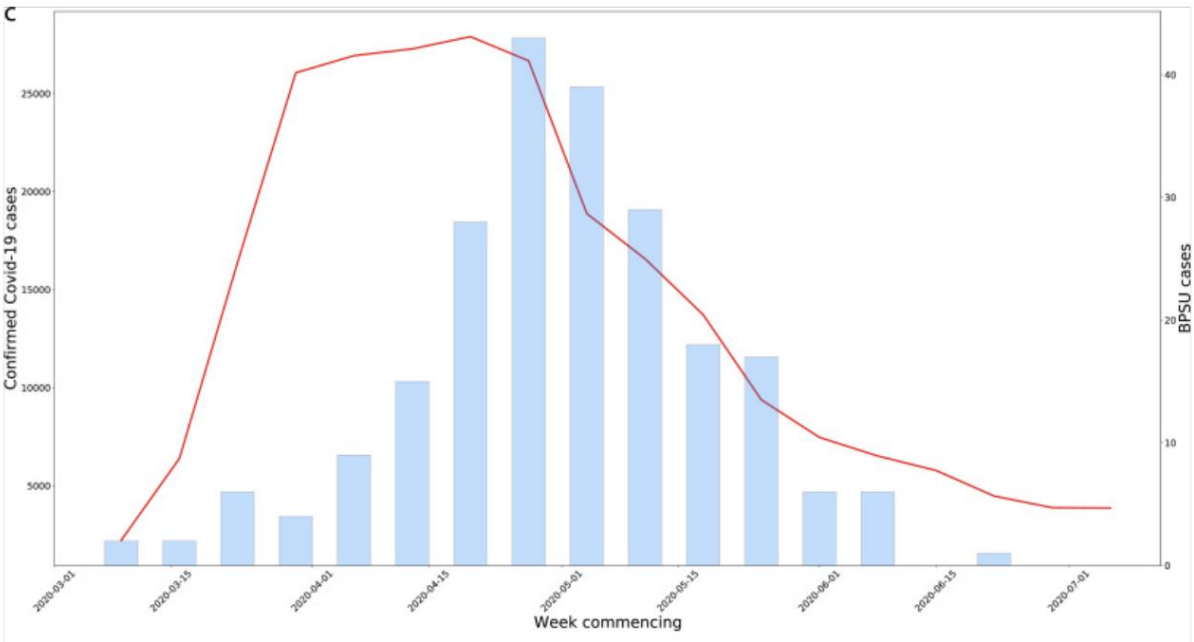

Figure 1-6 Temporal distribution of COVID-19 hospitalisations and MIS-C cases in the UK.

This figure is from Flood et al.[208]. The bar chart represents the number of cases of MIS-C, indicated by the y-axis on the right. The red line illustrates the number of COVID-19 hospitalisations indicated by the y-axis on the left.

Children most commonly present with fever, rash, GI symptoms and conjunctivitis[199,209,210]. The majority of children with MIS-C are SARS-CoV-2 seropositive but PCR negative[199,209,210]. Characteristic laboratory findings include raised neutrophils, CRP, procalcitonin (PCT), ferritin and D-dimer with low levels of haemoglobin (Hb), lymphocytes and albumin[199,209,210]. Cardiac markers, including troponin and brain natriuretic peptide (BNP), are elevated in those with cardiac involvement[199,209,211]. MIS-C is associated with a number of significant complications including cardiac involvement[199,209,212], neurological complications[199,213] and systemic thrombosis[202]. More than half of the patients have abnormal echocardiogram (ECHO) findings, with reduced left ventricular ejection fraction reported in up to 60%, and coronary artery aneurysms (CAAs) in 8-24%[199,209,212].

Children with MIS-C can deteriorate rapidly, developing shock and multi-organ dysfunction. Around 70% of patients require intensive care support, 50-60% require inotropic support, 20-30% necessitate invasive ventilation and 4% need extracorporeal membrane oxygenation (ECMO)[199,209]. Reassuringly, patients with MIS-C recover quickly with a relatively short duration of hospital stay (mean length of stay 8 days[199]) and a low mortality rate of approximately 1.5-2%[199,209].

Management of MIS-C involves a multidisciplinary approach focussed on providing supportive care, treating infection and measures to reduce inflammation and prevent thrombotic events. Due to the emergent nature of MIS-C, treatment regimens were extrapolated from similar inflammatory conditions to include intravenous immunoglobulin (IVIG), corticosteroids, and biological therapies (anti-IL6, anti-IL1 and anti-TNFα) and varied across different regions, based on local expertise and resources available at the time[211,214,215,215,216]. Patients are routinely followed-up with regular clinical reviews and investigations, including blood tests, ECHO, and neurological assessments, to detect any potential long-term sequelae.

1.5.1.1 Knowledge gaps in MIS-C clinical characteristics and pathogenesis at the beginning of this PhD

During the early stages of my research, MIS-C emerged as a novel clinical entity. Its sudden emergence presented a unique opportunity to investigate and address the significant knowledge gaps that existed across all aspects of the disease. Studies were needed to provide greater understanding of the clinical characteristics of MIS-C, diagnostic approaches, treatment options, and long-term outcomes. Additionally, the underlying pathogenesis and contributing factors, such as the innate and adaptive

immune responses, genetics, and other potential risk factors, required further exploration. I will now focus on some of these specific areas that I aimed to address during my PhD.

Large multi-centre MIS-C cohort description

The incidence of MIS-C is relatively low and while cases were being reported from various countries, there was a lack of multi-centre, international large datasets describing the full spectrum of disease. Obtaining comprehensive data on demographic and clinical features, laboratory findings, treatment approaches, disease severity and outcomes is vital for advancing the understanding of MIS-C. Furthermore, it would allow assessment of the disease burden, identification of risk factors and improved diagnosis and prognosis.

Diagnosis of MIS-C

The development of novel diagnostics became paramount for tackling the challenges presented by overlapping features between MIS-C and other diseases. The design of diagnostic scores or clinical decision-making tools offered an expedited approach for aiding the diagnosis of MIS-C. These tools often use a combination of clinical and routinely collected laboratory markers, offering an accessible and cost-effective means of facilitating timely decision making and prompt initiation of appropriate treatment.

I chose to focus on the development of a clinical diagnostic score for MIS-C as this offered a valuable alternative to biomarker-based diagnostic methods. While biomarker-based diagnostics provide greater specificity and accuracy, they often require significant time and resources for their discovery and implementation into diagnostic tests. In contrast, following rigorous validation, diagnostic scores have the advantage of being readily applicable in various healthcare settings, including in Middle- and Low-Income economies, where access to specialist tests may be limited.

Longitudinal trends of paediatric SARS-CoV-2 serology

The diagnostic landscape for MIS-C is dynamic, and along with exploring alternative diagnostic avenues, it is crucial to acknowledge that the diagnostic utility of SARS-CoV-2 serology testing for MIS-C may diminish over time. Recognising the need for a comprehensive understanding of this evolution, I decided to examine the longitudinal trends of paediatric SARS-CoV-2 serology.

MIS-C prognostic/severity markers

Patients with MIS-C can deteriorate rapidly and the identification of those at high risk of severe disease or cardiac complications can be challenging. Therefore, my research focussed on the identification of clinical and laboratory markers associated with severity and cardiac outcomes, and subsequent design of a severity score for classification of disease severity and identification of patients at risk of severe disease. This would enable risk stratification and help guide allocation of resources and tailored management, leading to improved patient outcomes. Not only that, standardised and validated severity scores can also be of value within research, for instance, as outcome measures for clinical studies or for advancing the understanding of MIS-C pathophysiology, through comparison of biological mechanisms across severity groups.

MIS-C pathogenesis and immunopathology

There was an urgent need to understand the pathogenesis and underlying mechanisms driving immune dysregulation and systemic inflammation, to help identify risk factors, potential diagnostic biomarkers, and therapeutic targets. The occurrence of MIS-C, several weeks after exposure to SARS-CoV-2, strongly indicated the involvement of the adaptive immune response in its pathogenesis. My research focussed on investigating the role of antibodies and T cells in the pathogenesis of MIS-C and their contribution to the development and progression of the disease.

Investigating the role of antibodies was a crucial area of research, particularly given the implications on vaccine design and delivery strategies. This included the examination of antibody profiles and levels, to determine if specific antibody responses were associated with the development or severity of MIS-C. Additionally, functional, and mechanistic studies were needed to help unravel underlying disease mechanisms.

T cell immunity is another important component of the adaptive immune response that warranted investigation. Characterising the T cell response, including the distribution, antigen specificity and functionality of T cell subsets could provide valuable insights into the disease mechanisms underlying MIS-C. In addition, studying these aspects of T cell immunity throughout the course of MIS-C, from acute illness to convalescence, could provide further insights into disease progression and severity.

Investigating the role of antibodies and T cells contributes to the broader research efforts investigating multiple factors such as genetics, innate immunity and environmental, which may be involved in MIS-

C pathogenesis and immunopathology; ultimately leading to better understanding of MIS-C and improved patient outcomes through enhanced strategies for prevention, diagnosis, and management.

1.5.1.2 Current understanding of MIS-C

Significant progress has been made in the understanding of various aspects of MIS-C. Studies conducted on large cohorts have provided detailed clinical descriptions of MIS-C, advancements have been made in diagnostics, prognostication, and therapeutics as well as substantial developments in the understanding of underlying aetiology and immunopathology. This section aims to highlight the progress made in the knowledge of MIS-C during the course of my PhD.

MIS-C clinical features and risk factors

The studies conducted in larger multi-centred cohorts have been consistent with the early reports of MIS-C, providing validation and confirmation of the initial findings. They also revealed additional insights and nuances of the disease, expanding our understanding of MIS-C. While the majority of children commonly present with rash, GI symptoms, conjunctivitis, and cardiac involvement, studies have reported a diverse range of manifestations. For example the cutaneous changes in MIS-C can be either local or generalised with a wide range of rashes including maculopapular, urticarial, vesicular, and diffuse erythematous[217–219]. GI symptoms typically include abdominal pain and diarrhoea, however more severe manifestations such as enteritis, appendicitis and pancreatitis have been noted[220,221]. Left ventricular dysfunction and coronary artery aneurysms are the most frequently reported cardiac findings, however, additional abnormalities including pericarditis, myocarditis, valvular involvement, and arrhythmias have been described[212,222]. While neurological involvement is uncommon, it can present with a range of symptoms such as an altered mental status, headache, seizures, cranial nerve palsies, peripheral neuropathy, and acute transverse myelitis[213,223–226]. It is important to note that cases of multisystem inflammation associated with SARS-CoV-2 have also been reported in neonates[227–230] and adults[231–234] (described later), expanding the spectrum of the condition across different age groups.

The initial reports of MIS-C indicated a number of potential risk factors which have been confirmed in subsequent studies, reinforcing their significance in the development of MIS-C. Furthermore, the subsequent studies provide a more comprehensive understanding, through in-depth analyses and quantification of the associated risks. Studies have consistently demonstrated increased risk of MIS-C in males compared to females and in those from Black and Hispanic ethnic backgrounds[197,235–237]. Pre-

existing conditions such as asthma, obesity and metabolic conditions have also been associated with increased risk[235,236,238]. Additionally, socio-economic factors, such as access to healthcare and inequities in resource allocation may contribute to increased vulnerability to MIS-C in certain populations[236,239,240].

Several studies have investigated the influence of host genetics in the development of MIS-C, revealing significant associations with immune-related genes. Rare genetic variants in immune-related genes, such as TLR3, TLR6, IFNB1, and IFNA6, have been associated with MIS-C and may contribute to early disease onset and treatment resistance[241]. Moreover, variants in the Suppressor of Cytokine Signalling 1 (SOCS1) gene have been shown to enhance IFN signalling and immune cell activation, which are likely to contribute to the hyperinflammation observed in MIS-C[242,243]. Genetic defects in the X-linked inhibitor of apoptosis protein (XIAP), and cytochrome b-245 beta chain (CYBB), which is involved in generation of reactive oxygen species, have also been described in MIS-C, suggesting their potential role in the dysregulated immune response[247]. In addition, patients with MIS-C were found to have variants in genes encoding the 2′-5′-oligoadenylate synthetase (OAS)–ribonuclease L (RNase L) viral RNA sensing pathway, which can amplify the inflammatory response in myeloid cells[244]. These findings provide valuable insights into the genetic contributions to MIS-C and possible underlying mechanisms and therapeutic targets which can be explored in future studies.

To summarise, these findings represent a selection of important studies which have significantly contributed to the understanding of MIS-C. They have provided insights into the diverse clinical features, risk factors and genetic factors associated with MIS-C that are guiding ongoing research in the field.

Diagnosis of MIS-C

Researchers have developed scoring systems and prediction models using different methodologies to help differentiate MIS-C from similar conditions like KD, TSS, and COVID-19. Sobh et al. constructed a prediction model using the following four variables identified from multivariate regression analyses: abdominal pain, vomiting, cervical lymphadenopathy, and platelet count, which had moderate accuracy (area under the curve (AUC) 0.7) for discriminating MIS-C from KD[245]. Similarly, Kostik et al. designed a score with five variables identified from regression analyses, including: age, CRP, D-dimer, platelet count and GI involvement, which could discriminate MIS-C from KD with 87.5% sensitivity and 89.1% specificity[246]. Another study conducted by Clark et al. identified predictors from regression analyses and used a backward selection model to limit the variables to hypotension and/or fluid

resuscitation, abdominal pain, rash, and serum sodium levels, which demonstrated excellent discrimination (concordance index 0.91) between MIS-C and febrile controls[247]. Godfred Cato et al. used the Least Absolute Shrinkage and Selection Operator (LASSO) method[248] to develop highly accurate (AUC 0.87-0.97) diagnostic scores incorporating comorbidities, clinical features, laboratory findings, and echocardiogram results for differentiating MIS-C from TSS, KD, and COVID-19[249]. Additionally, Lam et al. employed machine learning algorithms to create a clinical decision support tool for distinguishing MIS-C from other febrile conditions. By considering age, clinical markers, and laboratory markers, their tool exhibited exceptional accuracy with AUC values of 0.98-0.99[250,251]. Indeed, all these diagnostic scoring systems have shown high accuracy in guiding clinical decision-making for the diagnosis of MIS-C. Implementation of these scores following validation, could potentially lead to improved patient outcome through timely and appropriate management.

Researchers have identified biomarkers, immune and gene expression signatures and developed novel tools for differentiating MIS-C from other conditions. Raised levels of serum chemokine ligand nine (CXCL9), which is induced by IFNγ, could differentiate MIS-C from COVID-19 and febrile controls[252]. Soluble Triggering Receptor Expressed on Myeloid Cells-1 (sTREM-1), an inflammatory biomarker associated with immune cell activation and increased pro-inflammatory cytokines, has been shown to accurately (AUC 0.87) differentiate MIS-C from COVID-19[253]. Rajamanickam et al. identified unique immune profiles associated with MIS-C, characterised by variations in T cell, B cell, DCs and monocyte subsets, which can distinguish MIS-C from COVID-19 and other infectious diseases[254]. The use of the serum delta neutrophil index (DNI), which reflects the fraction of immature granulocytes, has been proposed as an easily accessible marker for diagnosing MIS-C[255]. Next-generation sequencing of nucleic acids (whole blood and saliva RNA and DNA) has allowed identification of distinct gene expression signatures associated with cellular injury and cellular death in MIS-C and COVID-19 and revealed enrichment of pyroptosis-related genes, and downregulation of T cell-associated pathways which were specific to MIS-C[256]. Moreover, gene expression analyses have identified a 5-gene signature (HSPBAP1, VPS37C, TGFB1, MX2, and TRBV11-2), which has been validated on qRT-PCR and shown to have high diagnostic accuracy (AUC 0.93) for distinguishing MIS-C from febrile controls, including Kawasaki disease, bacterial infections, and viral infections[257]. In addition to biomarker discovery, researchers have also focussed on the development of diagnostic tools for instance, Maltz-Matyschsyk et al. designed a grating-coupled fluorescence plasmonic (GCFP) biosensor chip for identification of biomarkers in saliva and serum samples, which has shown promise for diagnosing MIS-C[258].

MIS-C prognostic/severity markers

Several studies have investigated features associated with MIS-C disease severity, particularly in terms of shock, the level of organ support, requirement for invasive ventilation, inotropic support, paediatric intensive care unit (PICU) admission, length of PICU admission and death. Demographic features such as older age[259–262], male sex[263,264] and Black ethnicity[265] have been associated with severe MIS-C. Presenting clinical features including dyspnoea, abdominal pain and conjunctivitis were also more frequently present in children with severe disease[264–267]. In terms of laboratory markers, significantly elevated CRP[259,265,268–270], white blood cells (WBC)[259,270,271], ferritin[259,260,262,264–266,270,271], lactate[271], D-dimer[259,265,266,270,271], creatine kinase[271], troponin[265,272], pro-BNP[265,270,272,273], fibrinogen[266,270] and markedly reduced lymphocyte count[265,269,272], platelets[260,265,270,274], haemoglobin[272], albumin[272,275] and Vitamin D[267,275] were observed in severe disease compared to mild/moderate disease.

Several studies have combined features associated with disease severity in MIS-C, to develop severity prediction scores using admission or baseline values. Snipaitene et al. found that a composite score consisting of platelet count, mean platelet volume, plateletcrit, and platelet distribution width was able to accurately predict MIS-C severity (AUC 0.90), demonstrating its potential as a quick and reliable tool in clinical practice[270]. Similarly, Savorgnan et al. identified a combination of elevated creatinine, international normalised ratio (INR), pro-BNP, WBC, ferritin, respiratory rate, and decreased albumin could discriminate between mild and severe MIS-C with an AUC of 0.92[276]. In another study, Cetin et al. found that lymphocyte count, pro-BNP, albumin, ferritin, troponin and D-dimer, could be used to identify patients at high risk of developing severe MIS-C[261]. These findings highlight the potential of combining features associated with severe disease in MIS-C to develop high-performing severity prediction scores, which would be invaluable for risk stratification and informing clinical decision making.

Some studies have also evaluated laboratory markers associated with poor cardiac outcomes. Raised levels of CRP, BNP and low blood pH were associated with reduced cardiac function[266]. Moreover, raised cardiac markers such as pro-BNP and troponin, showed potential for early detection of cardiac involvement and predicting morbidity and mortality in MIS-C[277]. Abrams et al. showed that male patients, and those presenting with mucocutaneous changes or conjunctival injection, had higher likelihood of exhibiting coronary artery abnormalities[265]. Furthermore, severe MIS-C with myocarditis was characterised by elevated levels of pro-angiogenesis cytokines, chemokines, and a unique

monocyte and dendritic cell gene signature related to sustained NF-κB activity and TNFα signaling[278]. These findings provide insights into the underlying mechanisms of myocardial involvement in MIS-C and can be used to identify patients at risk of cardiac complications.

MIS-C pathogenesis and immunopathology

MIS-C is believed to be a post-infectious phenomenon occurring following exposure to SARS-CoV-2, although a causal link has not yet been established. The disease timeline suggests that an aberrant acquired immune response may be driving the pathogenesis[279], however, there are suggestions that innate immunity may also play a role[280–282]. Moreover, the similarities in clinical, laboratory and immunological features between MIS-C, KD, and COVID-19 hyperinflammation, indicate potentially overlapping disease mechanisms. This section will highlight some of the key hypotheses regarding the pathogenesis of MIS-C, including dysregulated innate immune response, antibody-mediated disease, immune complex formation, involvement of superantigens and persistent antigenaemia.

Innate immunity:

Various aspects of the innate immune response appear to be dysregulated in MIS-C. This includes increased activation of neutrophils and monocytes[280,283], as well as reduced expression of surrogate markers of antigen presentation (HLA-DR, CD86) in monocytes and dendritic cells[280,284]. Additionally, neutrophil extracellular traps (NETs), which are web-like structures composed of DNA and antimicrobial proteins released by neutrophils, have been implicated in the immunopathogenesis of MIS-C. Increased formation of NETs has been observed in MIS-C patients, potentially contributing to vascular inflammation and endothelial dysfunction[285]. Rare genetic variants in TLRs have been associated with MIS-C[241], which may impact their ability to detect viral pathogens, potentially leading to dysregulated immune responses and increased susceptibility to MIS-C. In addition, alterations in type I and II interferon responses have been observed in MIS-C[278], and this along with genetic variants in INFA and INFB genes[241], suggests a possible role for a dysregulated IFN response leading to impaired antiviral immune responses, uncontrolled viral replication and excessive inflammation. Complement dysregulation has also been implicated in the pathogenesis of MIS-C. Abnormalities in the complement system, including high levels of soluble C5b-9, have been reported in MIS-C patients[281]. Complement dysregulation can contribute to excessive inflammation, tissue damage and thrombosis, which are characteristic features of MIS-C[281]. This dysregulation may lead to delayed or improper priming of adaptive immunity or regulatory immune responses[280,284].

Cytokine response:

The hyperinflammatory cytokine response in MIS-C is similar to the dysregulated cytokine response seen in COVID-19 hyperinflammation[286]. There is a significant increase in pro-inflammatory cytokines and chemokines involved in the recruitment and activation of immune cells which is countered by a rise in anti-inflammatory cytokines, including IFNγ, IL1β, IL6, IL8, IL17, TNFα, IL10 and IP10[280,281,283,287,288]. Uncontrolled cytokine release, with an imbalance between proinflammatory and anti-inflammatory cytokines, can contribute to widespread inflammation, tissue damage and myocardial dysfunction. TNFα, IL6, IL10, and CXCL10, in particular, have been associated with adverse outcomes and cardiac manifestations in MIS-C[289,290]. IL6 plays a role in inflammation and cardiac function. Previous research has demonstrated that increased levels of IL6 can impair cardiac contractility and function[291,292]. The cardiac depressant effect of IL6 may be a contributing factor to the development of myocardial dysfunction and cardiac manifestations observed in MIS-C.

Antibody-mediated disease:

Numerous antibody-mediated mechanisms have been investigated in the pathogenesis of MIS-C. Studies investigating the differences in the humoral response in COVID-19 and MIS-C found that while the antibody response in MIS-C and convalescent COVID-19 were similar, the levels of anti-SARS-CoV-2 IgG were higher in MIS-C and had better neutralising efficacy[172,283]. Moreover, Yonker et al. showed increased levels of SARS-CoV-2 S IgM, IgG, and IgA in MIS-C compared to COVID-19 and controls[293]. SARS-CoV-2 S IgM remained elevated despite the delayed onset of MIS-C, while SARS-CoV-2 S IgG and IgA levels increased over time, suggesting ongoing viral antigenic exposure and inflammation of the GI mucosa in children with MIS-C[293]. Furthermore, Bartsch et al. found that children with MIS-C had persistent and enhanced Fc receptor-binding antibodies, which selectively activated monocytes[294]. These findings provide insight into the potential role of antibodies in the pathogenesis of MIS-C.

Vella et al. investigated the plasmablast (PB) responses in paediatric COVID-19 and MIS-C patients and found raised PB levels in both cohorts[295]. The PB response to viral infection is expected to peak 1-2 weeks after infection, followed by a rapid decline, therefore the findings indicate a prolonged response in MIS-C, suggesting ongoing immune activation and antibody production, which may be contributing to the immunopathology[295]. Additionally, increased T-box transcription factor (Tbet) expression in PBs was seen in MIS-C[295]. T-bet expression in PB has been linked to extra-follicular responses, autoimmunity, and class-switching[296–298] and its higher expression suggests potential dysregulation of immune responses and the development of autoimmune reactions in MIS-C.

ADE has also been investigated in MIS-C, given its similarity to COVID-19 hyperinflammation and the elevated SARS-CoV-2 antibody titres observed in MIS-C compared to paediatric COVID-19 cases and healthy controls[293]. Consiglio et al. tested the hypothesis of ADE by assessing seasonal coronavirus antibody titres in healthy controls, KD, MIS-C and COVID-19[287]. Seasonal coronavirus IgG were present in all cohorts except MIS-C, suggesting that they may in fact have a protective role, though the number of patients in this study was small[287].

The presence of autoantibodies in children with MIS-C has been explored. Gruber et al. identified numerous IgG and IgA peptide autoantigen candidates, including anti-La and anti-Jo-1, which are associated with the autoimmune disease systemic lupus erythematosus (SLE)[283]. Consiglio et al. observed enrichment for autoantigens involved in lymphocyte activation processes, signalling phosphorylation, and cardiovascular development[287]. Ramaswamy et al. found that IgG from severe MIS-C patients bound cardiac microvascular endothelial cells[284]. While Pfeifer et al. detected autoantibodies against IL1Rα in more than half of their MIS-C cohort[299]. These findings suggest the presence of autoantibodies against endothelial, mucosal, and immune antigens in MIS-C. Nevertheless, further validation is required to determine their significance, as these findings are not consistent, and the presence of autoantibodies does not confirm a pathological role.

Immune complex formation:

The role of immune complexes in inducing inflammation through Fc-γ receptor and complement activation has been extensively studied in the pathogenesis of KD[300–303]. Genetic studies have also demonstrated an increased risk of KD in children with genetic variants related to adaptive immunity and immune complex clearance[304]. In MIS-C, the deposition of SARS-CoV-2 antigen immune complexes on cell surfaces has been proposed as a potential mechanism for multisystem inflammation[181], and a dysregulated complement response has also been implicated[281]. In addition, results from the mechanistic study by Boribong et al. suggested a role for anti-Spike IgA immune complexes in increasing the inflammatory response in MIS-C, through activation of neutrophils and augmented NET formation[285]. Further studies to expand the understanding of the role of immune complexes and complement activation in MIS-C are required.

Dysregulated T cell response:

MIS-C is associated with profound lymphopenia[199,209,210], which indicates that T cells are likely to be involved in its pathogenesis. Several mechanisms have been proposed including SARS-CoV-2 inducing apoptosis of lymphocytes, suppression of the thymus and redistribution of T lymphocytes from the circulation to tissues or organs[305].

Single-cell transcriptomic and cell surface-marker approaches have revealed distinct features of T cell responses in MIS-C. These include reduced levels of $CD4^+$, $CD8^+$, and γδ T cells, consistent with the lymphopenia described in the observational studies[280,287,295,306]. There was also evidence of high levels of $CD4^+$ and $CD8^+$ T cell proliferation[295], expansion of $CD4^+CCR7^+$ T cells and activated tissue-homing T cells, suggesting T cell activation and migration to specific tissues[287,295,306]. MIS-C patients displayed a higher proportion of activated naive T cells, γδ T cells and innate lymphocytes[280], as well as increased proportions of proliferating and chronically stimulated $CD4^+$ and $CD8^+$ T cells compared to children and adults with COVID-19[295]. Of note, patients requiring inotropic support, showed higher levels of activated vascular patrolling $CD8^+$ T cells[295], suggesting their potential role in MIS-C pathophysiology.

These findings reveal a dysregulated T cell response in MIS-C, which warrants further investigation to unravel the underlying mechanisms involved.

Superantigen-mediated disease:

Researchers have investigated the potential involvement of SARS-CoV-2 superantigens in driving the hyperinflammatory response in MIS-C, due to the similarities between MIS-C and TSS, a condition known to be mediated by superantigens[307]. Superantigens can activate a large number of T cells by binding to the T cell receptor (TCR) and HLA molecules, leading to excessive cytokine release and dysregulated immune responses[308]. Computational modelling has demonstrated that the SARS-CoV-2 S protein contains putative superantigen fragments[309–311]. Analysis of T cell repertoires from patients with COVID-19 hyperinflammation and MIS-C revealed a skewed TCR Vβ repertoire and enrichment of Vβ genes, which is consistent with superantigenic activity[309–311]. However, studies comparing the pro-inflammatory cytokine production in response to SARS-CoV-2 Spike antigens and known superantigens did not demonstrate intrinsic superantigen-like activity of the Spike protein[312,313], and analysis of T cell responses to SARS-CoV-2 peptides suggested that the expanded T

cell repertoire was not specific to SARS-CoV-2[313,314]. It is important to note that superantigen-mediated diseases typically exhibit a rapid onset following exposure to the toxin or trigger[307], however, the development of symptoms in MIS-C occurs several weeks after SARS-CoV-2 infection, suggesting that other immune mechanisms may be involved.

Persistent antigenaemia:

Researchers have shown presence of SARS-CoV-2 antigens in the circulation[293,315] and GI tract[293] of patients with MIS-C, which have persisted weeks after the initial infection. Moreover, Yonker et al. demonstrated that prolonged SARS-CoV-2 S antigen in the GI tract leads to release of zonulin[293], a biomarker of intestinal permeability[316], which they proposed is a potential mechanism for SARS-CoV-2 antigens trafficking into the circulation and causing hyperinflammation[293]. Contrastingly, Sigal et al. did not find persistence of SARS-CoV-2 S antigen in the plasma of a large cohort of patients with MIS-C, opposing their involvement in MIS-C disease pathogenesis[317].

Management of MIS-C

The management of MIS-C evolved over the course of the pandemic. In the UK, a Delphi process was initially used to reach a consensus and provide national clinical guidance[318]. Guidance was provided on investigations to aid diagnosis, exclude other important causes, determine severity and cardiac involvement. The importance of early (within 24 hours) case-by-case assessment for any patients with suspected MIS-C by a multidisciplinary team (MDT) was highlighted[318]. Core members of the MDT included general paediatricians, paediatric infectious disease specialists, paediatric rheumatologists, paediatric cardiologists, and paediatric intensivists[318]. The general principles of treatments focussed on management of the inflammatory response, prevention of thromboses, and providing organ support, with variation according to disease severity and presence of KD criteria. The use of either IVIG or glucocorticoids was recommended as first-line therapy, along with broad spectrum antibiotics, anti-platelet medications and anticoagulants; with addition of biologics (e.g. IL1 receptor antagonist, anti-IL6 and anti-TNFα) in refractory cases[318].

Since then, several observational studies have been performed, including three large multi-centred studies which all used propensity score analysis to examine outcomes in patients with MIS-C following different treatment regimes. Son et al. reported that treatment with IVIG plus glucocorticoids was associated with a lower risk of cardiovascular dysfunction and reduced need for additional treatment

compared to IVIG alone[319]. McArdle et al. and Channon-Wells et al. reported findings of the Best Available Treatment Study (BATS), which compared outcomes in patients treated with IVIG alone, glucocorticoids alone and IVIG plus glucocorticoids and found no significant differences in recovery among these approaches, however the group receiving combination therapy did have reduced need for additional treatment[320,321]. Similarly, Ouldali et al. demonstrated that a combination of IVIG plus glucocorticoid led to reduced duration of fever and decreased need for additional treatment and haemodynamic support[322]. These large observational studies provided valuable insights and preliminary evidence of the effectiveness of different treatment regimens in MIS-C. Findings from the SwissPed Randomised Evaluation of COVID-19 Therapy (RECOVERY) trial[323], showed that children with MIS-C, when treated with methylprednisolone, exhibited a comparable length of hospital stay and a reduced need for respiratory support compared to those treated with IVIG[323], suggesting that methylprednisolone could be a viable first-line therapy for MIS-C. Additionally, the outcomes of the UK RECOVERY[324] trial revealed that methylprednisolone treatment led to reduced hospital stay durations compared to standard care, while tocilizumab reduced hospital stay duration specifically in cases of inflammation resistant to initial treatment, albeit with an associated increase in inotrope use[325]. Interestingly, the study observed no reduction in hospital stay duration with IVIG and anakinra treatments[325]. Results from the US Multisystem Inflammatory Syndrome Therapies In Children (MISTIC)[326] trial are awaited.

Long-term implications

Long-term outcome data is not yet available, however, results from medium-term follow-up at 6-12 months are reassuring with very few sequelae reported. Markers of inflammation normalise within weeks to months following hospital discharge[327–329], although some abnormalities like elevated D-dimer and ferritin may persist in a subset of patients at 1 year[327]. In terms of cardiac outcomes, markers of cardiac injury (e.g. BNP, troponin) and ECHO abnormalities, such as ventricular dysfunction and coronary artery abnormalities generally resolved within 4-6 weeks, although rare cases of persistent cardiac abnormalities have been reported[327–332]. Two small studies showed 17% (2/23) and 50% (10/20) of patients had late gadolinium enhancement on cardiac magnetic resonance imaging (CMRI) performed at 6 months, indicating myocardial scarring[331,332]. Gastrointestinal symptoms and liver enzyme abnormalities resolved by 6 months in most cases (87%)[329]. Although mild neurological abnormalities were detected on examination in 39% of patients at 6 months, there was minimal functional impairment[329]. Physical functioning and emotional lability showed improvement by 6 months and the majority of children returned to school[329].

1.5.2 COVID-19 vaccine-induced myocarditis

In April 2021, a causal association was made between COVID-19 vaccines and myocarditis after several reports of this adverse event in Israel, Europe and the US[333–337]. Myocarditis is a known rare side effect of some vaccines, including influenza[338] and smallpox[339]. COVID-19 vaccine-induced myocarditis gained significant attention due to the large-scale vaccination campaigns and the higher number of reported cases in male adolescents and young adults, following the second dose of the mRNA-based vaccines BNT162b2 (Pfizer-BioNTech) and mRNA-1273 (Moderna)[333–337].

1.5.2.1 Knowledge gaps in COVID-19 vaccine-induced myocarditis at the beginning of this PhD

As a novel condition, the understanding of COVID-19 vaccine-induced myocarditis was limited and required comprehensive research to gain better understanding of its epidemiology, clinical presentation and diagnosis, risk factors, management, underlying pathogenesis, and long-term outcomes. My research focussed on investigating the role of antibodies in the development of COVID-19 vaccine-induced myocarditis and its potential implications for vaccination strategies.

1.5.2.2 Current understanding of COVID-19 vaccine-induced myocarditis

As COVID-19 vaccination campaigns progressed, cases of vaccine-induced myocarditis were increasingly reported and the understanding of the disease has improved with time. Indeed, the rates of COVID-19 vaccine-induced myocarditis were found to vary with sex, age, vaccine type and dose, in line with the early reports[340–343].

Male adolescents and young adults (12-30 year olds) of White or Hispanic ethnicity had the highest risk[340,343], following the second dose of mRNA COVID-19 vaccination[340,343], with an estimated incidence as high as 1.4 per 10 000[343]. The incidence of myocarditis was higher after the mRNA-1273 (Moderna) vaccine compared to the BNT162b2 (Pfizer-BioNTech) vaccine[343], with a slight increase in risk if the second dose was administered less than 30 days after the first[343].

Patients with COVID-19 vaccine-induced myocarditis typically presented 2-4 days following vaccination with chest pain, dyspnoea, fever and myalgia[340,343–345]. Laboratory investigations showed raised cardiac troponin[340,341,344,346] and negative serology and PCR for common causes of viral myocarditis[340,346]. The most common abnormalities on cardiac investigations were ST elevation on

electrocardiogram (ECG), reduced left ventricular ejection fraction on ECHO and findings consistent with myocarditis on CMRI[340,344]. Although almost all individuals were hospitalised, they generally required only supportive treatment, most commonly with non-steroidal anti-inflammatory medication[340,343]. IVIG, glucocorticoids, anti-arrhythmic and heart-failure medication were required in a small proportion. Organ support with inotropes or invasive ventilation was rare[340]. Most patients recovered quickly[340,343] and had a short duration of hospital stay (mean 5.8 days[344]).

Long-term outcome data is awaited, however small studies with short-term (90 days) follow-up data post-diagnosis have provided some insights, up to half of the patients reported ongoing symptoms[343] and CMRI showed improved but persistent late gadolinium enhancement in 80% of the cases[347].

Although several mechanisms of diseases have been investigated, the pathogenesis of COVID-19 vaccine-induced myocarditis remains unknown. It is likely that multiple factors influencing the immune response play a role, including genetic susceptibility, sex and age. Molecular mimicry can result in antibodies against the SARS-CoV-2 S protein encoded by the mRNA vaccine, to cross-react with α-myosin[348–351] and cause damage to the cardiac tissue. However, the timing of the response may be considered a little early for an antibody-mediated disease process, moreover, viral vector vaccines also produce Spike protein, but have not been implicated. The T cell response in patients with COVID-19 vaccine-induced myocarditis was studied by Yonker et al. and no differences were observed between patients and asymptomatic vaccinated controls[352]. Of note, they did report a significantly higher level of unbound Spike protein in the plasma of myocarditis patients, which may play a role in disease pathogenesis[352]. An alternative hypothesis is a delayed hypersensitivity reaction, which is supported by evidence of eosinophilic myocarditis in some COVID-19 vaccine-induced myocarditis patients[353–355]. Finally, sex hormone variations are known to impact the immune response, for instance, testosterone can have an immunosuppressive effect on the immune response[356], which may contribute to increased risk in males.

Health authorities and experts continue to recommend COVID-19 vaccination for eligible individuals, as the benefits of vaccination in preventing COVID-19 and its complications outweigh the potential risks. For example, the risk of myocarditis following SARS-CoV-2 infection was found to be seven times greater than the risk of myocarditis following COVID-19 vaccination[357]. Some countries, including the UK, have chosen the BNT162b2 (Pfizer-BioNTech) vaccine over mRNA-1273 (Moderna) in children and young adults[358–360] to help reduce the risk of vaccine-induced myocarditis in the susceptible age group.

1.5.3 Other SARS-CoV-2 associated diseases

In addition to COVID-19, MIS-C and COVID-19 vaccine-induced myocarditis, which are the primary focus of my research, it is important to acknowledge the existence of other SARS-CoV-2 related conditions, such as Multisystem Inflammatory Syndrome in Adults (MIS-A), COVID-19 vaccine-induced MIS-C, and Long COVID. These conditions highlight the spectrum of post-SARS-CoV-2 antigen exposure sequelae and are areas of research interest within the broader context of the COVID-19 pandemic (Figure 1-7).

1.5.3.1 MIS-A

MIS-A is a rare but severe inflammatory syndrome observed in adults approximately 2-5 weeks following exposure to SARS-CoV-2, which shares many similarities with MIS-C. It predominately affects young males (19-34 years)[233,234], as well as individuals from Black or Hispanic ethnic groups[234], and has a higher mortality rate than MIS-C, at 5-7%[233,234] compared to 1.5-2%[199,209]. The diagnosis and management of MIS-A share principles with MIS-C[234,361]. The underlying mechanism of MIS-A may be similar to MIS-C with additional factors influencing the disease process such as age, comorbidities and medication.

1.5.3.2 Vaccine-induced MIS-C

Vaccine-induced MIS-C is believed to be an immune-mediated response triggered by the Spike protein encoded by mRNA COVID-19 vaccines[362,363]. Vaccine-induced MIS-C primarily affects individuals aged 12-20 years and has a slight male preponderance. The reported incidence is extremely low, ranging from 1.0 to 2.9 cases per million vaccinated individuals within this age group[362,363]. It is important to note that COVID-19 vaccination has significant benefits, including a reduced incidence of post-SARS-CoV-2 MIS-C[364,365]. Therefore, considering the minimal likelihood of vaccine-induced MIS-C and the potential benefits of vaccination, it remains highly recommended for eligible children and young adults.

1.5.3.3 Long COVID

Long COVID, refers to persistent symptoms experienced by approximately 10% of children and adults after acute COVID-19[366]. Symptoms can involve multiple systems and can last for months to years. The exact mechanisms are unclear, but persistent viral activity, inflammation, and autoantibodies

have been suggested[366]. The diagnosis is based on clinical assessment and management includes tailored approaches such as rehabilitation and mental health support[366–368].

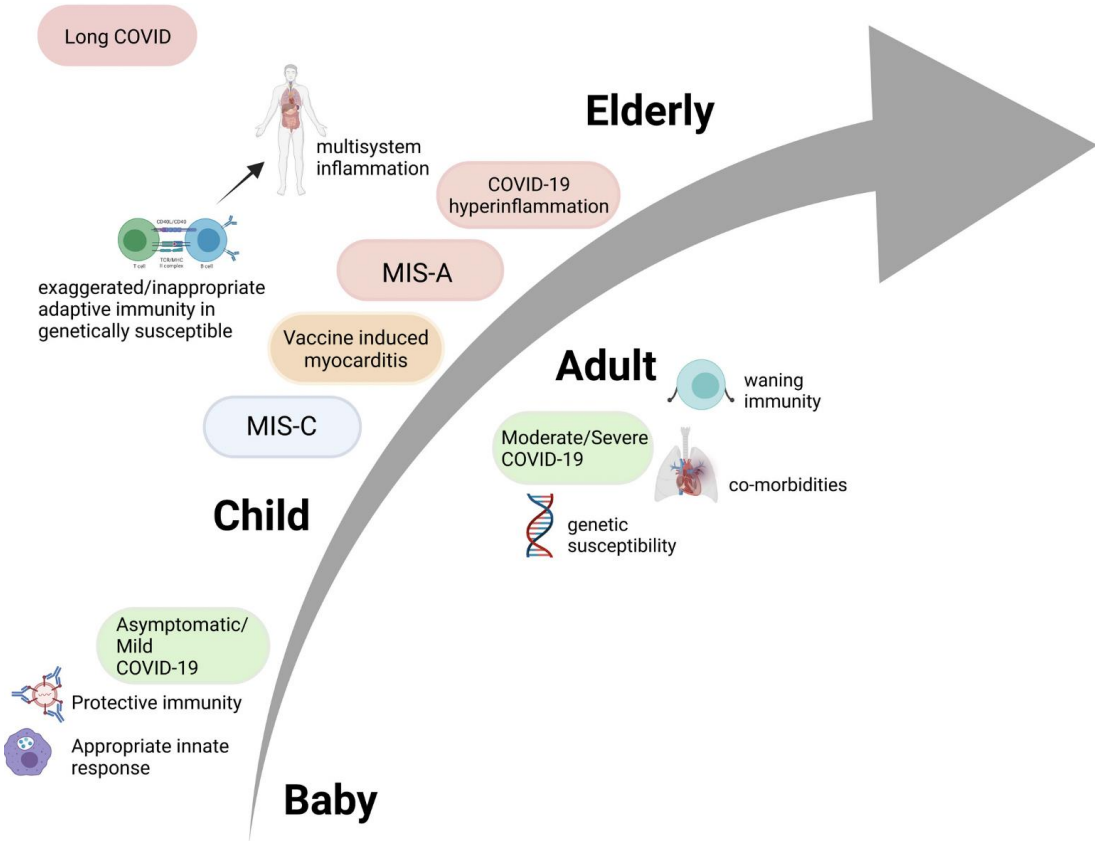

Figure 1-7 SARS-CoV-2 associated disease and underlying factors across different age groups.

This figure is from Patel et al.[286] *COVID-19 = Coronavirus Disease 2019, MIS-A = Multisystem Inflammatory Syndrome in Adults, MIS-C = Multisystem Inflammatory Syndrome in Children.*

1.6 Summary

This chapter provides a comprehensive background on viral infections and the host immune response. It also introduces SARS-CoV-2 infection, the COVID-19 pandemic and associated conditions which have emerged, including MIS-C and COVID-19 vaccine-induced myocarditis. The knowledge gaps present at the beginning of this PhD have been highlighted. By addressing some of these gaps, the research I conducted during this PhD aims to contribute to a deeper understanding of various aspects of SARS-CoV-2 associated diseases. In the subsequent chapters, this thesis will describe the specific approaches employed to tackle key research questions and will outline the contributions and implications of the findings within the broader context of the field.

Chapter 2: Project overview

During my PhD, I aimed to address some of the key knowledge gaps related to SARS-CoV-2 associated diseases in children, which are described in detail in Chapter 1. This broadly included studying age-related differences in COVID-19 severity, investigating the role of antibodies in COVID-19 and MIS-C disease severity, exploring the role of antibodies in COVID-19 vaccine-induced myocarditis and assessing the clinical characteristics and immunopathology of MIS-C. I integrated a range of approaches, including testing antibody profiles, analysing large clinical datasets, developing diagnostic and severity scoring systems, and performing mechanistic antibody and functional T cell experiments. This multidimensional approach allowed for a comprehensive understanding of the clinical, immunological, and pathogenic aspects of paediatric COVID-19, MIS-C and COVID-19 vaccine-induced myocarditis.

2.1 Hypotheses

The overarching hypotheses are:

1) Antibody dependent enhancement contributes to the age-related differences observed in COVID-19 disease severity.
2) MIS-C and COVID-19 vaccine-induced myocarditis are caused by an aberrant adaptive immune response to SARS-CoV-2 antigens.

2.2 Aims

Aim 1: To ascertain the role of cross-reactive seasonal coronavirus antibodies and SARS-CoV-2 specific antibodies in SARS-CoV-2 associated diseases (Chapter 4).

Hypotheses for Aim 1:

1a) Age-related differences in COVID-19 severity arise from antibody dependent enhancement caused by cross-reactive seasonal coronavirus antibodies.

1b) Cross-reactive seasonal coronavirus antibodies are associated with disease severity in paediatric COVID-19 and MIS-C.

1c) SARS-CoV-2 specific antibodies are associated with disease severity in paediatric COVID-19 and MIS-C.

Aim 2: To differentiate MIS-C from other infectious and inflammatory diseases through the comprehensive analysis of clinical features and laboratory parameters and develop a diagnostic score for MIS-C (Chapter 5).

Hypotheses for Aim 2:

2a) A diagnostic score based on clinical and laboratory variables can effectively differentiate MIS-C from other febrile conditions.

2b) The diagnostic utility of SARS-CoV-2 serology testing for MIS-C will diminish over time.

Aim 3: To comprehensively characterise the clinical and laboratory features of MIS-C and to develop a disease severity score for MIS-C using physiological and laboratory markers (Chapter 6).

Hypothesis for Aim 3:

3a) Existing and novel severity scoring systems based on physiological and laboratory markers will effectively identify MIS-C patients at risk of severe disease and cardiac complications.

Aim 4: To determine the role of SARS-CoV-2 specific antibodies in the pathogenesis of MIS-C and COVID-19 vaccine-induced myocarditis (Chapter 7).

Hypothesis for Aim 4:

4a) The cardiac pathology in MIS-C and COVID-19 vaccine-induced myocarditis is caused by an aberrant antibody immune response.

Aim 5: To understand the T cell response in MIS-C compared to febrile and healthy controls through functional studies (Chapter 8).

Hypothesis for aim 5:

5a) A dysregulated T cell response plays a significant role in the immunopathology of MIS-C.

Chapter 3: Methodology

This chapter presents an overview of the clinical studies included in this thesis and details of the laboratory methods employed in each results chapter.

3.1 Clinical cohorts

The historical and ongoing research studies from which I have used clinical data and biological samples will be described in this section. For all of the studies detailed below, recruited individuals gave written consent and assent (if applicable), with the exception of the Best Available Treatment Study (BATS), where consent was not required for use of anonymised routinely collected hospital data. Where samples from a historical study have been used, consent had been obtained for use in future ethically approved studies. My work is predominantly based on data and samples from the three studies described in sections 3.1.1, 3.1.2 and 3.1.3. Additional data and samples from patients and controls were used from the ten studies/bio-registries briefly outlined in section 3.1.4. The studies and samples used are summarised in Table 3-1Table 3-1. The clinical characteristics and demographic details of the cohorts, along with details of the samples used will be described in detail in Chapters 4-8.

Table 3-1 Summary of the studies, clinical cohorts and samples used for the work in this thesis.

Name of study	Study Dates	Clinical cohort	Samples/data used	Reference to Chapter in thesis
Diagnosis and Management of Febrile Illness using RNA Personalised Molecular Signature Diagnosis Study (DIAMONDS)	2020-ongoing	Children (< 18 years): MIS-C, Bacterial, Viral, KD, Inflammatory disease, healthy paediatric controls and healthy COVID-19 vaccinated adult controls (greater than (>) 21 years)	Clinical data Serum Whole blood	Chapters 5,7,8
Best Available Treatment Study (BATS)	2020-ongoing	Children (< 18 years) with MIS-C	Clinical data	Chapter 6
Delirium and Population Health Informatics Cohort (DELPHIC) COVID-19 Sub-study	2020-2022	Adults > 70 years: healthy, asymptomatic COVID-19, symptomatic COVID-19	Clinical data Serum	Chapter 4

Table 3-1 continued.

Name of study	Study Dates	Clinical cohort	Samples/data used	Reference to Chapter in thesis
Personalised Risk assessment in Febrile illness to Optimise Real-life Management (PERFORM)	2016-2019	Children (< 18 years): MIS-C, Bacterial, Viral, KD, Inflammatory disease and healthy paediatric controls	RNA-seq data	Chapter 8
European Union Childhood Life-threatening Infectious Disease Study (EUCLIDS)	2012-2015	Pre-COVID-19 children (< 18 years): Bacterial, Viral, KD, Inflammatory disease, healthy paediatric controls	Clinical data RNA-seq data Serum	Chapters 4,8
Genetic determinants of Kawasaki disease for susceptibility and outcome	2013-2022	Pre-COVID-19 children (< 18 years): KD	Clinical data Serum	Chapter 4
Imperial Health Knowledge Bank (IHKB)	2020-ongoing	Adults (> 21 years) with COVID-19 pneumonitis	Clinical data Serum	Chapter 4
Diagnosing and predicting risk in children with SARS-CoV-2 related illness study	2021-2022	Children (< 19 years): COVID-19 vaccine-induced myocarditis	Clinical data Serum	Chapter 7
Interferon Gamma Release Assay in Diagnostic evaluation of Active TB (IDEA) study	2011-2013	Pre-COVID-19 pandemic middle aged adults (30-70 years)	Serum	Chapter 4
The Graz Endomyocardial Biopsy Registry	2019-ongoing	Adults with myocarditis/inflammatory cardiomyopathy	Clinical data Serum	Chapter 7
Diagnosis and Risk Stratification in Myocarditis Study	2018-2020	Adults with myocarditis/inflammatory cardiomyopathy	Clinical data Serum	Chapter 7
The Structure and Functional Characterisation of Human Hearts Study	2016-2020	Healthy adults (> 18 years)	Clinical data Cardiac tissue	Chapter 7
Fever in children	2014-2017	Febrile children (< 18 years)	Clinical data Plasma	Chapter 4

3.1.1 Diagnosis and Management of Febrile Illness using RNA Personalised Molecular Signature Diagnosis Study (DIAMONDS)

DIAMONDS is a European Union (EU), Horizon 2020 funded, multi-centre study that aims to use individual ribonucleic acid (RNA) signatures detected in blood for rapid diagnosis of serious infectious and inflammatory diseases (London, Dulwich Research Ethics Committee: 20/HRA/1714)[369]. The DIAMONDS consortium includes 28 sites in 11 European countries and 3 non-European sites (The Gambia, Nepal, Taiwan) (Figure 3-1).

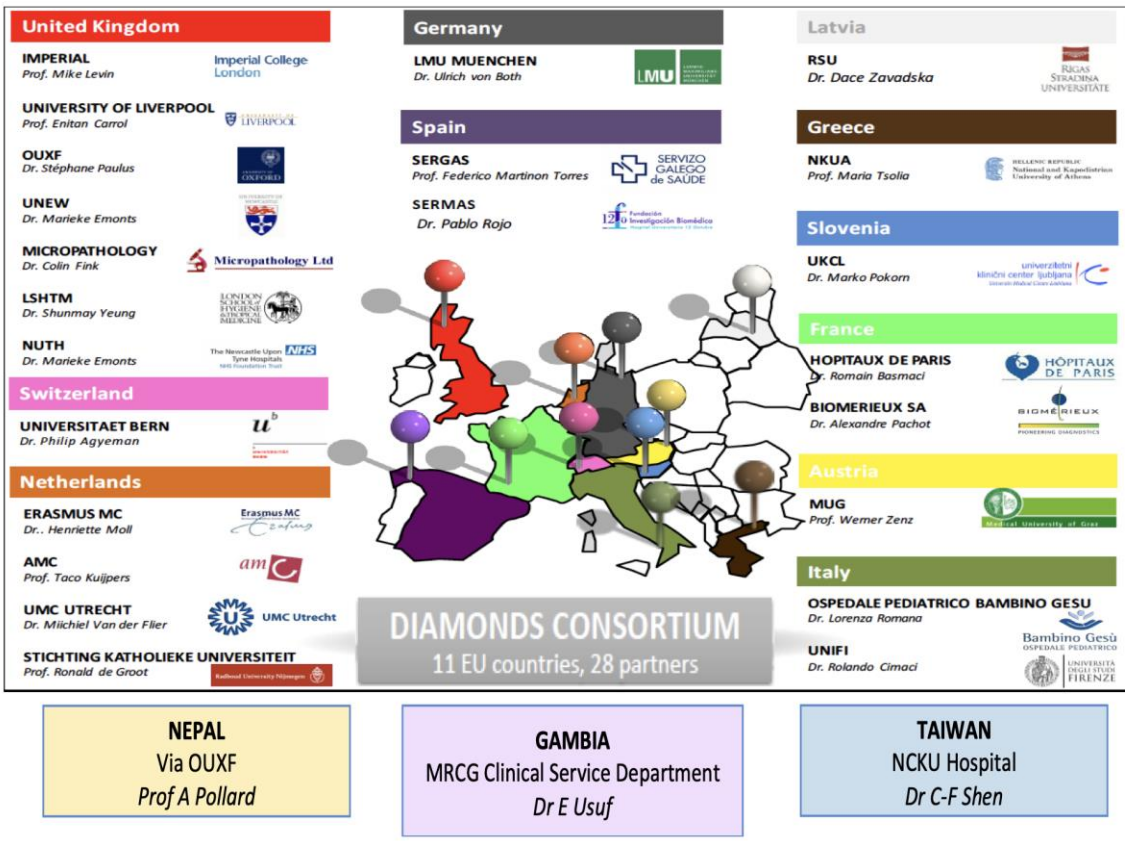

Figure 3-1 Diagnosis and Management of Febrile Illness using RNA Personalised Molecular Signature Diagnosis Study (DIAMONDS) Clinical Network[369].

3.1.1.1 DIAMONDS: patient recruitment and sampling

Patients of any age attending a participating hospital with fever, history of fever in the preceding 24 hours, or symptoms suggestive of infection or inflammation, were recruited into the study. The majority of patients were recruited in hospital accident and emergency departments, on transfer to inpatient wards or intensive care units. Individuals attending participating hospitals, with no fever and

no signs or symptoms of current or recent (within 3 weeks) infection or inflammation were recruited as controls (e.g. from outpatient appointments, minor trauma, minor operations). Individuals were excluded if they did not give consent or if they did not have a sample for PAXgene sample taken, for RNA sequencing.

All participating individuals were given a unique identification number and this along with date of birth is used for identification of individuals. A paper case record form (CRF) was completed for all individuals to collect anonymised data regarding the clinical presentation, symptoms, results of investigations and final diagnoses from health records. This information is uploaded onto a password protected, encrypted study database which conforms with current national and EU standards for data handling as well as the General Data Protection Regulations.

Research samples were collected at presentation to hospital during the acute illness (timepoint one (TP1)), following resolution of fever and improvement in blood markers e.g. fall in C-reactive protein (CRP) (timepoint two (TP2)) and following convalescence (timepoint three (TP3)). Where possible, the research samples were taken alongside the routine clinical tests, otherwise as agreed by the patient or carer/parent. As this study aims to develop novel diagnostic tests, a range of biological samples were collected including blood (whole blood, plasma, serum), respiratory secretions, urine and saliva. Samples were labelled with the unique identification number and stored in a centralised biobank. A total of 8000 individuals have been prospectively recruited between 01/01/2020 and 30/04/23; recruitment is ongoing.

3.1.1.2 DIAMONDS: clinical phenotyping

The local clinical research team assign a clinical phenotype to each patient by following the comprehensive phenotyping algorithm based on clinical data and results of investigations, as shown in Figure 3-2. The clinical cohorts used for my thesis include definite bacterial (DB), definite viral (DV), definite inflammatory syndrome (INF), healthy paediatric (HPC) and adult controls (HAC). The definite inflammatory syndrome group includes patients with MIS-C, KD and other inflammatory syndromes. A DB classification required the presence of clinical features in keeping with a bacterial illness, isolation of a pathogenic bacteria from a sterile site which matched the syndrome, CRP level greater than 60 mg/L and a neutrophil count greater than 12 x 10^9/L. Classification of DV required presence of clinical features of a viral illness, isolation of a virus matching the syndrome, a CRP level less than 60 mg/L and a neutrophil count less than 12 x 10^9/L. If the clinical features were present for a bacterial or viral illness, and the laboratory criteria (neutrophil count and CRP) were met, but a pathogen was not detected, then patients were classified as probable bacterial and probable viral respectively.

Patients were classified as having a definite inflammatory syndrome if they did not exhibit clinical and laboratory features consistent with an infection, but instead displayed characteristic indicative of an inflammatory illness. MIS-C classification was assigned if the WHO criteria for MIS-C were met[204]. KD classification was assigned if the American Heart Association (AHA) KD criteria were met[370]. Inclusion as healthy control required absence of fever and no recent vaccination, within the last 14 days.

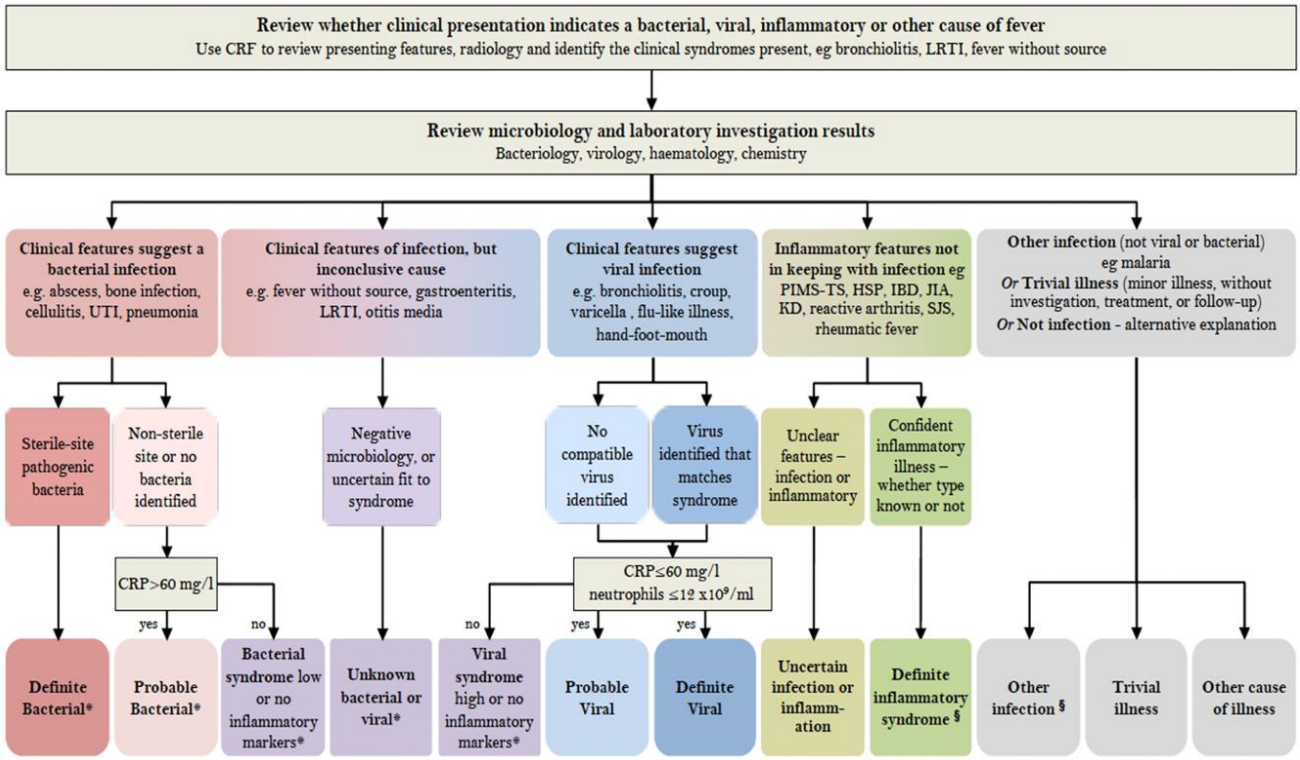

* Detection of virus does not exclude attribution of these infection phenotypes
§ Note that two phenotypes can be assigned to a patient if one is a non-viral/non-bacterial infection, or an inflammatory phenotype

Figure 3-2 The phenotyping algorithm for patients recruited into the Diagnosis and Management of Febrile Illness using RNA Personalised Molecular Signature Diagnosis Study (DIAMONDS)[371].

3.1.1.3 My role in DIAMONDS

I have worked as a clinical researcher at three London hospitals which are part of DIAMONDS: St Mary's Hospital, Evelina Children's Hospital and Great Ormond Street Hospital. I was involved in multiple aspects of DIAMONDS including a) recruitment of patients and controls, b) data collection and entry onto the study database c) sample collection, processing and biobanking d) phenotyping of patients recruited at St Mary's Hospital.

3.1.2 Best Available Treatment Study (BATS)

BATS is an international retrospective data collection study, which was set up following the emergence of the MIS-C[372]. MIS-C encompasses a condition with a wide spectrum of presentation and severity and in the absence of RCTs, patients were managed with a range of anti-inflammatory and immunomodulatory treatments by paediatricians across the world using their best judgement and available resources. Paediatricians worldwide were invited to join BATS and upload deidentified, routinely collected longitudinal data from suspected and confirmed cases of MIS-C, using a Web-based Research Electronic Data Capture (REDCap) database[373]. The primary aim of BATS was to evaluate clinical data to assess how different treatment strategies impact patient outcomes and to identify any adverse treatment effects. Patients between the ages of 0 to 19 years with confirmed MIS-C meeting the WHO[204], CDC[203], or UK[194] case definitions as well as suspected inflammatory cases related to SARS-CoV-2 not meeting these criteria were included. Suspected cases were included in this study as the spectrum of MIS-C is not known. Data collected include demographic characteristics, presenting symptoms, complications of disease or treatment, length of hospital stay, health status at discharge, echocardiogram (ECHO) findings following discharge and daily data for clinical features, laboratory markers, immunomodulatory treatments and level of organ support[321]. A total of 2101 children from 39 countries were recruited between 14/06/2020 and 25/04/2022. Recruitment remains open.

3.1.2.1 My role in BATS

I am a co-investigator for this study and led the ethics and UK clinical and regulatory management. This involved writing the clinical study protocol, obtaining ethical approval (London, Camden and Kings Cross Research Ethics Committee: 20/HRA/2957) and registering the study on the International Standard Randomised Controlled Trial Number (ISRCTN) registry (Trial ID: ISRCTN69546370). Together with the BATS working group, I helped design the CRF and completed data entry for patients admitted to St Mary's Hospital, London.

3.1.3 Delirium and Population Health Informatics Cohort (DELPHIC) COVID-19 sub-study

DELPHIC is a Wellcome Trust funded study, established in 2017 to investigate the determinants and consequences of acute illness in the elderly population (London, Camden and King's Cross Research Ethics Committee 16/LO/1217)[374]. The study has 1000 active participants, aged greater than 70 years and living in the London borough of Camden. Individuals were recruited from primary and secondary care, including general practice surgeries and memory clinics.

At the beginning of the COVID-19 pandemic, the established DELPHIC study cohort provided a unique and immediate opportunity, to undertake research aimed at understanding the epidemiology of transmission and factors (including age, frailty, comorbidities) associated with severe disease. The DELPHIC COVID-19 sub-study aimed to follow patients from the pre/early SARS-CoV-2 infection stage and throughout the course of their illness[375]. Baseline samples were taken from all participants including nasopharyngeal swab, PAXgene sample, plasma and serum samples. Participants were followed up with 2-weekly nasopharyngeal swab and health assessments for identification of COVID-19 cases. Individuals with COVID-19 symptoms and/or positive SARS-COV-2 PCR were sequentially re-sampled, during their illness and following recovery.

3.1.3.1 My role in DELPHIC COVID-19 sub-study

I helped process, aliquot and biobank the PAX-gene, plasma and serum samples collected from the study participants.

3.1.4 Other studies

3.1.4.1 Personalised Risk assessment in Febrile illness to Optimise Real-life Management (PERFORM)

The PERFORM study[376] (London, Central Research Ethics Committee, 16/LO/1684) is the predecessor of DIAMONDS. It was a prospective, multi-centre, EU-funded study carried out between 2016-2019. The study aimed to identify protein and gene diagnostic biomarkers for febrile children to differentiate between bacterial, viral and inflammatory disease. Children aged between 1 month and 18 years presenting to hospital with a fever or history of fever, as well as healthy controls were recruited to the study from participating hospitals across 10 European countries. Anonymised routinely collected demographic, clinical and microbiological data were compiled using a secure web-based platform.

Each participant was clinically phenotyped using a similar algorithm to the one described above for DIAMONDS. Biological samples including whole blood, serum, plasma and PAXgene were collected for biomarker discovery and biobanked for future research.

3.1.4.2 European Union Childhood Life-threatening Infectious Disease Study (EUCLIDS)

EUCLIDS preceded the PERFORM study and was an EU funded, prospective, multi-centre, study carried out across nine European countries and West Africa between 2012-2015 (National Research Ethics Service Committee London, Fulham, 11/LO/1982). The study aimed to understand the genetic basis of disease susceptibility and severity of life-threatening childhood bacterial infections[377]. Children aged 1 month to 18 years with suspected sepsis or severe focal infections along with healthy controls, attending participating hospitals in the UK, Austria, Germany, Lithuania, Spain, and the Netherlands were recruited into the study. Detailed anonymised routinely collected demographic, clinical and microbiological data were compiled using a secure web-based platform. Biological samples including whole blood, serum, plasma and PAXgene were collected as part of the study and biobanked for future research.

3.1.4.3 Fever In Children study

The Fever in Children study was a single-centre prospective cohort study, conducted at the Royal Alexandra Children's Hospital Emergency Department, Brighton, between February 2014 – January 2017. Children aged between 1 day to 17 years of age, with fever or history of fever above 37.5°C, requiring a blood test as part of their routine management were included in this study. Plasma samples and anonymised routinely collected demographic and clinical data were collected for each participant and biobanked for future research.

3.1.4.4 Genetic determinants of Kawasaki disease for susceptibility and outcome

The genetic determinants of Kawasaki disease for susceptibility and outcome study (London, Fulham Research Ethics committee, 13/LO/0026) aimed to identify genes underlying susceptibility to KD and development of coronary artery aneurysms (CAAs). It was a multi-centre study comprising of researchers from 42 UK National Health Service (NHS) hospitals. Children meeting the AHA clinical diagnostic criteria for KD and their biological parents were recruited through participating hospitals or through the records of the UK Kawasaki Support Group. Routine clinical and laboratory data was collected, and biological (blood, urine, throat swabs) samples were taken from children recruited

prospectively during acute illness. A study questionnaire was completed and saliva samples from affected children and their parents were taken from participants recruited retrospectively. A total of 1379 participants were recruited to the study between 25/03/2013 – 30/12/2022.

3.1.4.5 Imperial Health Knowledge Bank (IHKB)

IHKB aims to recruit patients admitted to any hospital within the Imperial College Healthcare NHS Trust, who provided consent for use of anonymised routinely collected clinical data and biological samples for research and teaching purposes. The aim of this biobank is to enable research which improves understanding of health conditions to facilitate earlier detection of disease and development of novel tests and treatments. 735 adults with COVID-19 were recruited into this study.

3.1.4.6 Diagnosing and predicting risk in children with SARS-CoV-2 related illness study

The Diagnosing and predicting risk in children with SARS-CoV-2 related illness study is part of the Predicting Viral Associated Inflammatory Disease Severity in Children with Laboratory Diagnostics and Artificial Intelligence initiative (PreVAIL kIds) by the National Institute of Health (UCSD #140220). This study aims to generate transcript and protein datasets for development of diagnostic and prognostic tests for SARS-CoV-2 associated diseases in children. Children with COVID-19, MIS-C, COVID-19 vaccine-induced myocarditis as well as febrile and healthy controls were recruited from Rady Children's Hospital, San Diego, United States.

3.1.4.7 Interferon Gamma Release Assay (IGRA) in Diagnostic Evaluation of Active TB (IDEA)

IDEA was a prospective, multi-centre, cohort study in secondary care in England (Northwest London Research Ethics Committee, 11/H0722/8). The aim of the study was to assess the accuracy of diagnostic strategies in suspected tuberculosis cases. Patients older than 16 years with suspected tuberculosis were recruited from inpatient and outpatient settings within NHS hospitals. Clinical data and blood samples, including serum, were collected from recruited patients.

3.1.4.8 The Graz Endomyocardial Biopsy Registry

The Graz Endomyocardial Biopsy Registry (Ethical approval reference: 32-575 ex 19/20) is a prospective registry that recruits patients above the age of 18 years undergoing endomyocardial biopsy at the University Heart Center, Graz. Clinical data, cardiac tissue, and various biomaterials are collected from participating patients and biobanked for use in research studies.

3.1.4.9 Diagnosis and Risk Stratification in Myocarditis Study

The Diagnosis and Risk Stratification in Myocarditis Study aims to evaluate the role of genetics in the development of dilated cardiomyopathy following acute myocarditis, and to identify novel diagnostic and prognostic biomarkers for myocarditis to allow prompt treatment and prevention of long-term complications in high-risk individuals (Southeast London Research Ethics committee, 18/LO/0676). Adults, over the age of 18 years, with acute myocarditis were recruited and samples were taken for genetic, protein expression and biomarker identification.

3.1.4.10 The Structure and Functional Characterisation of Human Hearts Study

The Structure and Functional Characterisation of Human Hearts Study is part of a larger body of work which aims to understand mechanisms underlying cardiac disease states in order to identify novel treatment targets (London Bridge Research Ethics Committee, 16/LO/1568). The purpose of this study is to obtain samples from healthy deceased donors for comparison with the disease states. Consent for research was given by the patient's family when all clinical usage was exhausted. Samples from explanted hearts from adults are used for isolation of cells from fresh tissue for functional work. Frozen and fixed tissue is used for RNA, DNA and protein expression studies as well as histology and imaging for assessment of structural changes.

3.2 Laboratory methods

This section includes the phlebotomy and sample processing methods I used for DIAMONDS participants included in the experiments described in Chapters 7 and 8. Following this, the experimental principles and protocols employed in each results chapter will be outlined. All the laboratory work was carried out in a containment level two (CL2) laboratory, either inside a class two microbiological safety cabinet or on the laboratory workbench top as appropriate. Personal and protective equipment were used in accordance with Imperial College London Laboratory Safety Training and departmental guidance.

3.2.1 Phlebotomy and sample processing

The materials and equipment used for phlebotomy and sample processing are shown in Table 3-2 and Table 3-3.

Table 3-2 Details of materials used for phlebotomy and sample processing.

Item	**Supplier**
2 ml screw-top microtubes, PCR grade	Sarstedt Ltd, Leicester, United Kingdom
Disposable container	Starlab, Milton Keynes, United Kingdom
Lithium heparin tubes	BD, New Jersey, United States
P1000, P200, P10/20 filter tips	Starlab, Milton Keynes, United Kingdom
P1000, P200, P20, P10 pipettes	Gilson, Madison, Wisconsin, United States
Polypropylene medical sharps container	Thermo Fisher Scientific, Horsham and Loughborough, United Kingdom
Sealable PathoPouch with Absorbent (UN3373 P650 packaging for Category B biological samples)	Intelsius, York, United Kingdom
Serum separation tubes	Becton, Dickinson and Company (BD), New Jersey, United States
Vacutainer holder	BD, New Jersey, United States
Vacutainer Safety Lok Blood Collection System	BD, New Jersey, United States
Virkon tablets	Thermo Fisher Scientific, Horsham and Loughborough, United Kingdom

Table 3-3 Details of the equipment used for phlebotomy and sample processing.

Item	Model	Company
Mid bench centrifuge	4K15	Sigma Laboratory Centrifuges, Germany

3.2.1.1 Phlebotomy

Best practices for phlebotomy including infection prevention and control practices were followed in accordance with the Imperial College Healthcare NHS Trust guidelines. Approximately 5 millilitres (mls) of blood was drawn into the blood bottle of choice e.g. serum separation tube (SST), using a vacutainer safety lok system, and needle discarded into a sharps bin following venepuncture. The blood-filled SST was inverted five times and labelled with unique patient identifier number, episode number, timepoint and the date and time of blood draw. Blood was allowed to clot at room temperature for 30-60 minutes and then stored at 4 degrees Celsius (°C) until processing. Samples were stored in Sealable PathoPouch for transportation to the laboratory. Waste was discarded into clinical waste bags.

3.2.1.2 Serum separation protocol

Serum is the liquid fraction of whole blood that is collected after centrifuging clotted blood, while plasma is the liquid fraction that is collected after centrifuging whole blood that contains anticoagulants e.g. ethylenediaminetetraacetic acid (EDTA). Traditionally serum has been used, instead of plasma, for research relating to proteins or antibodies for several reasons[378]. Serum has been shown to have higher metabolite concentrations, it does not contain anticoagulants which may interfere with immunoassays (e.g. enzyme-linked immunosorbent assay (ELISA)) and it does not contain fibrinogen and coagulation factors which can interfere with protein studies[378].

The DIAMONDS standard operating procedure (SOP) was followed for processing and storage of serum samples. Serum separation was performed within 4 hours and maximum 24 hours of blood collection. The SST was centrifuged at 4°C at 2000 relative centrifugal force (RCF) for 10 minutes. Following separation, serum was transferred into 2.0 ml microtubes into 100 microlitres (µl) aliquots and each tube labelled with unique identification number, episode, timepoint, aliquot number, volume, date and sample type. Samples were stored long term at minus (-) 80°C. Blood collection tubes and other plastic waste (e.g. pipette tips) were placed in a disposable container and decontaminated using Virkon disinfectant tablets.

3.2.2 Laboratory methods used for work shown in Chapters 4 and 5

3.2.2.1 Coronavirus antibody fluorescence-activated cell sorting (FACS) assay

H-CoV-OC43 N, SARS-CoV-2 N and SARS-CoV-2 S IgG, IgM and IgA antibodies were measured using a FACS-based assay. FACS is a technique which uses fluorescent markers to analyse cell surface or intracellular molecules by flow cytometry. Flow cytometry technology uses lasers to analyse particles/cells for light scatter and fluorescent parameters. Light scatter is measured in two different directions, forward scatter (FCS), which indicates the relative size of the particle/cell and side scatter (SCS), which provides information about the internal complexity of the particle/cell[379]. There are sensors within the flow cytometer which detect defined wavelengths of light. As each particle/cell passes through the laser beam, it creates of pulse of photon emission over time, which is recorded as an event. The total pulse area for an event correlates with its fluorescence intensity[380].

The assay utilised human embryonic kidney 293T (HEK293T) cells, a cell line consisting of immortalised human embryonic kidney cells. HEK239T cells were transfected to express coronavirus antigens, then treated with patient plasma and incubated with anti-human IgG/IgA/IgM conjugated with a fluorophore, prior to analysis on a flow cytometer for quantification of antibody levels given in absorbance units (a.u.). The principles of this assay are depicted in Figure 3-3.

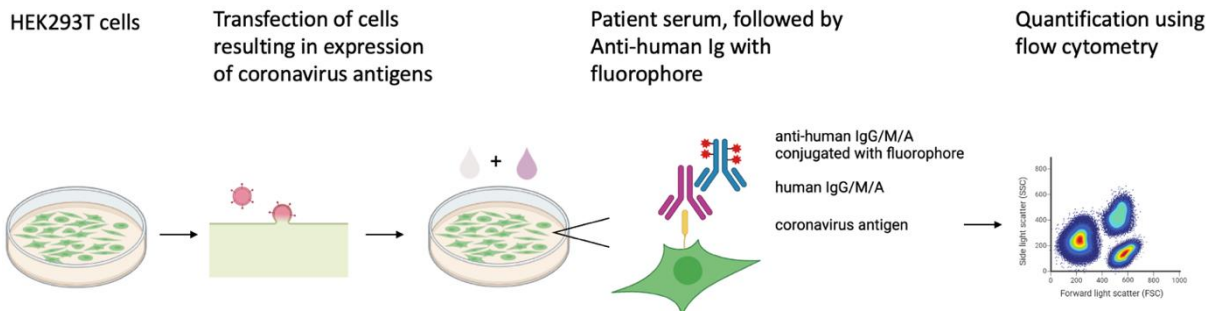

Figure 3-3 Principles of the coronavirus antibody fluorescence-activated cell sorting based assay.

Human embryonic kidney 293 T (HEK293T) cells were transfected to express coronavirus antigens and treated with patient plasma, followed by addition of anti-human immunoglobulin (Ig) G/M/A conjugated with a fluorophore. Cells were analysed on flow cytometry for antibody quantification.

Coronavirus antibody fluorescence-activated cell sorting (FACS) assay laboratory protocol

This assay was performed by the Kassiotis laboratory group at the Francis Crick Institute. The method is described briefly below and further details and optimisation data can be found in the supplementary text of the paper published by Ng et al.[180]. All reagents were supplied by Thermo Fisher Scientific, US, unless stated otherwise.

HEK293T cells (Cells Services facility, Francis Crick Institute, UK), were grown in Iscove's Modified Dulbecco's Medium (Sigma Aldrich, US) with 5% fetal bovine serum, L glutamine (2 mM), penicillin (100 U/ml), and streptomycin (0.1 mg/ml). Subsequently, HEK293T cells were transfected with an expression vector (pcDNA3) expressing SARS-CoV-2 N and SARS-CoV-2 S and an expression vector (pCMV3) expressing HCoV-OC43 S (SinoBiological, China). After two days, cells were trypsinised and transferred into V-bottom 96-well plates at a concentration of 20,000 cells/well. Cells were incubated with patient plasma (diluted 1:50 in Phosphate buffered saline (PBS) for 30 minutes. Cells were washed with FACS buffer (PBS, 5% Bovine Serum Albumin (BSA), 0.05% sodium azide) and stained for 30 minutes with the following antibodies which were all diluted 1:200 in FACS buffer: brilliant violet 421 anti-IgG (clone HP6017, Biolegend, US), allophycocyanin (APC) anti-IgM (clone MHM-88, Biolegend, US) and phycoerythrin (PE) anti-IgA (clone IS11-8E10, Miltenyi Biotec, Germany). Following incubation, cells were washed with FACS buffer and fixed using CellFIX buffer (BD Biosciences, US) for 20 minutes. Samples were run on an BD LSR Fortessa flow cytometer with a high throughput sampler (BD Biosciences, US) running BD FACSDiva software (Version 8.0) and analysed using FlowJo analysis software (Version 10).

3.2.2.2 Mesoscale Discovery (MSD) V-PLEX SARS-CoV-2 IgG assay

The MSD V-PLEX immunoassay was chosen for SARS-CoV-2 S and N IgG testing of 2022 samples due to practical considerations. The FACS-based assay at the Francis Crick Institute was not feasible for these samples due to the unavailability of the individual with expertise in running the assay, and the training required, which would have taken three months or more. Given that our research group already has expertise in using the MSD platform, this option was selected for efficiency. The MSD assay is validated (V-PLEX, V = validated) and a subset of samples from 2020-2021 originally run on the FAC-based assay were re-run on the MSD assay to ensure consistency and reliability. The change in assay was not expected to impact the results, as the focus of the longitudinal trends was on the qualitative assessment of antibody presence (positive or negative), and not on the quantitative measurement of antibody concentrations.

MSD immunoassays are based on proprietary technology which uses electrochemiluminescent labels (SULFO-TAG™) which generate light when stimulated with electricity in combination with multiarray technology for quantification of multiple proteins in a sample. The V-PLEX kit includes a plate coated with SARS-CoV-2 S and N antigens. When the sample is added, if SARS-CoV-2 S or N IgG are present, they will bind to their specific antigen and are subsequently detected using anti-human IgG antibodies conjugated with MSD SULFO-TAG™. When electricity is applied to the electrodes on the plate, light is emitted from the SULFO-TAGs and their intensity measured for quantification of SARS-CoV-2 S and N IgG. The schematic of this assay is shown in Figure 3-4.

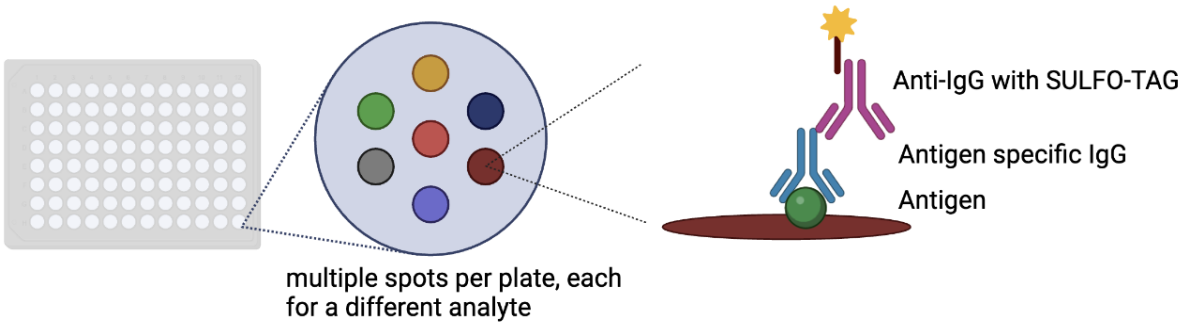

Figure 3-4 Schematic diagram of the V-PLEX Mesoscale Discovery assay.

Each well has multiple spots which are coated with a different antigen. Antigen specific IgG will bind to the antigen and is detected using anti-IgG conjugated with electrochemiluminescent labels termed SULFO-TAGs, which emit light when stimulated with electricity. This figure was made using Biorender.

The materials and equipment used for the MSD V-PLEX SARS-CoV-2 antibody assay are shown in Table 3-4 and Table 3-5 respectively and the assay protocol is detailed below. Ten samples that tested positive and ten samples that tested negative for SARS-CoV-2 S IgG on the FACS-based assay were re-run on the MSD assay to validate the results, so the two datasets could be merged for the longitudinal analyses.

Table 3-4 Details of the materials used for the Mesoscale Discovery V-PLEX SARS-CoV-2 IgG assay.

Item	**Supplier**
1.5 ml microcentrifuge tubes with cap	Starlab, Milton Keynes, United Kingdom
15 ml Falcon tubes	Starlab, Milton Keynes, United Kingdom
Duran laboratory bottles glass bottles (250 ml & 1L)	DWK Life Sciences, Mainz, Germany

Table 3-4 continued.

Item	Supplier
Mesoscale Discovery V-PLEX kit Contents: 96 well plate, Assay diluent, Blocker A, Detection antibody diluent, Phosphate buffer 5X, Read buffer, Standards, Stop solution	Mesoscale Diagnostics, Maryland, United States
P1000, P200, P10/20 filter tips	Starlab, Milton Keynes, United Kingdom
P1000, P200, P20, P10 pipettes	Gilson, Madison, Wisconsin, United States
P200 multichannel pipette	Gilson, Madison, Wisconsin, United States
Phosphate-buffered saline tablets 1x	Thermo Fisher Scientific, Massachusetts, United States
Plate sealers	Biolegend, California, United States
Reagent reservoirs	Thermo Fisher Scientific, Massachusetts, United States
Tween 20	Sigma Aldrich, Missouri, United States
Vacuum filter unit, 0.2µm filter, 500 ml	Thermo Fisher Scientific, Massachusetts, United States

Table 3-5 Details of the equipment used for the Mesoscale Discovery V-PLEX SARS-CoV-2 IgG assay.

Item	Model	Company
Microcentrifuge	Fresco™ 21	Thermo Fisher Scientific, Massachusetts, United States
MSD plate reader	MESO SECTOR S 600 MM	Mesoscale Diagnostics, Maryland, United States
Plate shaker	Orbi-shaker™ MP Microplate Shaker	Benchmark Scientific, New Jersey, United States
Vortex mixer	Whirlimixer	Fison, Ipswich, United Kingdom

MSD V-PLEX SARS-CoV-2 IgG assay laboratory protocol

Serum samples were thawed on ice and the MSD V-PLEX assay kit and reagents were brought to room temperature (RT) prior to use. Blocker A solution and wash buffer (PBS 0.05% Tween 20) were prepared as per manufacturer's instructions and vacuum filtered. Next, 150 µl of the Blocker A solution was added to each well, the plate sealed and incubated at RT on a plate shaker at 700 revolutions per minute (rpm) for 30 minutes. Next, the standards were prepared. To prepare the top standard (S1), the reference standard 1 (10x) was diluted 10-fold in assay diluent and vortexed briefly to mix. A 1:4 serial dilution of S1 was carried out using assay diluent to generate a total of 7 standards (S1-7). Assay diluent was used as a blank, as S8. Following incubation with Blocker A solution, the plate was washed three times, by addition and subsequent decanting of 150 µl of wash buffer in each well. After the final wash, the plate was gently tapped onto paper towels to remove any residual fluid. Thawed samples were pulse centrifuged (10,000 RCF for 5 seconds) prior to use, to remove any particulates. 50 µl of standards (S1-S8) were added to each of the standards wells and 50 µl of diluted sample (1:5000 dilution in assay diluent) was added to each of the sample wells. The standards were run in duplicates and the samples were run in singlicates. The plate was sealed and incubated at RT for 1 hour on a plate shaker at 700 rpm. The plate was washed three times, followed by addition of 50 µl of detection antibody solution (1x) to each well. The plate was incubated at RT for 1 hour on a plate shaker at 700 rpm and then washed again three times. Thereafter, 150 µl of read buffer was added to each well and the plate analysed using an MSD plate reader.

3.2.3 Laboratory methods used for work shown in Chapter 7

The materials and equipment used for immunohistochemistry (IHC) and enzyme-linked immunosorbent assays (ELISAs) are displayed in Table 3-6 and Table 3-7.

Table 3-6 Details of materials used for immunohistochemistry and enzyme-linked immunosorbent assays.

Item	Supplier
Acetone ACS reagent, ≥99.5% (-20^{o}C)	Sigma Aldrich, Dorset, United Kingdom
Aluminium foil	Thermo Fisher Scientific, Horsham and Loughborough, United Kingdom
Clear nail polish	A.S. Watson (Health & Beauty UK) Ltd
Eppendorf Safe-Lock 1.5 ml tubes	Eppendorf Ltd, Stevenage, United Kingdom
FITC IgA (2.0g/L), FITC IgM (2.0g/L), FITC IgG (2.0g/L)	Agilent Technologies, London, United Kingdom
Human Recombinant Troponin (100ug/ml)	Cambridge Bioscience Ltd, Cambridge, UK
Human TruFx, fc receptor block stain	Biolegend, San Diego, California, United States
Hydrophobic PAP pen	Abcam PLC, Cambridge, United Kingdom
Microscope glass slides	VWR, International, Randor, Pennsylvania, United States
Mounting coverslips	VWR, International, Randor, Pennsylvania, United States
Mounting medium with DAPI, aqueous, fluoroshield	Abcam PLC, Cambridge, United Kingdom
Myosin, from porcine heart (0.1-0.5 units/mg)	Sigma Aldrich, Dorset, United Kingdom
Opaque slide tray	VWR, International, Randor, Pennsylvania, United States
P1000, P200, P10/20 filter tips	Starlab, Milton Keynes, United Kingdom
P1000, P200, P20, P10 pipettes	Gilson, Madison, Wisconsin, United States
Phosphate-buffered saline (PBS, 1x), sterile-filtered	Thermo Fisher Scientific, Horsham and Loughborough, United Kingdom
Rabbit anti-human IgG conjugated with HRP (2mg/ml)	Abcam PLC, Cambridge, United Kingdom
Rabbit Serum	Abcam PLC, Cambridge, United Kingdom
Staining jar	VWR, International, Randor, Pennsylvania, United States

Table 3-6 continued.

Item	Supplier
TMB ELISA kit: Blocking Buffer, Diluent, ELISA microplates PBS 1x, Sealing Film, Stop Solution, TMB Liquid Substrate, Wash Buffer, 96-well ELISA microplates	Peprotech, London, United Kingdom
Wheat Germ Agglutinin with Texas Red	Thermo Fisher Scientific, Horsham and Loughborough, United Kingdom
Whole heart porcine lysate (5mg/ml)	Thistle Scientific Ltd, Glasgow, UK

Table 3-7 Details of the equipment used for immunohistochemistry and enzyme-linked immunosorbent assays.

Item	Model	Company
Cryostat	CM1850	Leica, Germany
ELISA plate reader	SpectraMax Paradigm multi-mode microplate reader	Beckham Coulter, California, United States
Mid bench centrifuge	4K15	Sigma Laboratory Centrifuges, Germany
Wide-field Microscope	HWF1, Zeiss Axio Observer	Zeiss, Cambridge, United Kingdom

3.2.3.1 Immunohistochemistry

Immunohistochemistry (IHC) is a method used for identifying specific antigens within tissue sections using antigen-specific antibodies. The antigen-antibody interaction is visualised on light microscopy by using an antibody conjugated with a fluorescent marker. Indirect IHC was used for detection of any anti-cardiac antibodies in the serum of patients with MIS-C and COVID-19 vaccine-induced myocarditis. The serum from patients and controls served as the unlabelled primary antibody, therefore if anti-cardiac antibodies were present in the serum, they would bind the cardiac tissue. Secondary labelled antibodies were used to bind to the primary antibody, these included anti-human IgG, IgM and IgA conjugated with fluorescein isothiocyanate (FITC), a green-fluorescent dye. Wheat Germ Agglutinin (WGA) with Texas Red, a red-fluorescent dye, was applied to the tissue to visualise the cell membranes, as WGA is known to bind cell membrane glycoproteins. 4',6-diamidino-2-phenylindole (DAPI) was used to visualise cell nuclei, as it emits a blue fluorescence when bound to DNA. The IHC slides were imaged using a wide-field microscope, and 10 images of each section were taken at 20x magnification. A diagram of the experimental design is shown in Figure 3-5. The details of the tissue preparation and optimised assay protocol are described overleaf and the details and results of the optimisation experiments are shown in Appendix 2 (2.1 IHC optimisation experiments).

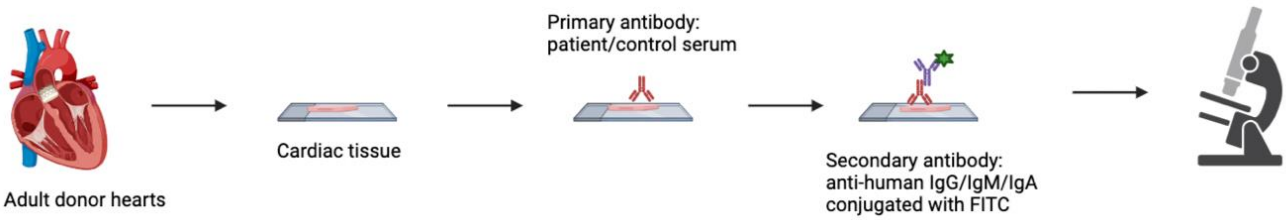

Figure 3-5 Schematic diagram of the immunohistochemistry experiment.

Donor cardiac tissue was incubated with serum from patient/controls (primary antibody), followed by addition of anti-human IgG/IgM/IgA conjugated with fluorescein isothiocyanate (FITC) (secondary antibody). The slides were visualised under a wide-field microscope. This figure was made using Biorender.

Cardiac donors and preparation of tissue section slides

Cardiac tissue samples from deceased donors were obtained from Harefield Hospital, UK. Details of the two selected donors are shown in Table 3-8. The hearts were flash-frozen in liquid nitrogen and then stored at −80 °C for cryosectioning. Heart tissue was cut into 7µm thick sections using a cryostat, placed on microscope slides and air-dried for 15 minutes before storing long-term at −80 °C freezer.

Table 3-8 Details of the selected cardiac donors.

	Donor A	**Donor B**
Age (years)	48	17
Sex	Male	Female
Past medical history	Nil recorded	No history of: hypertension/ cardiothoracic disease/ liver disease/ diabetes/ smoking/ alcohol drinking
Cause of death	Haemorrhage	Status epilepticus
Reason for unsuitability as transplant organ	Poor function	Deterioration on organ care system

IHC laboratory protocol

Serum samples were thawed on ice. A humid chamber was prepared using the opaque slide tray. Microscope slides with human cardiac tissue slices were removed from the freezer and fixed with acetone for ten minutes at RT. Next, the acetone was discarded and borders were drawn around each tissue section using a hydrophobic pen. 150ul of 2% human fc receptor block diluted in 5% rabbit serum (diluted in PBS) was applied to each tissue section for blocking at RT for 60 minutes. Serum samples were pulse centrifuged and diluted 1:50 with 5% rabbit serum. The slides were drained to remove blocking buffer and any excess buffer was wiped away. 150ul of diluted serum from each patient/control was applied to the tissue sections, alongside a PBS control. The slides were incubated overnight at 4°C. Following incubation, each section was washed three times by application of 200ul PBS for 5 minutes and subsequent drainage. After the third wash, any excess PBS was wiped away. Room lights were switched off for the next steps to prevent photobleaching. 150ul of anti-human IgG conjugated with FITC (diluted to 1:250 in PBS) was applied to each tissue section and incubated at RT for one hour. Each section was washed 3 times. WGA with Texas Red, diluted 1:50 with PBS, was applied to each section and incubated at RT for 15 minutes. This was followed by 3 washes. Next, 1-2

drops of mounting media containing DAPI were added to each section and a coverslip applied. The slides were covered and left to dry at RT for 30 minutes. The coverslips were sealed using clear nail polish and left to dry at RT for 15 minutes. The slides were visualised using a wide-field microscope and kept in an opaque slide box at 4°C for long-term storage. The same protocol was used for IgM and IgA using anti-human IgM (diluted to 1 in 250 in PBS) and anti-human IgA (diluted to 1 in 50 in PBS) respectively.

IHC imaging

A wide-field microscope (HWF1 Zeiss Axio Observer) and Zeiss Zen software (Zen 2, blue addition) were used to image the IHC slides. A preview image of the entire tissue section was taken at 10x magnification and used for random selection of ten positions for imaging; this ensured coverage of the entire tissue section and prevented any overlap. The WGA channel was used for focusing to avoid photobleaching of the FITC. Images were taken at 20x magnification with the WGA, FITC and DAPI channels. Microscope settings were kept consistent across all experiments.

3.2.3.2 Cardiac autoantibody Enzyme-Linked Immunosorbent Assay (ELISA)

ELISAs are used for detecting and quantifying an antigen within a sample, through measurement of highly specific antibody-antigen interaction. An indirect ELISA assay was designed for the detection of anti-cardiac antibodies in the serum of patients with MIS-C and COVID-19 vaccine-induced myocarditis. Three assays with different antigens were set up including porcine whole heart lysate, porcine myosin, and human recombinant troponin. The patient sera served as the primary antibody, and horseradish peroxidase (HRP) conjugated anti-human IgG was used as the secondary antibody. HRP is an enzyme that is commonly used in colorimetric assays in conjunction with the substrate 3,3',5,5'-Tetramethylbenzidine (TMB). When HRP and TMB are combined, HRP reduces hydrogen peroxide and oxidises the TMB, producing a colour change from colourless to blue. The addition of an acidic solution (e.g. sulphuric acid) can stop this reaction and turn the solution yellow, the intensity of which can be measured at the wavelength of 450 nm. Whole heart lysate was used as a first-line assay to detect the presence of any anti-cardiac antibodies, while the myosin and troponin assays allowed detection of specific antigen-antibody reactions. Porcine lysate and myosin were used as there is cross-reactivity between human and porcine antibodies/antigens and this also limits non-specific binding of human antibodies in patient serum with human heart lysate/myosin. The experimental design is shown in Figure 3-6.

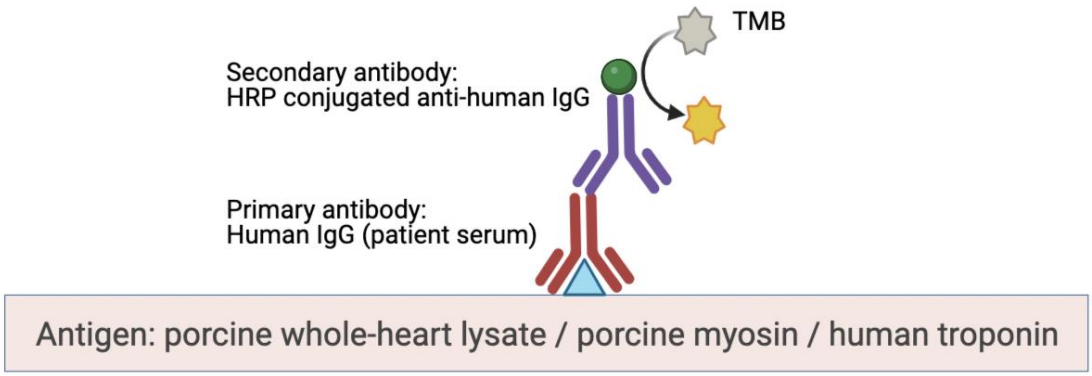

Figure 3-6 Schematic diagram of the indirect enzyme-linked immunosorbent assay.

Three different antigens were used: porcine whole heart, porcine myosin and human recombinant troponin. Patient serum served as the primary antibody, the secondary antibody was an HRP conjugated anti-human IgG and TMB was used as the colorimetric substrate for HRP. This figure was made using Biorender.

Cardiac autoantibody ELISA laboratory protocol

The materials and equipment used for the ELISAs are shown in Table 3-6 and Table 3-7. The optimised assay protocol is detailed below, and the details and results of the optimisation experiments are shown in Appendix 2 (2.2 ELISA optimisation experiments).

Whole heart lysate

The whole heart lysate was thawed and diluted to working concentration of 1.25ug/ml using PBS (1:4000 dilution). Next, 50ul of whole heart lysate was added to each well of a 96-well microplate. The plate was sealed and incubated overnight at 4°C (18 hours). The next day, the Peprotech TMB ELISA Buffer Kit and all the reagents were brought to RT and serum samples were thawed on ice prior to use. Wash buffer was prepared as per manufacturer's instructions. The plate was washed three times, by addition and subsequent decanting of 200 µl of wash buffer in each well. After the third wash, any residual fluid was removed by gently tapping the plate on a paper towel. 50 µl of blocking buffer was added to each well, the plate was sealed and incubated for one hour at RT. During this incubation step, the ELISA diluent was prepared as per manufacturer's instructions. Thawed samples were pulse centrifuged and diluted (1:100) using ELISA diluent. Following the blocking step, the plate was washed three times and 50 µl of the diluted serum was added to each well, along with three positive and negative (PBS) controls. All samples were run in duplicates. The plate was sealed and incubated at RT for 30 minutes. The HRP-conjugated anti-human IgG was brought to the working concentration of 0.33 µg/ml by diluting with blocking buffer (1 in 6000). The solution was protected from the light by covering with foil and kept on ice. The plate was washed three times, followed by addition of 50 µl of TMB to each well. The plate was sealed and covered with foil for 7 minutes, after which 25 µl of the stop solution was added to each well and the plate read using the ELISA plate reader at 450nm wavelength.

Myosin ELISA

The same protocol was followed for myosin ELISA with the following exceptions: a) myosin working concentration of $1.25x10^{-5}$ units/mg (1 in 40000 dilution) b) HRP conjugated anti-human IgG working concentration of 0.33 µg/ml (1 in 3000 dilution) c) HRP-TMB reaction time of 8 minutes.

Troponin ELISA

The same protocol was followed for the troponin ELISA with the following exceptions: a) troponin working concentration of 0.04 µg/ml (1 in 2500 dilution) b) HRP conjugated anti-human IgG working concentration of 0.33 µg/ml (1 in 3000 dilution) c) HRP-TMB reaction time of 9 minutes.

Positive controls

The positive controls serum samples were selected after reviewing the results of whole heart lysate, myosin, and troponin ELISAs performed on serum of adult myocarditis patients by Dr Alma Octavia as part of her PhD. For each assay, three patients with the highest readings above the positive threshold were selected as positive controls for my experiments.

3.2.4 Laboratory methods used for work shown in Chapter 8

The materials and equipment required for the SARS-CoV-2 QuantiFERON assay, multiplex cytokine assays and mass cytometry are shown in Table 3-9 and Table 3-10.

Table 3-9 Details of the materials used for the SARS-CoV-2 QuantiFERON assay, multiplex cytokine assay and mass cytometry.

Item	Supplier
0.5 ml screw-top microtubes, PCR grade	Sarstedt Ltd, Leicester, United Kingdom
1.5 ml microcentrifuge tubes with cap	Starlab, Milton Keynes, United Kingdom
1.8 ml cryovial, with self-sealing cap	Starlab, Milton Keynes, United Kingdom
15 ml falcon tube	Starlab, Milton Keynes, United Kingdom
1L Disposable Sweet Jars	Starlab, Milton Keynes, United Kingdom
250 ml, 500 ml, 1L Duran Laboratory glass bottles	DWK Life Sciences, Mainz, Germany
5 ml Eppendorf Tubes with screw cap	Eppendorf, Hamburg, Germany
Barcoding antibodies	Fluidigm, California, United States
Cell surface antibodies and intracellular antibodies	Biolegend, California, United States Fluidigm, California, United States
Cytodelics fixation buffer, lysis buffer, wash buffer and whole blood cell stabilizer	Cytodelics AB, Sweden
Element calibration beads	Fluidigm, California, United States
Ethylenediaminetetraacetic acid (0.5mM)	Thermo Fisher Scientific, Massachusetts, United States
Falcon™ round bottom polypropylene test tubes with cap	Thermo Fisher Scientific, Massachusetts, United States
Heparin 1000 units/10 ml solution	Medisave, Dorset, United Kingdom
Human FcX Trustain fc receptor blocker	Biolegend, California, United States
LEGENDplex™ Human Anti-Virus Response Panel (13-plex) with V-bottom Plate kit. Contents: Setup beads, Capture beads, Detection antibodies, Standard cocktail, SA-PE, Matrix B, Assay Buffer, Wash Buffer, Plate sealers, V-bottom plates	Biolegend, California, United States

Table 3-9 continued.

Item	Supplier
Maxpar cell staining buffer	Fluidigm, California, United States
Maxpar fix and perm buffer	Fluidigm, California, United States
Maxpar intercalator solution	Fluidigm, California, United States
Mesoscale Discovery U-PLEX kit Contents: 96 well plate, Linkers, Stop solution, Read buffer, Assay diluent, Detection antibody diluent, Standards, Biotinylated antibodies set 1: IL2, IL4, IL13, IL17A	Mesoscale Diagnostics, Maryland, United States
Methanol	Thermo Fisher Scientific, Massachusetts, United States
P1000, P200, P10/20 filter tips	Starlab, Milton Keynes, United Kingdom
P1000, P200, P20, P10 pipettes	Gilson, Madison, Wisconsin, United States
P200 multichannel pipette	Gilson, Madison, Wisconsin, United States
Phosphate-buffered saline tablets 1X	Thermo Fisher Scientific, Massachusetts, United States
Plate sealers	Biolegend, California, United States
QuantiFERON SARS-CoV-2 Starter Set Contents: blood collection tubes (Ag1, Mitogen, Nil)	Qiagen, The Netherlands
Reagent reservoirs	Thermo Fisher Scientific, Massachusetts, United States
Sealable PathoPouch with Absorbent (for transport of Category B biological samples)	Intelsius, York, United Kingdom
Tween 20	Sigma Aldrich, Missouri, United States
Vacutainer Lithium Heparin Tube, 8 ml	BD, New Jersey, United States

Table 3-10 Details of the equipment used for the SARS-CoV-2 QuantiFERON assay, multiplex cytokine assay and mass cytometry.

Item	Model	Company
Flow cytometer	BD LSR II Fortessa with high throughput sampler (HTS)	BD Biosciences, California, United States
Microbiological Incubator	Touch 190S	LEEC Ltd, Nottingham, United Kingdom
Microcentrifuge	Fresco™ 21	Thermo Fisher Scientific, Massachusetts, United States
Mid bench centrifuge	4K15	Sigma Laboratory Centrifuges, Germany
MSD Plate reader	MESO SECTOR S 600 MM	Mesoscale Diagnostics, Maryland, United States
Plate shaker	Orbi-shaker™ MP Microplate Shaker	Benchmark Scientific, New Jersey, United States
Vortex mixer	Whirl mixer	Fison, Ipswich, United Kingdom
Water bath	JB Nova	Grant Scientific, Cambridgeshire, United Kingdom

3.2.4.1 SARS-CoV-2 QuantiFERON assay

QuantiFERON assays allow assessment of cell-mediated immunity to a particular antigen. The principle of the assay entails stimulation of whole blood with a specific antigen, resulting in activation of antigen-specific lymphocytes in individuals with prior exposure to that antigen. The activated lymphocytes produce IFNγ, which can be measured using an ELISA. QuantiFERON assays are widely used to aid the diagnosis of *Mycobacterium tuberculosis* infection, whereby raised IFNγ levels indicate active or latent tuberculosis infection[381]. The SARS-CoV-2 QuantiFERON assay was developed by Qiagen to measure the production of IFN by activated T cells in response to SARS-CoV-2 antigens composed of peptides from the S1 subunit, S2 subunit and receptor binding domain of the Spike protein[382]. Phytohemagglutinin (PHA), a lectin which binds to T cell membranes resulting in non-specific activation of T cells, is used as the positive control (termed "mitogen (mit)" for the purpose of this assay). A negative control is also used for measurement of background and non-specific IFNγ (termed "nil" for the purpose of this assay). The principles of the SARS-CoV-2 QuantiFERON assay are illustrated in Figure 3-7.

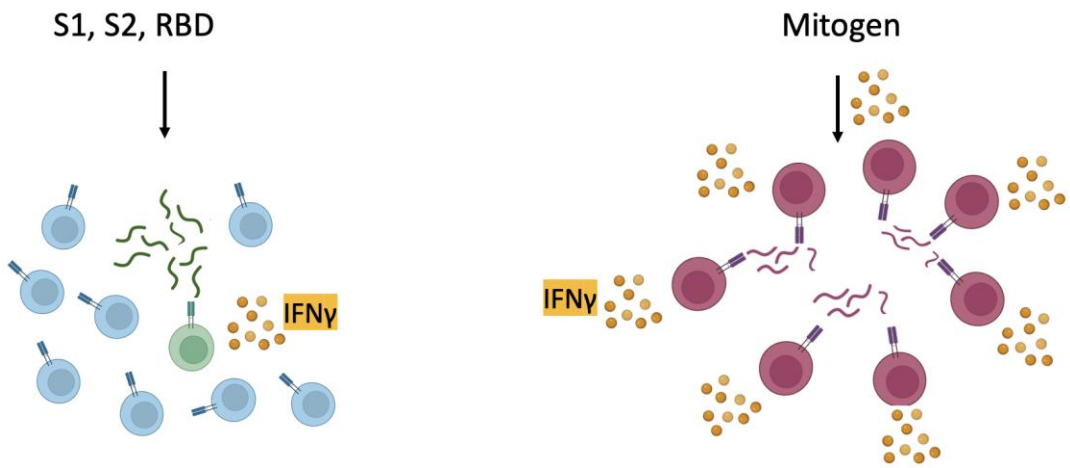

Figure 3-7 Principles of the SARS-CoV-2 QuantiFERON assay.

Exposure of SARS-CoV-2 antigens (peptides from the Spike S1 and S2 subunit and the receptor binding domain) results in activation of antigen-specific T cells and interferon gamma (IFNγ) production in individuals with prior exposure to SARS-CoV-2 antigens. Exposure of phytohemagglutinin (mitogen) results in non-specific activation of T cells and IFNγ production. This figure was made using Biorender.

SARS-CoV-2 QuantiFERON assay laboratory protocol

Figure 3-8 shows the experimental flow for the QuantiFERON assay. Lithium heparin tubes were used for collection of 4 ml of whole blood from patients and controls. For a small subset of patients and controls an aliquot (0.5 ml) of pre-incubation blood was taken for mass cytometry. After that, 1 ml of blood was pipetted into each of the SARS-CoV-2 QuantiFERON tubes (ag1, mitogen, nil) and incubated at 37°C for 17-24 hours. Following incubation, the entire blood volume of each tube was placed into a pre-labelled 5 ml Eppendorf tube and gently mixed to fully resuspend all blood components. For a small subset of patients and controls an aliquot of post-incubation blood (0.5ml) from each of the QuantiFERON tubes was taken for mass cytometry. The 5 ml Eppendorf tube was centrifuged at 3000 RCF for 15 minutes and the supernatant was aliquoted into 0.5 ml microtubes and stored at -80°C. Blood collection tubes and other plastic waste (e.g. pipette tips) were placed into a disposable container, sealed, sprayed with 70% ethanol and autoclaved.

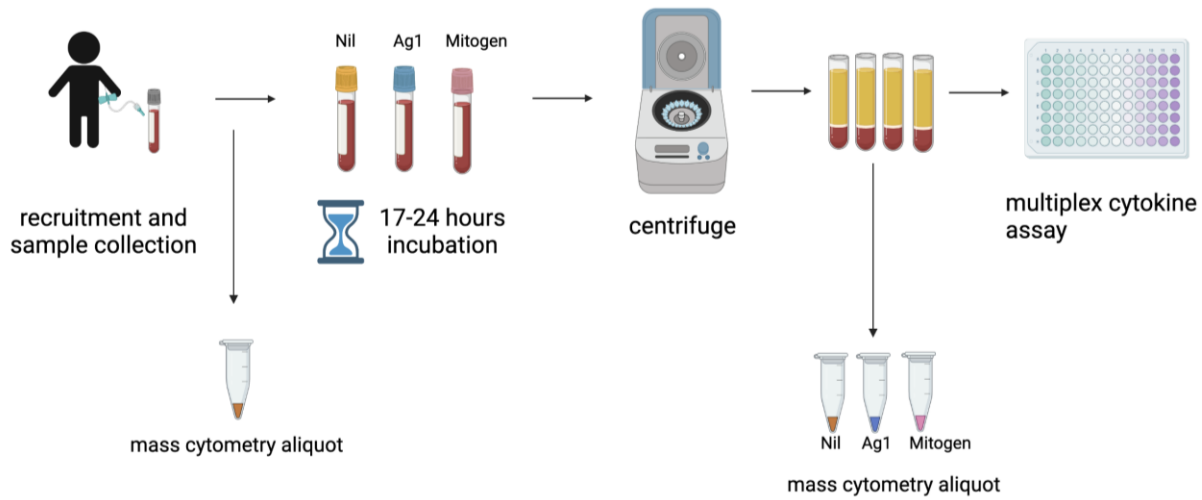

Figure 3-8 Experimental flow for the SARS-CoV-2 QuantiFERON assay and mass cytometry.

Whole blood was collected from recruited patients and transferred into three tubes containing 1) SARS-CoV-2 Antigen 1 (ag1) 2) Negative control (nil) 3) Positive control (mitogen) and incubated at 37°C for 17-24 hours. The samples were centrifuged, supernatant extracted and used for the multiplex cytokine assay. Mass cytometry samples were taken pre-and-post incubation on a subset of patients. This figure was created in Biorender.

3.2.4.2 LEGENDplex 13-plex cytokine assay

The LEGENDplex Human Anti-virus Response Panel allows measurement of 13 cytokines: IL1β, IL6, IL8, IL10, interleukin 12p70 (IL12p70), IFNγ, interferon alpha 2 (IFNα2), interferon beta (IFNβ), interferon lambda 1 (IFNλ1), interferon lambda 2/3 (IFNλ2/3), IP10, TNFα and GM-CSF.

I selected this panel as it includes IFNγ, which is produced by T cells and can serve as a marker for T cell activation and immune response. The panel also includes type I (IFNα2, IFNβ) and type III interferons (IFNλ1/IFNλ2/3) which allows a broader assessment of the interferon response. Additionally, the panel contains cytokines that are known to be dysregulated in MIS-C (e.g. IL6, IL10, TNFα) and would allow examination of their potential roles in the disease mechanism.

Bead-based immunoassays allow simultaneous detection of multiple analytes in one sample using flow cytometry. The basic principles of flow cytometry have been described previously (section 3.2.2.1). The principles of the LEGENDplex multiplex assay are illustrated in Figure 3-9. Each bead is coupled with a specific surface antibody for a particular analyte. When the beads are incubated with a sample containing that analyte, the analyte binds to its specific antibody. A biotinylated detection antibody is subsequently added, which binds to its specific antibody-bound analyte, forming a bead specific antibody-analyte-detection antibody complex. Streptavidin phycoerythrin (SA-PE) is used as a reporting agent for biotinylated antibodies. Streptavidin is a bacteria-derived biotin-binding protein and phycoerythrin is a red algae fluorescent protein which absorbs light at 565 nm. Analyte-specific populations can be identified on the flow cytometer, as the beads are differentiated by size and internal fluorescence intensity. Upon binding of SA-PE to biotinylated detection antibodies, fluorescence intensities proportionate to the quantity of bound analytes can be detected. The concentration of each analyte is calculated by using a standard curve generated in the same experiment.

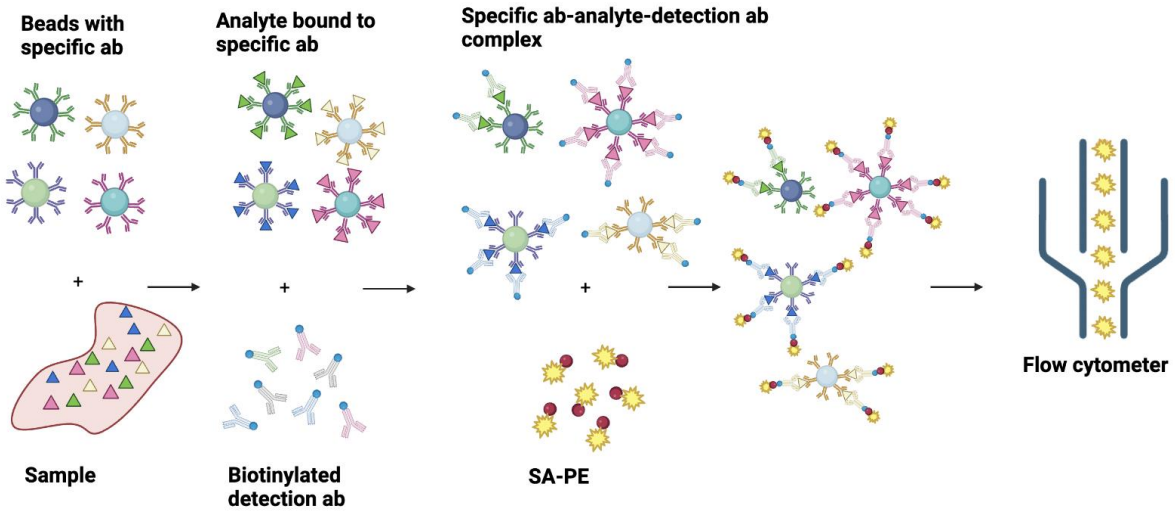

Figure 3-9 Principles of the LEGENDplex bead-based multiplex assay.

Beads are coupled with a specific antibody (ab) against target analytes. When the sample is added, analytes bind the specific ab, which is followed by the addition and binding of biotinylated detection antibodies. Streptavidin phycoerythrin (SA-PE) is used as a reporting agent for biotinylated antibodies, which enables quantification of each analyte on flow cytometry. This figure was made using Biorender.

LEGENDplex 13-plex cytokine assay laboratory protocol

Supernatant samples from the SARS-CoV-2 QuantiFERON were thawed on ice. The LEGENDplex Human Anti-Viral 13-plex assay kit and all reagents were brought to RT prior to use. Wash buffer solution, Matrix B and standard cocktail were prepared as per manufacturer's instructions. The standard cocktail was used for the top standard (S7) and a 1:4 serial dilution was performed using assay buffer to prepare S6-S1. Assay buffer was used as blank for S0. A 96-well V-bottom plate was used for this assay. Standards and samples were run in duplicates in vertical configuration for ease of data acquisition and analysis on the LEGENDplex software. 25 µl of Matrix B solution and 25 µl of each standard (S0-S7) were added to each of the standards wells. Thawed samples were pulse centrifuged prior to use. For the sample wells, 37.5 µl of assay buffer and 12.5 µl of each sample were added. Next, 25 µl of beads were added to each well, after vortexing for one minute to allow resuspension of beads. For each of the incubation steps, the plate was sealed using a plate sealer, wrapped in aluminium foil to protect from light and incubated at RT on a plate shaker at 800 rpm. The first incubation step was for two hours and was followed by centrifugation. For each of the centrifugation steps, the settings of 250 RCF for 5 minutes were used, thereafter, the supernatant was discarded into the sink, and the plate gently blotted once on a stack of paper towels. The plate was then washed by adding 200 µl of wash buffer, incubating for 1 minute and then centrifuging and discarding the supernatant. Following a 1:2 dilution with assay buffer, 25 µl of detection antibodies was added to each well and the plate

was incubated for one hour. Next, 25 µl of SA-PE, diluted 1:2 with assay buffer, was added to each well and the plate incubated for 30 minutes. The plate was centrifuged and supernatant discarded, followed by addition of 150 µl of wash buffer into each well, which was gently pipetted up and down to resuspend the beads. The samples were read on a flow cytometer within 4 hours.

LEGENDplex 13-plex cytokine assay flow cytometry set up

A BD LSR Fortessa flow cytometer with high-throughput sampler (HTS) was used. Phycoerythrin (PE) was used as the reporter channel (575-585 nm) and APC used as the classification channel (660 nm). The cytometer was started according to the manufacturer's recommendations. The LEGENDplex guide was followed to create a template for data acquisition and to set up the photomultiplier tube (PMT) voltages using the set-up beads and the FACSDiva software (Version 6.0). The HTS was used for rapid automated sample acquisition and the total events per well were limited to 10,000. This approach allowed acquisition of greater than 100 events per analyte as recommended by the manufacturer and prevented the experiment from being excessively time consuming.

LEGENDplex 13-plex cytokine assay data acquisition

The LEGENDplex Data Analysis Software Suite was used for initial quality control (QC) checks. The flow cytometry files were loaded onto the software and the automated gating of bead population was reviewed for any misclassifications. A 5-parameter logistic (PL) equation was used to fit the standard curves using logistic regression. The threshold for the R^2 value, which is a statistical measure of how closely the regression line fits the standard curve data, was set at > 0.95. A minimum of 100 events were required for each bead and the coefficient of variation (between replicates) threshold was set at < 30%. For values which were lower than the lower limit of detection, the software was able to provide estimated results. For values higher than the upper limit of detection, the highest concentration on the standard curve of that analyte was used.

3.2.4.3 MSD U-Plex assay for multiplex cytokine testing

The principles of the MSD immunoassays have been described previously. U-PLEX MSD assays were used as they allow custom design of multiplex assays. In these assays, biotinylated capture antibodies are conjugated to U-PLEX linkers, which then bind the specific spots on the plate. The principles of the U-PLEX assay are shown in Figure 3-10. The following four cytokines were selected: IL2, IL17A, IL4 and IL13. IL2 was selected as it is primarily produced by activated T cells and is involved in activation and proliferation of $CD4^+$ T cells and Tregs. IL17A was included as it is associated with Th17 cells and promotes generation of inflammatory cytokines and chemokines. IL4 and IL13 were selected to assess the type II immune response, along with IL10 which is included in the LEGENDplex panel.

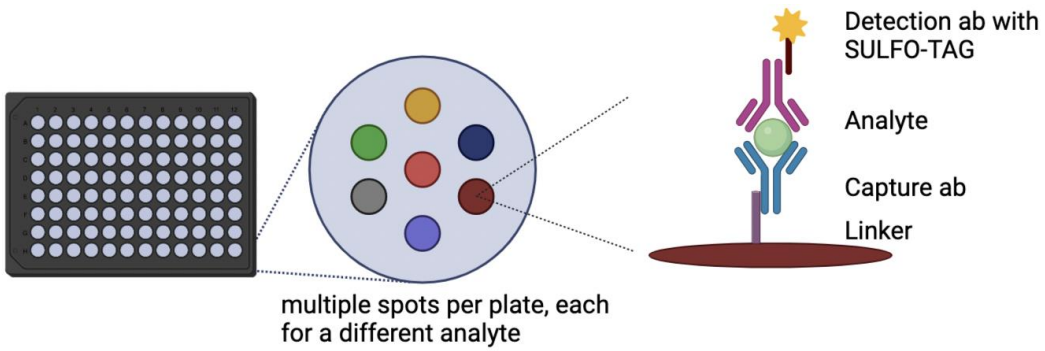

Figure 3-10 Principles of the U-PLEX Mesoscale Discovery assay.

Each well has multiple spots. Linkers are used to bind a capture antibody (ab) to a particular spot. The target analyte will bind to the capture antibody, and this is detected by anti-human antibodies conjugated with electrochemiluminescent labels (SULFO-TAGs) which emit light when stimulated with electricity. This figure was made using Biorender.

MSD 4-plex assay laboratory protocol

Supernatant samples from the SARS-CoV-2 QuantiFERON assay were thawed on ice. The MSD U-PLEX assay kit and all the reagents were brought to RT prior to use. Wash buffer was prepared as per manufacturer's instructions. Each biotinylated capture antibody was assigned a unique Linker (Figure 3-11) and 1x Linker-coupled antibody coating solution was prepared as per manufacturer's instructions. 50 µl of the coating solution was added to each well, the plate was sealed and incubated at RT on a plate shaker at 850 rpm for one hour. The plate was washed three times, by addition of 150 µl of wash buffer into each well and subsequent decanting. After the third wash, the plate was gently tapped on a paper towel to remove any residual fluid. Next, the standards solution was reconstituted as per manufacturer's instructions. 30 µl of each calibrator corresponding to individual analytes, was

added to the standards solution (4x). Assay diluent was added to make up a 1x solution of the top standard (S1). A serial dilution of 1:4 was carried out using assay diluent to generate a total of 7 standards (S1-S7). Assay diluent was used as a blank, S8. Thawed samples were pulse centrifuged prior to use. 25 µl of assay diluent was added to each well, followed by 25 µl of standards to each of the standards wells and 25 µl of sample to each of the samples well. Samples were run in singlicates. The plate was incubated for one hour, followed by three washes. 50 µl of 1x detection antibody solution was added to each well and the plate was incubated for one hour. The plate was washed again three times and thereafter, 150 µl of read buffer was added to each well and the plate was analysed using an MSD plate reader.

Linker 1: IL4
Linker 2: IL13
Linker 3: IL2
Linker 8: IL17A

Figure 3-11 Spot map for the U-PLEX assay with four active spots.

Linker numbers were allocated to each capture antibody. This figure was made using Biorender.

MSD 4-plex assay data acquisition

Data were acquired using the MSD plate reader (MESO SECTOR S 600 MM) and the Methodical Mind Software. The data were exported as a text file to the Discovery Workbench Application (Version 4.0) for generation standard curves (using a 4 PL algorithm and R^2 threshold of > 0.95) and calculation of the concentrations of analytes measured. QC acceptance criteria were defined as coefficient of variation between replicates < 30%. For results with values below the lower limit of detection, the software estimated values were used. For values above the detection threshold, the top concentration from the standard curve of that analyte was used.

3.2.4.4 Mass cytometry

Mass cytometry was carried out on a subset of samples from the SARS-CoV-2 QuantiFERON assay, following stimulation with nil, ag1 and mitogen. The same experiment was carried out on whole blood samples taken prior to stimulation from the same individuals by Dr Michael Carter (Figure 3-8). Samples were stained for cell surface markers (activation/proliferation/exhaustion/apoptosis) and intracellular cytokines (IL2, IL6, TNFα, IFNγ) to allow a comprehensive assessment of immune cell phenotype, function and cytokine production.

Mass cytometry or cytometry at time-of-flight (Cy-TOF) allows phenotypic and functional analysis of single cells. It uses similar principles of flow cytometry, however the antibodies used to stain cells/beads are labelled with heavy metal ion tags rather than fluorochromes. Metal ions form discrete, non-overlapping, isotopic peaks, which removes the need for compensation, reduces background autofluorescence, and increases the number of reporter antibodies that can be used per sample[383,384]. A barcoding approach is often used for mass cytometry. This entails tagging individual samples with a unique "barcode", using different combinations of metal ion tags, then pooling the samples so they can be run together, This reduces technical variability and enhances throughput[385,386]. Following staining, cells are passed in a single cell suspension into a nebuliser, which places cells into droplets for introduction into the mass cytometer. Individual cells pass through argon plasma at over 6700°C, which vaporises the cell into a cloud of single-atom ions, which are subsequently filtered by a quadrupole, leaving only the heavy metal ions tagged to the staining antibodies[384]. In the time-of-flight analyser, the ions are separated based on their velocity as they travel through a flight region, and the ion counts are converted to electrical potential signals for analysis[384].

The list of antibodies and metal tags used for barcoding and surface markers and intracellular cytokines are shown in Table 3-11 and Table 3-12 respectively and the experiment protocol is shown below. Antibodies were purchased from Fluidigm (California, United States) unless specified otherwise.

Table 3-11 Barcoding mastermix antibodies and metal ion tags.

Sample	Antibody conjugated with metal isotopes
Sample 1	CD45-106Cd
	CD45-110Cd
Sample 2	CD45-106Cd
	CD45-198Pt
Sample 3	CD45-106Cd
	CD45-89Y
Sample 4	CD45-110Cd
	CD45-198Pt
Sample 5	CD45-110Cd
	CD45-89Y
Sample 6	CD45-198Pt
	CD45-89Y

Table 3-12 Antibodies and metal ion tags for cell surface and intracellular cytokine staining.

Cell surface staining antibodies	Metal Tag
CD3 UCHTP1 (Biolegend)	111Cd
CD4 RPA-T4 (Biolegend)	113Cd
CD25 (2A3)	169Tm
CD127/IL-7Ra (A019D5)	176Yb
CD45RO (UCHL1)	149Sm
HLA-DR (G46- 6)	151Eu
CD197/CCR7 (G043H7)	167Er
CD45RA (HI100)	155Gd
CD38 HB-7 HIT2 (Biolegend)	161Dy
CD8a RPA-T8 (Biolegend)	116Cd
TCR $\boldsymbol{\gamma\delta}$ (11F2)	152Sm
CD19 HIB19 (Biolegend)	112Cd
CD14 RMO52 M5E2 (Biolegend)	114Cd
CD15 W6D3 (Biolegend)	142Nd
CD16 (3G8)	209Bi
CD20 (2H7)	171Yb

Table 3-12 continued.

Cell surface staining antibodies	**Metal Tag**
CD11c (Bu15)	159Tb
CD27 (L128)	162Dy
CD5 UCHT2 (Biolegend)	141Pr
CD64 10.1 (Biolegend)	116Cd
CD278/ICOS (C398.4A)	143Nd
CD11b/Mac-1 (ICRF44)	144Nd
CD223/LAG-3 (11C3C65)	150Nd
CD10 HI10a	156Gd
CD134/OX40 (ACTP35)	158Gd
CD95/Fas DX2 (Biolegend)	163Dy
CD161 (HP- 3G10)	164Dy
CD206/MMR (15-2)	168Er
CD279/PD-1 (EH12.2H7)	174Yb
CD28 (CD28.2)	160Gd
Intracellular cytokines staining antibodies	Metal Tag
IL6 (MQ2- 13A5)	154Sm
IFNγ (B27)	165Ho
TNFα (MAb11)	146Nd
IL2 MQ1-17H12 (Biolegend)	145Nd

Mass cytometry sample collection

Following SARS-CoV-2 QuantiFERON assay incubation, 100 µl of blood was taken from each of the three tubes: SARS-CoV-2 ag1, mitogen (mit) and negative control (nil) and transferred to three cryovials containing 100 µl of cell stabilisation solution (1:1). The cryovial was inverted 10 times to gently mix the blood with the cell stabilisation solution, then incubated at RT for 10 minutes before transferring to -80°C storage.

Mass cytometry laboratory protocol

Buffers and solutions were prepared as per manufacturer's instructions and kept at RT. One 15 ml falcon tube per sample was labelled and prepared with 2.5 ml of fixation buffer and 250 µl of 0.5mM EDTA. Mass cytometry samples were thawed in a water bath set at 37°C. 200 µl of each sample was pipetted into the prepared falcon tubes and incubated at RT for 15 minutes. The samples were centrifuged at 800 RCF for 5 minutes and supernatant aspirated. Five ml of lysis buffer was added to each falcon tube, gently mixed by inverting and incubated at RT for 15 minutes. During this incubation period, the cell surface antibodies mastermix was thawed on ice. The samples were centrifuged at 1000 RCF for 5 minutes and the supernatant aspirated. All the centrifugation steps had the same setting unless specified. Next, the cells were washed by gently resuspending with 10 ml of wash buffer and then centrifuged. The supernatant was aspirated, and the cells were resuspended with 500 µl of wash buffer and transferred to a microcentrifuge tube. To ensure all the cells are transferred from the falcon tube, a further 500 µl of wash buffer was added to the falcon tube and mixed prior to adding to the microcentrifuge tube (total volume 1000 µl per tube). The samples in the microcentrifuge tubes were centrifuged and supernatant was aspirated. Cells were resuspended in 50 µl of Fc receptor blocking solution, gently mixed and incubated at RT for 10 minutes. The samples were centrifuged and the supernatant aspirated. The cell surface antibodies mastermix was vortexed and then 100 µl was added to each sample tube and gently pipetted to mix. Thereafter, the samples were incubated at RT for 30 minutes. During the incubation period, the intracellular cytokine antibodies were thawed on ice. Following incubation, one ml of cell staining buffer was added to each tube to wash the cells, followed by centrifugation and removal of supernatant. This was repeated. Next, the cells were resuspended in one ml of fix and perm buffer and incubated for 10 minutes at RT. The samples were centrifuged and supernatant discarded and cells resuspended with one ml of fix and perm buffer and centrifuged again. After removal of the supernatant, the cells were resuspended in 50 µl intracellular cytokine solution. The total volume in each tube was brought up to 100 µl with fix and perm buffer. This was followed by 30 minutes incubation at RT. After incubation, cells were washed by addition of one ml of cell staining buffer to each tube, centrifuging, and aspiration of supernatant. The wash step

with the cell staining buffer was repeated. The cells were resuspended in one ml of intercalation solution, gently vortexed and incubated at RT for 30 minutes. The supernatant was discarded and cells resuspended in residual intercalation solution and stored at -80°C. Samples were thawed and manufacturer's cell retrieval protocol was followed prior to addition of element calibration beads and data acquisition at the NIHR BRC Flow Core Facility. The mass cytometry data were de-barcoded, QC carried out and manual and automated cell gating performed to obtain cell proportion and cell expression data.

3.2.4.5 RNA sequencing

RNA sequencing (RNA-seq) is a high-throughput technique used for examining the quantity and sequences of the total cellular content of RNA in a sample. Briefly, total RNA is extracted from the sample and reverse transcribed into complementary DNA (cDNA) libraries. The cDNA libraries are sequenced using next-generation sequencing technologies, generating millions of short sequence reads. The reads are aligned to a reference genome to determine their origin and for quantification or can be assembled to discover novel transcripts[387]. One of the primary applications of RNA-seq is differential gene expression analysis across different samples or conditions for biomarker discovery or for characterisation of the biology. The laboratory methods for RNA extraction are described briefly below, with further details reported in Jackson et al.[257].

Sample collection and RNA extraction

Samples were collected from patients recruited into the EUCLIDS, PERFORM and DIAMONDS studies, at the earliest timepoint after hospital attendance, prior to any immunomodulatory treatment. Whole blood was collected into PAXgene Blood RNA vacutainers (Pre-Analytix, Germany) and stored at –80^{o}C. Total RNA was extracted, using RNA extraction kits as per manufacturer's recommendation and was followed by DNAse treatment. The sample integrity and quality were assessed using Nanodrop™ spectrophotometer (Thermo Fisher Scientific, United States), QIAxcel (Qiagen, The Netherlands), Bioanalyser (Agilent Technologies, United States) and Qubit fluorometer (Invitrogen, United States) prior to plating for sequencing. The samples were sequenced at The Wellcome Centre for Human Genetics in Oxford, UK.

3.3 Data analysis

All of the data analysis for this thesis was performed using R Statistical Computing Language (R programming: Version 4.2.1, 23.06.2022)[388] in R Studio (Version 421 2.04.2022)[389], and GraphPad Prism software (Version 99.4.1, 18.07.2022)[390]. Significance level was set at a p value of < 0.05 for all the analyses performed. The specific R packages used, pre-processing and QC protocols and data analysis methods will be described in each results chapter.

Chapter 4: The role of antibodies in SARS-CoV-2 associated diseases

4.1 Introduction

As the COVID-19 pandemic progressed, it quickly became apparent that while significant numbers of adults suffered severe disease, children were largely spared[391,392]. This is notable because most other respiratory viruses affect the very young and the elderly with two peaks of disease susceptibility[150]. I sought to test the hypothesis that pre-existing antibodies against seasonal coronaviruses (e.g. HCoV-OC43), which may have accumulated in adults during their lifetime, contribute to the severe disease through an antibody dependent enhancement mechanism. Early studies noted the relationship between SARS-CoV-2 IgG titres and COVID-19 severity in adults[66,67,69]. Consequently, I investigated the role of seasonal coronavirus antibodies and SARS-CoV-2 specific antibodies in severity of paediatric COVID-19. This analysis was extended to include MIS-C, as the timing of the disease, which occurs several weeks after exposure to SARS-CoV-2 when antibodies are being produced, suggests that antibodies may play a role in driving the immunopathology in MIS-C. Understanding the relationship between antibodies and disease severity could provide valuable insights into the mechanisms underlying the distinct manifestations of SARS-CoV-2 infections across different age groups. Not only that, but it also holds important implications for vaccine development and delivery strategies.

<u>The primary aim of this chapter is:</u>

To ascertain the role of cross-reactive seasonal coronavirus antibodies and SARS-CoV-2 specific antibodies in SARS-CoV-2 associated diseases.

<u>The objectives of this chapter are:</u>

1) Measure and compare titres of seasonal coronavirus (HCoV-OC43) antibodies in pre-COVID-19 samples from children and adults of different ages to investigate the potential contribution of cross-reactive antibodies to age-related differences seen in COVID-19.
2) Measure and compare titres of seasonal coronavirus (HCoV-OC43) antibodies in samples taken during the COVID-19 pandemic from different disease groups (COVID-19, MIS-C, KD, febrile controls) to investigate the potential contribution of cross-reactive antibodies to disease severity in COVID-19 and MIS-C.

3) Measure and compare titres of SARS-CoV-2 specific antibodies across different disease groups (COVID-19, MIS-C, KD, febrile controls) to investigate the potential contribution of SARS-CoV-2 specific antibodies to disease severity in COVID-19 and MIS-C.

The key findings from this chapter are:

The work in this chapter contributes to the understanding of the role of seasonal coronavirus antibodies and SARS-CoV-2 specific antibodies in COVID-19 and MIS-C. At the beginning of the COVID-19 pandemic, little was known about these diseases and many hypotheses were being rapidly tested to gain better understanding of these new diseases. ADE leading to COVID-19 disease severity in adults, was a critical hypothesis to address. This work provides evidence against ADE as a reason for age-related differences seen in COVID-19 disease severity. Moreover, while early studies had shown a relationship between SARS-CoV-2 IgG titres and COVID-19 severity in adults, this trend was not observed in the paediatric COVID-19 and MIS-C cohort studied in this chapter. Overall, this research helps to advance the understanding of COVID-19 and MIS-C, informs future research studies, and has implications for vaccine strategies.

4.2 Methodology

4.2.1 Clinical cohorts and study design

To investigate age-related differences in levels of seasonal coronavirus antibodies, I identified and assembled serum samples collected during the early/pre-COVID-19 pandemic era, from individuals representing a diverse age group. To understand the role of SARS-CoV-2 specific antibodies in the severity of SARS-CoV-2 associated disease, I assembled samples from adult COVID-19, paediatric COVID-19, MIS-C, healthy paediatric controls, and febrile paediatric controls collected during the COVID-19 pandemic (2020-2022). The paediatric febrile controls were from DIAMONDS and included children with bacterial illness (definite bacterial and probable bacterial), viral illness (definite viral and probable viral), inflammatory disease (non-SARS-CoV-2 associated) and KD. Further details of the DIAMONDS clinical phenotyping can be found in Chapter 3 (section 3.1.1.2). Patients and controls were recruited into multiple studies in the UK and across Europe. Table 4-1 summarises the clinical cohorts included for the work presented in this chapter. Further details of the individual studies from which these patients were recruited can be found in Chapter 3 (section 3.1).

Table 4-1 Summary of the clinical cohorts selected for antibody testing.

Cohort	Criteria for selection	Study
Pre-pandemic adults	> 18 years of age Sampled prior to the COVID-19 pandemic	IDEA study
Pre-pandemic children	< 18 years of age Sampled prior to the COVID-19 pandemic	EUCLIDS, Fever in Children study, Genetic determinants of KD for susceptibility and outcome study
Early COVID-19 pandemic: Asymptomatic Elderly	> 70 years of age No acute febrile illness Sampled early in the COVID-19 pandemic	DELPHIC
COVID-19 pandemic: Symptomatic Elderly	> 70 years of age Symptoms of COVID-19 Sampled during the COVID-19 pandemic	DELPHIC

Table 4-1 continued.

Cohort	Criteria for selection	Study
COVID-19 pandemic: Febrile children	< 18 years age Admitted to hospital with a febrile illness (Bacterial/Viral/Inflammatory/KD/COVID-19/MIS-C) Sampled during the COVID-19 pandemic	DIAMONDS
COVID-19 pandemic: Adult COVID-19	> 18 years of age Symptomatic COVID-19	DIAMONDS, IHKB

4.2.2 Coronavirus antibody fluorescence-activated cell sorting (FACS) assay

H-CoV-OC43 Nucleocapsid (N), SARS-CoV-2 N and SARS-CoV-2 Spike (S) IgG, IgM and IgA antibodies were measured using a FACS-based assay. Briefly, HEK293T cells expressing coronavirus antigens were treated with patient plasma and incubated with anti-human IgG/IgM/IgA conjugated with a fluorophore. The intensity of the fluorophores was measured using a flow cytometer, which correlated with antibody titres. The detailed laboratory method can be found in Chapter 3 (section 3.2.2.1).

4.2.3 Data analysis

4.2.3.1 FACS-based assay threshold

The antibody titre results were determined using fluorescence intensity (absorbance units (a.u.)) and the threshold for a definite positive antibody titre result was set at > 2.0, definite negative at < 1. Results between 1-2 were considered indeterminant. Indeterminant results were excluded from the analyses, specifically for the non-continuous data analysis where definitive positive and negative results were required.

These thresholds were set by the laboratory team following assay optimisation as described in Ng et al.[180]. Though they serve as assay-specific benchmarks, it's important to acknowledge potential variations in biological thresholds. Furthermore, when exploring trends or correlations in values below these established cut-offs, it's crucial to consider the limitations. Weak correlations with borderline significance may pose challenges in interpretation, as values near the thresholds may lack the robustness required for definitive conclusions.

4.2.3.2 Assessment of batch effects threshold

As the samples were run across multiple plates, the data were assessed for batch effects, using principal component analysis (PCA). PCA is a statistical method that allows unsupervised analysis of the data variance, by reducing the dimensions of a large dataset into a few principal components (PCs) which explain the greatest variation in the data.

4.2.3.3 Laboratory markers quality control (QC)

The laboratory markers underwent QC check prior to data analysis. The QC criteria were as follows:

- Each laboratory marker unit was checked and values were converted to conventional UK unit values.
- Data distribution was assessed for any skewness or abnormalities. Data points that deviated significantly were reviewed individually to check if the results were consistent with other related blood markers e.g. total white blood cells (WBCs) matched the total of the WBC differential (neutrophils + lymphocytes + monocytes + eosinophils).
- Extreme outliers where there are no explanations for the deviation (e.g. different units/decimal point in the incorrect place) and which are not consistent with other blood markers and clinical information (e.g. creatinine of 1744 but normal urea in a previously well patient with a mild viral illness) were excluded from the analysis.

4.2.3.4 Age-related analyses

The age-related analyses included children (< 18 years) and adults (18-70 years) sampled prior to the COVID-19 pandemic and healthy asymptomatic elderly adults (greater than (>) 70 years) sampled early in the COVID-19 pandemic (pre-pandemic cohort). The correlation between HCoV-OC43 and SARS-CoV-2 antibody levels and age was assessed using Spearman rank's correlation, which is suitable for assessing relationships between continuous variables which do not follow a normal distribution. Wilcoxon pairwise comparisons were performed to assess the relationship between sex and antibody levels of HCoV-OC43 and SARS-CoV-2. Only Nucleocapsid (N) IgG, IgM and IgA were tested for both viruses. These analyses may offer insights into the potential role of pre-existing immunity in explaining the sex differences observed in COVID-19 severity.

4.2.3.5 Cross-reactive antibodies

To investigate the impact of pre-existing immunity and assess for potential cross-reactivity, Spearman rank's correlation was used to examine the relationship between HCoV-OC43 (N) and SARS-CoV-2 (N and S) antibody levels in both the pre-pandemic and pandemic cohorts. The pandemic cohort comprised of children (COVID-19, MIS-C, febrile controls), adults (COVID-19) and elderly (asymptomatic, symptomatic for COVID-19) sampled during the COVID-19 pandemic.

To further evaluate the effects of pre-existing immunity, the relationship between HCoV-OC43 antibody titres and COVID-19 within different age groups, as well as among individuals with and without COVID-19, was investigated by comparing median HCoV-OC43 antibody titres across cohorts sampled during the COVID-19 pandemic. Wilcoxon pairwise comparisons were performed, with correction for multiple testing (as > 10 comparisons) using the Benjamini Hochberg (BH) method[393].

4.2.3.6 SARS-CoV-2 specific antibodies and disease severity

Paediatric COVID-19

Spearman rank's correlation was used to assess the relationship with SARS-CoV-2 specific antibody levels and clinical and laboratory markers associated with disease severity. The laboratory markers recorded during acute illness, including maximum CRP, maximum neutrophils, and minimum lymphocytes were used. Length of PICU admission and length of hospital admission were used as clinical markers of severity. To further assess clinical severity, each patient was assigned a maximal disease severity score during their hospital admission, which was adapted from the WHO COVID-19 ordinal severity scale[394] (Table 4-2). Since all the samples from the paediatric COVID-19 cohort were from hospitalised patients, the scores ranged from 3-8. Children with trivial illness and negative SARS-CoV-2 PCR, who were recruited to DIAMONDS, were selected as uninfected controls and assigned a score of "0". The antibody levels were compared across severity groups using Wilcoxon pairwise comparisons with BH correction for multiple testing.

Adult COVID-19

The analyses for adult COVID-19 patients were performed by Dr Claire Broderick. Each patient was assigned a maximal WHO ordinal severity score for COVID-19 during their acute illness (Table 4-2). An

additional category "11" was added to include patients with a severity score of "3" who were admitted to hospital for reasons other than COVID-19. Levels of SARS-CoV-2 antibodies were plotted against the severity scale and symptom duration.

Table 4-2 COVID-19 disease severity scale, adapted from the World Health Organisation COVID-19 ordinal severity scale[394].

Patient State	Descriptor	Score
Uninfected	No clinical or microbiological signs of infection	0
Ambulatory	No limitations of activities	1
	Limitations of activities	2
Hospitalised – mild disease	Hospitalised, no oxygen therapy	3
	Oxygen via mask/nasal prongs	4
Hospitalised – severe disease	High-flow oxygen or Non-invasive ventilation	5
	Invasive ventilation	6
	Invasive ventilation + additional organ support including vasopressors, renal replacement therapy or extracorporeal membrane oxygenation	7
Death	Patient died	8
Hospitalised – mild disease (adults only)	SARS-CoV-2 positive, but admitted to hospital for reasons other than COVID-19	11

MIS-C

Spearman rank's correlation was used to assess the relationship between SARS-CoV-2 specific antibody levels and clinical and laboratory markers of severity, including: maximum CRP, maximum neutrophils, minimum lymphocytes, maximum troponin, length of PICU admission and length of hospital admission. Each patient was assigned a disease severity score (Table 4-3), using an adapted version of the MIS-C disease severity scale used for the severity prediction analyses presented in Chapter 6. The antibody levels were compared across severity groups using Wilcoxon pairwise comparisons with BH correction for multiple testing.

The relationship between SARS-CoV-2 specific antibody and presence of cardiac complications in MIS-C was assessed using Spearman rank's correlation for continuous variables (troponin levels, coronary artery diameter, coronary artery z-score) and by Wilcoxon pairwise comparisons for categorical variables (presence/absence of left ventricular dysfunction, low cardiac output, myocarditis, and valvular regurgitation on echocardiogram). The echocardiogram findings were extracted from reports written by specialists performing the scan.

Table 4-3 MIS-C disease severity scale.

Severity	**Descriptor**	**Score**
Mild	Admitted on a ward No other support	1
Moderate	Oxygen therapy AND/OR Non-invasive ventilation AND/OR PICU admission	2
Severe	Invasive ventilation OR Vasopressors	3
Very Severe	Invasive ventilation AND Vasopressors OR Invasive ventilation AND renal replacement therapy / extracorporeal membrane oxygenation OR Vasopressors AND renal replacement therapy / extracorporeal membrane oxygenation OR Invasive ventilation AND Vasopressors AND renal replacement therapy / extracorporeal membrane oxygenation	4
Death	Patient died	5

4.3 Results

The following section presents the results obtained from the analysis of the HCoV-OC43 N and SARS-COV-2 N and S IgG, IgM and IgA antibody levels from pre- and post-COVID-19 pandemic cohorts. The results presented are organised according to the chapter objectives: 1) age-related effects 2) cross-reactive antibodies 3) SARS-CoV-2 IgG specific antibody titres and severity of SARS-CoV-2 associated diseases. Table 4-4 provides a summary of the number of participants in each cohort and type of coronavirus antibody assay performed. The results of the principal component analysis did not indicate any significant batch effects between plates (Appendix 3 Figure A3-1).

Table 4-4 Summary of the number of participants and coronavirus antibody assays performed.

Cohort	**HCoV-OC43 N IgG/M/A (Number of participants)**	**SARS-CoV-2 N IgG/M/A (Number of participants)**	**SARS-CoV-2 S IgG/M/A (Number of participants)**
Pre-pandemic paediatric (< 18 years)	236	39	39
Pre-pandemic adults (18-69 years)	133	0	0
Early pandemic/ COVID-19 Pandemic Elderly (70+ years)	Asymptomatic/healthy: 89 Symptomatic for COVID-19: 112 TOTAL: 212	Asymptomatic/healthy: 89 Symptomatic for COVID-19: 112 TOTAL: 212	Asymptomatic/healthy: 89 Symptomatic for COVID-19: 112 TOTAL: 212
COVID-19 Pandemic febrile children (< 18 years)	MIS-C: 35 COVID-19: 4 Febrile controls: 54 TOTAL: 93	MIS-C: 203 COVID-19: 30 Febrile controls: 54 Trivial illness: 10 TOTAL: 297	MIS-C: 203 COVID-19: 30 Febrile controls: 54 Trivial illness: 10 TOTAL: 297
COVID-19 adults (> 18 years)	233	471	471

4.3.1 Age-related analyses

The analyses investigating age and sex related differences in antibody titres were performed on a total of 458 pre-pandemic samples tested for HCoV-OC43 N and SARS-CoV-2 N IgG, IgM and IgA antibodies. SARS-CoV-2 S antibody results were not included in these analyses as this assay was not performed on the adult cohort (18-70 years). The age range of the entire cohort was 0.1 to 95 years, with 236 children (< 18 years), 133 adults (18-70 years) and 89 elderly participants (> 70 years). The proportion of females in each age group was: children - 47% (112/236), adults - 44% (59/133) and elderly - 67% (60/89). The distribution of participants by age and sex is shown in Figure 4-1.

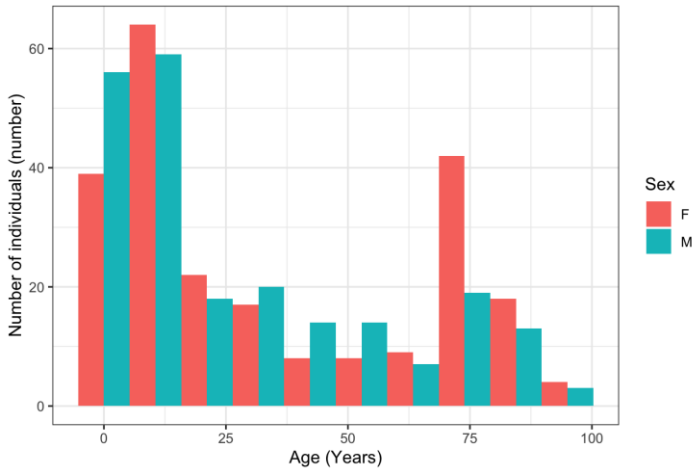

Figure 4-1 Histogram showing the age and sex distribution of the participants included in the age-related antibody analyses. F = female. M = Male. Total n = 458

Of the participants tested for HCoV-OC43 antibodies, 20% (n = 92) were positive for HCoV-OC43 N IgG, 4% (n = 20) were positive for IgM and 0% (n = 0) were positive for IgA (Table 4-5). None of the participants tested positive for SARS-CoV-2 N IgG, IgM or IgA (Table 4-5).

Table 4-5 Summary of HCoV-OC43 and SARS-CoV-2 antibody results for individuals sampled in the pre/early COVID-19 pandemic era. N = Nucleocapsid, n = Number of participants.

	Positive, n (%)	Negative, n (%)	Indeterminant, n (%)
HCoV-OC43 N IgG	92/458 (20.1%)	299/458 (65.3%)	67/458 (14.6%)
HCoV-OC43 N IgM	20/458 (4.4%)	384/458 (83.8%)	54/458 (11.8%)
HCoV-OC43 N IgA	0/458 (0%)	457/458 (99.8%)	1/458 (0.2%)
SARS-CoV-2 N IgG	0/458 (0%)	457/458 (99.8%)	1/458 (0.2%)
SARS-CoV-2 N IgM	0/458 (0%)	457/458 (99.8%)	1/458 (0.2%)
SARS-CoV-2 N IgA	0/458 (0%)	456/458 (99.6%)	2/458 (0.4%)

A weak negative correlation was seen between HCoV-OC43 N IgM and age (R = -0.49, p < 2.2 x 10^{-16}) (Figure 4-2B), however the majority of the results fell below the positive threshold (84% tested negative, Table 4-5). No significant correlation was observed between age and HCoV-OC43 N IgG and IgA (Figure 4-2A and Figure 4-2C). Although there were no positive results for SARS-CoV-2 antibodies, a weak negative correlation was seen between SARS-CoV-2 N IgG and age and SARS-CoV-2 N IgM and age (Figure 4-2D and Figure 4-2E). Additionally, although there were no positive results for HCoV-OC43 N IgA and SARS-CoV-2 N IgA, there was a trend of higher levels of IgA in both the young children and the elderly compared to the adults.

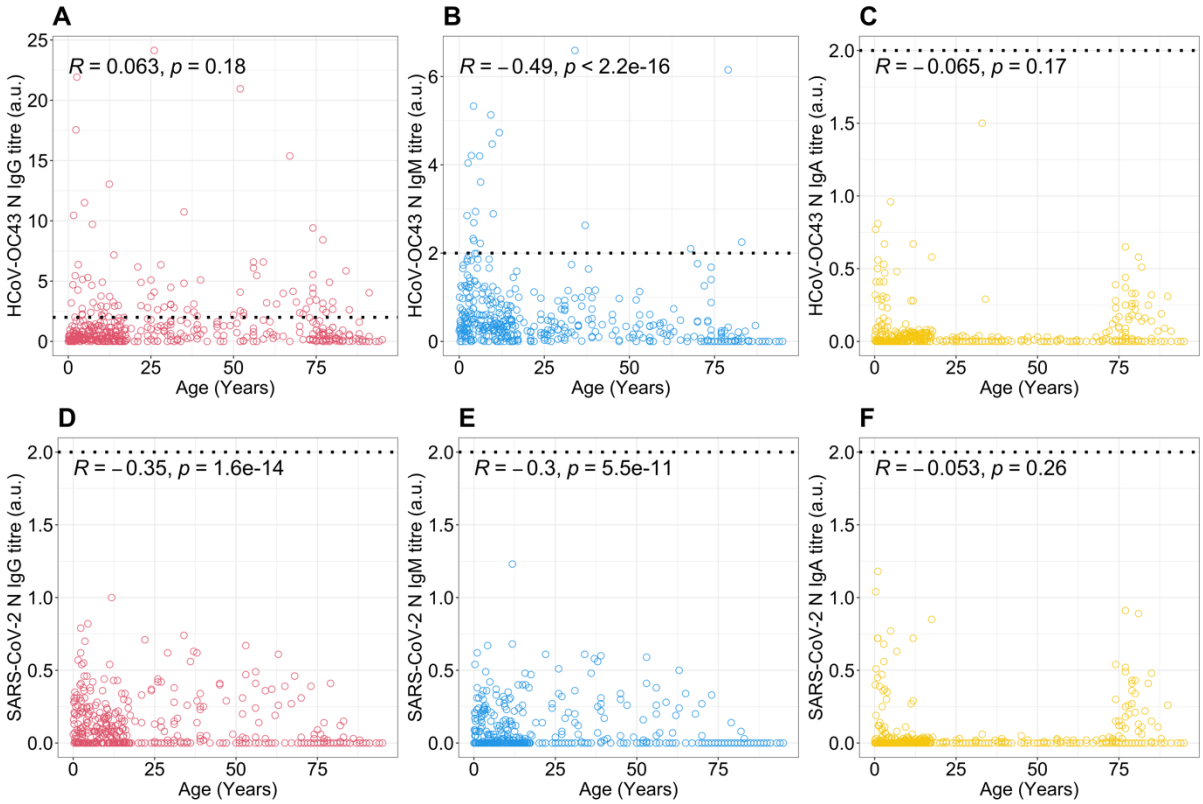

Figure 4-2 Scatterplots showing the relationship between age and titres of HCoV-OC43 Nucleocapsid (N) IgG (A), HCoV-OC43 N IgM (B), HCoV-OC43 N IgA (C), SARS-CoV-2 N IgG (D), SARS-CoV-2 N IgM (E) and SARS-CoV-2 N IgA (F) in pre-COVID-19 pandemic samples (n = 391-456).

The antibody titres were determined using fluorescence intensity measured in absorbance units (a.u.). The threshold for positive antibody level (> 2.0) has been demarcated by the horizontal dotted line. Spearman's correlation coefficient (R) and p value have been displayed on each plot.

When considering the effect of sex on antibody levels, HCoV-OC43 N IgM levels were higher in males compared to females (p = 0.001) (Figure 4-3B), but IgG and IgA levels did not differ significantly by sex (Figure 4-3A and Figure 4-3C). Although none of the SARS-CoV-2 antibody results met the threshold for positivity, SARS-CoV-2 N IgG and IgM titres were significantly higher in males (p = 0.005 and p = 0.0007, respectively) (Figure 4-3D and Figure 4-3E); no sex differences were observed for SARS-CoV-2 IgA titres.

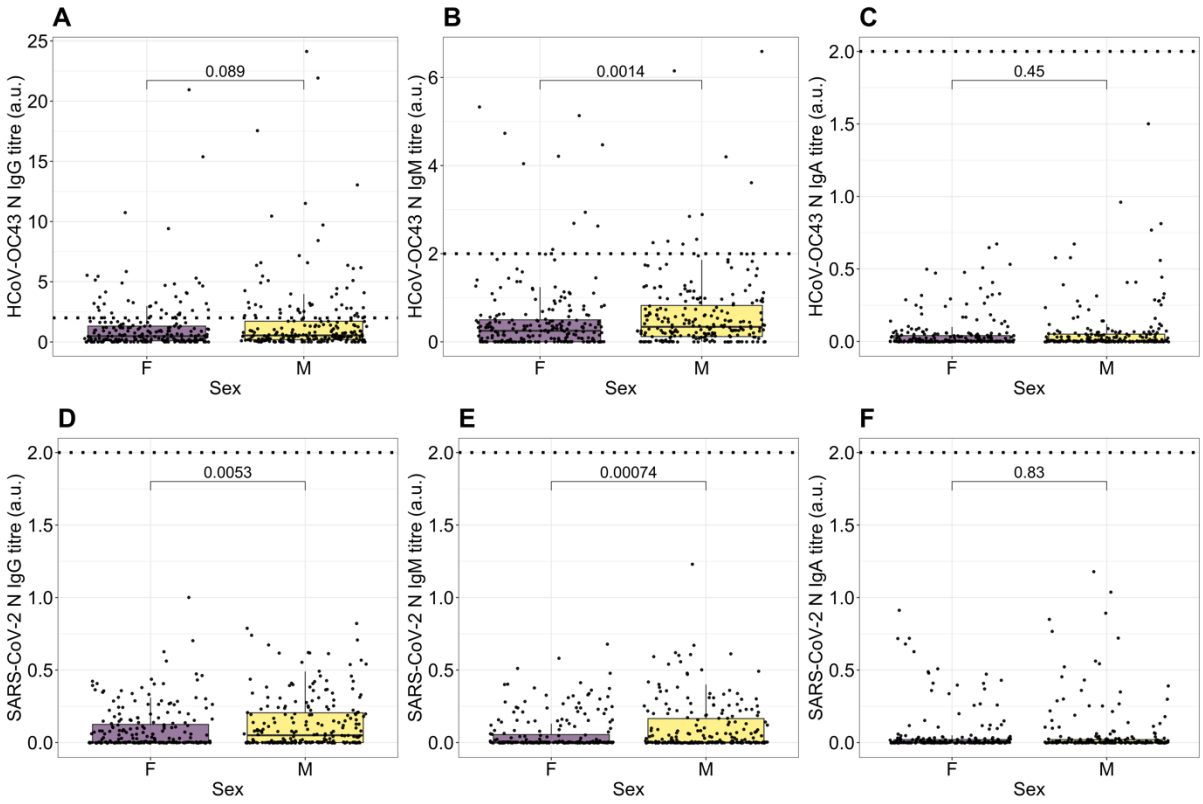

Figure 4-3 Boxplots showing titres of HCoV-OC43 Nucleocapsid (N) IgG (A), HCoV-OC43 N IgM (B), HCoV-OC43 N IgA (C), SARS-CoV-2 N IgG (D), SARS-CoV-2 N IgM (E) and SARS-CoV-2 N IgA (F) by sex: female (F) n = 231, male (M) n = 223.

The antibody titres were measured in absorbance units (a.u.). The threshold for positive antibody level (> 2.0) has been demarcated by the horizontal dotted line. P values from Wilcoxon pairwise comparison have been displayed.

4.3.2 Cross-reactive antibodies

4.3.2.1 Pre-COVID-19 pandemic samples

Figure 4-4 displays the scatterplots of HCoV-OC43 N antibodies (IgG, IgM and IgA) plotted against SARS-CoV-2 N and S antibodies (IgG, IgM and IgA) in pre-COVID-19 pandemic samples, to investigate for any potential cross-reactivity. Notably, none of the samples reached the positive threshold (> 2.0) for any of the SARS-CoV-2 N antibodies and only two individuals were positive for SARS-CoV-2 S antibodies (Figure 4-4), indicating the absence of substantial pre-existing immunity to SARS-CoV-2 in this pre-pandemic cohort. Although the majority of the results were below the positivity threshold, a weak positive correlation was observed between HCoV-OC43 N and SARS-CoV-2 N IgG, IgM and IgA titres and HCoV-OC43 N and SARS-CoV-2 S IgM and IgA titres, suggesting that there may be a degree of cross-reactivity between these antibodies.

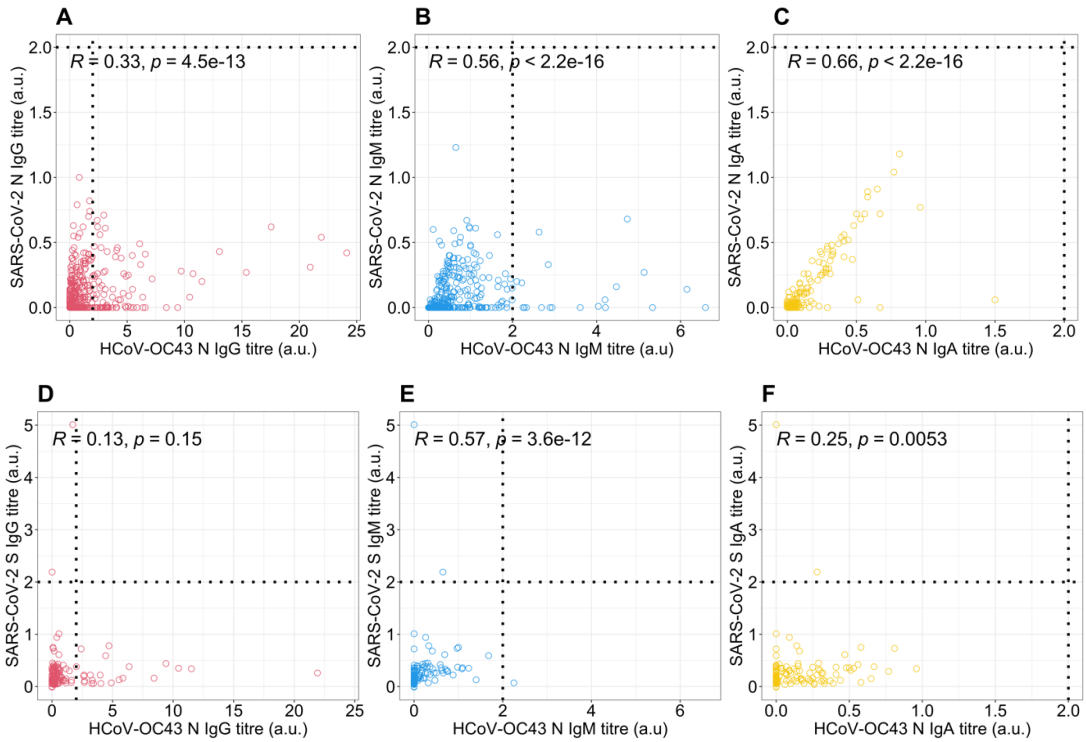

Figure 4-4 Scatterplots showing the relationship between HCoV-OC43 and SARS-CoV-2 antibody titres in the pre-COVID-19 pandemic samples.

*HCoV-OC43 Nucleocapsid (N) IgG titre and SARS-CoV-2 N IgG (**A**), HCoV-OC43 N IgM titre and SARS-CoV-2 N IgM (**B**), HCoV-OC43 N IgA titre and SARS-CoV-2 N IgA (**C**) (n = 456), HCoV-OC43 N IgG titre and SARS-CoV-2 Spike (S) IgG (**D**), HCoV-OC43 N IgM titre and SARS-CoV-2 S IgM (**E**), HCoV-OC43 N IgA titre and SARS-CoV-2 S IgA (**F**) (n = 128). The antibody titres were measured in absorbance units (a.u.). The thresholds for positive antibody level (> 2.0) have been demarcated by the horizontal and vertical dotted lines. Spearman's correlation coefficient (R) and p value have been displayed on each plot.*

4.3.2.2 COVID-19 pandemic samples

Samples taken from individuals during the COVID-19 pandemic were tested for HCoV-OC43 N and SARS-CoV-2 N and S IgG, IgM and IgA levels, to investigate the effect of pre-existing immunity and assess for potential cross-reactive antibodies. This included asymptomatic elderly (n = 89), symptomatic COVID-19 elderly (n = 112), adult COVID-19 (n = 233), paediatric COVID-19 (n = 4), MIS-C (n = 35) and paediatric febrile controls (n = 54).

On assessment of HCoV-OC43 titres by cohort, adults with COVID-19, children with MIS-C and paediatric febrile controls were found to have higher IgG titres than the asymptomatic and symptomatic COVID-19 elderly (Figure 4-5A). However, no significant differences were seen across the different cohorts when comparing only the positive HCoV-OC43 IgG titres (> 2.0) (Figure 4-6). Although significant differences were seen between the cohorts for IgM and IgA, the vast majority of the results (98.7% and 100% respectively) fell below the threshold required to be classified as positive (Figure 4-5B and Figure 4-5C).

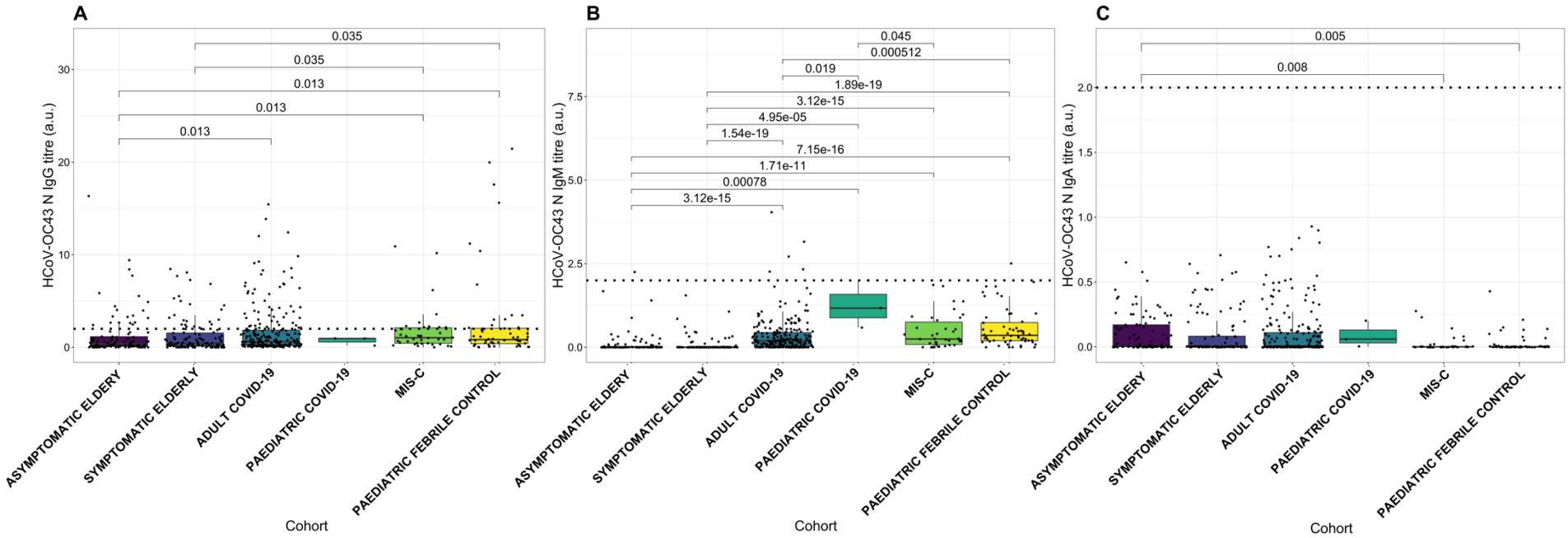

Figure 4-5 Boxplot showing titres of HCoV-OC43 Nucleocapsid (N) IgG (A), HCoV-OC43 N IgM (B), HCoV-OC43 N IgA (C) by disease groups from samples taken during the COVID-19 pandemic.

Asymptomatic elderly (n = 89), symptomatic COVID-19 elderly (n = 112), adult COVID-19 (n = 233), paediatric COVID-19 (n = 4), MIS-C (n = 38), paediatric febrile control (n = 56). The antibody titres were measured in absorbance units (a.u.). The threshold for positive antibody level (> 2.0) has been demarcated by the horizontal dotted line. Significant p values (< 0.05) from Wilcoxon pairwise comparisons with Benjamini Hochberg correction have been displayed.

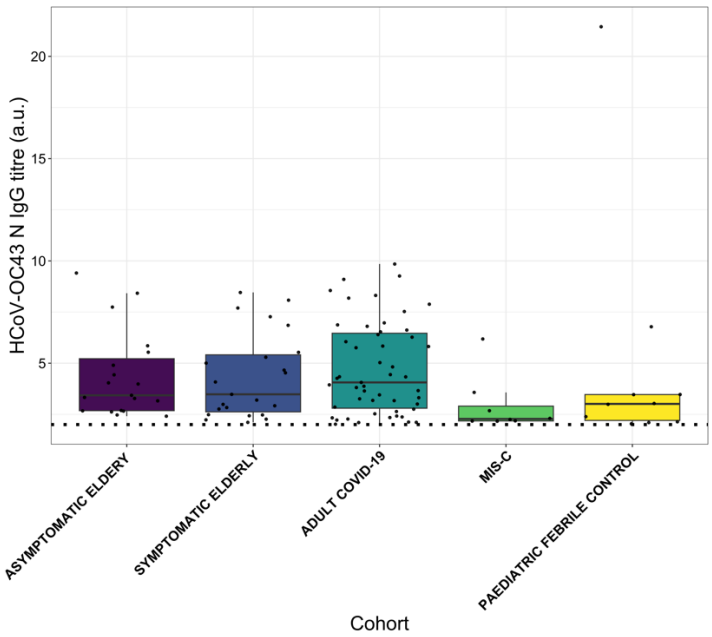

Figure 4-6 Boxplot showing titres of HCoV-OC43 Nucleocapsid (N) IgG which met the threshold for positive result (> 2.0) in samples taken from individuals during the COVID-19 pandemic.

Asymptomatic elderly (n = 19), symptomatic COVID-19 elderly (n = 23), adult COVID-19 (n = 51), MIS-C (n = 8), paediatric febrile control (n = 10). The antibody titres were measured in absorbance units (a.u.). Positive antibody level (> 2.0) has been demarcated by the horizontal dotted line. Significant p values (< 0.05) from Wilcoxon pairwise comparisons with Benjamini Hochberg correction have been displayed.

The analysis of the relationship between HCoV-OC43 and SARS-CoV-2 antibody levels revealed a positive correlation (Figure 4-7). Specifically, a weak positive correlation was observed between HCoV-OC43 N IgG and SARS-CoV-2 (N and S) IgG levels (Figure 4-7A and Figure 4-7D). Although the majority of participants tested negative for HCoV-OC43 N and SARS-CoV-2 (N and S) IgM and IgA antibodies, a weak positive correlation was observed between HCoV-OC43 and SARS-CoV-2 IgM and IgA titres (Figure 4-7).

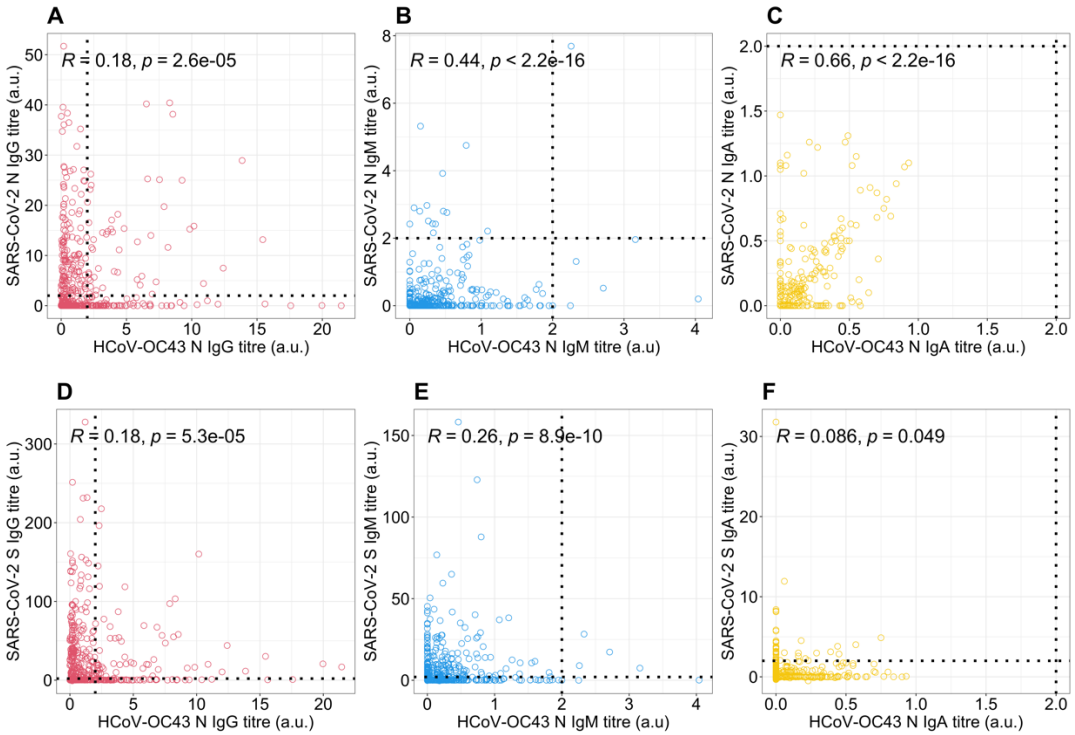

Figure 4-7 Scatterplots showing the relationship between HCoV-OC43 and SARS-CoV-2 antibody titres in the COVID-19 pandemic samples.

*HCoV-OC43 Nucleocapsid (N) IgG titre and SARS-CoV-2 N IgG (**A**), HCoV-OC43N IgM titre and SARS-CoV-2 N IgM (**B**), HCoV-OC43N IgA titre and SARS-CoV-2 N IgA (**C**) (n = 539), HCoV-OC43N IgG titre and SARS-CoV-2 Spike (S) IgG (**D**), HCoV-OC43N IgM titre and SARS-CoV-2 S IgM (**E**), HCoV-OC43 N IgA titre and SARS-CoV-2 S IgA (**F**) (n = 539). The antibody titres were measured in absorbance units (a.u.). Positive antibody level (> 2.0) has been demarcated by the horizontal and vertical dotted lines. Spearman's correlation coefficient (R) and p value have been displayed on each plot.*

4.3.3 SARS-CoV-2 specific antibodies and disease severity

4.3.3.1 Paediatric COVID-19

A total of 30 paediatric COVID-19 patients were included in the analysis. The median age was 13 years (Interquartile Range (IQR) 7.5-14 years) and 45% (n = 14) were female. Of the 30 patients, 20 (67%) required PICU admission, 12 (40%) required invasive ventilation, 7 (23%) required inotropic support and 2 (7%) patients died. The median length of hospital stay was 7 days (IQR 7-15 days) and median length of PICU stay was 4 days (IQR 0-8 days). SARS-CoV-2 S IgG was positive in 67% (n = 20), IgM positive in 37% (n = 11) and IgA positive in 27% (n = 8) (Table 4-6).

Table 4-6 SARS-CoV-2 antibody results in the paediatric COVID-19 cohort.

	Positive, n (%)	**Negative, n (%)**	**Indeterminant, n (%)**
SARS-CoV-2 Spike IgG	20/30 (66.7%)	9/30 (30%)	1/30 (3.3%)
SARS-CoV-2 Spike IgM	11/30 (36.7%)	18/30 (60%)	1/30 (3.3%)
SARS-CoV-2 Spike IgA	8/30 (26.7%)	5/30 (16.7%)	17/30 (56.7%)

Laboratory and clinical markers of disease severity

The median maximum CRP level was 43 mg/L (IQR 18-161 mg/L), the median maximum neutrophil count was 4.2 x 10^9/L (IQR 6.8-9.3 x 10^9/L) and the median minimum lymphocyte count was 0.5 x 10^9/L (IQR 0.9-1.7 x 10^9/L). A trend of positive correlation was seen between SARS-CoV-2 IgG titres and maximum neutrophil count (R = 0.31, p = 0.09) and SARS-CoV-2 IgM titres and maximum neutrophil count (R = 0.35, p = 0.06) (Figure 4-8B and Figure 4-8E). No association was seen between SARS-CoV-2 antibody titres (IgG and IgM) and maximum CRP or minimum lymphocyte count (Figure 4-8). SARS-CoV-2 IgG titres had no significant correlation with length of hospital stay or length of PICU stay in paediatric COVID-19 (Figure 4-9). The other clinical markers of severity (e.g. level of organ support) were not assessed individually as they were incorporated into the COVID-19 severity score.

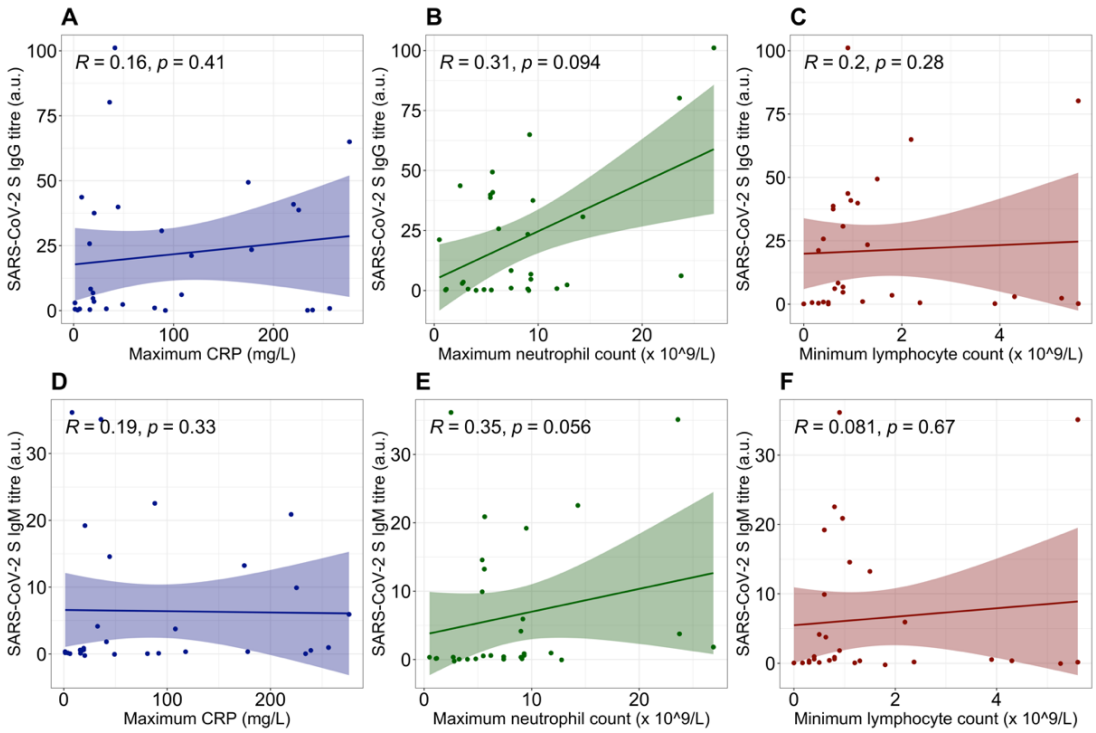

Figure 4-8 Scatterplots showing the relationship between SARS-CoV-2 Spike (S) IgG and IgM titres in paediatric COVID-19 (n = 30) and maximum C-reactive protein (CRP) (mg/L) (A,D), maximum neutrophil count (x 10^9/L) (B,E) and minimum lymphocyte count (x 10^9/L) (C,F).

The antibody titres were measured in absorbance units (a.u.). Spearman's correlation coefficient (R) and p value have been displayed on each plot, along with the regression line and 95% confidence intervals.

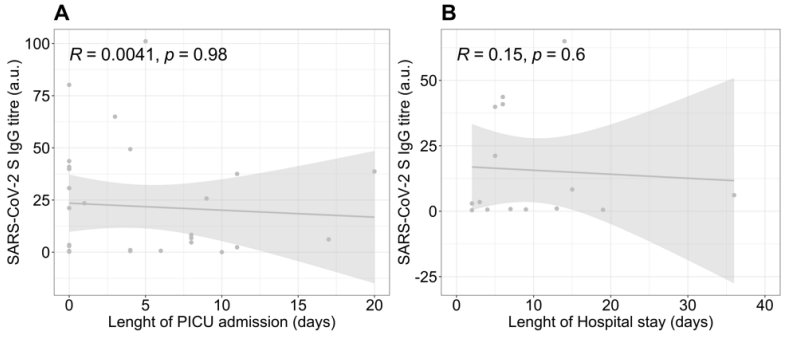

Figure 4-9 Scatterplots showing the relationship between SARS-CoV-2 Spike (S) IgG titres and length of paediatric intensive care unit (PICU) admission (A) and hospital admission (B) in paediatric COVID-19 (n = 25).

The antibody titres were measured in absorbance units (a.u.). Spearman's correlation coefficient (R) and p value have been displayed on each plot, along with the regression line and 95% confidence intervals.

COVID-19 disease severity score

The results of the WHO COVID-19 severity score (Table 4-2) applied to paediatric patients with trivial illness and COVID-19 are shown in Table 4-7. There was a spread of patients across each score category, with the highest proportion of paediatric COVID-19 patients (21%, n = 8) scoring 3 – hospitalised with mild disease, not requiring oxygen. The small number of patients in each score category limited the ability to comment on sex distribution (Table 4-7). The adult COVID-19 data showed a similar spread across the score categories, with the highest proportion of patients (37% n = 91) scoring 4 – hospitalised with mild disease, requiring oxygen (Table 4-8). In adult COVID-19 cases, a higher proportion of females had a score of "1" indicating COVID-19 with no limitations on activity, whereas a greater proportion of males had scores ranging from 3 to 8, representing more severe disease (Table 4-8).

Table 4-7 Paediatric patients with trivial illness and COVID-19 categorised by WHO COVID-19 severity score[394] and sex. Number (n) and percentage (%) of patients in each category is presented.

WHO COVID-19 severity score	**0**	**3**	**4**	**5**	**6**	**7**
Male, n (%)	2 (20%)	6 (75%)	0 (0%)	3 (43%)	4 (80%)	2 (40%)
Female, n (%)	7 (70%)	2 (25%)	3 (100%)	4 (57%)	1 (20%)	3 (60%)
Unknown, n (%)	1 (10%)	0 (0%)	0 (0%)	0 (0%)	0 (0%)	0 (0%)
TOTAL, n (% of total)	10 (26%)	8 (21%)	3 (8%)	7 (18%)	5 (13%)	5 (13%)

Table 4-8 Adult patients with COVID-19 categorised by maximum WHO COVID-19 severity score[394] and sex. Number (n) and percentage (%) of patients in each category is presented.

WHO COVID-19 severity score	**1**	**2**	**3**	**4**	**5**	**6**	**7**	**8**	**11***
Male, n (%)	7 (33%)	0 (0%)	23 (62%)	50 (55%)	10 (62%)	16 (76%)	15 (58%)	16 (70%)	4 (36%)
Female, n (%)	14 (67%)	0 (0%)	14 (38%)	41 (45%)	6 (38%)	5 (24%)	11 (42%)	7 (30%)	7 (64%)
TOTAL, n (% of total)	21 (8.5%)	0 (0%)	37 (15%)	91 (37%)	16 (6.5%)	21 (8.5)	26 (11%)	23 (9%)	11 (4.5%)

*An additional category “11” was added to include patients with a severity score of “3” who were admitted to hospital for reasons other than COVID-19. The data from this table was provided by Dr Claire Broderick.

Next, the relationship between SARS-CoV-2 S IgG and WHO severity scores was evaluated. Although a bell-shaped trend was observed in the paediatric COVID-19 data, with peak SARS-CoV-2 S IgG and IgM titres at WHO severity score of 4, no statistically significant differences were detected (Figure 4-10A and Figure 4-10B). A similar trend was observed in the adult COVID-19 data, with peak antibody titres at WHO severity score of 5 (Figure 4-10C and Figure 4-10D).

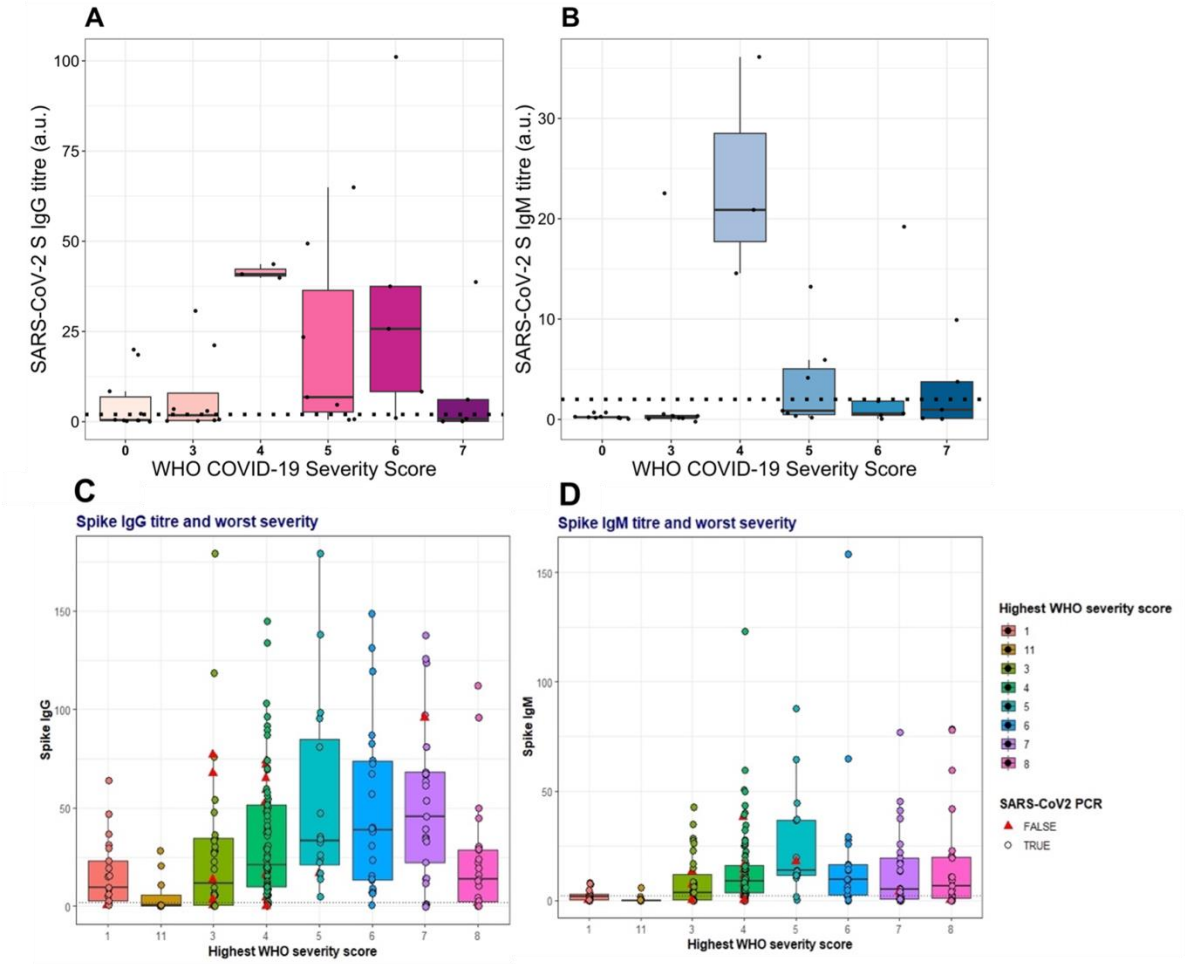

Figure 4-10 Boxplots showing SARS-CoV-2 Spike (S) IgG and IgM titres for paediatric COVID-19 cases (A and B) and adult COVID-19 cases (C and D) by the maximum WHO COVID-19 severity score.

Paediatric COVID-19 cases, n=30. Adult COVID-19 cases, n = 246. Antibody titres were measured in absorbance units (a.u.), with the positive antibody level (> 2.0) indicated by the horizontal dotted line. Significant p values (< 0.05) from Wilcoxon pairwise comparisons with Benjamini-Hochberg correction have been displayed. An additional severity category "11" was added to the adult data to include patients with a severity category of "3" who were admitted to hospital for reasons other than COVID-19. Graphs C and D were made by Dr Claire Broderick.

To assess whether symptom length was contributing to the observed trend of rising antibody titres with severity, the SARS-CoV-2 S IgG titres were plotted against the number of days of symptoms at blood sampling. The analysis revealed no significant relationship between the two variables in both the paediatric (Figure 4-11A) and adult (Figure 4-11B) data, indicating that other factors are driving the association between COVID-19 severity and antibody titres.

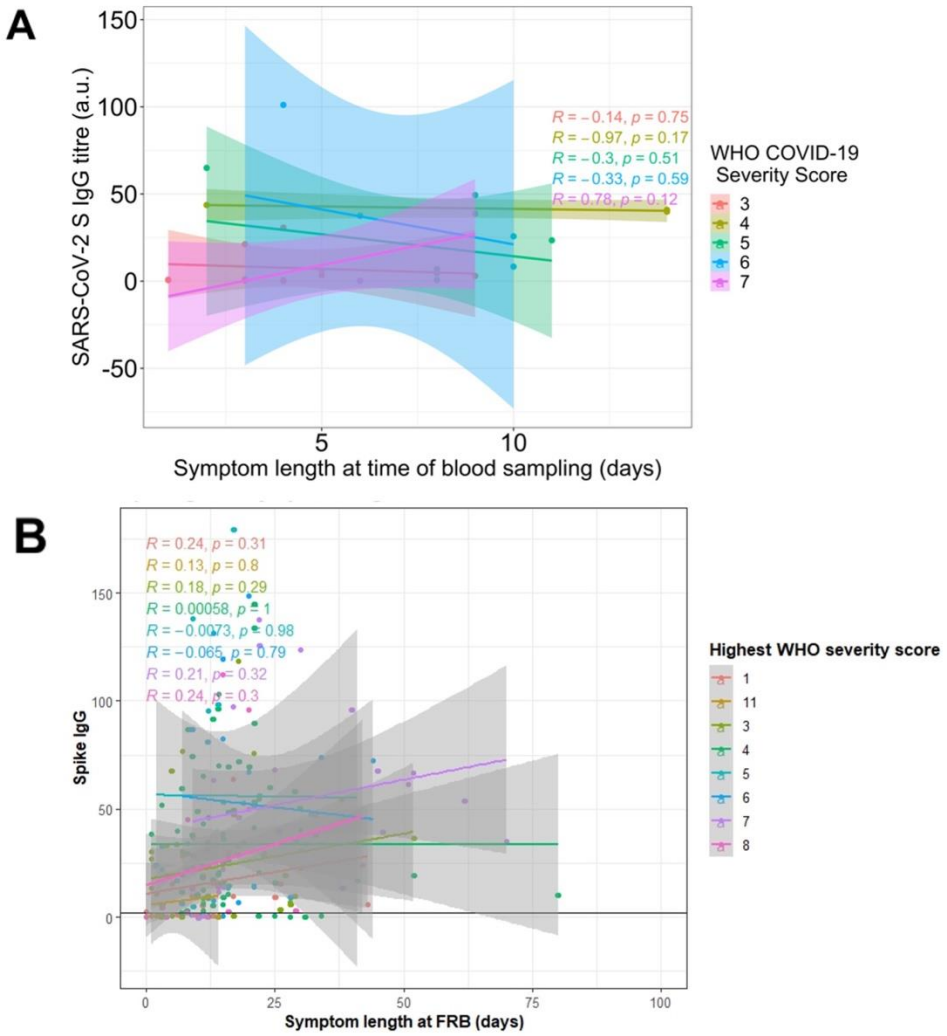

Figure 4-11 Scatterplots showing the relationship between SARS-CoV-2 Spike (S) IgG titres and length of symptoms (days) by WHO COVID-19 severity scores of paediatric COVID-19 cases (n = 30 (A) and adult COVID-19 cases (n = 246) (B).

The antibody titres were measured in absorbance units (a.u.). Spearman's correlation coefficient (R) and p values have been displayed, along with the regression lines and 95% confidence intervals for each severity category. Graph B was made by Dr Claire Broderick. FRB = first research bloods.

4.3.3.2 MIS-C

The following analysis aimed to evaluate the association of SARS-CoV-2 S antibodies with MIS-C disease severity. A total of 120 children with MIS-C were included, with a median age of 10 years (IQR 7-12 years), and 50% (n = 60) were female. A considerable proportion, 68% (n = 82), were admitted to PICU, 7% (n = 8) required invasive ventilation, 61% (n = 73) required inotropic support and no patients died. The median length of hospital stay was 8 days (IQR 6-10 days), and the median length of PICU stay was 2 days (IQR 0-3 days). Among the participants, 93% (n = 111) were positive for SARS-CoV-2 S IgG, 33% (n = 40) were positive for IgM and 23% (n = 27) were positive for IgA (Table 4-9).

Table 4-9 SARS-CoV-2 antibody results in children with MIS-C.

N (%)	Positive	Negative	Indeterminant
SARS-CoV-2 Spike IgG	111/120 (92.5%)	3/120 (2.5%)	6/120 (5%)
SARS-CoV-2 Spike IgM	40/120 (33.3%)	61/120 (50.8%)	19/120 (15.8%)
SARS-CoV-2 Spike IgA	27/120 (22.5%)	71/120 (59.2%)	22/120 (18.3%)

Laboratory and clinical markers of disease severity

The median maximum CRP level was 221 mg/L (IQR 168-288 mg/L), the median maximum neutrophil count was 11 x 10^9/L (IQR 7.5-16 x 10^9/L), and the median minimum lymphocyte count was 0.7 x 10^9/L (IQR 0.4-1.1 x 10^9/L). No significant associations were detected between SARS-CoV-2 S antibody titres (IgG and IgM) and maximum CRP level, maximum neutrophil count and minimum lymphocyte count (Figure 4-12). Furthermore, SARS-CoV-2 antibody titres did not correlate with length of stay in hospital or PICU (
Figure 4-13). The other clinical markers of severity (e.g. level of organ support) were not assessed individually as they were incorporated into the MIS-C disease severity score.

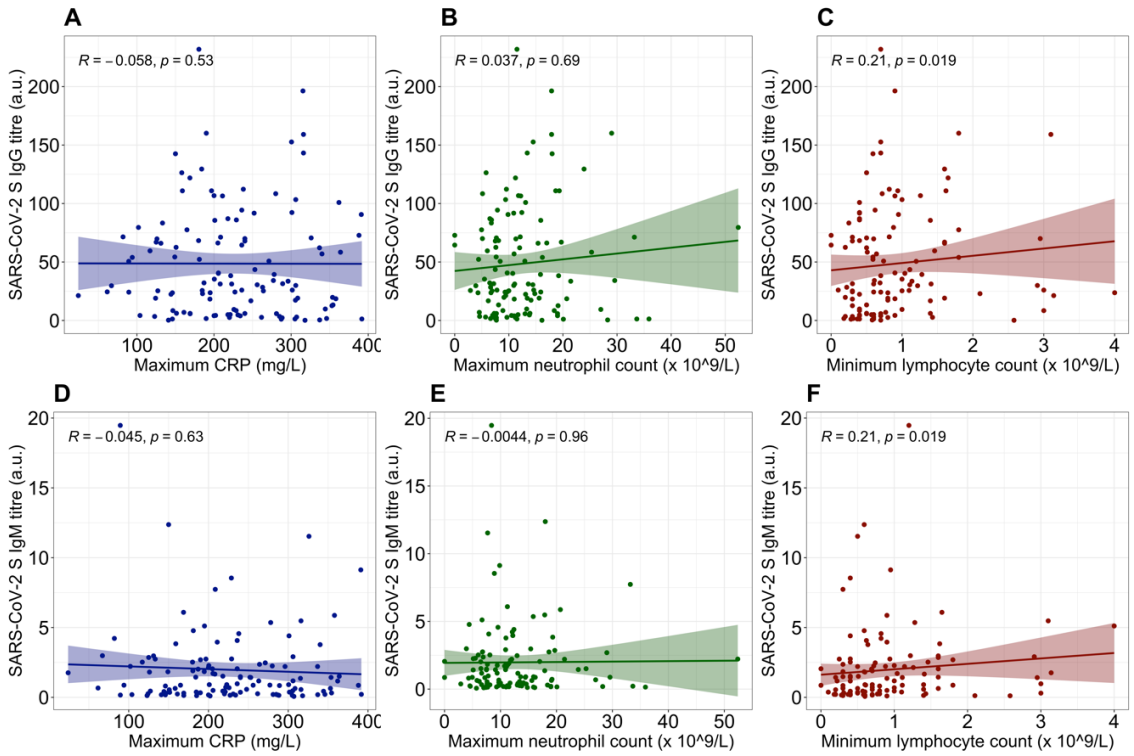

Figure 4-12 Scatterplots showing the relationship between SARS-CoV-2 Spike (S) IgG and IgM titres in patients with MIS-C (n = 120) and maximum C-reactive protein (CRP) (mg/L) (A,D), maximum neutrophil count (x 10^9/L) (B,E) and minimum lymphocyte count (x 10^9/L) (C,F).

Antibody titres were measured in absorbance units (a.u.). Spearman's correlation coefficient (R) and p value have been displayed on each plot, along with the regression line and 95% confidence intervals.

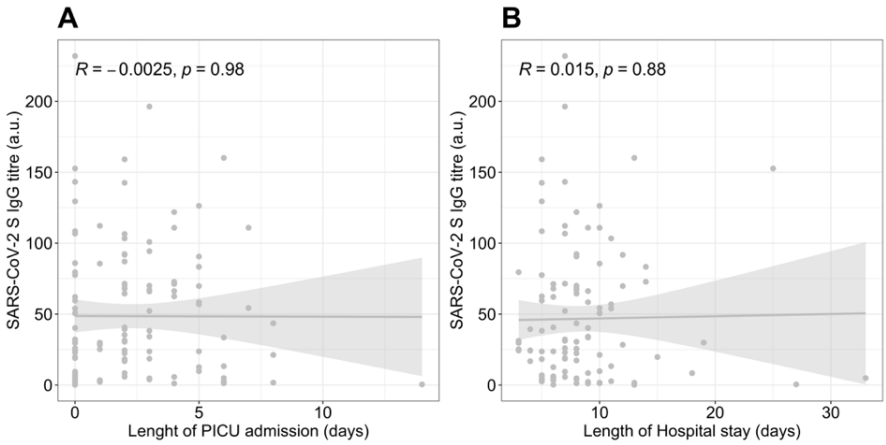

Figure 4-13 Scatterplots showing the relationship between SARS-CoV-2 Spike (S) IgG titres and length of paediatric intensive care unit (PICU) admission (A) and hospital admission (B) in children with MIS-C (A: n = 120, B: n = 110).

Antibody titres were measured in absorbance units (a.u.). Spearman's correlation coefficient (R) and p value have been displayed on each plot, along with the regression line and 95% confidence intervals.

MIS-C disease severity score

Table 4-10 presents the distribution of children with MIS-C by maximum disease severity category (Table 4-3) and sex. The highest proportion of patients (54%, n = 65) were classified as having severe disease. The next highest category was mild disease, accounting for 26% (n = 31) of the patients. The proportions of patients with moderate (13%, n = 16) or very severe disease (7%, n = 8) were smaller. When considering differences by sex, a higher number of males were categorised as having mild or moderate disease compared to females. Conversely, a higher proportion of females were found in the severe and very severe categories compared to males. Additionally, on assessment of disease severity scores and SARS-CoV-2 S IgG and IgM titres, no significant relationship was seen (Figure 4-14).

Table 4-10 Number of children with MIS-C categorised by maximum disease severity score and sex.

MIS-C Disease severity score	Mild	Moderate	Severe	Very Severe
	1	**2**	**3**	**4**
Male	22	12	23	3
Female	9	4	42	5
TOTAL	31	16	65	8

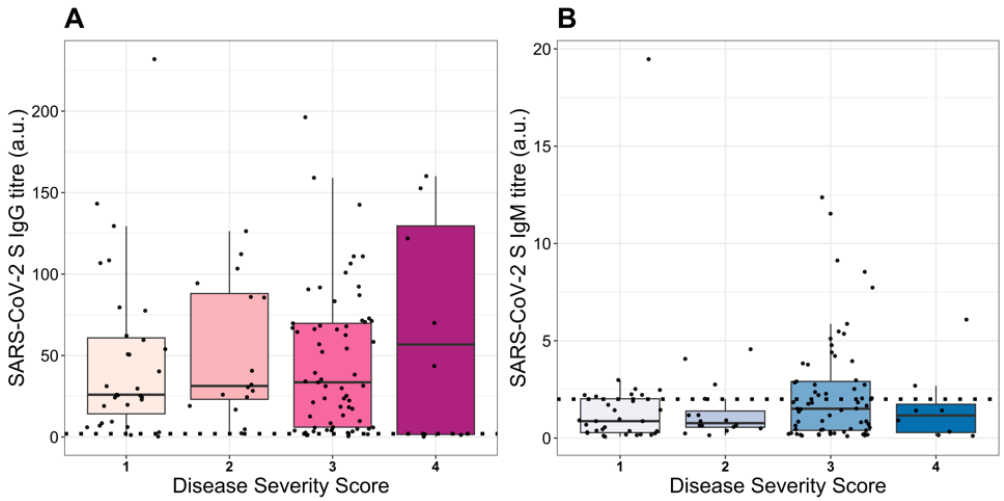

Figure 4-14 Boxplots showing SARS-CoV-2 Spike (S) IgG (A) and IgM (B) titres by the maximum MIS-C disease severity score (n = 120).

The antibody titres were measured in absorbance units (a.u.). Positive antibody level (> 2.0) is demarcated by the horizontal dotted line. Significant p values (< 0.05) following Wilcoxon pairwise comparisons with Benjamini Hochberg correction have been displayed.

Cardiac involvement

The relationships between markers of cardiac involvement in MIS-C and SARS-CoV-2 S IgG titres were investigated. The results revealed no significant associations between SARS-CoV-2 S IgG titres and cardiac involvement in MIS-C. This included troponin levels (Figure 4-15), echocardiogram abnormalities (left ventricular dysfunction, low cardiac output, myocarditis and valvular regurgitation) (Figure 4-16), and coronary artery measurements (Figure 4-17).

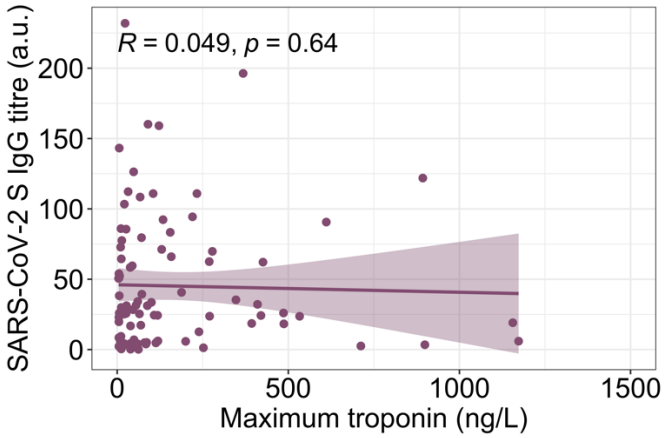

Figure 4-15 Scatterplot showing the relationship between SARS-CoV-2 Spike (S) IgG titres in children with MIS-C (n = 95) and maximum troponin levels (ng/L).

The antibody titres were measured in absorbance units (a.u.). Spearman's correlation coefficient (R) and p value have been displayed, along with the regression line and 95% confidence intervals.

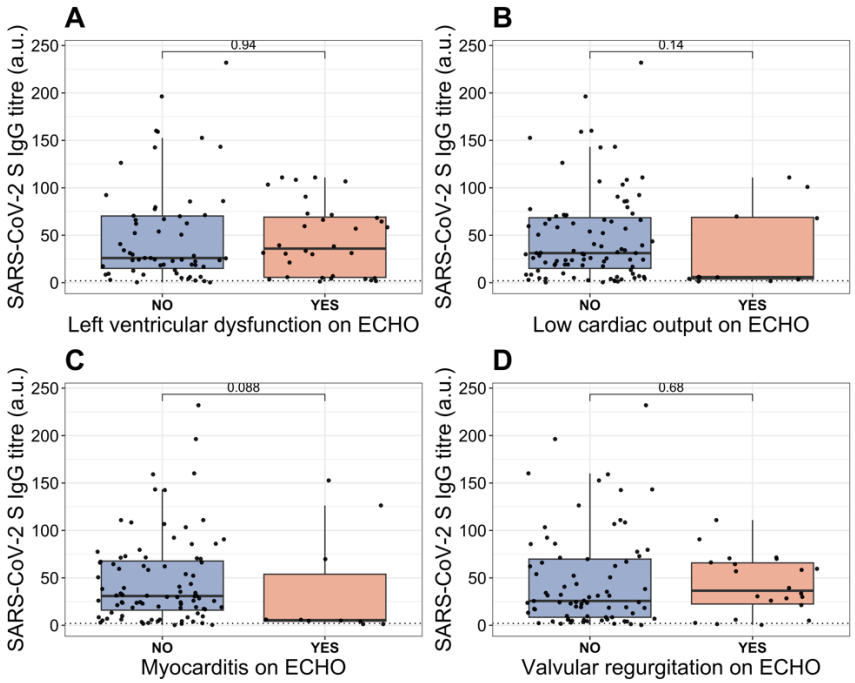

Figure 4-16 Boxplots showing SARS-CoV-2 Spike (S) IgG titres by echocardiogram findings in children with MIS-C: left ventricular dysfunction (n = 91) (A), low cardiac output (n = 102) (B), myocarditis (n = 98) (C) and valvular regurgitation (n = 99) (D).

The antibody titres were measured in absorbance units (a.u.). P values following Wilcoxon pairwise comparisons have been displayed.

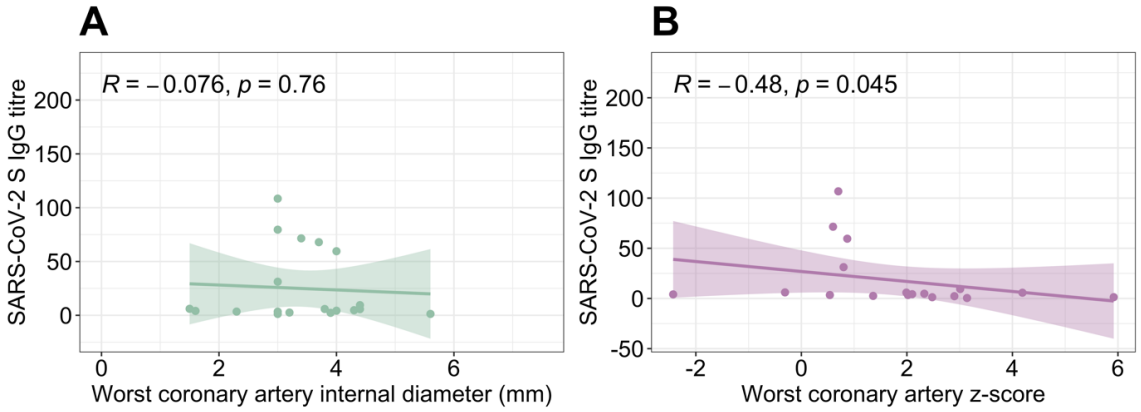

Figure 4-17 Scatterplots showing the relationship between SARS-CoV-2 Spike (S) IgG titres and maximum coronary artery internal diameter in millimetres (mm) (A) and maximum coronary artery z-score (B) measured on echocardiography in children with MIS-C (n = 20).

The antibody titres were measured in absorbance units (a.u.). Spearman's correlation coefficient (R) and p value have been displayed on each plot, along with the regression line and 95% confidence intervals.

4.4 Discussion

During the early stages of the COVID-19 pandemic, it quickly became apparent that while adults were experiencing severe, life-threatening illness, children were largely spared from the severe manifestations of COVID-19[395]. The work in this chapter investigates the age-related differences in COVID-19, specifically investigating the hypothesis that antibody dependent enhancement (ADE) due to cross-reactive antibodies from seasonal coronaviruses may contribute to severe disease in adults, as they have had more opportunities for exposure to seasonal coronaviruses over their lifetime. In addition, following early reports of raised SARS-CoV-2 IgG levels in adults with severe COVID-19, this chapter investigates the relationship between SARS-CoV-2 antibody titres and disease severity in both paediatric COVID-19 and MIS-C.

In the pre-pandemic cohort, which included adults and children, 20% tested positive for HCoV OC43 N IgG, indicating prior exposure, and 4% tested positive for HCoV OC43 N IgM, indicating recent infection (Table 4-5). These results are consistent with the global prevalence of respiratory tract infections due to seasonal coronaviruses, reported to be 0.5-18.4%[29]. There were no compelling age-related differences in the levels of HCoV OC43 N IgG, IgM and IgA in the pre-pandemic cohort (Figure 4-2). Additionally, there was no clear evidence of cross-reactive antibodies in the samples taken before or during the COVID-19 pandemic. While it is important to acknowledge that only one of the four seasonal coronavirus antibodies was tested due to time and cost constraints, limiting the comprehensive understanding of potential cross-reactivity with SARS-CoV-2, the current body of literature does not strongly support ADE in COVID-19[396]. Conversely, an alternate hypothesis suggests that pre-existing immunity from seasonal coronaviruses could provide protection against severe COVID-19. Ng et al. showed that a greater proportion of children have cross-reactive antibodies compared to adults and that these antibodies have neutralising effects on SARS-CoV-2 *in vitro*[180]. However, this is conflicted by findings from Lv et al., who reported that while increased cross-reactive antibodies are seen in children, they rarely have neutralising effects[177].

In the adult COVID-19 cohort, a rise in WHO COVID-19 severity score was associated with increased levels of SARS-CoV-2 S IgG and IgM titres (Figure 4-10C and Figure 4-10D). The antibody titres peaked at a severity score of 7, with lower antibody titres observed in patients who died (severity score 8). It was speculated that the lower antibody levels in deceased patients could be due to symptom duration at the point of blood sampling; however, no relationship was seen between symptom duration, antibody titres and disease severity in this cohort (Figure 4-11). These findings suggest that while SARS-CoV-2 specific antibodies may have an impact on COVID-19 disease severity, other factors also contribute to disease severity, particularly in fatal cases. This is concurrent with previous studies associating higher SARS-CoV-2

antibody levels with more severe disease in adult COVID-19 cases[66,67,69] with lower levels seen in fatal cases[165].

In contrast, the SARS-CoV-2 S IgG, IgM and IgA titres did not show significant associations with clinical or laboratory markers of disease severity in paediatric COVID-19. However, a non-significant trend of rising SARS-CoV-2 S IgG and IgM titres with increasing maximum neutrophil count was observed (Figure 4-8). Neutrophilia is commonly reported in severe COVID-19 cases[199,209,397]. This may be attributed to the overall immune response to SARS-CoV-2 which includes neutrophil activation and antibody production, or neutrophils could be influencing antibody production by interacting with other cells e.g. B cells – further studies are needed to explore this relationship. The limited sample size in the paediatric COVID-19 cohort (n = 30) may have contributed to the absence of significant associations with clinical severity, as observed in adults. There are limited studies investigating antibody titres in paediatric COVID-19 of varying severity, however two studies have reported an association of higher SARS-CoV-2 IgG levels with increased severity of paediatric COVID-19 cases[171,398].

The association of ADE with other viral infections, such as Dengue, has been established through diverse methodologies. In Dengue, observational studies in endemic regions highlighted increased disease severity during secondary infections with a distinct serotype. Subsequent experimental evidence from animal models and *in vitro* studies demonstrated that pre-existing antibodies facilitate the entry of a different serotype into host cells, primarily through Fc receptors on immune cells, leading to increased viral replication, pro-inflammatory response, and severe disease[399–401]. In contrast, my investigation into the role of antibodies in SARS-CoV-2 infections represents an initial and exploratory examination, focusing on identifying any preliminary evidence of ADE. If such evidence had been detected, the study would have been followed by more comprehensive experiments, mirroring those conducted in Dengue and RSV research.

In the context of MIS-C, the analyses did not find any significant associations between SARS-CoV-2 IgG and IgM and disease severity or cardiac involvement, which adds valuable insights to the current research landscape. Indeed, studies have shown that SARS-CoV-2 IgG titres are higher in MIS-C compared to convalescent COVID-19 [293,402,403], however, the specific relationship between antibody levels and disease severity in MIS-C had not been explored until now. It is important to consider that apart from their abundance, antibodies can have significant impact on the immune response through mechanisms such as antibody-mediated cellular cytotoxicity or development of autoantibodies, as suggested by some researchers[287,299,402].

This study is unique in that it provides a comprehensive comparison of HCoV-OC43 and SARS-CoV-2 antibody titres in adults and children from both pre-pandemic and pandemic periods, to address important hypotheses regarding the role of pre-existing antibodies and SARS-CoV-2 specific antibodies in the severity of SARS-CoV-2 associated diseases. However, this work has some limitations. Only antibodies against HCoV-OC43 were tested; expanding the investigation to include other seasonal coronaviruses could provide a more comprehensive exploration of potential cross-reactivity with SARS-CoV-2. Due to the rarity of severe paediatric COVID-19, only 30 paediatric COVID-19 cases were included, which may limit the ability to detect significant associations with disease severity; a larger sample size could improve the statistical power and reliability of the results. Additionally, while this work primarily involved exploratory analyses, the presence of multiple comparisons was addressed through p-value correction. However, it is important to recognise that despite these corrections, the potential for issues related to multiple comparisons persists (e.g., increased risk of Type I errors, overestimation of significance) and warrants consideration. The analysis was focused solely on antibodies against the Nucleocapsid and Spike proteins of SARS-CoV-2; inclusion of a broader range of antibodies (e.g. membrane or non-structural proteins), could provide a deeper understanding of the humoral immune response to SARS-CoV-2. Future research could extend beyond titres to assess the breadth, diversity, and quality (avidity) of the antibody response. Additionally, investigating antibody functionality through neutralization or antibody-dependent cellular cytotoxicity (ADCC) assays could provide valuable insights into the role of antibodies in disease pathogenesis.

4.5 Conclusion

The findings in this chapter provide valuable insights into several important aspects related to COVID-19 and MIS-C. The results contribute to the understanding that observed differences in severity of COVID-19 between children and adults are unlikely to be due to cross-reactive antibodies leading to ADE. It was crucial to investigate this hypothesis early in the pandemic, as ADE could have had significant implications for treatment approaches and vaccination strategies. Additionally, the results showed an association between SARS-CoV-2 specific antibody titres and disease severity in adult COVID-19, however, this was not observed in paediatric COVID-19 and MIS-C.

This chapter provides evidence against ADE and role of antibodies in disease severity in paediatric SARS-CoV-2 associated diseases. It is essential to build upon this work by conducting functional studies to gain further insights into the role of antibodies in the pathogenesis of paediatric SARS-CoV-2 associated disease, which will be addressed in Chapter 7. Understanding the pathophysiological mechanisms underlying the

disease is crucial for the development of effective diagnostic tools and management strategies and the work in this chapter contributes to this ongoing effort.

Chapter 5: Distinguishing MIS-C from other inflammatory and infectious diseases

5.1 Introduction

MIS-C emerged as a concerning complication of SARS-CoV-2 infection in children. In May 2020, paediatricians in the UK raised an alert, after noticing a cluster of cases of previously healthy children developing persistent fever and inflammation affecting multiple organ systems following exposure to SARS-CoV-2[194]. Subsequently, similar cases were reported worldwide[214,404–406]. Despite the publication of case definitions by RCPCH, WHO and CDC (Appendix 1,Table A1-1) to aid recognition and surveillance of MIS-C, there was a great degree of diagnostic uncertainty during this period, as little was known about the novel condition and it encompassed a spectrum of symptoms and severity. Moreover, MIS-C shares many clinical and laboratory features with other childhood infectious and inflammatory conditions, such as KD and TSS[196,202], further increasing the diagnostic challenge.

There was an urgent need for MIS-C diagnostics to support clinicians in making timely decisions and promptly initiating appropriate treatment. The work in this chapter summarises the effort to distinguish MIS-C from other paediatric febrile illnesses by conducting exploratory analyses on clinical, laboratory and SARS-CoV-2 serology data. Additionally, I chose to focus on the development of a clinical diagnostic score for MIS-C as this offered an expedited, accessible, and cost-effective alternative, during the time when biomarker diagnostics were still in development. The WHO and CDC case definitions of MIS-C include positive SARS-CoV-2 antigen or serology testing. However, as the number of children exposed to SARS-CoV-2 antigens increases over time, either through infection or vaccination, the utility of SARS-CoV-2 serology testing for MIS-C diagnosis may diminish, further complicating the diagnostic process. I therefore also investigated the trends of SARS-CoV-2 serology results in children over time.

<u>The primary aim of this chapter is:</u>

To differentiate MIS-C from other infectious and inflammatory diseases through comprehensive analysis of clinical features and laboratory parameters and development of a MIS-C diagnostic score.

The objectives of this chapter are:

1) Compare clinical features, laboratory markers and SARS-CoV-2 serology results in MIS-C, KD, Bacterial illness, Viral illness, and other Inflammatory diseases to identify variables associated with MIS-C.
2) Develop a diagnostic score for MIS-C using clinical and laboratory variables which distinguish MIS-C from other febrile illness.
3) Perform longitudinal analysis of SARS-CoV-2 serology results in MIS-C and febrile controls to assess the diagnostic utility of SARS-CoV-2 serology testing in MIS-C over time.

The key findings from this chapter are:

The work presented in this chapter provides valuable insight into the clinical and laboratory features that distinguish MIS-C from other febrile diseases, shedding light on the distinct pathophysiological mechanisms underlying MIS-C. The diagnostic score based on easily available clinical and laboratory features was able to distinguish MIS-C from other conditions with good accuracy (AUC 0.90). Following validation, this diagnostic score can be easily applied in a range of healthcare settings and can be a highly valuable tool for facilitating timely and informed clinical decision making. Furthermore, the analyses demonstrate a significant association between SARS-CoV-2 IgG seropositivity and MIS-C. However, longitudinal analyses showed a rise in SARS-CoV-2 IgG seropositivity over time, either through natural infection or vaccination, which diminishes the utility of this test. These findings highlight the need to potentially revise the MIS-C diagnostic criteria and emphasize the need for development of alternative diagnostic tests.

5.2 Methodology

5.2.1 Clinical cohort

The cohort consisted of children recruited into DIAMONDS during the COVID-19 pandemic era with MIS-C, Bacterial illness (definite bacterial and probable bacterial), Viral illness (definite viral and probable viral), Inflammatory disease (non-SARS-CoV-2 associated) and KD. Further details of the DIAMONDS clinical phenotyping are shown in Chapter 3 (section 3.1.1.2). For some of the sub-analyses, the MIS-C cohort was divided into "MIS-C", patients fulfilling the WHO MIS-C criteria, and "Incomplete MIS-C", patients who were treated by clinicians as MIS-C but did not fulfil the complete WHO MIS-C criteria. The samples from all patients were taken during acute illness.

5.2.2 Coronavirus antibody fluorescence-activated cell sorting (FACS) assay – 2020-2021 samples.

SARS-CoV-2 S IgG, IgM and IgA antibodies were measured using a FACS-based assay, as described in Chapter 3 (section 3.2.2.1).

5.2.3 Mesoscale Discovery (MSD) assay for SARS-CoV-2 antibody testing – 2022 samples

The MSD V-PLEX immunoassay was chosen for SARS-CoV-2 S and N IgG testing of 2022 samples due to practical considerations. The MSD assays use electrochemiluminescent labels (SULFO-TAGs) and multiarray technology to quantify proteins in a sample. If SARS-CoV-2 S or N IgG is present in a sample, it will bind to its specific capture antigen, and is detected using anti-human IgG antibodies conjugated with SULFO-TAGs. When electricity is applied, the SULFO-TAGs emit light, and its intensity is measured for quantification of SARS-CoV-2 IgG. Detailed methodology is provided in Chapter 3 (section 3.2.2.2).

5.2.4 Data analysis

5.2.4.1 FACS-based assay threshold

The antibody titres were determined using fluorescence intensity (absorbance units (a.u.)) and the threshold for a definite positive antibody titre result was set at > 2.0, definite negative at < 1. Results between 1-2 were considered indeterminant. Indeterminant results were excluded from the analyses.

5.2.4.2 MSD assay threshold

The MSD immunoassay results in arbitrary units per ml (AU/ml) were converted to the WHO international standard units, binding antibody units per ml (BAU/ml), using the conversion factor provided by MSD. The MSD recommended thresholds for positive results were used: SARS-CoV-2 S IgG > 18 BAU/ml and SARS-CoV-2 N IgG > 12 BAU/ml.

5.2.4.3 R packages

The following R packages were used for analysis and graphical representation of the data: ggfortify, ggplot2, ggpubr, gtsummary, dplyr, rstatix, Rcolorbrewer, beeswarm, tidyverse, epitools, nnet and finalfit.

5.2.4.4 Batch effects and laboratory marker QC

Any batch effects in the SARS-CoV-2 antibody dataset were assessed through principal component analysis and QC of laboratory markers were performed as previously described in Chapter 4 (section 4.2.3.3).

5.2.4.5 SARS-CoV-2 S IgG

In order to detect significant differences in the frequency of SARS-CoV-2 S IgG positivity between disease groups (MIS-C, Incomplete MIS-C, Bacterial, Viral, Inflammatory, KD), multiple Wilcoxon pairwise comparisons with BH correction were performed. Univariable logistic regression analysis was conducted to determine the association between positive SARS-CoV-2 S IgG result and the log odds of each diagnosis. Next, the median levels of SARS-CoV-2 S IgG were compared across disease groups using multiple Wilcoxon pairwise comparisons with BH correction, to investigate the potential utility of SARS-CoV-2 IgG titre in aiding MIS-C diagnosis.

5.2.4.6 Clinical features

Multivariable logistic regression analysis was performed to determine the log odds ratios of the presence of each clinical feature predicting diagnosis of MIS-C and Incomplete MIS-C. Log odds of above zero indicate increased likelihood of the diagnosis, while log odds of below zero indicate decreased likelihood of the diagnosis. To ensure the results were valid and reliable, model oversaturation and overfitting were avoided by ensuring there were 10 patients diagnosed with MIS-C/Incomplete MIS-C for each independent variable (clinical feature) included in the model. Variables were selected based on the principles of

parsimony and interpretability. Initially, a univariable analysis was performed to identify the clinical features most strongly associated with the disease outcome, then forward modelling was used to add variables one at a time, considering their statistical significance and predictive value, until the model reached a point of saturation.

5.2.4.7 Laboratory markers

A multivariable generalised linear regression model was used to determine the association of laboratory markers with MIS-C compared to all other disease groups. It's important to note that in the context of binary outcomes, such as the presence or absence of MIS-C, the multivariable generalized linear regression model utilized logistic regression. This statistical approach allowed me to assess the relationship between the selected laboratory markers and the likelihood of developing MIS-C, considering multiple variables simultaneously and accounting for the binary nature of the outcome variable (MIS-C vs no MIS-C). The analysis was conducted separately for each disease group (e.g., MIS-C versus (vs) Incomplete MIS-C, MIS-C vs Bacterial, MIS-C vs Viral, MIS-C vs Inflammatory, MIS-C vs KD) as well as combined (MIS-C vs all other disease groups), to determine if the associations with MIS-C were specific to certain disease groups, or if they were consistent across all comparisons. A multivariable regression model was used as it allows examination of the independent effects of each laboratory marker while adjusting for potential confounding factors. BH correction for multiple testing was applied. The following admission laboratory markers were included: Hb, WBC, neutrophils, lymphocytes, monocytes, eosinophils, platelets, fibrinogen, D-dimer, urea, creatinine, ALT, bilirubin, albumin, CRP, ferritin, troponin, BNP, LDH, creatine kinase and lactate. Patients with missing values for any of the specified laboratory markers were not included in the analysis for the respective marker.

5.2.4.8 MIS-C diagnostic score

The MIS-C diagnostic score was designed by using the results of the logistic regression models that evaluated clinical features and laboratory markers associated with MIS-C. The clinical significance of each variable was also taken into consideration. The diagnostic score aimed to include a restricted set of blood markers, to potentially allow for use in resource limited settings. The following presenting clinical features were included: fever, conjunctivitis, cardiac involvement, gastrointestinal symptoms, respiratory symptoms, headache, and rash along with the following admission blood markers: CRP, albumin, lymphocytes and monocytes. The log odds ratio (LOR) from the logistic regression model and the coefficients from the generalised linear regression model were used to assign weights to each variable. The blood markers were scaled and adjusted for direction of change, by using the normal range values.

Although SARS-CoV-2 S IgG was significantly associated with MIS-C, it was not included in the model due to possible reduced utility over time.

The distribution and overlap of the MIS-C diagnostic scores were examined for each disease group to understand the range and variability of results within each group and to assess the discriminative ability of the score. The median scores were compared across all disease groups using Wilcoxon pairwise comparisons, and the sensitivity and specificity of the score were determined. The optimal threshold for classifying patients as MIS-C was determined using receiving operator characteristic curve (ROC) analysis and Youden's index. Youden's index maximizes the sum of sensitivity and specificity in discriminating between two classes. Graphically, this can be seen as the point which maximizes the vertical distance between the ROC curve and the diagonal line (random chance line) connecting (0,0) and (1,1)[407] (Figure 5-1).

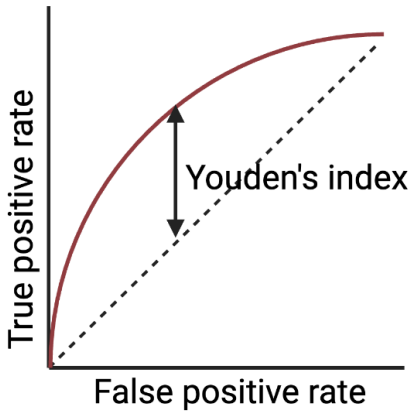

Figure 5-1 Receiving operator curve and Youden's index.

The receiving operator curve (ROC) is dependent on the true positive rate (sensitivity) and the false positive rate (1 – specificity). The diagonal dashed line represents the random chance line. The Youden's index is the point on the ROC curve that maximises the distance from the random chance line[407]*. This figure was made using Biorender.*

The calculation for Youden's index is: Sensitivity + Specificity – 1.

- Sensitivity = True Positive (TP) / (TP + False Negative (FN))
- Specificity = True Negative (TN) / (TN + False Positive (FP))

The performance of the diagnostic score was evaluated by calculating the accuracy ((TP + TN) / (TP + TN + FP + FN)), positive predictive value (PPV = TP / (TP + FP)), negative predictive value (NPV = TN / (TN + FN)) and area under the curve (AUC), which measures the model's ability to discriminate MIS-C from other diseases. An AUC of 1 indicates perfect discrimination, while an AUC of 0.5 is equivalent to random chance.

5.2.4.9 Longitudinal analysis of SARS-CoV-2 serology results in children

The proportion of children with positive SARS-CoV-2 S IgG serology in each disease group (MIS-C, Incomplete MIS-C, Bacterial, Viral, Inflammatory and KD) were assessed over a span of three years: 2020, 2021 and 2022 to provide insights into the temporal trends. Most individuals infected with SARS-CoV-2 will generate antibodies against the viral structural proteins (including the Spike and Nucleocapsid proteins)[408]. Whereas the vaccines licensed in Europe exclusively contain the Spike protein/gene and as a result, vaccinated individuals will primarily generate antibodies against the Spike protein[408]. Therefore to assess the seropositivity associated with natural infection, independent of vaccination, SARS-CoV-2 N IgG results were analysed. SARS-CoV-2 N IgG results were only available for the 2022 samples. Given that children under the age of 5 years are most susceptible to MIS-C due to limited exposure and lack of vaccination, and most difficult to differentiate from those with KD, a sub-analysis was conducted for this age group.

5.3 Results

The cohort consisted of patients with MIS-C (n = 170), Incomplete MIS-C (n = 33), Bacterial illness (n = 208), Viral illness (n = 143), Inflammatory disease (n = 64) and KD (n = 21) recruited between 2020 and 2021. The clinical and demographic features of the cohort are shown in (Appendix 4 Table A4-1).

5.3.1 SARS-CoV-2 S IgG

Patients diagnosed with MIS-C had the highest percentage of positive SARS-CoV-2 S IgG results (98%), followed by those with Incomplete MIS-C (83%) (Table 5-1). Smaller proportions of children in the Bacterial (33%), Viral (28%), Inflammatory (29%) and KD (29%) groups tested positive for SARS-CoV-2 S IgG (Table 5-1). The frequency of positive SARS-CoV-2 S IgG results in MIS-C and Incomplete MIS-C was significantly higher compared to the other disease groups (Table 5-2). Logistic regression results showed increased log odds of the diagnosis of MIS-C (LOR 4.32, $p = 5.90 \times 10^{-17}$) and Incomplete MIS-C (LOR 1.63, p = 0.001) when SARS-CoV-2 S IgG was positive (Table 5-3). The distribution of SARS-CoV-2 S IgG titres varied widely among all disease groups, with significantly higher titres in patients with MIS-C (all $p < 0.0001$) and Incomplete MIS-C (all $p < 0.01$) compared to all other disease groups (Figure 5-2).

Table 5-1 SARS-CoV-2 S IgG results by disease group. n = number of children.

Condition	SARS-CoV-2 S IgG Negative (n)	SARS-CoV-2 S IgG Positive (n)	Percentage (%) SARS-CoV-2 S IgG positive
MIS-C	4	157	98%
Incomplete MIS-C	5	25	83%
KD	11	7	39%
Bacterial	132	64	33%
Inflammatory	44	18	29%
Viral	97	37	28%

Table 5-2 Wilcoxon pairwise comparisons with Benjamini Hochberg adjustment for SARS-CoV-2 Spike IgG positivity frequency in different disease groups. Significant p values have been highlighted.

	Bacterial	Incomplete MIS-C	Inflammatory	KD	MIS-C
MIS-C	$1.08x10^{-34}$	0.01	$2.77x10^{-27}$	$2.75x10^{-15}$	NA
Incomplete MIS-C	$8.94x10^{-7}$	NA	NA	NA	NA
Inflammatory	0.81	$6.43x10^{-6}$	NA	NA	NA
KD	0.84	0.01	0.77	NA	NA
Viral	0.59	$1.27x10^{-7}$	0.97	0.65	$1.08x10^{-34}$

Table 5-3 Logistic regression analysis of the association between positive SARS-CoV-2 Spike IgG and the log odds of diagnostic outcomes.

Log odds ratio, confidence intervals (CI) and p values are shown. Significant p values have been highlighted. Orange = increased odds. Purple = reduced odds.

	Log odds ratio (CI)	p value
MIS-C	4.32 (3.43-5.51)	$5.90x10^{-17}$
Incomplete MIS-C	1.63 (0.73-2.72)	0.001
Bacterial	-1.14 (-1.50-(-0.78)	$4.79x10^{-10}$
Viral	-1.29 (-1.72 -(-0.87)	$2.02x10^{-09}$
Inflammatory	-1.04 (-1.64-(-0.49)	0.0004
KD	-0.52 (-1.53-0.43)	0.292

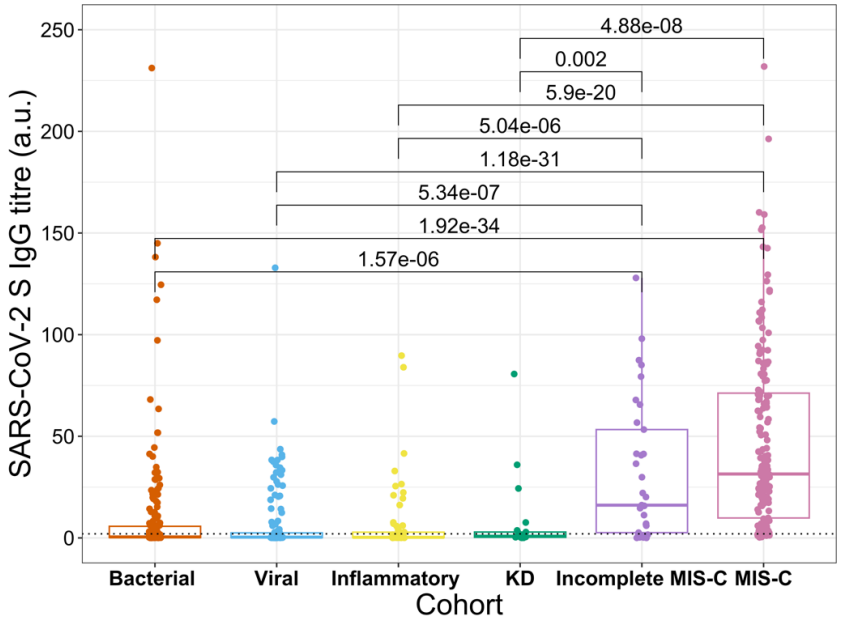

Figure 5-2 Boxplot showing SARS-CoV-2 Spike (S) IgG titres across different disease groups.

Bacterial (n = 196), Viral (n = 134), Inflammatory disease (n = 62), Kawasaki Disease (KD) (n = 18), Incomplete MIS-C (n = 30) and MIS-C (n = 161). Median values and interquartile range have been displayed. Only significant p values following Wilcoxon pairwise comparisons with Benjamini Hochberg adjustment have been displayed.

5.3.2 Clinical features associated with MIS-C

Logistic regression analysis was conducted to identify clinical features associated with the diagnosis of MIS-C and Incomplete MIS-C. The following clinical features were associated with increased log odds of the diagnosis of MIS-C: conjunctivitis (LOR 2.75, p = $4.66x10^{-14}$), cardiac symptoms (LOR 2.17, p = $7.21x10^{-6}$), gastrointestinal symptoms (LOR 1.98, p = $1.14x10^{-9}$), headache (LOR 0.87, p = 0.007) and rash (LOR 0.86, p = 0.002) (Table 5-4). Conversely, the presence of lymphadenopathy (LOR 1.54, p = 0.001), oedema/ascites (1.62, p = 0.015) and sensory symptoms (LOR 2.1, p = 0.003) were associated with increased log odds of the diagnosis of Incomplete MIS-C (Table 5-4).

Table 5-4 Multivariable logistic regression analysis of presenting clinical features associated with the diagnosis of MIS-C and Incomplete MIS-C.

Log odds ratio, confidence intervals (CIs) and p values have been shown. Significant p values have been highlighted.

	MIS-C (n = 170)		**Incomplete MIS-C (n = 33)**	
Clinical feature	**Log odds (CI)**	**p value**	**Log odds (CI)**	**p value**
Fever	16.47 (-5.05-236.30)	0.980	-	-
Conjunctivitis	2.75 (2.06-3.50)	$4.66x10^{-14}$	-	-
Cardiac	2.17 (1.24-3.15)	$7.21x10^{-06}$	-	-
Gastrointestinal	1.98 (1.37-2.65)	$1.14x10^{-09}$	-	-
Headache	0.87 (0.24-1.51)	0.007	-	-
Rash	0.86 (0.31-1.42)	0.002	-	-
Musculoskeletal	0.76 (-0.07-1.60)	0.073	-	-
Lymphadenopathy	0.59 (-0.31-1.50)	0.197	1.54 (0.54-2.44)	0.001
Neurological symptoms	0.59 (-0.33-1.47)	0.198	-	-
Oedema/ascites	-0.03 (-1.5-1.48)	0.974	1.62 (0.11-2.83	0.015
Mucositis	-0.45 (-1.68-0.74)	0.468	-	-
Shock	-0.51 (-1.42-0.37)	0.264	-	-
Respiratory	-0.61 (-1.3-0.10)	0.102	-	-
Inflamed extremities	-1.20 (-2.7-0.28)	0.115	-	-
Sensory	-0.79(-3.08-1.00)	0.440	2.10 (0.52-3.42)	0.003

5.3.3 Laboratory markers associated with MIS-C

Multivariable generalised linear regression was conducted to identify laboratory markers that were associated with MIS-C (Table 5-5). Compared to all other disease groups combined (MIS-C vs all), patients with MIS-C had significantly higher fibrinogen (coefficient = 0.89, p = $8.54x10^{-10}$), D-dimer (coefficient = $1.38x10^{-05}$, p = 0.04), urea (coefficient = 0.008, p = 0.004), creatinine (coefficient = 0.002, p = $6.6x10^{-07}$), bilirubin (coefficient = 0.004, p = 0.02), CRP (coefficient = 0.002, p = $3.15x10^{-36}$), BNP (coefficient = $2.96x10^{-05}$, p = 0.01) and lactate (coefficient = 0.05, p = 0.02), indicated by the positive coefficient values. On the other hand, patients with MIS-C significantly lower lymphocytes (coefficient = -0.06, p = $8.47x10^{-10}$), monocytes (coefficient = -0.18, p = $9.2x10^{-14}$) and albumin (coefficient = -0.018, p = $6.29x10^{-13}$) compared to all other disease groups, indicated by the negative coefficients associated with these variables. Of these, raised fibrinogen and CRP and reduced lymphocytes, monocytes, and albumin (except in KD) were consistently observed when comparing MIS-C with Bacterial, Viral, Inflammatory and KD separately. On comparing MIS-C with Incomplete MIS-C, MIS-C had higher fibrinogen (coefficient = 0.06, p = 0.004) and CRP (coefficient = 0.001, p = 0.001) and lower albumin (coefficient = -0.01, p = 0.02) and LDH (coefficient = -0.0002, p = 0.004); indicating that Incomplete MIS-C may encompass a milder form of the MIS-C.

Table 5-5 Multivariable generalised linear model of laboratory markers as predictors of MIS-C compared to other paediatric febrile illnesses.

Coefficients and Benjamini Hochberg adjusted p values have been displayed. Significant p values (< 0.05) have been highlighted: orange = positive association, purple = negative association. "all" = Incomplete MIS-C + Bacterial + Viral + Inflammatory + Kawasaki disease (KD)

	MIS-C vs all		**MIS-C vs Incomplete MIS-C**		**MIS-C vs Bacterial**		**MIS-C vs Viral**		**MIS-C vs Inflammatory**		**MIS-C vs KD**	
	Coefficient	p value	Coefficient	p value	Coefficient	p value	Coefficient	p value	Coefficient	p value	Coefficient	p value
Haemoglobin	-0.0003	0.9117	-0.0017	0.4893	-0.0006	0.7229	-0.0022	0.2176	0.0027	0.2469	0.0038	0.0377
WCC	-0.0020	0.6062	0.0002	0.9672	-0.0112	0.0060	0.0160	0.0026	0.0032	0.6763	-0.0096	0.0296
Neutrophils	0.0052	0.1634	0.0026	0.6400	-0.0066	0.1847	0.0312	1.42×10^{-08}	0.0085	0.2469	-0.0021	0.7373
Lymphocytes	-0.0572	8.47×10^{-10}	-0.0540	0.0554	-0.0940	2.67×10^{-12}	-0.0809	8.71×10^{-09}	-0.1295	1.32×10^{-06}	-0.1204	3.00×10^{-16}
Monocytes	-0.1810	9.20×10^{-14}	-0.1841	0.0554	-0.2213	4.41×10^{-12}	-0.4120	4.01×10^{-15}	-0.4253	3.15×10^{-09}	-0.3394	5.13×10^{-13}
Eosinophils	-0.0026	0.9364	-0.0645	0.5417	0.2100	0.0459	0.4701	0.0002	-0.0344	0.2201	-0.2862	0.0018
Platelets	7.83×10^{-16}	1.0000	0.5000	0.4893	-1.29×10^{-14}	1.0000	1.0000	0.1750	-1.07×10^{-14}	1.0000	1.31×10^{-15}	1.0000
Fibrinogen	0.0898	8.54×10^{-10}	0.0557	0.0044	0.0566	0.0060	0.1380	6.49×10^{-16}	0.0443	0.0225	0.0302	0.0970
D Dimer	1.38×10^{-05}	0.0465	8.51x10-07	0.9045	1.03×10^{-05}	0.1651	1.66×10^{-05}	0.0073	1.29×10^{-06}	0.8438	7.22×10^{-07}	0.9136
Urea	0.0080	0.0038	-0.0017	0.6400	0.0084	0.0193	0.0103	0.0077	0.0054	0.2469	0.0035	0.3081
Creatinine	0.0017	6.60×10^{-07}	0.0003	0.5310	0.0015	0.0006	0.0021	1.17×10^{-05}	0.0006	0.2469	0.0006	0.0970
ALT	-8.29×10^{-05}	0.7483	-0.0007	0.1210	9.87×10^{-05}	0.7560	-0.0004	0.1304	0.0007	0.3502	0.0004	0.5119
Bilirubin	0.0036	0.0216	0.0005	0.8711	0.0019	0.3731	0.0110	1.17×10^{-05}	0.0015	0.5955	0.0028	0.1678
Albumin	-0.0176	6.29×10^{-13}	-0.0106	0.0262	-0.0202	1.38×10^{-9}	-0.0313	5.86 x10-16	-0.0142	0.0028	0.0015	0.7541
CRP	0.0020	3.15×10^{-36}	0.0011	0.0014	0.0018	1.12×10^{-12}	0.0035	2.63×10^{-69}	0.0021	2.63×10^{-15}	0.0010	0.0001
Ferritin	2.27×10^{-05}	0.2133	-2.13×10^{-05}	0.2171	5.43×10^{-05}	0.0167	3.67×10^{-05}	0.0694	-9.16×10^{-06}	0.6763	1.91×10^{-05}	0.3318
Troponin	7.86×10^{-05}	0.0713	2.03×10^{-05}	0.5417	4.86×10^{-05}	0.2144	2.37×10^{-05}	0.4311	1.05×10^{-05}	0.7658	2.17×10^{-05}	0.5119

Table 5-5 continued.

	MIS-C vs all		MIS-C vs Incomplete MIS-C		MIS-C vs Bacterial		MIS-C vs Viral		MIS-C vs Inflammatory		MIS-C vs KD	
	Coefficient	p value	Coefficient	p value	Coefficient	p value	Coefficient	p value	Coefficient	p value	Coefficient	p value
BNP	$2.96x10^{-05}$	0.0106	$1.45x10^{-05}$	0.2171	$3.53x10^{-05}$	0.0044	$1.55x10^{-05}$	0.0832	$1.54x10^{-06}$	0.8748	$1.35x10^{-06}$	0.9136
LDH	-0.0001	0.0534	-0.0002	0.0044	$-7.11x10^{-05}$	0.7229	-0.0005	0.0036	-0.0002	0.2469	-0.0003	0.0970
Creatine Kinase	$1.19x10^{-05}$	0.9364	$-6.68x10^{-05}$	0.5417	0.0002	0.2281	-0.0001	0.1274	$6.80x10^{-05}$	0.5955	$6.42x10^{-05}$	0.5030
Lactate	0.0490	0.0150	0.0321	0.2171	0.0358	0.1722	0.0460	0.0555	0.0236	0.3502	0.0149	0.5030

5.3.4 MIS-C Diagnostic score

A diagnostic score was developed to help identify patients with a greater likelihood of having MIS-C, based on the clinical and laboratory features associated with the condition. The MIS-C diagnostic score algorithm is as follows:

(Conjunctivitis present + 2.75) + (Cardiac involvement present + 2) + (Gastrointestinal symptoms present + 2) + (Headache present + 1) + (Rash present + 1) + (Fever present + 1) + (Respiratory symptoms present – 2) + ([7 – lymphocyte count] x 0.5] + ([1 – monocyte count] x 3) + ([50 – albumin] x 0.02) + (CRP x 0.02)

The median results of the diagnostic score were significantly higher in MIS-C compared to all other disease groups (MIS-C vs Incomplete MIS-C: $p = 1.43x10^{-08}$; MIS-C vs Bacterial: $p = 1.25x10^{-48}$; MIS-C vs Viral: $p = 1.46\ x10^{-49}$; MIS-C vs KD: $p = 2.94x10^{-07}$ (Figure 5-3A)). The median results of the score were also significantly higher in Incomplete MIS-C compared to Bacterial ($p = 0.002$), Viral ($p = 1.43x10^{-08}$) and Inflammatory ($p = 0.007$), but not KD ($p = 0.34$) (Figure 5-3A). The scores were normally distributed in all disease groups (Figure 5-3B). The MIS-C group formed a distinct peak which was shifted to the right indicating higher scores, with some overlap with the other disease groups (Figure 5-3B). The ROC analysis and Youden's Index identified the optimal threshold of the score as 11.7, which corresponded to a sensitivity of 0.93 and specificity of 0.86 (Figure 5-4). The performance of the diagnostic score was tested using this threshold and results are summarised in Table 5-6. The score had good performance at distinguishing MIS-C from all other groups combined (AUC 0.90) and separately (Bacterial AUC 0.88, Viral AUC 0.97, Inflammatory AUC 0.90 and KD AUC 0.80). Of note, the NPV of the score for MIS-C versus KD was lower than other comparisons at 56% (Table 5-6).

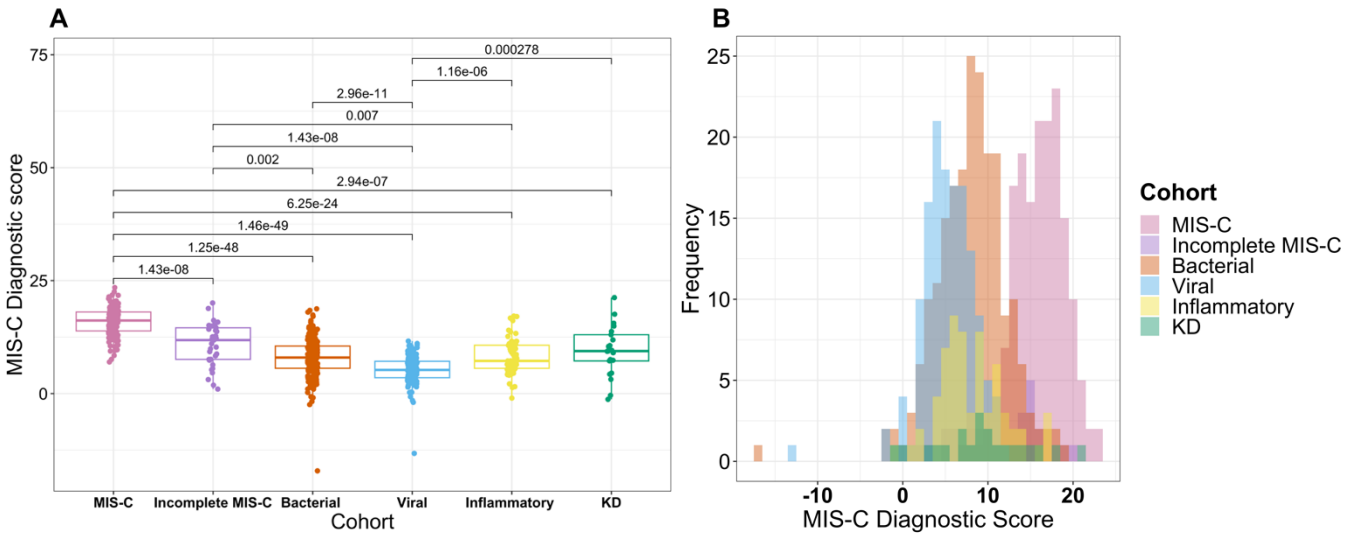

Figure 5-3 Boxplot showing the MIS-C diagnostic score results by disease group (A) and Histogram showing the distribution of the MIS-C diagnostic score results by disease group (B).

MIS-C (n = 169), Incomplete MIS-C (n = 33), Bacterial (n = 208), Viral (141), Inflammatory (n = 63) and Kawasaki disease (KD) (n = 21). Median values, IQR and significant p values following Wilcoxon pairwise comparisons with Benjamini Hochberg correction have been displayed for the boxplot.

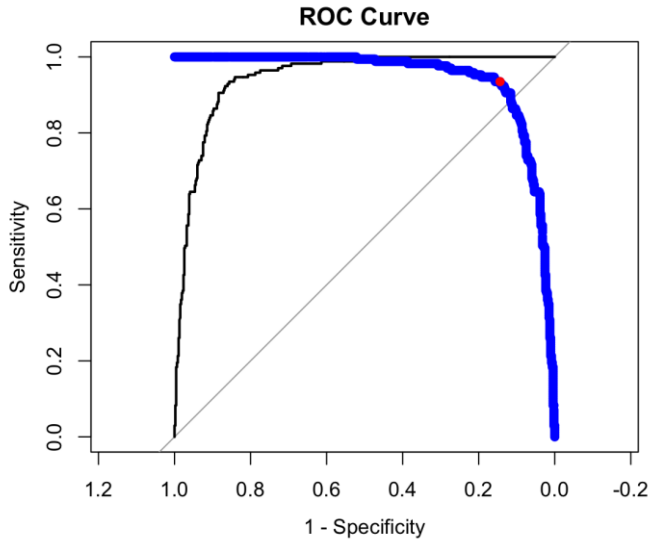

Figure 5-4 Receiver Operating Characteristic (ROC) curve analysis and Youden's index for selecting the optimal threshold for the MIS-C diagnostic score.

The blue line represents the sensitivity and specificity values at different diagnostic score thresholds. Each blue point on the line represents a specific threshold point and its corresponding sensitivity and specificity. The optimal threshold is shown as the red dot, set at 11.7, which corresponds to a sensitivity of 0.93 and specificity of 0.86.

Table 5-6 Performance of the MIS-C diagnostic score in distinguishing MIS-C from all other disease groups combined and at an individual level.

PPV = positive predictive value. NPV = negative predictive value. AUC = area under the curve. KD = Kawasaki Disease

	MIS-C vs ALL	MIS-C vs Bacterial	MIS-C vs Viral	MIS-C vs Inflammatory	MIS-C vs KD
Accuracy	88%	88%	96%	92%	91%
PPV	70%	82%	100%	95%	96%
NPV	97%	94%	93%	83%	56%
AUC	0.90	0.88	0.97	0.90	0.80

5.3.5 Longitudinal analysis of SARS-CoV-2 antibody titres in children

5.3.5.1 SARS-CoV-2 Spike (S) IgG titres

An increasing proportion of SARS-CoV-2 S IgG positive results was observed within all disease groups across the years 2020, 2021 and 2022 (Table 5-7 and Figure 5-5). The proportion of positive results in the non-MIS-C groups was 16% in 2020, 45% in 2021 and 80% in 2022 (Table 5-7). Although the number of individuals in the under 5 years of age sub-group was smaller, the same trend of increasing SARS-CoV-2 S IgG seropositivity over time was observed (2020: 12%, 2021: 40%, 2022: 88%). Of note, there were smaller numbers of MIS-C and Incomplete MIS-C cases in 2022, compared to the preceding two years (Table 5-7 and Figure 5-5).

Table 5-7 Longitudinal analysis of SARS-CoV-2 Spike IgG results in children under the age of 18 years, with a sub- analysis of children under the age of 5 years.

	SARS-CoV-2 Spike IgG positive results in children under the age of 18 years, number of individuals (%)		
	2020 (< 18 years)	**2021 (< 18 years)**	**2022 (< 18 years)**
MIS-C	36/39 (92.3%)	121/122 (99.2%)	14/14 (100%)
Incomplete MIS-C	5/7 (71.4%)	19/22 (86.4%)	1/1 (100%)
Bacterial	20/108 (18.5%)	44/88 (50%)	43/58 (74%)
Viral	8/55 (14.6%)	28/78 (35.8%)	59/69 (86%)
Inflammatory	3/28 (10.7%)	15/31 (48.4%)	13/16 (81%)
KD	1/7 (14.3%)	6/11 (54.6%)	5/7 (71%)
TOTAL Non-MIS-C	32/198 (16.2%)	93/208 (44.7%)	120/150 (80%)
	Sub-analysis of SARS-CoV-2 Spike IgG positive results in children under the age of 5 years, number of individuals (%)		
	2020 (< 5 years)	**2021 (< 5 years)**	**2022 (< 5 years)**
MIS-C	7/8 (87.5%)	21/22 (95.5%)	1/1 (100%)
Incomplete MIS-C	1/3 (33.3%)	5/5 (100%)	NA
Bacterial	5/39 (12.8%)	16/35 (45.7%)	17/20 (85%)
Viral	3/35 (8.6%)	13/48 (27.1%)	19/25 (76%)
Inflammatory	1 / 2 (50%)	5/13 (38.5%)	4/5 (80%)
KD	0/5 (0%)	5/9 (55.6%)	4/6 (66.7%)
TOTAL Non-MIS-C	10/82 (12.2%)	44/110 (40%)	44/50 (88%)

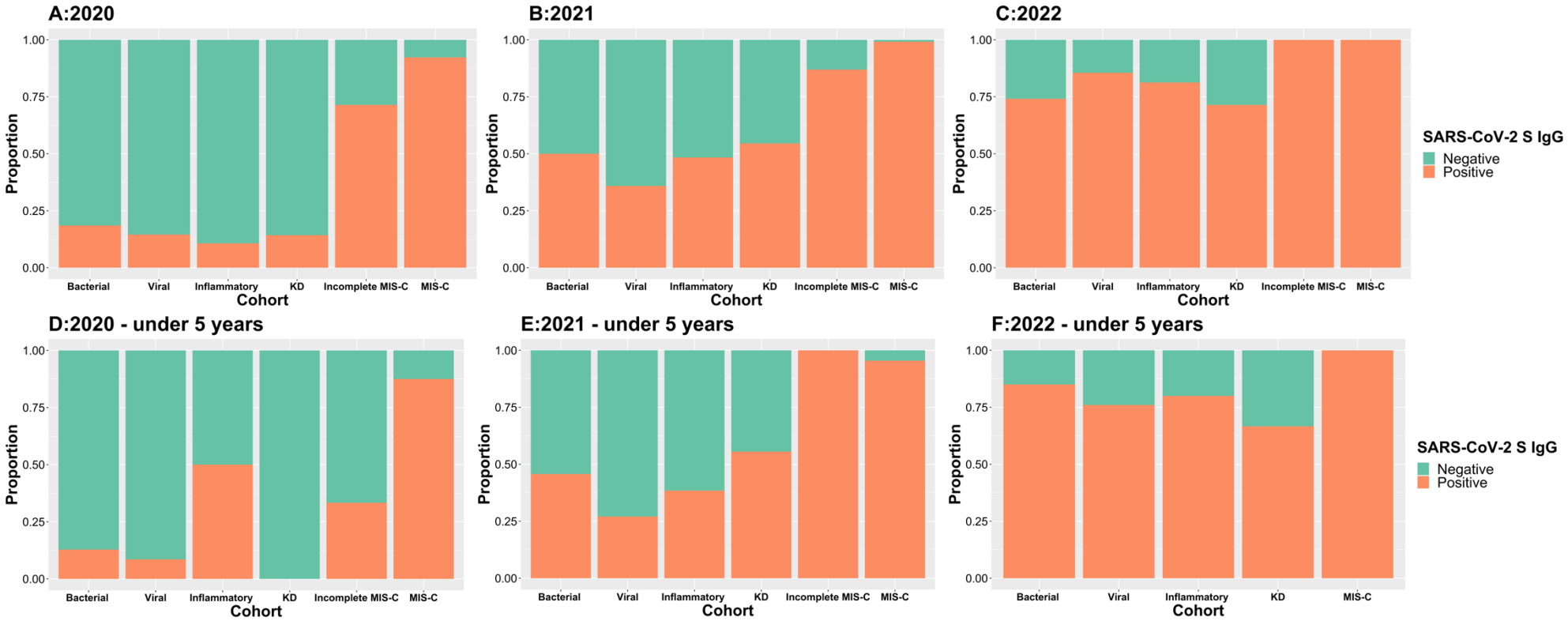

Figure 5-5 Bar charts showing the proportion of children positive and negative for SARS-CoV-2 Spike (S) IgG in 2020, 2021 and 2022.

Graphs in Panels A, B, C and include children under the age of 18 years, while graphs in panels D, E, F represent children under the age of 5 years. 2020: MIS-C n = 39, under 5 n = 8; Incomplete MIS-C n = 7 under 5 n = 3; Bacterial n = 108 under 5 n = 39; Viral n = 55 under 5 n = 35; Inflammatory n = 28 under 5 n = 2; KD n = 7 under 5 n = 5. 2021: MIS-C n = 112 under 5 n = 22; Incomplete MIS-C n = 22 under 5 n = 5; Bacterial n = 88 under 5 n = 35; Viral n = 78 under 5 n = 48; Inflammatory n = 31 under 5 n = 13; KD n = 11 under 5 n = 5. 2022: MIS-C n = 14 under 5 n = 1; Incomplete MIS-C n = 22 under 5 n = 0; Bacterial n = 88 under 5 n = 20; Viral n = 78 under 5 n = 25; Inflammatory n = 31 under 5 n = 5; KD n = 11 under 5 n = 6.

5.3.5.2 SARS-CoV-2 Nucleocapsid (N) IgG titres

The results of SARS-CoV-2 N IgG titres for samples collected in 2022 are shown in Table 5-8 and Figure 5-6. Although the proportion of SARS-CoV-2 N IgG positive cases in the non-MIS-C group for children < 18 years of age was lower than the SARS-CoV-2 S IgG results, over 70% of children were SARS-CoV-2 N IgG positive (N IgG 73% vs S IgG 80%). A lower proportion, but still considerable number of cases (23/57) were positive for SARS-CoV-2 N IgG in the < 5 years of age sub-group (N IgG 40% vs S IgG 80%).

Table 5-8 SARS-CoV-2 Nucleocapsid IgG results of samples collected in 2022.

	SARS-CoV-2 Nucleocapsid IgG positive, n (%)	
	2022 < 18 years	**2022 < 5 years**
MIS-C	13/14 (93%)	0/1 (0%)
Incomplete MIS-C	1/1 (100%)	NA
Bacterial	42/58 (72%)	6/20 (30%)
Viral	47/69 (68%)	11/25 (44%)
Inflammatory	14/16 (88%)	2/5 (40%)
KD	6/7 (86%)	4/6 (66.7%)
TOTAL Non-MIS-C	109/150 (73%)	23/57 (40%)

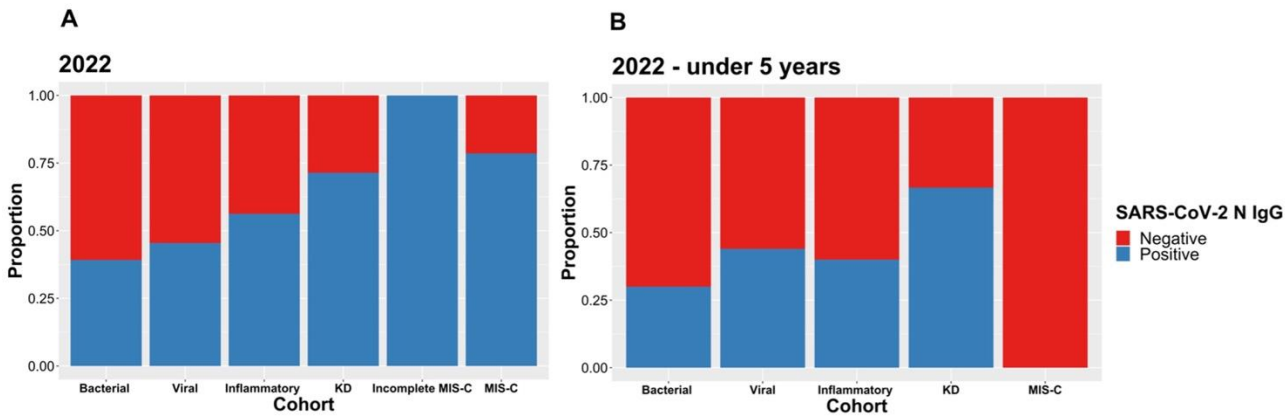

Figure 5-6 Bar charts showing the proportion of children positive and negative for SARS-CoV-2 Nucleocapsid (N) IgG from samples collected in 2022.

Graph A includes data from children under the age of 18 years, while graphs B includes children under the age of 5 years. MIS-C n=14, under 5 n=1; Incomplete MIS-C n=1 under 5 n=0; Bacterial n= 58 under 5 n=20; Viral n=69 under 5 n=25; Inflammatory n=16 under 5 n= 5; KD n=7 under 5 n=6.

5.4 Discussion

Following the emergence of MIS-C there was increased diagnostic uncertainty, due to the similarities with other inflammatory and infectious diseases (e.g. KD, TSS) and the absence of a diagnostic test. Exposure to SARS-CoV-2, including positive SARS-CoV-2 IgG, is part of the WHO and CDC MIS-C case definitions. Early data (2020-2021) demonstrated that MIS-C had the highest proportion of SARS-CoV-2 S IgG seropositivity, compared with other diagnoses (Bacterial, Viral, Inflammatory and KD) (Table 5-1), and that a positive IgG result was significantly associated with an increased likelihood of an MIS-C diagnosis (Table 5-3). These results confirm that SARS-CoV-2 seropositivity is specific to MIS-C and may aid its diagnosis. Additionally, patients with MIS-C and Incomplete MIS-C had significantly higher titres of SARS-CoV-2 IgG compared to patients with Bacterial, Viral, KD and other Inflammatory diseases – suggesting the potential diagnostic value of SARS-CoV-2 IgG titres (Figure 5-2). Similar findings have been reported in other studies where higher antibody levels were seen in MIS-C compared to other diseases[289,409]. This indicates while antibody quantity may not be playing a role in MIS-C disease severity, as indicated by the results in Chapter 4, it could be an important factor in the pathogenesis or immunopathology of MIS-C.

The longitudinal analyses presented in this chapter reveal an increase in SARS-CoV-2 S and N IgG seropositivity among non-MIS-C cases from 2020 to 2022 (Figure 5-5 and Figure 5-6). Notably, no studies have reported SARS-CoV-2 antibody results over time prior to this. These trends are likely due to natural infection or vaccination and highlight the reduced diagnostic utility of this marker over time. Moreover, the findings suggest the need to revise the current WHO and CDC MIS-C case definitions, which include SARS-CoV-2 seropositivity, to reflect the evolving epidemiology and they emphasize the need for more specific diagnostic tests.

Additionally, this prompts a discussion on the evolving significance of predictive values. In the early stages of the pandemic, a positive antibody result held significant positive predictive value (PPV), aiding in early detection and management. However, as seropositivity becomes more widespread, the relative importance of the negative predictive value (NPV) of a negative antibody result increases, reflecting the need for adapted diagnostic strategies over time.

Moreover, serological assays extend beyond producing binary results. Assessment of additional parameters, including titre, avidity, acute/convalescent status, and the IgM/IgG ratio, has the potential to provide invaluable insights into the recency of infection. This, in turn, contributes to a more refined understanding of the temporal aspects of immune responses to SARS-CoV-2.

Evaluation of clinical and laboratory markers allowed identification of features which distinguished MIS-C from other febrile illnesses including: conjunctivitis, gastrointestinal symptoms, cardiac involvement, lymphopenia, hypoalbuminemia, and elevated CRP levels. These findings align with existing literature and provide further evidence of the distinct clinical profile of MIS-C[196,199,410]. Of note, monocytopenia was also found to be highly associated with MIS-C, which has yet to be reported in other clinical descriptions of MIS-C. This finding aligns with the results from Gruber et al., who reported reduced non-classical monocytes in peripheral blood immunophenotyping studies[402]. Their findings, combined with their reporting of increased mediators of monocyte chemotaxis, suggests possible migration of monocytes to affected tissues[402]. The clinical significance of this novel association awaits validation in an external cohort, but if confirmed, monocytopenia's specificity for MIS-C could impact diagnosis, management strategies, and future research into the pathophysiology of MIS-C. Finally, it appears that while there are similarities in the clinical, laboratory and serological profiles of MIS-C and Incomplete MIS-C, some differences remain; with Incomplete MIS-C likely representing a milder spectrum of disease which is not being captured by the current diagnostic criteria.

The MIS-C diagnostic score demonstrated excellent performance with an AUC of 0.9 in the analysed cohort, suggesting its potential as a valuable tool for expediting clinical decision-making and initiating timely, targeted treatment and ultimately contributing improved patient outcomes. However, it's crucial to acknowledge the inherent limitations associated with retrospectively developing clinical diagnostic scores using parameters from diagnostic criteria. This approach may introduce biases such as verification bias, spectrum bias, recall bias, and selection bias. Despite these challenges, when there is no gold standard for diagnosis and the goal is to establish a tighter definition of the disease, this methodology can be a valid and pragmatic approach. To increase the reliability of the diagnostic score and mitigate biases, external validation in independent cohorts and prospective studies is essential and ensures the generalisability of the score across diverse populations. Furthermore, the incorporation of unsupervised machine learning techniques or variable selection methods (e.g. Least Absolute Shrinkage and Selection Operator), could further enhance the performance of the score.

While other MIS-C clinical diagnostic tools have been developed by various groups[246–250], this score offers a simple, cost-effective, and reliable approach to facilitate the diagnosis of MIS-C. Similar diagnostic scoring systems have been successfully employed in other infectious and inflammatory conditions. For instance, the American College of Rheumatology/European League Against Rheumatism (ACR/EULAR) criteria are often used for classification of rheumatoid arthritis[411] and the

Modified Centor Score[412] assesses streptococcal pharyngitis probability, guiding diagnostic test and management decisions – highlighting the versatility and effectiveness of diagnostic scores.

Researchers have also identified biomarkers[252,253], immune[254] and gene expression signatures[256,257] associated with MIS-C, which have the potential to be developed into more specific and accurate diagnostic tests. Ultimately, it is important to consider the evolving nature of MIS-C and ongoing monitoring and refinement of diagnostic scores and tests to ensure their applicability and accuracy in future clinical practice.

This work benefits from a large dataset of patients recruited from multiple sites across Europe. This comprehensive dataset enhances the generalisability of the findings and provides valuable insights which are applicable to a broad population. Despite having a rigorous data collection protocol in the DIAMONDS study, missing data was observed in the clinical features and laboratory markers fields. Moreover, the lack of reporting on the absence of clinical features and the potential bias introduced by the likelihood of missingness being related to the output or exposure are important to consider. Imputation of missing blood markers was considered but ultimately not carried out, to maintain the integrity of the data and to avoid biases associated with imputation. Additionally, it is crucial to highlight that while this work primarily involved exploratory analysis, the presence of multiple comparisons was addressed through p-value correction. However, it is important to recognise that despite these corrections, the potential for issues related to multiple comparisons persists (e.g., increased risk of Type I errors, overestimation of significance) and warrants consideration.

5.5 Conclusion

In conclusion, this work contributes valuable insights into the understanding and diagnosis of MIS-C. The presence of higher SARS-CoV-2 S IgG antibody titres in MIS-C compared to all other disease groups, suggests the potential role of antibodies in MIS-C disease pathogenesis, which warrants further exploration. However, the prevalence of SARS-CoV-2 seropositivity in the population has increased over time, which highlights the need to revise the WHO and CDC MIS-C case definitions and the need to identify specific diagnostic markers for MIS-C. The diagnostic score based on clinical and laboratory features has demonstrated excellent performance in distinguishing MIS-C from other diseases, with an AUC of 0.9. Future research should focus on external validation and refinement of the MIS-C diagnostic score, before implementing it in the clinical setting. It is important to recognise that the reported cases may represent only the tip of the iceberg, as shown by the milder phenotype observed in the Incomplete MIS-C group, and the additional diagnostic challenges posed by the

increasing background rates of SARS-CoV-2 seropositivity. Continued collaborative efforts and multi-centred studies are crucial for keeping pace with the changing epidemiology and clinical presentation of MIS-C and for developing alternative and specific diagnostic strategies, such as protein and RNA-signatures, to improve accuracy and specificity. Overall, these findings contribute to the understanding of MIS-C and provide valuable insights for clinical practice and future research endeavours.

Chapter 6: Clinical characterisation of MIS-C and development of a severity prediction score

6.1 Introduction

MIS-C is a complex and evolving condition which has presented unique challenges in clinical diagnosis and management. Building upon the insights gained from Chapter 5, which focussed on distinguishing MIS-C from other diseases, the work in this chapter delves into the clinical characterisation of MIS-C, identification of factors associated with disease severity and development of a MIS-C severity prediction score.

Children with MIS-C present with a wide spectrum of disease severity and can deteriorate rapidly, with a significant proportion developing shock (60%), cardiac dysfunction (54%) and multiorgan failure requiring intensive care (71%)[192]. Among the cardiac complications, left ventricular dysfunction (LVD), coronary artery aneurysms (CAAs) and myocarditis, are the most frequently reported[212,413,414]. The potential long-term impacts on cardiovascular health associated with CAA and severe myocarditis, raise significant concerns. Studies on Kawasaki Disease (KD), which shares many overlapping features with MIS-C, have shown a dramatic reduction in risk, severity and complications of CAA through early detection and prompt management[415–417]. Hence, early identification of children at risk of developing severe MIS-C and associated cardiac complications is crucial for optimising clinical management and preventing long-term complications.

In response to the emergence of MIS-C in May 2020, numerous studies were rapidly initiated to enhance the understanding of the novel paediatric inflammatory condition, with emphasis on advancing diagnostic abilities and establishing safe and efficacious treatment approaches. The Best Available Treatment Study (BATS) is a prime example of the efforts made by paediatricians across the globe, coming together to answer critical research questions regarding treatment safety and efficacy in the absence of randomised control trials. I was part of the BATS study working group and helped to set up the BATS consortium in June 2020, which now comprises of partners from over 70 centres in 39 countries. The study involved comprehensive, retrospective collection of daily deidentified data on patients with MIS-C including symptoms, blood markers, physiological markers, treatment, complications, and outcomes. The primary aim of BATS was to compare outcomes following different treatments. The results of the interim and final analyses have been published, showing no significant difference in the two primary outcomes 1) composite of ventilator and inotropic support and 2) death,

following treatment with IVIG alone, glucocorticoids alone or IVIG and glucocorticoids combined [320,321].

The BATS dataset provided an invaluable opportunity to address important research questions including descriptive analyses of MIS-C from a large, international cohort, identification of factors associated with disease severity and development of a severity prediction score. Several studies have identified risk factors for severe disease in MIS-C [236,262,413,418] and Brisca et al. highlighted the value of using severity classifications for guiding clinical management[419]. However, the development of prognostic tools for MIS-C remains limited. Savorgnan et al. made strides in this area by developing a scoring system consisting of physiological and laboratory parameters which was able to stratify MIS-C disease severity with good performance (AUC 0.90)[276]. However, this study focussed exclusively on PICU patients, and scoring systems that can effectively assess disease severity in a broad range of MIS-C patients are needed. Thus, the work in this chapter will focus on the analysis of the BATS dataset to address these gaps.

<u>The primary aim of this chapter is:</u>

To comprehensively characterise the clinical and laboratory features of MIS-C and to develop a disease severity score using physiological and laboratory parameters.

<u>The objectives of this chapter are:</u>

1) Conduct descriptive analyses on the international BATS MIS-C cohort to gain insights into the demographic, clinical and laboratory variables associated with MIS-C.
2) Evaluate the associations of demographic, clinical and laboratory variables with MIS-C disease severity and cardiac complications.
3) Assess existing and novel scores to determine their ability to identify patients with MIS-C at risk of developing severe disease and cardiac complications.

<u>The key findings from this chapter are:</u>

The work in this chapter makes valuable contributions to the field of MIS-C research. The descriptive analyses conducted on a large, international cohort provide a comprehensive understanding of the clinical characteristics of this condition. Variables associated with MIS-C disease severity were identified, leading to the development of a highly accurate severity classification and prediction score

(AUC 0.88). Following validation, the integration of the severity score into clinical practice holds significant implications for clinical management. The severity score offers a valuable approach for early risk stratification, enabling appropriate resource allocation and timely interventions for at-risk patients, potentially leading to improved patient outcomes.

6.2 Methodology

6.2.1 Clinical Cohort

The BATS international cohort consists of patients between the ages of 0 to 19 years with confirmed MIS-C meeting the WHO[204], CDC[203], or UK[194] case definitions as well as suspected inflammatory cases related to SARS-CoV-2 not meeting these criteria. Further details on BATS can be found in Chapter 3 (section 3.1.2).

6.2.2 Data QC

The dataset underwent QC checks prior to analysis, including data cleaning to address missing values and outliers, appropriate data transformation and resolution of data inconsistency. Interpolation was employed for imputing missing values where applicable, for example, if the level of respiratory support was recorded as "oxygen" on day 1 and day 3, but there is a missing value for day 2, the level of respiratory support for day 2 was estimated to be “oxygen”. Additionally, variables with different units, such as laboratory markers, were standardised to the units used in the UK. Data consistency checks were performed to identify any discrepancies, for example if oxygen saturations are recorded as less than 90% but respiratory support recorded as “none”.

6.2.3 R packages

The following R packages were used for the analysis and graphical representation of the data: gtsummary, ggpubr, dplyr, beeswarm, ggplot2, scales, tidyverse, hrbthemes, viridis, Hmisc, tidyr and pROC.

6.2.4 Descriptive analyses

The descriptive analysis of the demographic, clinical and laboratory variables included the use of medians and interquartile range for continuous variables and proportions for categorical variables. These analyses were performed for the entire cohort and then repeated following stratification by disease severity categories.

The demographic features included in the analysis were: age, sex, self-reported ethnicity, weight z-scores, significant comorbidities, and resource settings[420]. The following conditions which were classified as significant comorbidities: asthma, severe allergy, obesity, autoimmune disease, primary immunodeficiency, secondary immunodeficiency, HIV, juvenile idiopathic arthritis, chronic lung disease, congenital heart disease, chronic kidney disease, chronic liver disease, chronic neurological disorder, previous KD, malignancy and sickle cell disease.

Clinical features consisted of presenting symptoms, results of SARS-CoV-2 PCR and serology, whether the KD criteria were met, treatment received, ECHO findings and markers of clinical severity (inotropic support, invasive ventilation, renal replacement therapy (RRT), extracorporeal membrane oxygenation (ECMO) requirement, death, and length of admission).

The admission blood test results were used for the analysis of laboratory markers. These included: Hb, WBC, neutrophils, lymphocytes, platelets, sodium, phosphate, creatinine, ALT, albumin, D-dimer, fibrinogen, activated partial thromboplastin time (APTT), troponin, BNP, CRP, ferritin, lactate, and Vitamin D.

6.2.5 Disease severity and cardiac complications

6.2.5.1 Severity categories

Key variables, including location of care, medical interventions, and organ support were used to design the severity categories. Patients previously admitted to hospital for the same illness episode (e.g. local hospital prior to transfer to tertiary centre), were excluded from the severity analyses, to ensure baseline severity was accurately reflected. The rules for severity classification are presented in Table 6-1. Of note, the decision to include patients admitted to PICU without need for extensive organ support in the “Moderate” category, was based on the observation that many MIS-C patients were admitted to PICUs for close monitoring, despite not requiring significant organ support. This may be attributed to the uncertainty surrounding the novel condition and rapid deterioration seen in these patients or due to different thresholds for admission to PICU across the globe.

Table 6-1 Disease severity categories for MIS-C.

Severity	Descriptor
Mild	Admitted on a ward AND No support
Moderate	Oxygen therapy AND/OR Fluid bolus AND/OR Non-invasive ventilation AND/OR PICU admission
Severe	Invasive ventilation OR Vasopressors
Very Severe	Invasive ventilation AND Vasopressors OR Invasive ventilation AND RRT/ECMO OR Vasopressors AND RRT/ECMO OR Invasive ventilation AND Vasopressors AND RRT/ECMO OR Invasive ventilation AND Vasopressors AND RRT AND ECMO OR Patient died

The proportion of patients in each severity category was assessed at baseline, 24 hours, 48 hours, 72 hours, 96 hours, and 120 hours, along with maximum severity during admission. Preliminary analyses showed that the highest proportion of patients categorised as Severe or Very Severe was at the 48-hour timepoint. Consequently, the 48-hour timepoint was selected for the prediction of future severity analyses. The change in severity from baseline to 48 hours was assessed by assigning patients to either the "Stable/Improvement group" or the "Deterioration" group using the rules shown in Table 6-2.

Table 6-2 Rules for assignment of patients to Stable/Improvement or Deterioration group according to the change in their severity status from baseline to 48 hours.

Stable/Improvement group		**Deterioration group**	
Baseline	**48 hours**	**Baseline**	**48 hours**
Mild	Mild	Mild	Moderate/Severe/Very Severe
Moderate	Moderate/Mild	Moderate	Severe/Very Severe
Severe	Moderate/Mild	Severe	Very Severe
Very Severe	Severe/Moderate/Mild		

6.2.5.2 Cardiac complications

Cardiac complications were defined as the presence of any of the following ECHO findings: CAA, myocarditis, LVD, persistent CAA, and any abnormal echocardiogram finding (endocarditis, pericarditis, pericardial effusion, CAA, myocarditis, LVD or valvular dysfunction). All the patients included in the analyses had an ECHO during their hospital admission. The ECHO findings were entered into the BATS database using reports from clinical notes written by the healthcare professional performing the scan. CAA was defined as a z-score greater than 2.5[417,421]. Z-scores are used to assess the relative size of an individual's coronary arteries compared to a healthy population; they represent the number of standard deviations away from the mean value of measurements in a healthy population. Persistent CAA was defined as CAA present on the pre-hospital discharge ECHO.

6.2.5.3 Severity analyses

<u>The associations of demographic, clinical and laboratory variables with disease severity and cardiac complications</u>

The demographic features, clinical features, laboratory markers and cardiac complications were stratified by severity to identify any differences across severity categories. The severity categories were then converted to binary outputs, “Mild/Moderate” and “Severe/Very Severe”, for statistical testing, to see if significant differences existed in the distribution of characteristics between severity groups. Categorical variables were analysed using the Chi-squared test, while continuous variables were compared using Wilcoxon pairwise comparisons. The proportion of missing laboratory results were also compared amongst severity groups using the Chi-squared test to assess for any bias.

A multivariable logistic regression model was used for calculation of odds ratios (OR), to quantify the strength and direction of the associations between demographic, clinical and laboratory variables and 1) disease severity and 2) cardiac complications. For the demographic features, the reference variables were: sex = female, ethnicity = Caucasian and resource setting = High-Income. To ensure validity of the analysis and reduce bias introduced by missing values, laboratory markers with high proportion of missing values were excluded from the model including phosphate, Vitamin D, BNP and ferritin. WBC was also excluded from the model to prevent multicollinearity with neutrophils and lymphocytes.

Physiological score

A previously published physiological score[422] was applied to assess its association with disease severity and utility in identifying patients at risk of Severe/Very Severe disease. The total physiological score comprises of cardiovascular, neurological, and respiratory components, added together in a 1:1:1 ratio. The cardiovascular, neurological, and respiratory scores are calculated using the first available vital signs on presentation to a hospital as described in Table 6-3. Multiple different weightings for the cardiovascular, respiratory, and neurological elements were trialled to reflect the MIS-C clinical picture (e.g. higher weighting of cardiovascular element 2:1:1). However, the optimal performance was seen when using a 1:1:1 ratio. This piece of work was carried out by Dr Clare Wilson.

Table 6-3 Total physiological score calculation.

HR = heart rate, SBP = systolic blood pressure, CRT = Capillary refill time, RR = respiratory rate, AVPU score = neurological assessment tool used to evaluate level of consciousness[423]*.*

Score	**Calculation**
Cardiovascular:	(HR – mean HR for age) + (mean SBP for age – SBP) + (25 x CRT)
Neurological:	(SBP – mean SBP for age) + (mean HR for age – HR) + (25 x AVPU score)
Respiratory:	(RR – mean RR for age) + (5 x (100 – oxygen saturation)
Total physiological score	Cardiovascular + Neurological+ Respiratory

Laboratory score

The logistic regression analysis identified significant variables for the laboratory severity score. These variables were scaled and adjusted based on normal range values to align with typical healthy values, incorporating a systematic refinement for accurate representation of changes. Weights, initially informed by clinical judgment and odds ratio results from the logistic regression analysis, were added and subsequently refined. The score was refined iteratively for accuracy and clinical applicability. After initial scaling and addition of weights, further adjustments were made systematically, aligning with clinical outcomes and clinician feedback. Sensitivity analyses were used to optimise the balance between sensitivity and specificity.

Only a small proportion of patients (27%, 346/1285) had complete data to generate a laboratory score. Therefore, imputation was used to replace the missing values with the median value of the respective variable for the specific severity category to which the patient belonged.

Combined physiological and laboratory score and performance of scores

The physiological score results and laboratory score results were combined after scaling. The score results were compared across disease severity categories, stable/deterioration categories and cardiac complications using Wilcoxon pairwise comparisons with BH correction. ROC and AUC were used to evaluate the performance of the physiological score, laboratory score and the combined score in predicting the distinction between a) Mild/Moderate and Severe/Very Severe disease categories at baseline and at 48 hours b) stable patients and deteriorating patients c) cardiac complications.

6.3 Results

6.3.1 Descriptive analyses of demographic features, clinical characteristics, and laboratory markers in MIS-C

A total of 1,285 patients were included in this analysis from 39 countries. The demographic features, clinical characteristics and laboratory results are outlined in Table 6-4, Table 6-5, and Table 6-6, respectively.

The cohort had a male preponderance (59%), the median age was 7.2 years (IQR 3-8 – 11 years) and Caucasian (41%) and Hispanic (31%) ethnicities were more prevalent than others in this cohort. The median weight z-score was 0.47 (IQR -0.3 – 1.4) and 6% of the cohort had significant comorbidities. The majority of the patients were from High-Income (47.9%) or Upper Middle-Income (44%) resource settings. The median fever duration was 5 days (IQR 3-6 days), with gastrointestinal symptoms (52%), rash (58%), conjunctivitis (53%), and mucocutaneous changes (49%) being the most common presenting features. SARS-CoV-2 serology positivity was observed in 68% of the cohort, while a smaller subset was SARS-CoV-2 PCR positive (22%). The baseline laboratory results showed lymphopenia, raised markers of inflammation (CRP and ferritin), deranged coagulation (raised D-dimer and fibrinogen), poor renal function (hyponatremia and raised creatinine), and low Vitamin D levels. Of note, several laboratory markers, including phosphate, BNP, ferritin, lactate, and Vitamin D, had a high percentage of missing values (40-95%). Around half of the cohort (52%) had abnormal ECHO findings, with LVD (21%) and CAA (12%) being the most commonly reported cardiac complications. Persistent CAA was noted in a small portion of patients (6%). Majority of the patients were treated with IVIG (49%) and corticosteroids (46%), with a small proportion receiving other immunomodulatory agents. In terms of clinical severity markers, 24% required inotropic support, 8% required invasive ventilation, 1% had RRT, and 0.4% underwent ECMO. The overall mortality rate was 1%, and the median length of hospital stay was 9 days (IQR 6 – 13 days).

Table 6-4 Demographic features of the Best Available Treatment Study MIS-C cohort.

n = counts, % = percentages, IQR = interquartile range

Demographic features	**(n = 1285)**
Age (years), median [IQR]	7.2 [3.8 - 11]
Sex	
Female, n (%)	530 (41%)
Male, n (%)	755 (59%)
Ethnicity	
Asian, n (%)	61 (5%)
Black, n (%)	111 (9%)
Caucasian, n (%)	522 (41%)
Hispanic, n (%)	400 (31%)
Other or not known, n (%)	191 (15%)
Weight z-score, median [IQR]	0.47 [-0.3 - 1.4]
Significant Comorbidity, n (%)	75 (6%)
Resource setting	
Low and Lower Middle-Income Economies, n (%)	102 (8%)
Upper Middle-Income Economies, n (%)	568 (44%)
High-Income Economies, n (%)	615 (48%)

Table 6-5 Clinical characteristics of the Best Available Treatment Study MIS-C cohort.

n = counts, % = percentages, IQR = interquartile range, BCG = Bacillus Calmette–Guérin.

Clinical features	**Overall (n = 1285)**
Days of fever, median [IQR]	5.0 [3.0 - 6.0]
Sore cough, n (%)	317 (25%)
Cough, n (%)	270 (21%)
Respiratory distress, n (%)	132 (10%)
Abdominal pain, n (%)	761 (59%)
Diarrhoea, n (%)	545 (42%)
Vomiting, n (%)	683 (53%)
Headache, n (%)	387 (30%)
Seizures, n (%)	21 (2%)
Encephalopathy, n (%)	47 (4%)
Irritable, n (%)	253 (20%)
Lethargy, n (%)	423 (33%)
Joint pain, n (%)	119 (9%)
Rash, n (%)	751 (58%)
Conjunctivitis, n (%)	682 (53%)
Oedema, n (%)	333 (26%)
Mucocutaneous changes, n (%)	627 (49%)
Skin peeling, n (%)	68 (5%)
Lymphadenopathy, n (%)	358 (28%)
BCG reactivation, n (%)	10 (0.8%)
Full KD criteria met, n (%)	338 (26%)
SARS-CoV-2 PCR Positive, n (%)	285 (22%)
SARS-CoV-2 Serology Positive, n (%)	871 (68%)

Clinical features	**Overall (n = 1285)**
TREATMENT	
Corticosteroids, n (%)	1016 (46%)
IVIG, n (%)	1081 (49%)
Anti-IL1,n (%)	69 (3%)
Anti-IL6,n (%)	43 (2%)
Anti-TNFα,n (%)	11 (0.5%)
Other, n (%)	10 (0.5%)
ECHOCARDIOGRAM FINDINGS	
Left ventricular dysfunction, n (%)	260 (21%)
Myocarditis, n (%)	107 (9%)
Coronary artery aneurysm, n (%)	152 (12%)
Persistent coronary artery aneurysm, n (%)	48 (6%)
Any abnormal findings, n (%)	636 (52%)
Inotropic agents, n (%)	309 (24%)
Invasive ventilation, n (%)	95 (8%)
Renal Replacement therapy, n (%)	17 (1%)
ECMO, n (%)	5 (0.4%)
Death, n (%)	17 (1%)
Length of admission (days), median [IQR]	9.0 [6.0 - 13]

Table 6-6 Baseline laboratory markers in the Best Available Treatment Study MIS-C cohort.

IQR = interquartile range, NR = normal range, NR values are from the Royal College of Paediatrics and Child Health[424]

Laboratory markers	**Overall: n = 1285**	**Missing, n (%)**
Haemoglobin (g/L), median [IQR] NR: 110 – 140	120 [110 - 130]	51 (4%)
White Blood Count (x10^9/L), median [IQR] NR: 5 – 12	10 [7.1 - 15]	52 (4%)
Neutrophils (x10^9/L), median [IQR] NR:2 – 8	7.9 [5.2 - 11]	143 (11%)
Lymphocytes (x10^9/L), median [IQR] NR: 1.5 – 9.5	1.3 [0.73 - 2.1]	107 (8%)
Platelets (x10^9/L), median [IQR] NR: 150 – 450	180 [120 - 270]	65 (5%)
Sodium (mmol/L), median [IQR] NR: 135 – 146	130 [130 - 140]	221 (17%)
Phosphate (mmol/L), median [IQR] NR: 0.8 – 1.5	1.1 [0.94 - 1.4]	891 (69%)
Creatinine (μmol/L), median [IQR] NR: 13 – 90	47 [35 - 64]	206 (16%)
ALT (U/L), median [IQR] NR: 0 – 37	32 [19 - 58]	256 (20%)
Albumin (g/L), median [IQR] NR: 35 – 50	34 [30 - 39]	383 (30%)
D dimer (ng/ml), median [IQR] NR: < 500	2400 [1200 - 4200]	507 (40%)
Fibrinogen (g/L), median [IQR] NR: 1.5 – 4	5.3 [4.2 - 6.5]	480 (37%)
APTT (s), median [IQR] NR: 28 – 45	33 [28 - 38]	449 (35%)
Troponin (ng/L), median [IQR] NR: < 10	18 [5.0 - 50]	597 (47%)
BNP (pg/ml), median [IQR] NR: NA	140 [33 - 620]	1066 (83%)

Table 6-6 continued.

Laboratory markers	**Overall: n = 1285**	**Missing, n (%)**
CRP (mg/L), median [IQR] NR: < 5	140 [82 - 220]	194 (15%)
Ferritin (ng/ml), median [IQR] NR: 12 – 200	390 [210 - 730]	572 (45%)
Lactate (mmol/L), median [IQR] NR: 1-2	1.8 [1.2 - 2.4]	808 (63%)
Vitamin D (nmol/L), median [IQR] NR: 50 – 250	33 [22 - 45]	1223 (95%)

6.3.2 The associations of demographic, clinical and laboratory variables with disease severity and cardiac complications

Having conducted the descriptive analyses of this cohort, I proceeded to assess the proportion of individuals in each of the pre-defined disease severity categories (Table 6-1) at multiple timepoints, as well as the maximum severity during hospital admission. The maximum disease severity results showed that the majority of patients with MIS-C had Mild (37%) or Moderate (35%) disease with smaller proportions with Severe (21%) and Very Severe disease (7%) (Figure 6-1). There was an increase in the proportion of patients with Severe or Very Severe disease from 15% at baseline, to 19% at 24 hours, peaking at 22% at 48 hours and subsequently falling.

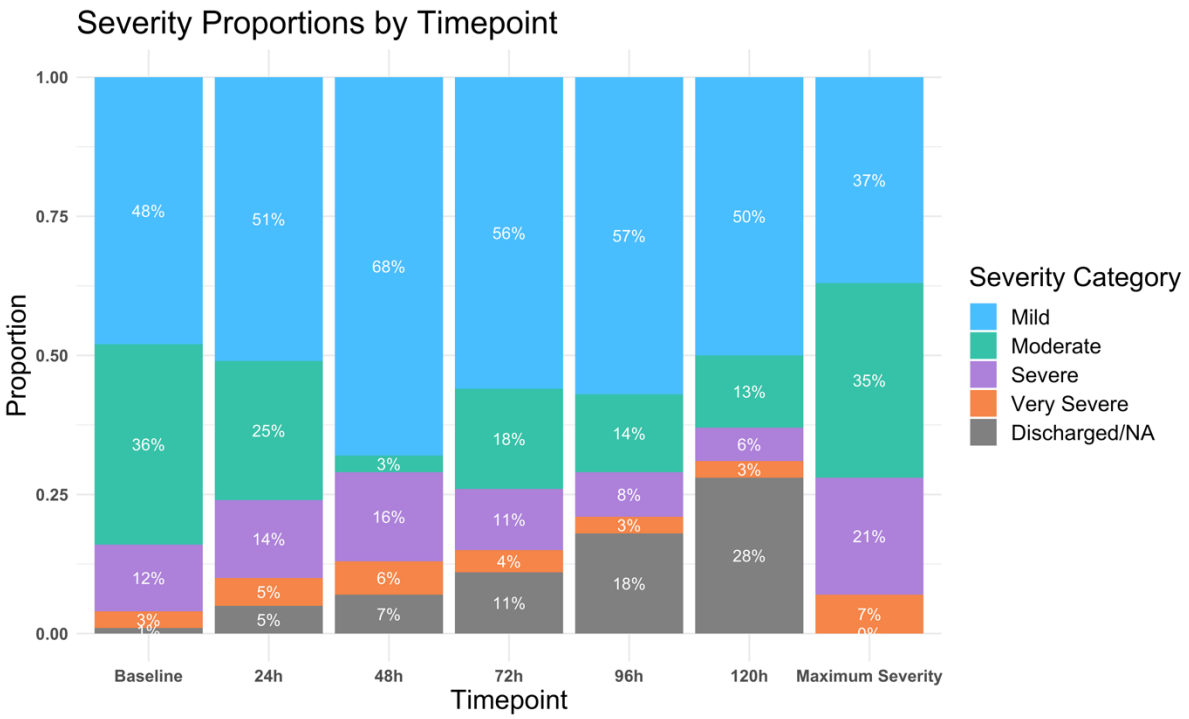

Figure 6-1 Stacked bar chart showing the proportion of MIS-C patients in each disease severity category over time.

Severity at the time of hospital admission (baseline), 24 hours, 48 hours, 72 hours, 96 hours and 120 hours following admission as well as maximum severity during hospital stay is displayed. N = 1285.

6.3.3 Variables associated with MIS-C disease severity

The demographic, clinical and laboratory variables categorised by maximum disease severity are presented in Appendix 5 Table A5-1, Table A5-2 and Table A5-3, respectively. Statistical comparisons using binary disease severity categories (Mild/moderate and Severe/Very Severe) revealed older age, female sex, Hispanic ethnicity, and Upper Middle-Income resource setting to be associated with Severe/Very Severe disease (all $p < 0.01$) (Appendix 5 Table A5-1).

Regarding clinical features, respiratory distress, gastrointestinal symptoms, encephalopathy, lethargy, BCG scar reactivation, skin peeling and positive SARS-CoV-2 PCR were more frequently present in the Severe/Very Severe group (all $p< 0.02$), while rash, lymphadenopathy and meeting the full KD criteria were more frequently present in the Mild/Moderate group (all $p < 0.05$) (Appendix 5 Table A5-2).

In terms of laboratory markers, significantly increased levels of WBC, neutrophils, ALT, D-dimer, fibrinogen, troponin, BNP, creatinine, CRP, ferritin, and lactate and significantly reduced levels of haemoglobin, lymphocytes, platelets, sodium, potassium, albumin were observed in Severe/Very Severe disease (all $p < 0.01$) (Appendix 5 Table A5-3). Overall, a significantly higher percentage of missing laboratory variable values were observed in the Mild/Moderate disease group compared to the Severe/Very Severe group (Appendix 5 Table A5-3).

A higher proportion of patients with Severe/Very Severe disease had cardiac involvement including, the presence of any echocardiogram abnormality, LVD and myocarditis (all $p < 0.0001$) (Appendix 5 Table A5-2). The length of admission was greater in patients with Severe/Very Severe disease ($p < 0.001$). No significant differences were seen in the treatments received (Appendix 5 Table A5-2).

The multivariable logistic regression analysis showed increased odds of Severe/Very Severe disease with increasing age, female sex and presence of respiratory distress, diarrhoea, vomiting, lethargy, and positive SARS-CoV-2 serology (all $p < 0.05$) (Figure 6-2). In terms of laboratory markers, increased levels of lactate and neutrophils, and reduced levels of Hb and lymphocytes were associated with increased odds of Severe/Very Severe disease (all $p < 0.05$) (Figure 6-2).

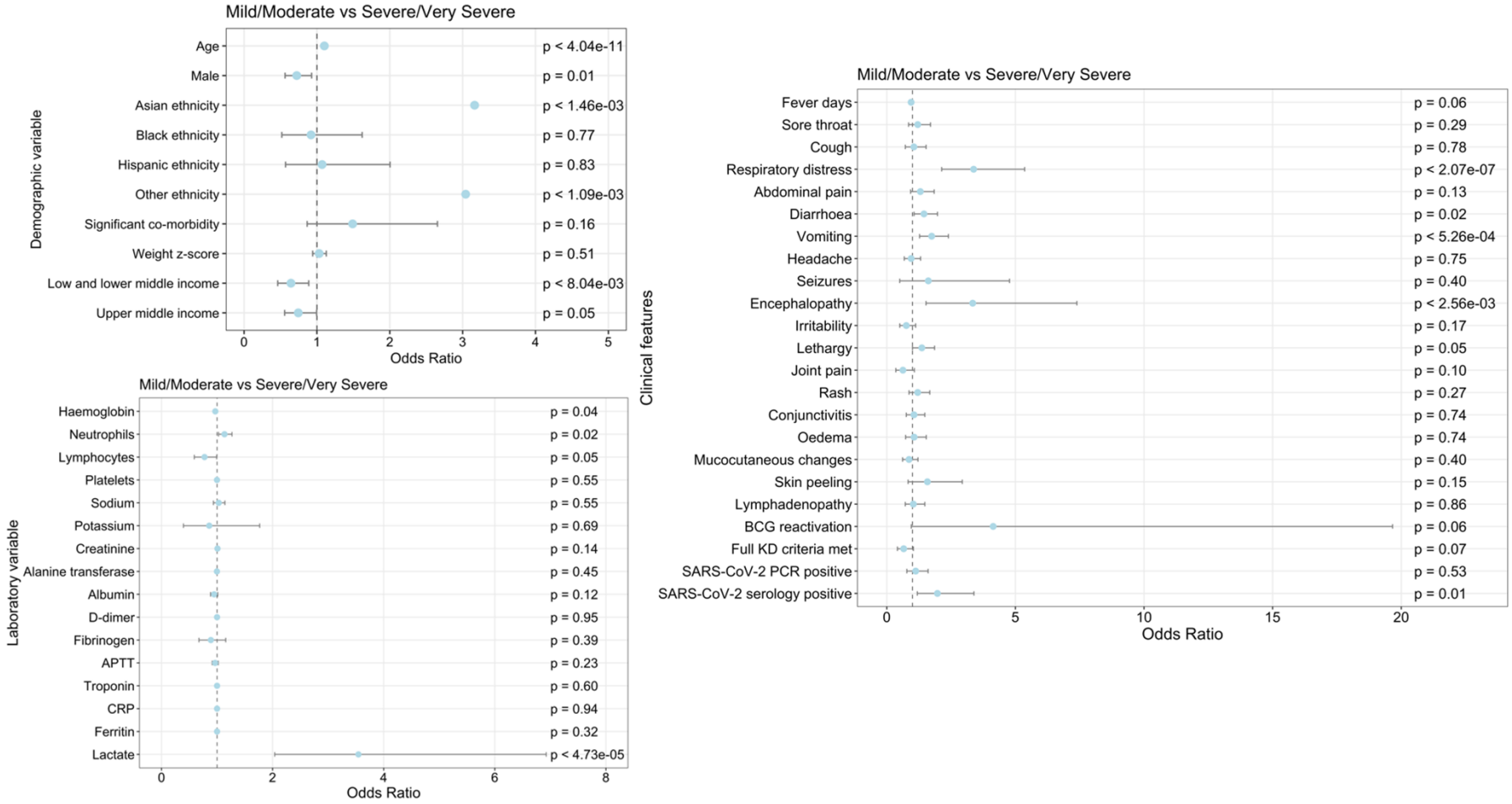

Figure 6-2 Odds Ratio plot for demographic, clinical and laboratory risk factors for Severe/Very Severe disease in MIS-C.

Odds ratios are derived from multivariable logistic regression analysis. N = 1285. Reference variables: Sex = Female, Ethnicity = Caucasian, Resource setting = High-Income setting. Adjusted p values are shown.

6.3.4 Variables associated with cardiac complications in MIS-C

The results of the multivariable logistic regression analyses of demographic and clinical variables associated with an increased risk of cardiac complications are presented in Figure 6-3 and Figure 6-4, respectively.

Similar to the preceding analysis, older age was associated with a higher risk of any abnormal echocardiogram findings, LVD and myocarditis (all $p < 0.05$) (Figure 6-3). Asian ethnicity was associated with a higher risk of any abnormal echocardiogram findings ($p < 0.05$), LVD ($p = 0.09$) and myocarditis ($p = 0.25$). Male sex was identified as risk factor for persistent CAA ($p < 0.01$) (Figure 6-3). Patients from Upper Middle-Income economies had an increased risk for all cardiac complications (all $p < 0.05$), while patients from Low and Lower Middle-Income resource settings had a lower risk of any abnormal echocardiogram findings and myocarditis (all $p < 0.0001$) (Figure 6-3).

With regards to clinical features, respiratory distress, abdominal pain, encephalopathy, and positive SARS-CoV-2 serology were associated with an increased risk of having any abnormal echocardiogram findings (all $p < 0.05$) (Figure 6-4). Presence of abdominal pain, encephalopathy, and rash were associated with an increased risk of LVD (all $p < 0.05$). Presence of diarrhoea and encephalopathy were associated with an increased risk of myocarditis (all $p < 0.05$). While positive SARS-CoV-2 PCR was associated with a reduced risk of myocarditis ($p = 0.03$). Patients who met the full KD criteria had increased odds of developing CAA ($p = 0.05$) (Figure 6-4). No significant associations were observed with persistent CAA.

The majority of the laboratory markers evaluated did not show a significant relationship with any cardiac complications. However, reduced sodium, reduced APTT and raised ALT were associated with increased risk of any abnormal echocardiogram findings (all $p \leq 0.05$). Raised lactate, raised CRP and reduced albumin were associated with increased odds of myocarditis (all $p \leq 0.02$) (Appendix 5 Figure A5-1).

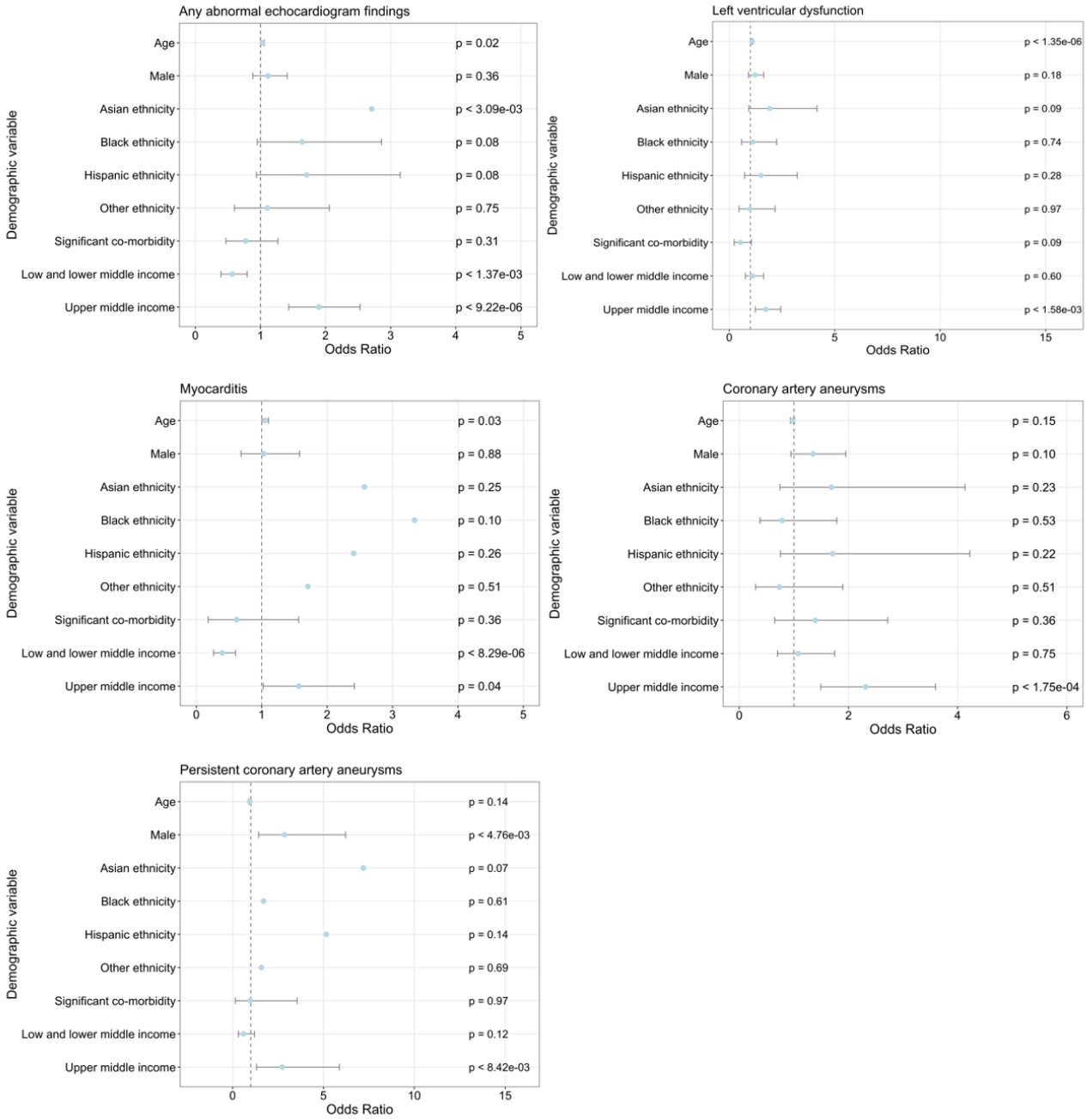

Figure 6-3 Odds ratio plot for demographic risk factors for cardiac complications in MIS-C.

Odds ratios are derived from multivariable logistic regression analysis. N = 1285. Reference variables: Sex = Female, Ethnicity = Caucasian, Resource setting = High-Income setting. Adjusted p values are shown.

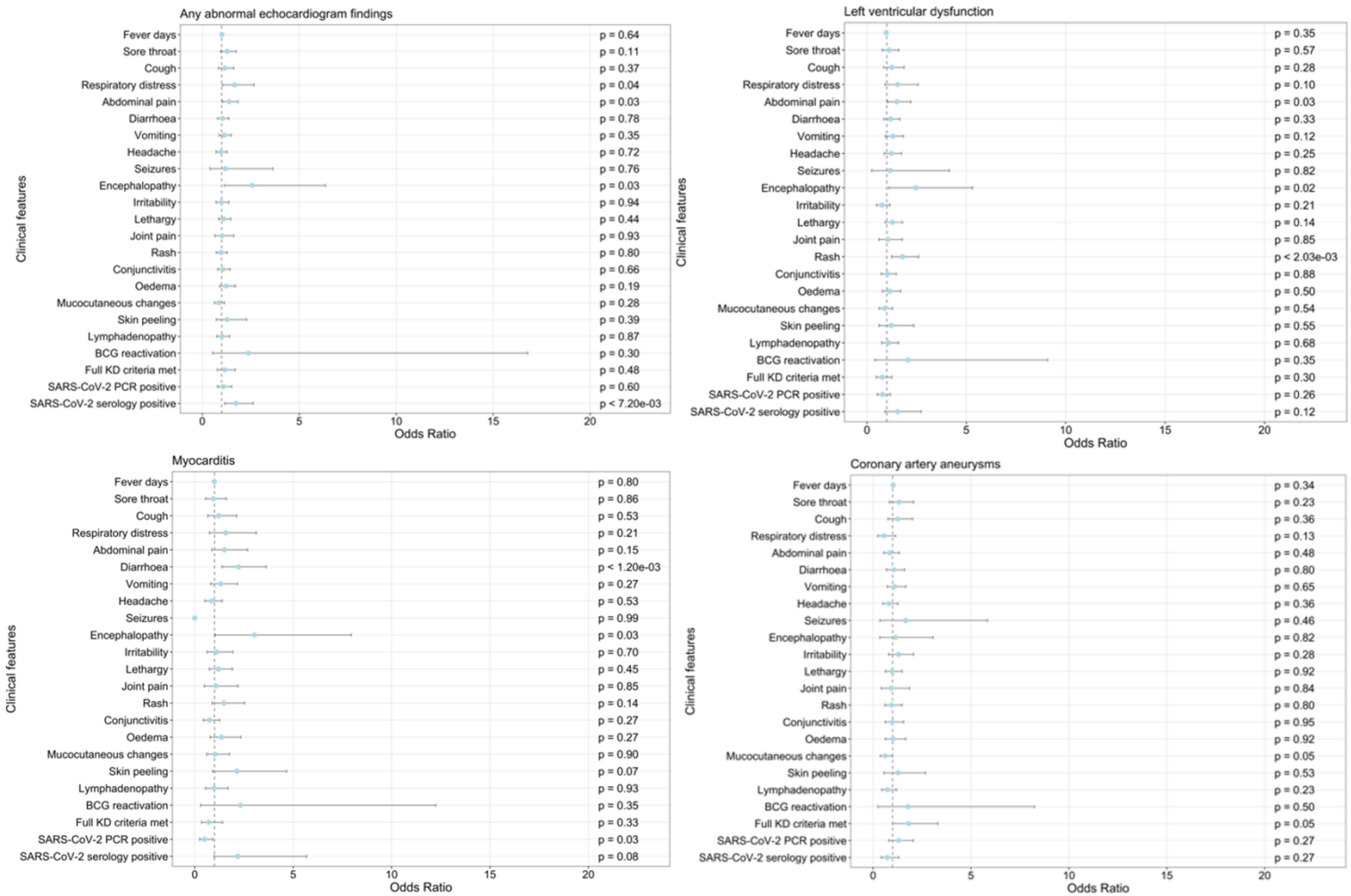

Figure 6-4 Odds ratio plot for clinical risk factors for cardiac complications in MIS-C.

Odds ratios are derived from multivariable logistic regression analysis. N = 1285. Reference variables: Sex = Female, Ethnicity = Caucasian, Resource setting = High-Income setting. Adjusted p values are shown.

6.3.5 Physiological score, laboratory score and combined scores

6.3.5.1 Scores

The physiological score:

Total physiological score = cardiovascular score + neurological score + respiratory score.

Further details of the score calculations are shown in Table 6-3.

The laboratory score:

([7 – lymphocyte count] x 2.5) + (neutrophil count x 1.5) + ([50 – albumin] x 1.5) + (creatinine x 0.2) + ([275 – platelets] x 0.08) + (lactate x 4)

The combined score:

combined score = (physiological score x 0.5) + laboratory score

6.3.5.2 Disease severity

On assessment of physiological, laboratory and combined scores with disease severity, there was a significant increase in all three scores with worsening severity at baseline and at 48 hours (all $p < 0.0001$) (Figure 6-5). The change in severity status was assessed to identify patients who were stable or improving and those who were deteriorating from baseline to 48 hours: 62% (n = 757) of patients remained stable, 22% (n = 275) improved, and 14% (n = 170) deteriorated. The physiological, laboratory, and combined scores were significantly higher in patients who deteriorated compared to those who remained stable or improved (all $p < 0.01$) (Figure 6-5).

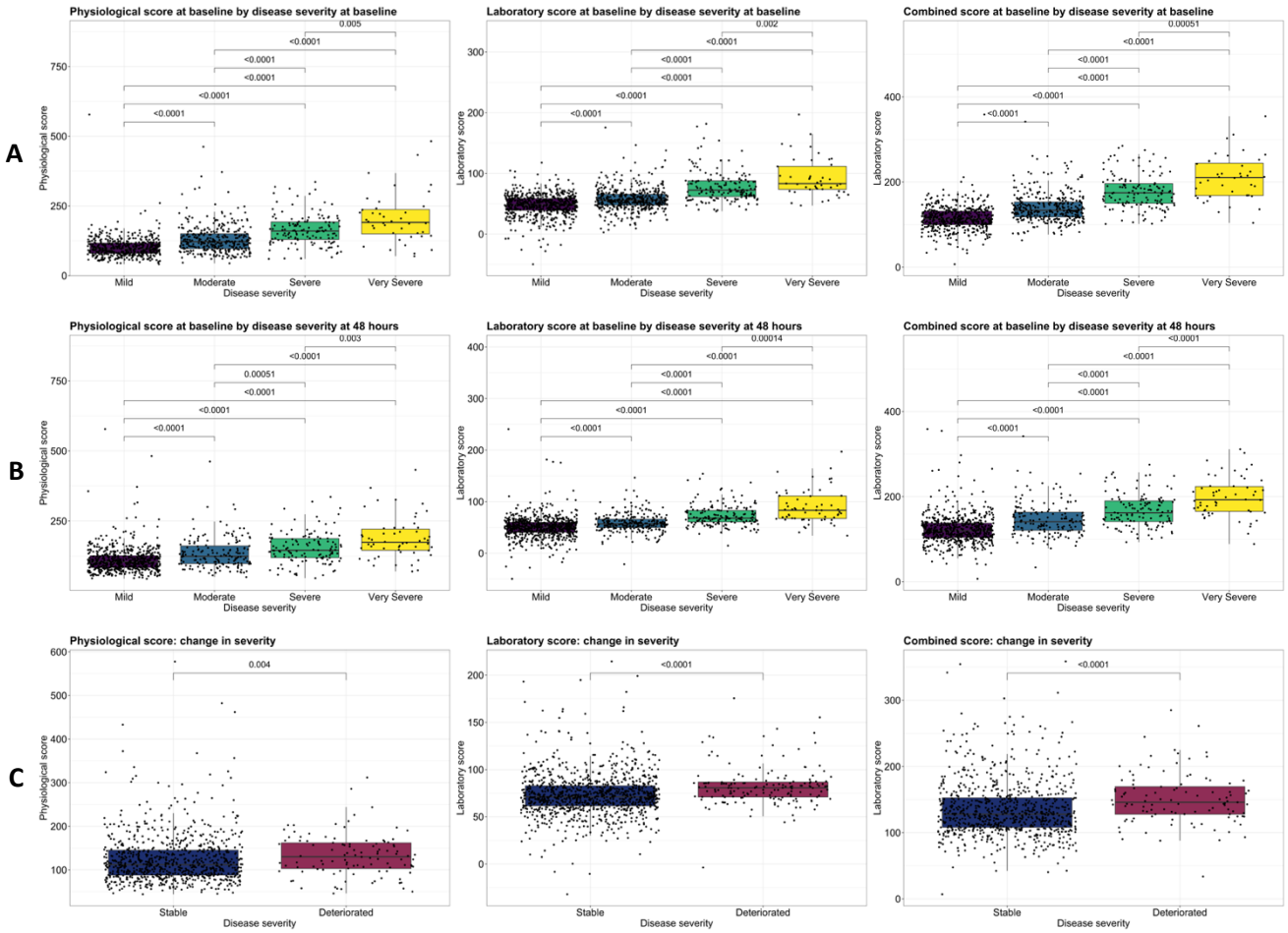

Figure 6-5 Boxplots of baseline physiological, laboratory and combined scores by MIS-C disease severity at baseline (A), 48 hours (B) and change in disease severity from baseline to 48 hours (C).

Physiological score baseline n = 994, 48 hours n = 930; change in severity n = 942; Lab score: baseline n = 1268, 48 hours n = 1189, change in severity n = 1201; Combined score – same numbers as physiological score. P values from Wilcoxon pairwise comparisons have been displayed.

6.3.5.3 Cardiac complications

The combined scores were also significantly higher in patients with any abnormal echocardiogram findings, LVD and myocarditis (all $p < 0.0001$) (Figure 6-6). There was no significant difference in the combined scores between patients with and without CAA (Figure 6-6). Of note, the combined scores in patients with persistent CAA were lower compared to those without persistent CAA (Figure 6-6). These findings were consistent when analysing the physiological and laboratory scores separately.

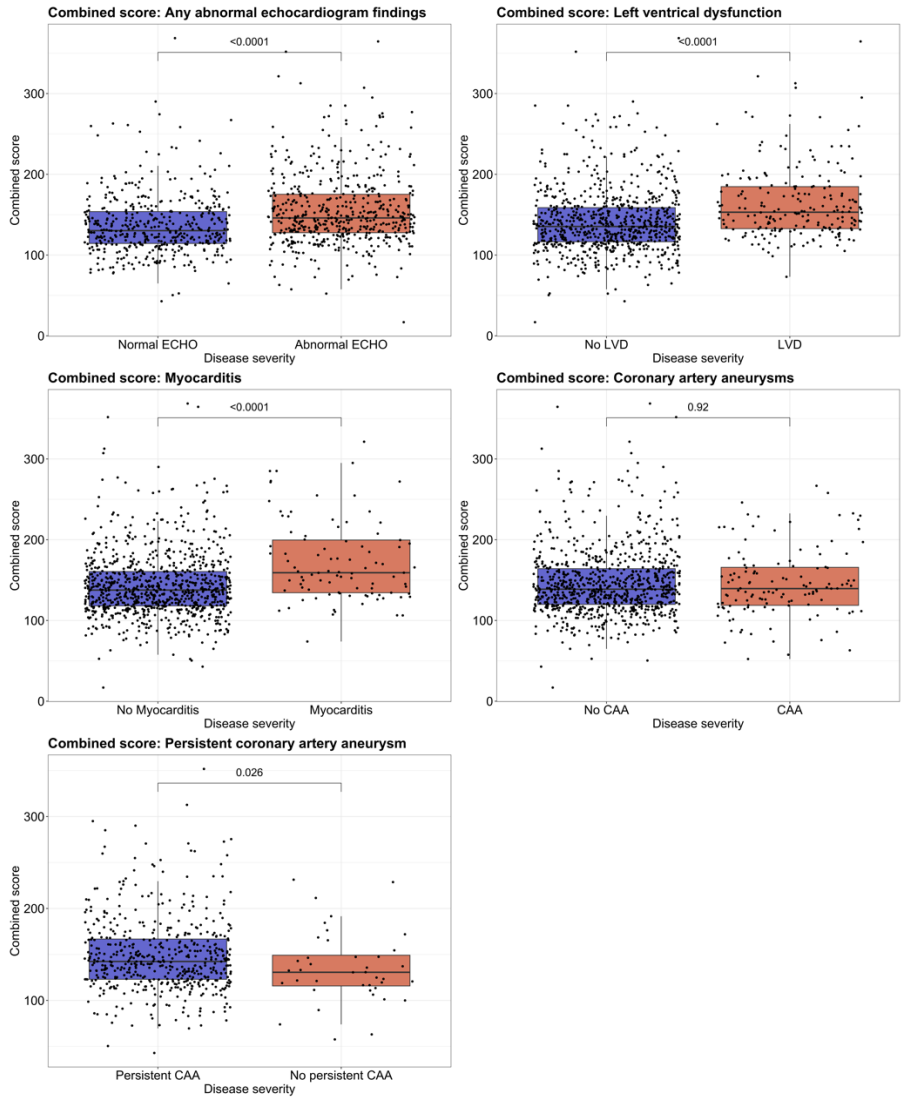

Figure 6-6 Boxplots of the combined physiological and laboratory scores by cardiac complications in MIS-C.

N = 965. P values from Wilcoxon pairwise comparisons have been displayed.

6.3.5.4 Performance of physiological, laboratory, and combined scores

Figure 6-7 displays the ROC curves for the physiological, laboratory, and combined scores using baseline values for classification of severity at baseline, prediction of 48-hour severity, prediction of change in severity, and prediction of any abnormal echocardiogram findings. Overall, the combined score demonstrated a higher AUC compared to the physiological or laboratory scores alone. The AUC for the combined score in predicting baseline severity was 0.88, for 48-hour severity the AUC was 0.83 and for change in severity the AUC was 0.65. The AUC for the combined score in predicting any abnormal echocardiogram findings was 0.64, and similar AUC values were observed for the other cardiac complications (LVD, myocarditis, CAA, persistent CAA).

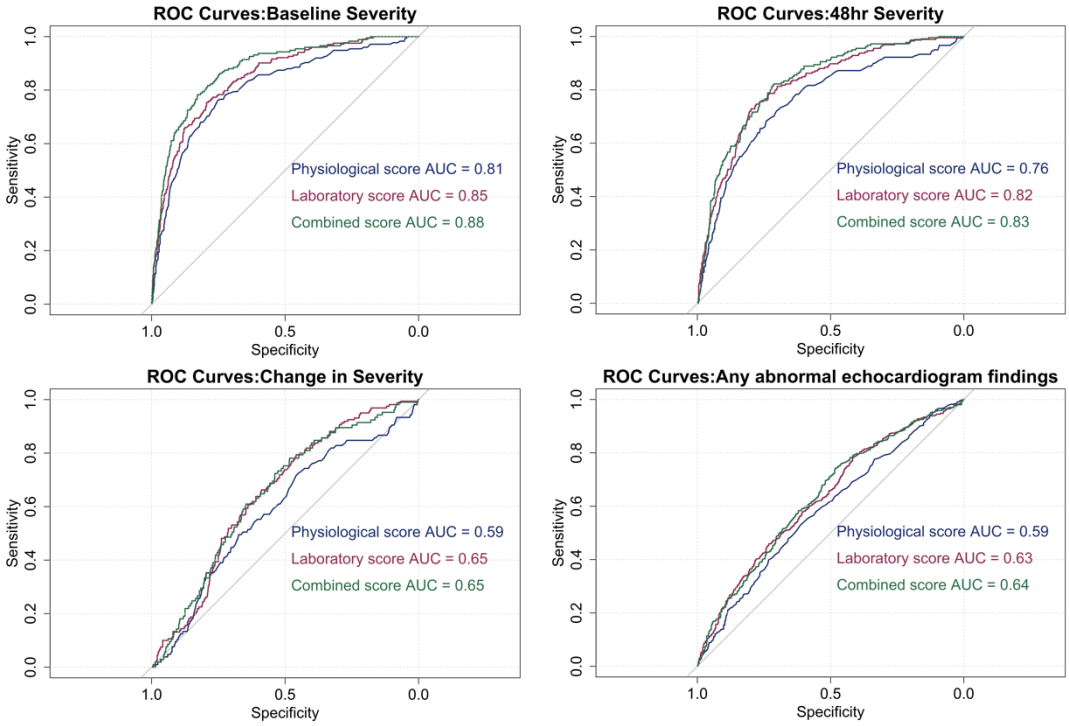

Figure 6-7 Receiver Operating Characteristic curve plots illustrating the performance of the physiological score, laboratory score, and combined score for classification of baseline severity and prediction of 48-hour severity, change in severity, and any abnormal echocardiogram findings.

The area under the curve (AUC) has been displayed for each score.

6.4 Discussion

The results presented in this chapter provide a comprehensive description of MIS-C and capture a broad spectrum of disease severity in a large international cohort (n = 1285). Examination of the associations of demographic, clinical and laboratory variables with disease severity provided valuable insight into factors influencing the severity of MIS-C and guided the development of severity prediction scores.

The study population had a male preponderance, which has been reported across a number MIS-C cohorts[210,397,425]. However, a greater proportion of the females in BATS developed Severe or Very Severe disease. A recent longitudinal cohort study by Auger et al. showed that while greater proportions of males developed MIS-C, the risk factors for MIS-C were more strongly associated in females[236]. The observed sex differences in susceptibility and severity are noteworthy, however they are not unique to MIS-C and have also been reported in other infectious and inflammatory conditions, including Influenza and Guillain-Barré syndrome[426–430]. Biological, genetic, hormonal, and behavioural differences are among the many interlinked factors that should be explored further to understand the underlying mechanisms.

The median age of the cohort was 7.2 years (IQR 3.8-11 years), which is consistent with previous reports indicating that MIS-C is primarily a disease of school-aged children (> 5 years), with smaller numbers of younger children and adults being affected[210,397,425,431,432] . The age distribution of MIS-C could be related to differences in maturity of the immune system and increased risk of exposure to SARS-CoV-2 in school environments. Of note, a recent study of an international MIS-C cohort (n = 2017) by McCrindle et al. comparing MIS-C characteristics with prevalent SARS-CoV-2 variants, showed that MIS-C patients during the delta (B.1.617.2) and omicron (B.1.1.529) periods were younger and had less severe disease than the earlier alpha+ (B.1.1.7 and others) and ancestral (Wuhan-Hu-1) periods[433]. Several factors, including differential genetic susceptibility to variants and differences in immune responses, may influence the observed trends and they warrant further research to fully understand the mechanisms driving these changes.

Studies have shown increased prevalence of MIS-C in children from Black, Hispanic and Asian ethnic backgrounds[205,434]. However, the BATS MIS-C cohort was predominantly Caucasian (41%) and Hispanic (31%), with smaller numbers of children from Black, Hispanic and other ethnic groups. The study by McCrindle et al., showed an increase in the proportion of Caucasian children with MIS-C with

over time[433]. Analysis of the BATS dataset by SARS-CoV-2 prevalent variant periods can confirm if similar trends exist, providing insight into the generalisability of these findings. No obvious trend relating to ethnicity and disease severity was seen, however Asian (OR 2.7 $p < 0.01$), Black (OR 1.6 $p = 0.08$) and Hispanic (OR 1.7 $p = 0.08$) children had increased odds of having any echocardiogram abnormalities.

At the onset of MIS-C, it was initially hypothesised that children with immune deficiencies may be at greater risk of developing MIS-C. However, this was not supported in later reports[199,209,397] or seen in the BATS cohort where only a small minority were found to have any significant comorbidities (6%). There was a higher proportion of patients with significant comorbidities in the Very Severe group (10%), and presence of significant comorbidities also corresponded with increased odds of Severe or Very Severe disease, but the results did not reach statistical significance. Although obesity has been reported as a risk factor for MIS-C in several studies[235,236,418,435], the median weight z-scores in the BATS cohort was 0.47, indicating that the weights of children in BATS are only slightly above the average for their age and sex. The weight z-scores were higher in High and Upper Middle-Income resource settings compared to Low-Income resource settings, however, when weight was assessed as an independent variable, no significant relationship with disease severity was observed.

The distribution of patients across resource settings in the BATS cohort largely reflected the participating sites, with a majority of patients coming from High or Upper Middle-Income settings. Initial analyses revealed that a greater proportion of patients from Upper Middle-Income settings had Severe/Very Severe disease compared to patients from High-Income settings, however, this relationship did not remain statistically significant on multivariable analysis. Furthermore, patients from Upper Middle-Income settings had significantly increased risk of all cardiac complications compared to patients from High-Income settings, which could be attributed to the impact of socioeconomic factors on overall health, immune function and cardiovascular health[436–438]. It is important to consider and further investigate the potential factors that may influence the observed relationship including lifestyle factors, access to and utilisation of healthcare and genetic variation. Additionally, efforts to reduce barriers and increase outreach and education, are vital for increasing the diversity of participating research sites and minimising recruitment bias, leading to more generalisable and impactful research.

The potential utility of a case-control approach in defining epidemiological risk factors deserves consideration. While the descriptive analysis of proportions in this study offers valuable insights into

the characteristics of the MIS-C cohort, a case-control design could enhance our understanding by comparing these findings with those of an unaffected group or the background population. This approach enables the assessment of relative risks and odds ratios, providing a quantitative measure of the observed associations in the study.

MIS-C was characterised by the presence of gastrointestinal symptoms, rash, conjunctivitis and mucocutaneous changes, in line with findings from the DIAMONDS cohort presented in Chapter 5 and other published studies[196,199,410]. Respiratory distress, encephalopathy and lethargy were associated with disease severity, this is not surprising given that these symptoms reflect significant systemic involvement. All the presenting symptoms were included in the multivariable model to identify the individual contribution of each symptom. However, to avoid potential multicollinearity and explore the compound effect, an alternative approach would be to group similar symptoms by system e.g. the presence of one, two or three gastrointestinal symptoms. Regarding laboratory features, patients with MIS-C displayed anaemia, lymphopenia, high inflammatory markers, deranged coagulation, and poor renal function, reflecting multi system involvement, consistent with previous reports[199,209,397]. Raised lactate and reduced lymphocytes exhibited the highest odds for having severe disease suggesting that mechanisms related to tissue hypoperfusion and immune dysregulation are likely to be contributing to the severity of MIS-C. Unfortunately, data on monocyte counts were not collected in BATS to allow corroboration of the novel association with MIS-C seen in the DIAMONDS cohort in Chapter 5.

On assessment of cardiac complications, 52% of the cohort were found to have an abnormal echocardiogram, 21% had LVD and 12% had CAA, these findings fall on the lower spectrum of what has been reported in other studies[199,210,212,397]. The demographic and clinical variables associated with increased risk of cardiac complications were similar to those associated with increased risk of Severe or Very Severe disease. It is worth highlighting that patients meeting the full KD criteria had increased odds of developing CAA (OR 1.8 p = 0.05). This could represent the heterogeneity of MIS-C with a distinct subset that has shared underlying pathophysiology to KD, or it could be due to disease misclassification. It's important to acknowledge the limitations of this analysis. Only patients who had echocardiogram findings reported were included, introducing potential selection bias. The lack of standardised ECHO time points adds complexity and may introduce additional biases. Despite these constraints, a pragmatic approach was chosen to utilise available data, recognising the inherent limitations, and emphasising the need for future studies with more comprehensive and standardised cardiac evaluation.

Similar to the cardiac findings, a smaller proportion of patients in the BATS cohort required inotropic support (24%) and invasive ventilation (8%) compared to previous reports[199,210,397]. This could be due to numerous reasons including differences in patient characteristics, availability of treatments, variability in treatment protocol and changes in treatment strategies over time. Intriguingly, the proportion of patients receiving different treatments did not differ across disease severity group, however combination therapy was not analysed and may reveal differences, with patients with more severe disease receiving multiple agents. Finally, the low mortality rate (1%) observed in this cohort is reassuring and contributes to the body of evidence supporting the favourable outcomes in children with MIS-C, despite the significant severity of illness observed during the acute phase.

Within paediatrics, various severity scoring systems have been established, including disease-specific scores and generalised scores e.g. those commonly used in PICUs. An example of a disease-specific score is the Paediatric Ulcerative Colitis Activity Index score. Its development involved a Delphi group for variable selection and regression modelling for weighting the selected variables[439]. In contrast, the Paediatric Index of Mortality 3 is a general severity score for critically ill paediatric patients[440]. It represents a refined version of the Paediatric Index of Mortality score, originally designed through a comprehensive process involving data collection from multiple PICUs, logistic regression, variable selection, and validation across different units to ensure accurate mortality prediction in paediatric intensive care settings[441]. The MIS-C severity score followed a comparable approach, utilising clinical significance and results of the regression modelling for variable selection. By integrating physiological and laboratory parameters, it aims to comprehensively evaluate disease severity tailored to the unique characteristics of this inflammatory syndrome.

The physiological, laboratory and combined scores using baseline results were effective at assessing MIS-C disease severity at baseline and 48 hours, with consistent trends of increasing scores with worsening severity. Furthermore, patients who experienced deterioration in their severity status had higher scores compared to those who remained stable or improved. The performance of the combined score for classification of severity at baseline was better than individual physiological or laboratory scores, as indicated by a higher AUC (Combined score AUC: 0.88, Physiological score AUC:0.81, Laboratory score AUC:0.85). Other researchers have developed similar scores for classification or prediction of MIS-C severity, which have comparable or superior performance[1]. However, a key difference is that these other scores often include markers which may not be easily accessible in low resource settings such as platelet distribution width, BNP and D-dimer[261,270].

Although significant differences were seen in the combined scores for patients who deteriorated compared to those who remained stable, and in those with and without cardiac complications, the performance of the combined score for predicting change in severity from baseline to 48 hours and identifying abnormal echocardiogram findings was limited. This is likely due to the overlap of scores and lack of clear separation between stables and deteriorating patients and patients with and without echocardiogram abnormalities. This could be due to several reasons. Disease progression is a complex process affected by multiple factors, it is possible that not all factors which play a role in predicting deterioration or cardiac complications were captured by the score. The 48-hour timepoint may not be optimal for assessing change in severity, and more frequent recording of clinical and laboratory data (e.g. every 6-12 hours) could provide more insight. Additionally, patients with MIS-C display a variability in disease progression, with some patients deteriorating rapidly, while others have more a stable course, which adds to the challenge of developing a score that is widely applicable. Finally, the design of the score may have limitations related to selection of variables and their weighting. Refinement of the scores with assistance of feature selection and machine learning algorithms could help improve the performance and accuracy.

Furthermore, considering the rapid deterioration observed in MIS-C, it is crucial to establish community resources for early recognition, including targeted training for community health care professionals and educational programs for parents/care givers. Such initiatives can facilitate earlier identification of symptoms, enabling timely interventions that have the potential to improve overall outcomes in children with MIS-C.

Despite the significant advantage of BATS being a large, multi-centred MIS-C study, the analyses presented in this chapter have several limitations. Factors such as variations in healthcare access and utilisation, recruitment bias, sample selection bias, and misclassification of data or coding errors can impact the robustness of the results. Moreover, the collaborative and inclusive approach of BATS sought a comprehensive representation of MIS-C cases. Moreover, due to BATS' collaborative and inclusive nature, potential participant overlap with other published study populations should be considered when interpreting cross-study comparisons. Missing and incomplete data also presented challenges, particularly with the laboratory score where data imputation was required, therefore, the bias introduced by imputation should be considered when interpreting the results. Additionally, the severity scores are based on available data, which may not capture all the relevant features influencing disease severity, as these may not have been collected or may be unknown. Lastly, the severity scores have not been externally validated, which is crucial for assessing generalisability and reliability.

6.5 Conclusion

Comprehensive analysis of the large, international MIS-C BATS cohort presented in this chapter has enhanced our understanding of MIS-C, specifically, the clinical and laboratory profile of MIS-C, risk factors associated with disease severity and through the development of severity scores which hold potential for use as clinical decision support tools.

The results have also highlighted areas of research that require further exploration. Investigating the maturation of the immune system and how age influences the development and severity of MIS-C may provide valuable insights into the underlying disease mechanisms. In addition, understanding the evolution of MIS-C with time and impact of different SARS-CoV-2 variants is crucial for improving preparedness for future waves and changes in disease patterns. Gaining better understanding of sex specific vulnerabilities, disease process and treatment responses could ultimately lead to improved patient care and tailored approaches for clinical management. Understanding the impact of other identified risk factors such as ethnicity and comorbidities in the development and progression of MIS-C is also essential for this goal. Addressing these research gaps will advance our understanding of MIS-C, the underlying pathophysiological mechanisms, and factors contributing to disease severity, ultimately leading to targeted approaches to clinical management and improved patient outcomes.

The combined severity score based on physiological and laboratory markers demonstrates potential for being developed as a simple tool for assessing MIS-C severity. The score could be incorporated into a mobile phone application for use in the emergency department to aid timely decision making, streamline assessment practises and minimise over-treatment by ensuring interventions are appropriately tailored to each child's specific needs. However, additional research is needed to address the limitations, refine the scores and ensure their validity in external cohorts.

In summary, the results presented in this chapter provide valuable contributions to the understanding of MIS-C and highlight the importance of collaboration and comprehensive data collection. The findings also establish the foundation for future mechanistic studies and the development of prognostic scores, which are crucial for unravelling the complexities of MIS-C and aiding improvements in diagnosis, management and outcomes of children affected by MIS-C.

Chapter 7: Mechanistic studies investigating the role of antibodies in SARS-CoV-2 associated diseases in children

7.1 Introduction

MIS-C and COVID-19 vaccine-induced myocarditis are two conditions which occur several weeks following exposure to SARS-CoV-2 antigens and are both associated with cardiac pathology.

MIS-C is associated with high rates of cardiac involvement including cardiogenic shock (50-80%), elevated troponin (68-95%) and BNP levels (78-100%), and echocardiogram abnormalities such as LVD (51-76%) and coronary artery dilatation or aneurysm (14-48%)[212]. Severe cases require intensive care with inotropic support and ECMO. Despite the significant cardiac dysfunction during acute illness, the majority of patients make complete recovery[328,329,442,443].

COVID-19 vaccine-induced myocarditis is a rare complication predominantly affecting young adult (12–24-year-old) males following the second dose of mRNA-based COVID-19 vaccination, with an estimated incidence as high as 1.4 per 10000[343]. Presenting symptoms include chest pain, palpitations, and shortness of breath. Cardiac troponin levels are significantly elevated with ST elevation seen on electrocardiogram and LVD commonly detected on ECHO. In most cases the disease is self-limiting and only necessitates supportive treatment.

The timing of both of these conditions, days to weeks after exposure to SARS-CoV-2 antigens, suggests that a dysregulated adaptative immune response, specifically antibodies, could be driving the cardiac pathology. Consequently, the work in this chapter investigates the potential role of antibody-mediated cardiac pathology in MIS-C and COVID-19 vaccine-induced myocarditis.

<u>The primary aim of this chapter is:</u>

To determine the role of SARS-CoV-2 specific antibodies in the pathogenesis of MIS-C and COVID-19 vaccine-induced myocarditis through mechanistic studies.

The objectives of this chapter are:

1) Use immunohistochemistry (IHC) to provide evidence for an antibody-mediated mechanism driving the cardiac pathology in MIS-C and COVID-19 vaccine-induced myocarditis.
2) Develop ELISAs to investigate the presence of autoantibodies targeting the myocardium in MIS-C and COVID-19 vaccine-induced myocarditis.

The key findings from this chapter are:

This work contributes to the understanding of the underlying mechanisms of the cardiac complications seen in MIS-C and COVID-19 vaccine-induced myocarditis, which are yet to be elucidated. The findings challenge the initial hypothesis of a direct anti-cardiac antibody-mediated cardiac pathology in MIS-C and COVID-19 vaccine-induced myocarditis. This is an important negative finding, with implications for COVID-19 vaccination strategies in children. Moreover, it opens alternative avenues for investigation to help unravel the intricacies of SARS-CoV-2 associated disease pathophysiology. The immunohistochemistry work in this chapter has been published in the Journal of American Medical Association Network Open[444].

7.2 Methodology

7.2.1 Clinical cohorts

The work in this chapter includes 6 clinical cohorts consisting of children with MIS-C (n = 10), children with COVID-19 vaccine myocarditis (n = 10), adults with non-SARS-CoV-2 associated myocarditis/inflammatory cardiomyopathy (IHC n = 8, ELISA positive control n = 9), healthy COVID-19 vaccinated adult controls (n = 10) and healthy pre-pandemic paediatric controls (n = 10). The patients and controls were recruited into multiple studies in the UK, Austria, and the US. Serum samples were used for this piece of work. An overview of the cohorts is given below and the details of individual studies from which these patients were recruited can be found in Chapter 3 (section 3.1).

7.2.1.1 MIS-C

Children and young adults aged less than 19 years admitted to St Mary's Hospital London and Evelina Children's Hospital, London, with an acute inflammatory febrile illness meeting the WHO case definition of MIS-C[204] were recruited as part of DIAMONDS. Ten patients were selected for this study. Five patients with cardiac involvement requiring intensive care and five patients with no cardiac involvement and no organ support requirement. Cardiac involvement was defined by significant abnormalities in cardiac troponin levels (> 100 ng/L) and/or abnormal echocardiogram findings. Serum samples were obtained from patients within 72 hours of admission to hospital, during the acute inflammatory phase of the illness, and prior to the initiation of any immunomodulatory treatment. Patients with other confirmed concurrent infectious disease(s) were excluded.

7.2.1.2 Vaccine myocarditis

Children and young adults ages less than 19 years presenting to Rady Children's Hospital in San Diego, US, with symptoms of myocarditis (including chest pain, shortness of breath, palpitations, fever) following the second dose of the COVID-19 mRNA vaccination, where other causes of myocarditis had been excluded, were recruited to the Diagnosing and Predicting Risk in Children with SARS-CoV-2 related illness study (n = 10). Serum samples were taken on the day of admission to hospital prior to receiving any treatment.

7.2.1.3 Adult myocarditis/inflammatory cardiomyopathy

Adults with acute myocarditis/inflammatory cardiomyopathy (IHC n = 8, ELISA positive control n = 9) were included from two research studies: 1) The Graz Endomyocardial Biopsy Registry, Graz, Austria 2) Diagnosis and Risk Stratification in Myocarditis Study, London, UK. They both included patients with biopsy confirmed acute myocarditis/inflammatory cardiomyopathy, where infectious causes of myocarditis had been excluded. Serum samples were taken during acute illness.

7.2.1.4 Healthy COVID-19 vaccinated adults

Healthy adults aged more than 21 years, with no recent (within 7 days) febrile illness, who had received COVID-19 vaccination were recruited as part of DIAMONDS (n = 10). Serum samples were taken at least two weeks following vaccination. Adult vaccinated controls were selected since at the time of this study, COVID-19 vaccinations had not been rolled out in the paediatric and young adult populations.

7.2.1.5 Healthy pre-COVID-19 pandemic children

Healthy children recruited to the EUCLIDS study prior to the COVID-19 pandemic, with no underlying immunological health conditions, no recent (within 3 weeks) febrile illness and no recent (within 3 weeks) vaccination were included (n = 10).

7.2.1.6 Cardiac tissue donors

Two donors, one male and one female, from The Structure and Functional Characterisation of Human Hearts Study were used for this work. Donors were excluded if they had pre-existing cardiovascular disease, autoimmune conditions, or prolonged ischemia before tissue was harvested from the left ventricle apex.

7.2.2 Blood sample collection and serum separation

The blood samples were collected from patients with MIS-C and healthy COVID-19 vaccinated adults and processed for serum separation using the protocol described in Chapter 3 (section 3.2.1).

7.2.3 Immunohistochemistry

Immunohistochemistry (IHC) is a method used for detecting specific antigens or proteins within tissue samples. Indirect IHC was employed to identify anti-cardiac antibodies in the serum of MIS-C and COVID-19 vaccine-induced myocarditis patients. Serum from patients and controls served as the primary antibody, binding to cardiac tissue if anti-cardiac antibodies were present. Secondary antibodies, including anti-human IgG, IgM, and IgA conjugated with FITC, were used for detection. The IHC slides were imaged using a wide-field microscope, and 10 images were taken at 20x magnification from each section. Details of the cardiac donors, preparation of cardiac tissue section slides and IHC experimental and imaging protocols are shown in Chapter 3 (section 3.2.3.1).

7.2.3.1 IHC Image Analysis

Images were processed and switched to a colour-blind friendly palate using ImageJ/Fiji software (Version 2.3.0/1.53q). Immunoglobulin deposition was assessed qualitatively for specific staining patterns. Results were quantified by calculating FITC fluorescence intensity. Kruskal-Wallis test (for non-parametric data) was performed to compare median fluorescence intensity of IgG, IgM and IgA staining between clinical cohorts and controls.

7.2.4 Cardiac autoantibody ELISAs

ELISAs are used for detecting and quantifying an antigen or protein within a sample, through measurement of highly specific antibody-antigen interaction. An indirect ELISA was designed to detect anti-cardiac antibodies in MIS-C and COVID-19 vaccine-induced myocarditis patient serum. Three assays with different antigens were used: porcine whole heart lysate, porcine myosin, and human recombinant troponin. Patient serum served as the primary antibody, and HRP-conjugated anti-human IgG was used for the secondary antibody. The colorimetric substrate 3-3',5,5'-tetramethylbenzidine (TMB) was used to induce a colour change following interaction with HRP, which enabled quantification of the anti-cardiac antibodies. The detailed laboratory protocols are shown in Chapter 3 (section 3.2.3.1).

7.2.4.1 ELISA results data analysis

As the samples were run in duplicates, the average optical density reading was taken for each sample. Next, the median optical density readings for each clinical cohort were compared using the Kruskal-Wallis test for non-parametric data.

7.3 Results

7.3.1 Demographic and clinical characteristics of the cohorts

A total of 48 patients and controls were included; the demographic information and clinical characteristics are shown in Table 7-1 and Appendix 6 Table A6-1. The median age for each cohort was: MIS-C – 10 years (IQR 13-14 years); COVID-19 vaccine-induced myocarditis – 15 years (IQR 14-16 years); adult myocarditis/inflammatory cardiomyopathy – 55 years (IQR 46-62 years); healthy paediatric controls – 8 years (IQR 12.5-14 years); healthy vaccinated adults > 21 years. There was a male preponderance in MIS-C (6/10 male), adult myocarditis/inflammatory cardiomyopathy (6/8 male) and COVID-19 vaccine-induced myocarditis (10/10 male) cohorts. Children with South Asian ethnicity were more prevalent in MIS-C (4/10), while the COVID-19 vaccine-induced myocarditis cohort was primarily made up of children from Caucasian (5/10) and Hispanic (4/10) ethnic backgrounds.

One of the eight adult myocarditis/inflammatory cardiomyopathy patient samples stained positive for IgG, which was used as a positive control for the IHC experiment. This sample was from a 41-year-old South Asian man with a diagnosis of acute lymphocytic myocarditis. The clinical characteristics of the remaining seven adult myocarditis/inflammatory cardiomyopathy patients can be found in Appendix 6 Table A6-1. One male and one female cardiac donor were selected for the IHC work, the details of these donors are shown in Chapter 3 (Table 3-8).

Table 7-1 Demographic and clinical features of patients and controls.

n = count, IQR = interquartile range, % = percentage. Normal range values are from the Royal College of Paediatrics and Child Health[424]*. IVIG = intravenous immunoglobulin.*

	COVID-19 vaccine-induced myocarditis (n = 10)	**MIS-C (n = 10)**	**Healthy pre-pandemic paediatric controls (n = 10)**	**Healthy vaccinated adults (n = 10)**	**Adult myocarditis (n = 1)**
Age, median (IQR) [years]	15 (14, 16)	10 (13, 14)	8 (12.5, 14)	> 21 years	41
Male – n (%)	10 (100%)	6 (60%)	5 (50%)	5 (50%)	1 (100%)
Ethnicity – n (%)					
Arab	0 (0%)	0 (0%)	2 (20%)	0 (0%)	
Black	0 (0%)	2 (20%)	2 (20%)	1 (10%)	
Caucasian	5 (50%)	2 (20%)	3 (30%)	7 (70%)	
Hispanic	4 (40%)	0 (0%)	0 (0%)	1 (10%)	
South Asian	0 (0%)	4 (40%)	2 (20%)	1 (10%)	1 (100%)
Mixed	1 (10%)	1 (10%)	0 (0%)	0 (0%)	
Unknown	0 (0%)	1 (10%)	0 (0%)	0 (0%)	
Comorbidities – n (%)					
ADHD	1 (10%)	0 (0%)	Not determined	Not determined	Nil recorded
Asthma	0 (0%)	1 (10%)			
Autism	1 (10%)	0 (0%)			
Developmental delay	1 (10%)	0 (0%)			
Eczema	0 (0%)	2 (20%)			
Myelomeningocele	1 (10%)	0 (0%)			
Obesity	2 (20%)	1 (10%)			
Maximum troponin, median (IQR) [ng/L] [normal range: < 14 ng/L]	7355 (2562.5, 17262.5)	86 (26, 384)	Not determined	Not determined	2596
Maximum c-reactive protein, median (IQR)[mg/L) [normal range: < 5 mg/L]	34 (16, 37.5)[b]	227 (189, 293)	Not determined	Not determined	89

Table 7-1 continued.

	COVID-19 vaccine-induced myocarditis (n = 10)	**MIS-C (n = 10)**	**Healthy pre-pandemic paediatric controls (n = 10)**	**Healthy vaccinated adults (n = 10)**	**Adult myocarditis (n = 1)**
Echocardiogram findings					
Coronary artery z-score > 2.5	0 (0%)	2 (20%)	Not determined	Not determined	0 (0%)
Left ventricular ejection fraction < 55%	5 (50%)	3 (30%)			1 (100%)
Right ventricular dysfunction	1 (10%)	0 (0%)			0 (0%)
Valvular regurgitation[a]	1 (10%)	1 (10%)			0 (0%)
Cardiac MRI findings					
T1 hyperenhancement	5 (50%)	Not determined	Not determined	Not determined	Not determined
T2 hyperenhancement	4 (40%)				
Post-contrast delayed enhancement	3 (30%)				
Shock – n (%)	0 (0%)	6 (60%)	Not applicable	Not applicable	1 (100%)
Inotrope requirement – n (%)	0 (0%)	6 (60%)	Not applicable	Not applicable	1 (100%)
Intensive care support – n (%)	0 (0%)	5 (50%)	Not applicable	Not applicable	1 (100%)
SARS-CoV-2 PCR positive – n (%)	0 (0%)	0 (0%)	Not determined	Not determined	0 (100%)
SARS-CoV-2 Spike IgG, median (IQR) [normal range: 0-2]	76.9 (73.6, 94.4)[c]	4.7 (4.7, 4.7)[d]	0.27(0.34, 0.46)	1.9 (2.3, 3.0)	Not determined
SARS-CoV-2 Nucleocapsid IgG positive	1 (10%)	Not determined	Not determined	Not determined	Not determined
Immunomodulatory treatment	Prednisolone – 1 (10%) Ibuprofen – 10 (100%)	No immunomodulators – 3 (30%) Glucocorticoids – 6 (60%) IVIG – 5 (50%) Tocilizumab – 3 (30%) Anakinra – 1 (10%)	Not applicable	Not applicable	No immunomodulators – 1 (100%)

a: Valvular regurgitation defined as >/= mild tricuspid or mitral regurgitation
b: Performed on 7/10 patients
c: Performed on 3/10 patients
d: Performed on 7/10 patients

7.3.2 IHC images

7.3.2.1 IgG staining

IgG staining was performed using serum from all study participants. No specific binding was observed in cardiac tissue treated with serum from patients with MIS-C and COVID-19 vaccine-induced myocarditis (Figure 7-1). A sample from one of the adult myocarditis patients showed specific binding of IgG to myocardial structures in cardiac tissue, which served as the positive control (Figure 7-1). This finding was reproducible on three separate experiments in cardiac tissue from both Donors A and B (Figure 7-2). No specific binding for IgG was seen in the remaining 7/8 adult myocarditis/inflammatory cardiomyopathy cases (Figure 7-3).

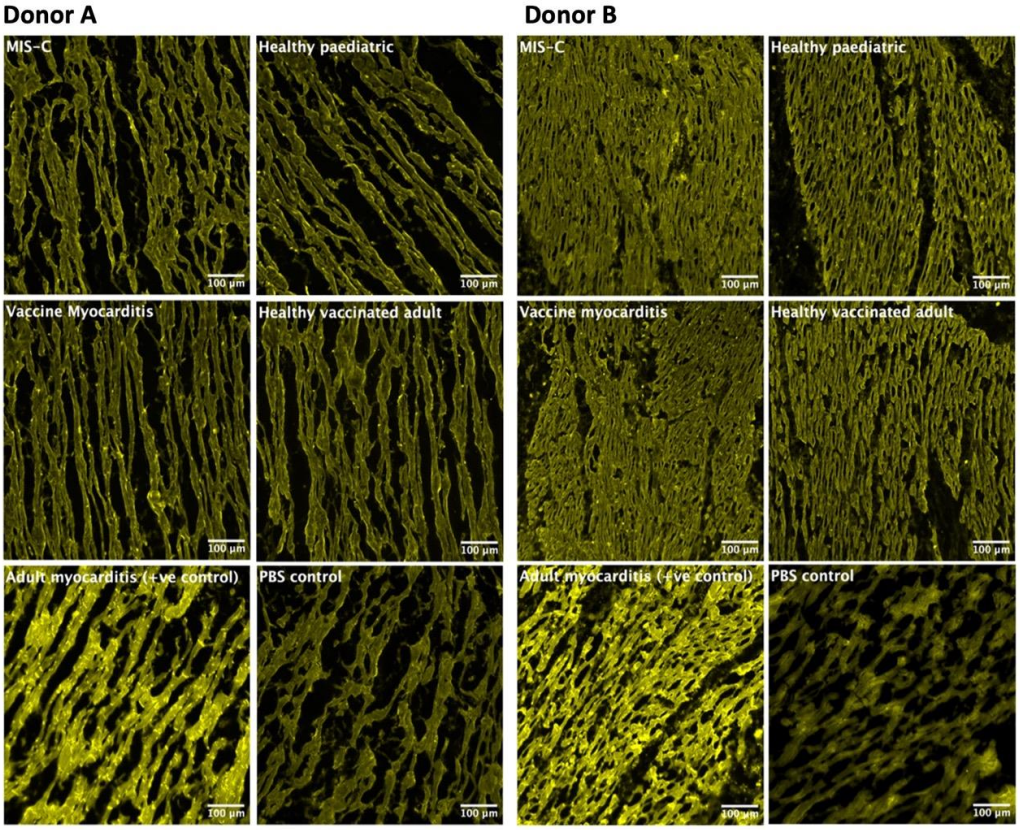

Figure 7-1 Immunohistochemistry images of IgG staining.

Immunohistochemistry images of cardiac tissue from Donors A and B treated with serum (1 in 50) from patients and controls and stained with fluorescein isothiocyanate (FITC) conjugated anti-human Immunoglobulin G (IgG). An example image from each of the following groups has been shown: phosphate buffered saline (PBS) – negative control, healthy pre-COVID-19 pandemic paediatric controls, healthy COVID-19 vaccinated adults, COVID-19 vaccine-induced myocarditis and MIS-C Images were taken on a wide-field microscope at 20x magnification.

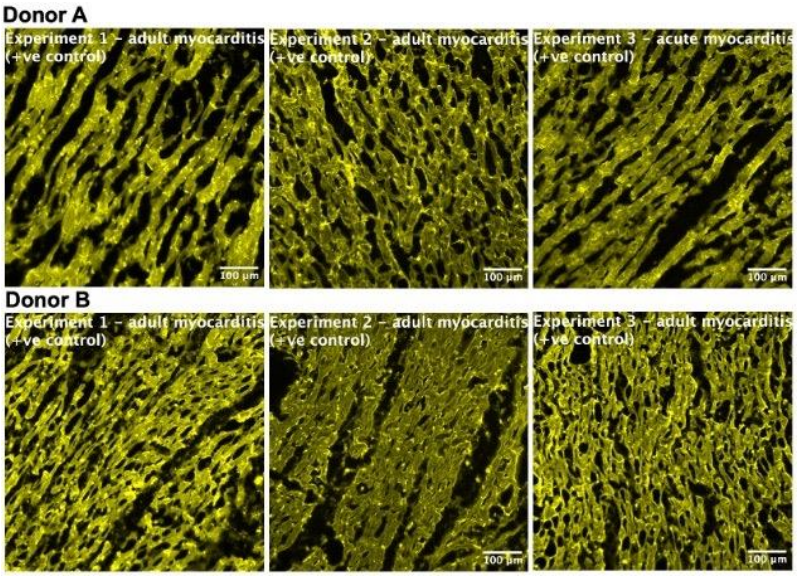

Figure 7-2 Immunohistochemistry images of IgG staining – positive control.

Immunohistochemistry images of cardiac tissue from Donors A and B treated with serum (1 in 50) from an adult with non-SARS-CoV-2 myocarditis and stained with fluorescein isothiocyanate (FITC) conjugated anti-human Immunoglobulin G (IgG), repeated on three separate experiments. Images were taken on a wide-field microscope at 20x magnification.

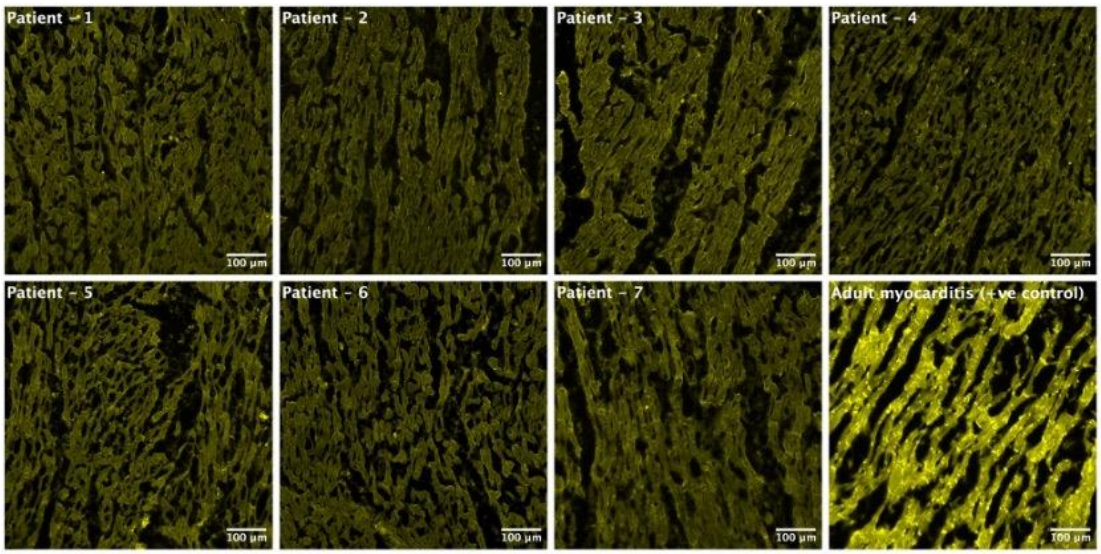

Figure 7-3 Immunohistochemistry images of IgG staining – adults with myocarditis/inflammatory cardiomyopathy.

Immunohistochemistry images of cardiac tissue from Donor A treated with serum (1 in 50) from adults with myocarditis/inflammatory cardiomyopathy stained with fluorescein isothiocyanate (FITC) conjugated anti-human Immunoglobulin G (IgG). An example image from each patient has been shown. Images were taken on a wide-field microscope at 20x magnification.

7.3.2.2 IgM and IgA staining

IgM and IgA staining was performed using serum from patients with MIS-C patients and COVID-19 vaccine-induced myocarditis, healthy paediatric controls, healthy COVID-19 vaccinated adults and one adult myocarditis patient (IgG staining positive control). No specific staining was seen for IgM and IgA in any patients or controls (Figure 7-4 and Figure 7-5, respectively).

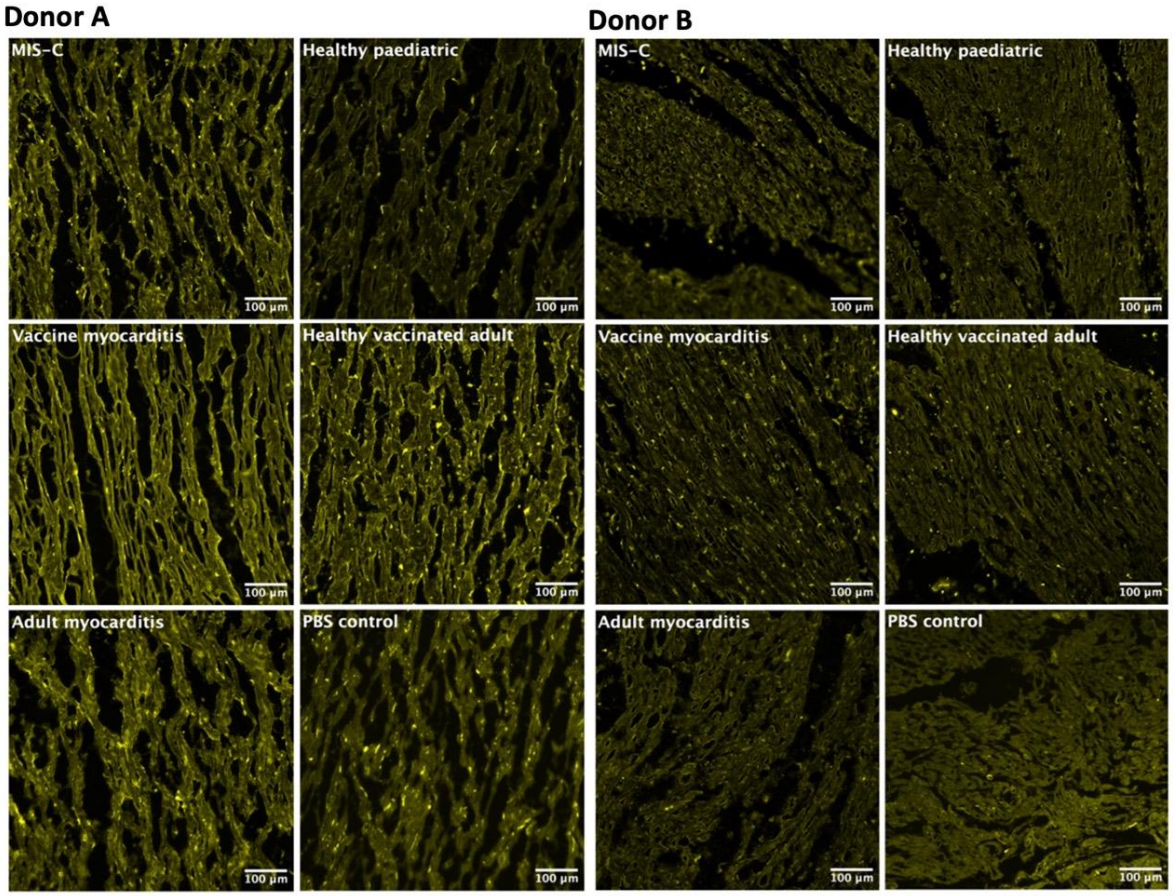

Figure 7-4 Immunohistochemistry images of IgM Staining.

Immunohistochemistry images of cardiac tissue from Donors A and B treated with serum (1 in 50) from patients and controls and stained with fluorescein isothiocyanate (FITC) conjugated anti-human Immunoglobulin M (IgM). An example image from each of the following groups has been shown: phosphate buffered saline (PBS) – negative control, healthy pre-COVID-19 pandemic paediatric controls, healthy COVID-19 vaccinated adults, COVID-19 vaccine-induced myocarditis and MIS-C. Images were taken on wide-field microscope at 20x magnification.

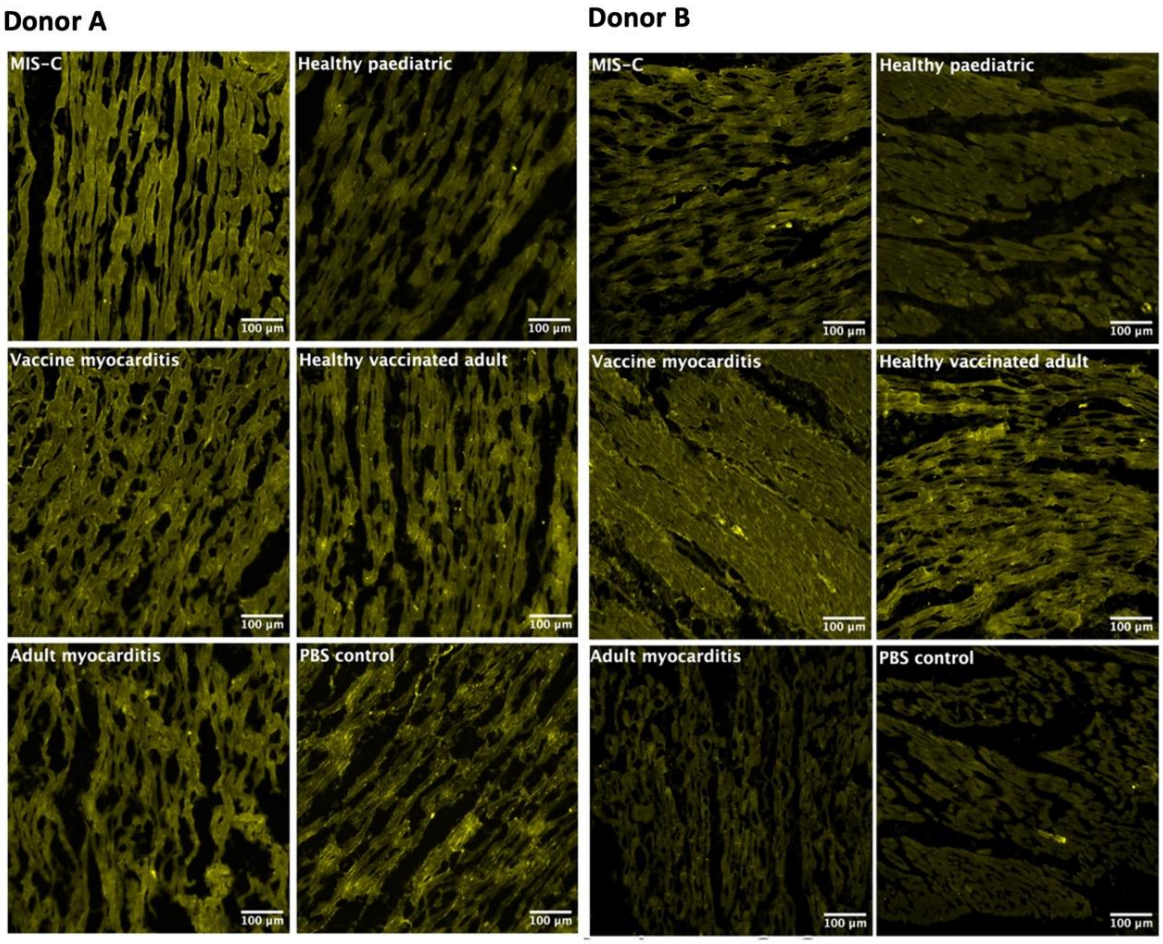

Figure 7-5 Immunohistochemistry images of IgA Staining.

Immunohistochemistry images of cardiac tissue from Donors A and B treated with serum (1in 50) from patients and controls and stained with fluorescein isothiocyanate (FITC) conjugated anti-human Immunoglobulin A (IgA). An example image from each of the following groups has been shown: phosphate buffered saline (PBS) – negative control, healthy pre-COVID-19 pandemic paediatric controls, healthy COVID-19 vaccinated adults, COVID-19 vaccine-induced myocarditis and MIS-C. Images were taken on wide-field microscope at 20x magnification.

7.3.2.3 FITC signal intensity

The quantified fluorescence intensity signal of FITC IgG, IgM and IgA for patients and controls is shown in Figure 7-6. The FITC IgG signal intensity of patients with MIS-C, COVID-19 vaccine-induced myocarditis and 7/8 adult myocarditis/inflammatory cardiomyopathy patients were similar to healthy controls ($p > 0.05$ for all Kruskal-Wallis comparisons). The FITC IgG signal intensity of the adult myocarditis positive control was distinctly higher than the other patients and controls.

On comparison of the fluorescence intensity signal of FITC IgM and FITC IgA between patients and controls, no significant difference was observed ($p > 0.05$ for all Kruskal-Wallis comparisons).

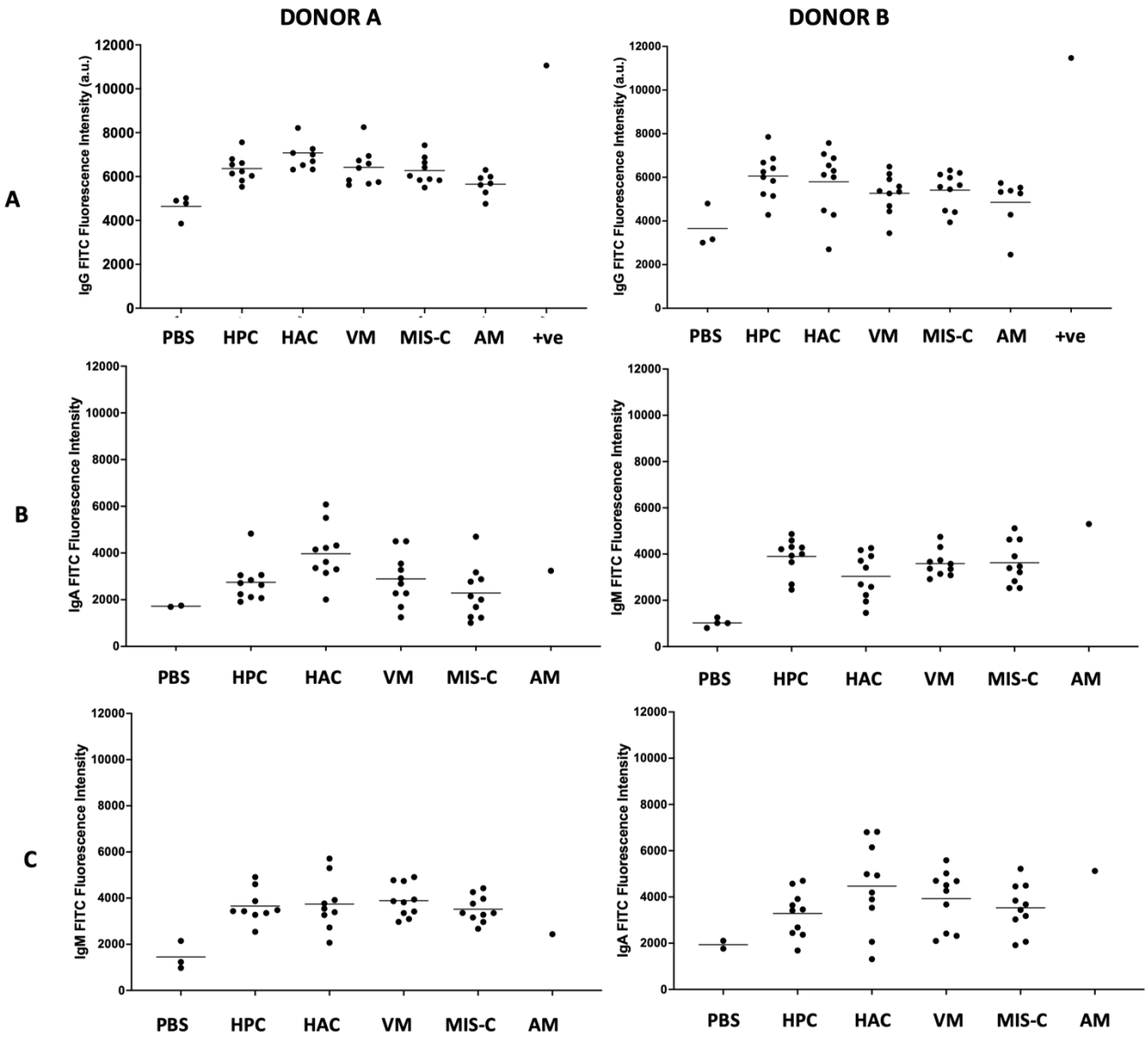

Figure 7-6 Fluorescence intensity of fluorescein isothiocyanate (FITC) conjugated with anti-human IgG (A), IgM (B), and IgA (C) in MIS-C, COVID-19 vaccine-induced myocarditis and controls.

Cardiac tissue from Donors A and B was treated with serum (1 in 50) from healthy pre-pandemic paediatric controls (HPC, n=10), healthy COVID-19 vaccinated adults (HAC, n=10), COVID-19 vaccine-induced myocarditis (VM, n=10), MIS-C (n=10), adult myocarditis positive control (+VE, n=1), adult myocarditis/inflammatory cardiomyopathy (AM, n=7) and phosphate buffered saline (PBS) – negative control (PBS, n=2-4). Only IgG measurements were taken for the adult myocarditis/inflammatory cardiomyopathy cases (n=7). The median signal intensity readings are displayed for each cohort. No significant differences were seen between MIS-C, vaccine myocarditis, adult myocarditis/inflammatory cardiomyopathy and healthy controls on Kruskal-Wallis analysis.

7.3.3 Cardiac autoantibodies ELISAs

The whole heart lysate, myosin and troponin anti-IgG ELISA results are shown in Figure 7-7, Figure 7-8, and Figure 7-9, respectively. The optical density for children with MIS-C and COVID-19 vaccine-induced myocarditis as well as the adult myocarditis/inflammatory myocarditis were significantly lower than the positive controls for all three assays. One healthy pre-pandemic paediatric control had a high reading for the whole heart lysate assay (Figure 7-7). There was no significant difference between the healthy COVID-19 vaccinated adults and the healthy pre-pandemic paediatric controls for the myosin and troponin assays (Figure 7-8 and Figure 7-9).

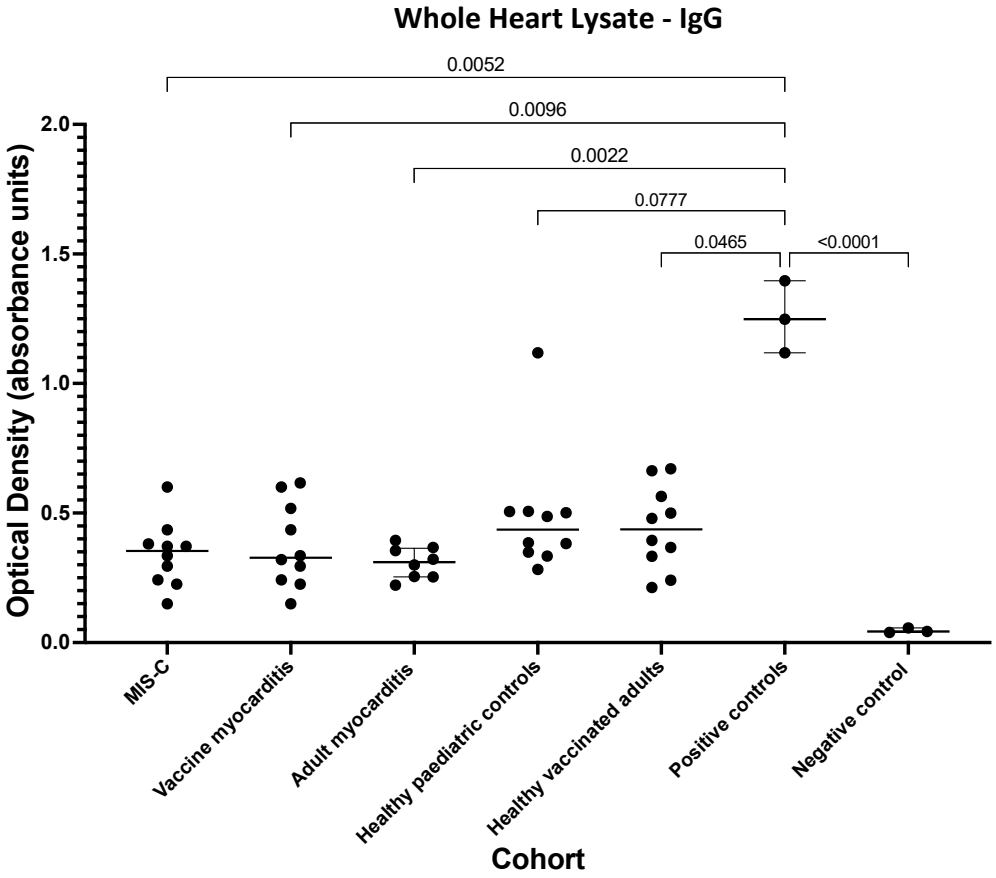

Figure 7-7 Whole heart lysate IgG ELISA results.

Patients with MIS-C (n = 10), COVID-19 vaccine-induced myocarditis (n = 10), adult myocarditis/inflammatory cardiomyopathy (n = 8), healthy paediatric controls (n = 10), healthy COVID-19 vaccinated adults (n = 10), adult myocarditis – positive controls (n = 3) and ELISA diluent – negative control (n = 3). The median optical density readings are displayed. P values from Kruskal-Wallis analysis are displayed.

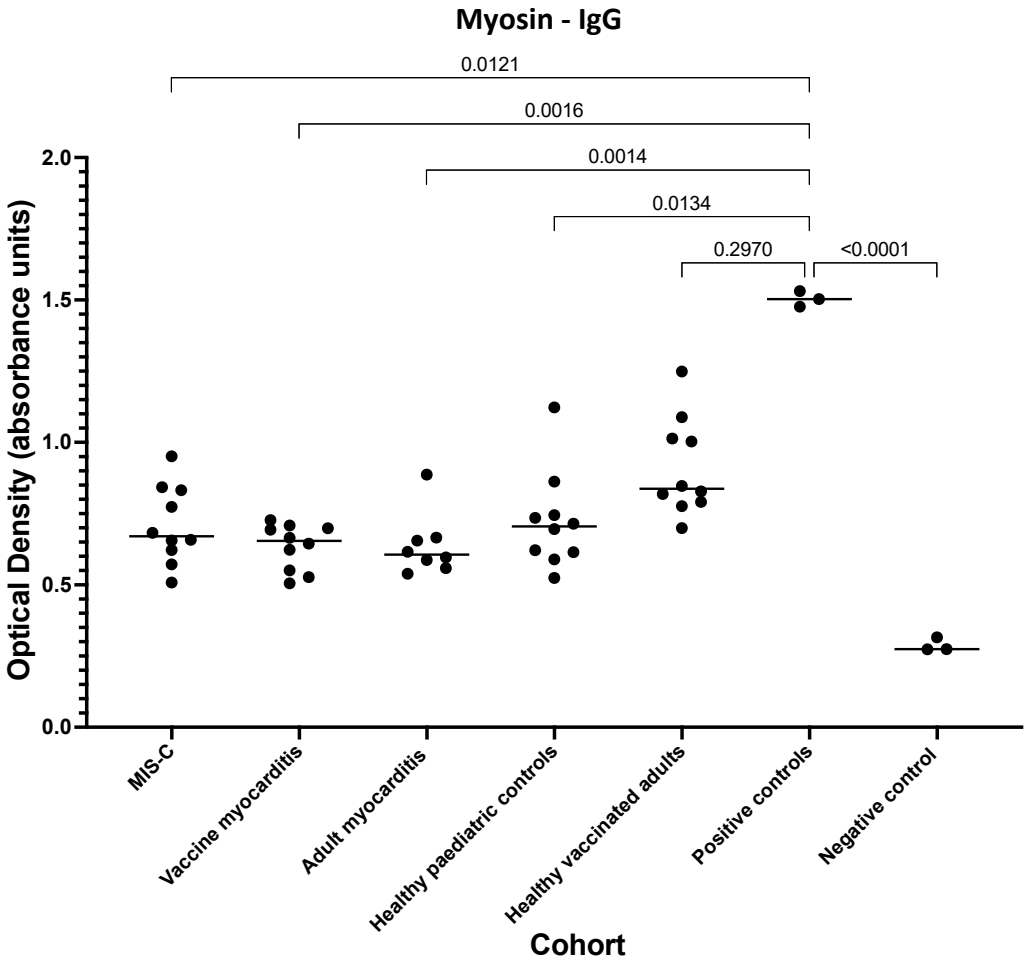

Figure 7-8 Myosin IgG ELISA results.

Patients with MIS-C (n = 10), COVID-19 vaccine-induced myocarditis (n = 10), adult myocarditis/inflammatory cardiomyopathy (n = 8), healthy paediatric controls (n = 10), healthy COVID-19 vaccinated adults (n = 10), adult myocarditis – positive controls (n = 3) and ELISA diluent – negative control (n = 3). The median optical density readings are displayed. P values from Kruskal-Wallis analysis are displayed.

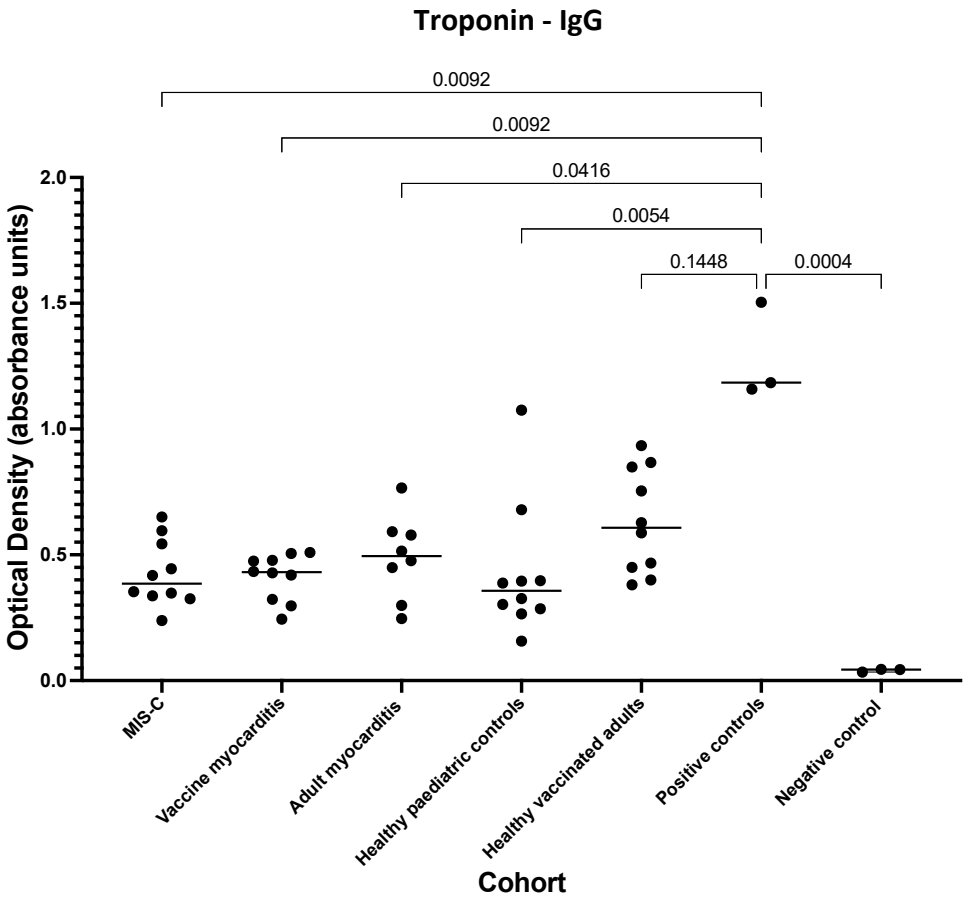

Figure 7-9 Troponin IgG ELISA results.

Patients with MIS-C (n = 10), COVID-19 vaccine-induced myocarditis (n = 10), adult myocarditis/inflammatory cardiomyopathy (n = 8), healthy paediatric controls (n = 10), healthy COVID-19 vaccinated adults (n = 10), adult myocarditis – positive controls (n = 3) and ELISA diluent – negative control (n = 3). The median optical density readings are displayed. P values from Kruskal-Wallis analysis are displayed.

7.4 Discussion

The primary objective of the work in this chapter was to investigate the role of antibody-mediated mechanisms in cardiac pathology associated with MIS-C and COVID-19 vaccine-induced myocarditis. IHC was used to directly visualise the binding of anti-cardiac antibodies from patient serum to donor cardiac tissues and ELISAs were employed to quantitatively assess the presence of general (whole heart lysate) and specific (myosin and troponin) anti-cardiac antibodies. Together, these techniques allowed the exploration of the potential involvement of anti-cardiac antibodies in the observed cardiac pathology of both conditions.

The absence of positive IHC and ELISA results suggests that the cardiac pathology in both MIS-C and COVID-19 vaccine-induced myocarditis is unlikely to be driven by direct anti-cardiac antibody-mediated mechanisms alone. However, it is worth considering that both viral antigens and antibodies may be required for antibody-mediated cardiac pathology, as indicated by the findings from Yonker et al. showing viral antigenaemia in MIS-C and COVID-19 vaccine-induced myocarditis patients[293,352]. Conversely, another study revealed that the majority of MIS-C patients had undetectable levels of SARS-CoV-2 Nucleocapsid and Spike antigens in their blood[317].

Building on these insights, published autopsy reports of MIS-C cases reveal inflammatory changes in cardiac tissue along with the detection of SARS-CoV-2, indicating potential virus-induced injury[445–447]. The presence of viral particles in various cardiac cell types suggests possible mechanisms, including direct viral effects, local inflammation, cardiomyocyte necrosis, and possible hematogenous spread, all contributing to the observed cardiac injury. Despite the rarity of fatal outcomes, these insights contribute to our understanding of MIS-C pathophysiology, providing valuable information on potential mechanisms from direct viral injury to hyperimmune responses. Histological data from vaccine-induced myocarditis is unavailable due to its self-limiting nature and relatively milder inflammatory response.

Considering the distinct clinical profiles, variations in cardiac involvement and disease severity of MIS-C and COVID-19 vaccine-induced myocarditis, it is plausible that these conditions may be triggered by different dysregulated immune responses. In MIS-C, the presence of a systemic hyperinflammatory response with excessive cytokine release[199,209], along with the rapid onset of severe cardiac dysfunction[212], which is reversible through immunomodulation, suggests a role for heightened levels of pro-inflammatory cytokines (such as IL6, IFNγ, TNFα) or other soluble factors. Soluble factors,

potentially exerting transient or reversible effects on myocyte function in MIS-C, may play a pivotal role in the dynamic pathophysiology of this condition; similar to what has been observed in meningococcal septicaemia, where raised IL6 has demonstrated myocardial depressant effects[291,292]. Future research endeavours could focus on identifying the specific role of cytokines and other soluble factors by utilising *ex vivo* or *in vitro* models to study myocyte function and contractility in the presence or absence of fractions of serum containing these factors. Conversely, the inflammatory response observed in COVID-19 vaccine-induced myocarditis is relatively milder and specific to the organs affected[344], with reports of eosinophilia supporting the hypothesis of a delayed hypersensitivity response[353–355].

The occurrence of both MIS-C and COVID-19 vaccine-induced myocarditis, several days or weeks after exposure to SARS-CoV-2 antigens, strongly suggests an aberrant adaptive immune response as the underlying mechanism. T cells play a critical role in coordinating the adaptive immune response and can contribute to the development of inflammation and tissue damage in certain circumstances. Thus, investigating the role of T cells in the immunopathology of these conditions is crucial.

Ultimately, it is likely that the aetiology of these conditions is multifactorial. Exposure to a novel antigen, such as SARS-CoV-2, can trigger a cascade of immune responses in genetically susceptible individuals. These responses may involve a dysregulated adaptive immune response, leading to an exaggerated immune reaction against cardiac tissues. Understanding the complex interplay between viral antigens, antibodies, and T cell responses in MIS-C and COVID-19 vaccine-induced myocarditis is crucial for unravelling the underlying mechanisms and developing targeted therapies.

Both the IHC and ELISA work have several limitations. For the IHC, there was only one positive control to confirm the validity of the immunoglobulin detection methods. To overcome this, the experiment was repeated using serum from this positive control on three separate occasions and showed reproducible findings on cardiac tissue from two different donors. This ensured the reliability of the method for detecting antibodies in human serum binding to cardiac tissue. MIS-C and COVID-19 vaccine-induced myocarditis are predominantly paediatric conditions; however, an adult positive control and adult cardiac donors were used. To obtain a more accurate representation, future studies would aim to include paediatric positive controls and cardiac tissue from paediatric donors. It is important to consider that the absence of antibody signal in the donor cardiac tissue used in the experiments may be due to a lack of the required genetic predisposition in the cardiac donors. Cardiac complications in MIS-C and COVID-19 vaccine-induced myocarditis may arise from specific genetic

factors that differ from the general population. This genetic variability could influence the immune response and the development of cardiac pathology in these conditions.

For the ELISAs, porcine whole heart lysate and porcine myosin were used to limit non-specific binding that occurs when using human heart lysate and myosin. Some of the limitations of using porcine lysate/myosin include species differences (e.g. inherent differences in protein compositions/post translations modifications), variations in immunogenicity of porcine antigens in human samples and disparity in epitope recognition. Of note, the positive control used in the IHC IgG experiment did not have a positive result for the whole heart/myosin/troponin ELISA assays. A possible explanation could be differences in antibody specificity between the IHC and ELISA, which could be due to the use of porcine lysate in the ELISA. This work relied on optical density results instead of quantifying antibody concentrates, which limits the interpretation of the data. However, a statistically significant difference was observed between the positive controls and MIS-C and vaccine myocarditis. Future studies should include standard curves and known antibody concentrations, to accurately quantify the antibody levels in patients and controls, facilitating identification of statistically and clinically significant positive results.

7.5 Conclusion

In conclusion, the results of the IHC and ELISA experiments, which show the lack of patient serum antibodies binding donor cardiac tissue and the lack of detection of anti-cardiac autoantibodies, strongly suggest that direct anti-cardiac antibody-mediated mechanisms are unlikely to be the primary drivers of cardiac immunopathology in both MIS-C and COVID-19 vaccine-induced myocarditis. This work contributes to the understanding of the underlying mechanisms of the cardiac complications seen in MIS-C and COVID-19 vaccine-induced myocarditis, which remain unclear. This is an important negative finding, with implications for COVID-19 vaccination programs in children, providing reassurance about the potential risk of direct antibody-mediated cardiac pathology. In addition, these findings highlight the need for further functional investigations, particularly involving T cell immunity, to identify the specific mechanisms underlying the cardiac pathology observed in these conditions. As a result, the next chapter will focus on investigating the role of T cells in the immunopathology of MIS-C.

Chapter 8: Functional studies investigating the role of T cells in MIS-C

8.1 Introduction

The timing of MIS-C, which is typically 4-6 weeks following exposure to SARS-CoV-2, indicates that a dysregulated adaptive immune response is driving the disease process. The results of the antibody analyses (Chapter 4), mechanistic antibody work (Chapter 7) and studies by other researchers[286] suggest that antibodies alone are unlikely to be solely responsible for the development of MIS-C. T cells are another key component of the adaptive immune response and their role in MIS-C immunopathogenesis has been explored. Early descriptions of MIS-C noted profound lymphopenia and alternation in T cell subsets, with reduced proportions of naïve cells and increased proportions of activated and proliferating $CD4^+$ and $CD8^+$ T cells[280,283,287,295]. Furthermore, studies have shown the upregulation of a specific T cell receptor (TCR) beta variable clonotype (TRBV11-2/TRBV21.3) in activated $CD4^+$ and $CD8^+$ T cells suggesting a "super-antigenic" effect of Spike protein antigens in triggering MIS-C[309,311,448].

While numerous studies have characterised T cell populations in MIS-C, those investigating T cell function are limited. Two studies have investigated functionality of specific T cells in convalescent MIS-C and reported normal function[449,450]. However, T cell function in acute MIS-C as well as comparison with other febrile illness remains largely unexplored. The work presented in this chapter aims to fill this gap in knowledge and further the understanding of the role of T cells in the immunopathogenesis of MIS-C.

<u>The primary aim of this chapter is:</u>

To gain better understanding of the T cell response in MIS-C compared to febrile and healthy controls through functional studies.

The objectives of this chapter are:

1) Perform SARS-CoV-2 QuantiFERON assays using acute and convalescent samples from MIS-C, febrile controls, and healthy controls to understand the role of T cells in MIS-C immunopathology.
2) Perform mass cytometry experiments on stimulated samples from the SARS-CoV-2 QuantiFERON assays to gain further insights into T cell function in acute and convalescent MIS-C.
3) Use RNA-seq data for corroboration of the findings from functional and immunological studies.

The key findings from this chapter are:

The work in this chapter expands the understanding of the T cell immune response in acute and convalescent MIS-C using multiple methodologies and provides comparison with febrile and healthy paediatric controls. The results provide valuable insights into immunological pathways that are both unique to MIS-C and shared by paediatric febrile illnesses. The finding of reduced specific T cell response to stimulation in acute MIS-C with recovery in convalescence suggests possible transient T cell exhaustion. However, further research is necessary for gaining a deeper understanding of the underlying mechanisms involved. If T cell exhaustion is indeed identified as an important driver of MIS-C pathogenesis, development of targeted interventions to reverse T cell exhaustion could yield significant benefits and lead to improved patient outcomes. The work described in this chapter has been submitted for publication to Nature Communications.

8.2 Methodology

8.2.1 Clinical cohorts and study design

The work in this chapter comprises of clinical data and samples from individuals recruited from St Mary's Hospital, London and Evelina Children's Hospital, London as part of DIAMONDS. These include children with MIS-C, severe bacterial illness (SBI), severe viral illness (SVI), Kawasaki disease (KD) and inflammatory disease (INF). Healthy paediatric controls (HPC) were included as age and sex-matched controls and healthy COVID-19 vaccinated adult controls (HAC) were included as healthy controls with prior exposure to SARS-CoV-2. Vaccinated children could not be included as COVID-19 vaccinations had not been rolled out into the paediatric population at the time this study was conducted.

The individuals underwent thorough phenotyping using a well-established algorithm, which is described in detail in Chapter 3 (section 3.1.1.2). The definite bacterial (DB) patients were designated to the "Severe Bacterial Illness (SBI)" group and the definite viral (DV) patients were designated to the "Severe Viral Illness (SVI)" group, as this cohort represents severely unwell children with febrile illnesses, defined by a substantial proportion (55%) of children requiring intensive care support. Study participants were sampled at two timepoints: acute illness (TP1) and convalescence (TP3) for SARS-CoV-2 QuantiFERON and cytokines assays. Samples for mass cytometry were taken from a small subset of patients. The whole blood RNA-seq data, used for corroboration of results, was generated from a separate cohort of children with acute febrile illness from the EUCLIDS, PERFORM and DIAMONDS studies recruited at a separate and earlier timeframe to the patients above.

8.2.2 SARS-CoV-2 QuantiFERON assay

QuantiFERON assays assess cell-mediated immunity to a specific antigen. Whole blood is stimulated with an antigen, activating antigen-specific lymphocytes in samples of individuals with prior exposure to the antigen. The activated antigen-specific lymphocytes produce IFNγ, which is measured using an ELISA. These assays are widely used for diagnosing *Mycobacterium tuberculosis* infection, where elevated IFNγ levels indicate active or latent tuberculosis[381]. The Qiagen SARS-CoV-2 QuantiFERON assay was used for measurement of IFNγ and other cytokines following stimulation of whole blood with SARS-CoV-2 antigens composed of peptides from the Spike protein (referred to as ag1)[382]. The assay included a positive control: phytohemagglutinin (PHA), a non-specific T cell stimulant (referred to as mitogen) and a negative control (referred to as nil). The detailed laboratory protocol is provided in Chapter 3 (section 3.2.4.1).

8.2.3 LEGENDplex 13-plex cytokine assay

The LEGENDplex Human Anti-virus Response Panel 13-plex cytokine assay was used for the measurement of cytokines in the QuantiFERON supernatant. It is a bead-based immunoassay, which allows measurement of multiple cytokines of interest in MIS-C immunopathology. These include: IL1β, IL6, IL8, IL10, IL12p70, IFNγ, IFNα2, IFNβ, IFNλ1, IFNλ2/3, IP10, TNFα and GM-CSF. The LEGENDplex bead-based immunoassays allow simultaneous detection of multiple analytes in one sample using flow cytometry. Beads are coupled with specific antibodies for each analyte. Addition of biotinylated detection antibodies results in formation of specific antibody-analyte-detection antibody complexes and SA-PE is used for reporting of biotinylated antibodies. Flow cytometry is used for identification and quantification of analyte-specific populations based on bead characteristics. The detailed laboratory protocol is provided in Chapter 3 (section 3.2.4.2).

8.2.3.1 LEGENDplex 13-plex cytokine assay data analysis

The following R packages were used for the analysis and graphical representation of the data: tidyverse, dplyr, pcatools, ggplot2 and rstatix.

Principal component analysis was conducted to detect any batch effects as the samples were run across 20 plates. Raw data were used for unstimulated (nil) samples. Percentage change from unstimulated samples was used for evaluating the stimulated samples (ag1 and mitogen). To address the skewness of data and improve visualisation, data were log10 transformed. Pairwise comparisons using the Wilcoxon

test (non-parametric) were performed across clinical cohorts and timepoints, with BH[393] correction for multiple testing.

A proportion of patients had research blood sampling following immunomodulatory treatment. K-means clustering was used to evaluate the effects of immunomodulatory treatment on cytokine levels. K-means clustering is an unsupervised algorithm used for clustering data into a pre-defined number of clusters (K). K was set at six, for each treatment group: 1) none, 2) IVIG, 3) Corticosteroids, 4) IVIG and Corticosteroids, 5) Corticosteroids and monoclonal antibodies (Mab) and 6) IVIG and Corticosteroids and Mab. K-mean clustering aims to minimise the within-cluster sum of squares, which is the sum of squared distance between each data point and the centre of the assigned cluster, to create tightly grouped clusters. The analyses were performed on raw data from acute (TP1) samples, separately for unstimulated (nil), ag1 stimulated and mitogen stimulated samples. Healthy controls were excluded from this analysis, to focus on the variations in cytokine data between patient treatment groups.

8.2.4 Mesoscale Discovery (MSD) U-Plex assay for multiplex cytokine testing

MSD U-PLEX assay was used for the measurement of IL2, IL17A, IL4 and IL13 in the QuantiFERON supernatant. MSD U-PLEX assay was selected as it allows custom design of single or multiplex assays, by using U-PLEX linkers that are conjugated to the biotinylated capture antibodies, which bind to specific spots in each well. The detailed description of MSD U-PLEX assay principles along with the laboratory protocol can be found in Chapter 3 (section 3.2.4.3). The data analysis followed the same approach as described for the LEGENDplex 13-plex assay above.

8.2.5 Mass cytometry

Mass cytometry was carried out on a subset of samples from the SARS-CoV-2 QuantiFERON assay, following stimulation with nil, ag1 and mitogen. Mass cytometry or cytometry at time-of-flight (Cy-TOF) allows phenotypic and functional analysis of single cells. Heavy metal ions are used for tagging antibodies. The tags have distinct peaks which can be detected on mass spectrometry, allowing characterisation of cells. Samples were stained for cell surface markers (activation, proliferation, exhaustion, apoptosis) and intracellular cytokines (IL2, IL6, TNFα, IFNγ) to allow a comprehensive assessment of immune cell phenotype, function, and cytokine production. Barcoding methodology was used to combine multiple samples, reduce variability, and enhance throughput. Details of the principles of mass cytometry, the staining and barcoding laboratory protocol can be found in Chapter 3 (section 3.2.4.4).

8.2.5.1 Mass cytometry data analysis

The following R packages were used for the analysis and graphical representation of the data: rstatix, ggpubr, ggprism, patchwork, magrittr, dplyr, ggplot2.

Targeted analyses were performed on variables relating to T cell immunity. Unsupervised hierarchical clustering was used to present the median values of the variables using the raw data for each group for comparisons of unstimulated samples. To assess the effect of stimulation and to bring the data onto the same scale, the fold change from unstimulated data to stimulated data was calculated for all variables. Next, to identify significant features within cell proportions and cell expression markers data, Wilcoxon pairwise comparisons with BH adjustment[393] were performed, comparing results between MIS-C TP1, MIS-C TP3 and HPC.

Due to a relatively small number of mass cytometry samples and a large number of variables (631), only a few samples had no missing data. This meant it was not feasible to do K-means clustering or unsupervised hierarchical clustering to assess the effect of immunomodulatory treatments. Therefore, PCA was performed instead. Combined raw data for TP1 and TP3 nil, ag1 and mitogen stimulated samples were used for the analysis as it was not possible to do the analysis separately by different stimulation states or timepoints due to small number of samples. Healthy controls were excluded from the analysis, to focus on the variations in data between patient treatment groups.

The mass cytometry samples from the SARS-CoV-2 QuantiFERON assay had undergone 17-24 hours of incubation at 37°C. To assess the effect of incubation on the mass cytometry results, PCA and unsupervised hierarchical clustering approaches were used. The results of the unstimulated mass cytometry samples from the SARS-CoV-2 QuantiFERON assay (incubated) were compared with results from whole blood mass cytometry samples (unincubated) taken from the same individuals. Wilcoxon pairwise comparisons with BH correction were conducted to identify statistically significant differences.

8.2.6 RNA sequencing

RNA sequencing (RNA-seq) is a high-throughput technique used for examining the quantity and sequences of the total cellular content of RNA in a sample. RNA-seq was used for targeted analyses of selected genes to help explain the SARS-CoV-2 QuantiFERON and mass cytometry findings. The laboratory methods for RNA extraction and sequencing are described in Chapter 3 (section 3.2.4.5).

8.2.6.1 Processing of raw data and generation of gene counts

The data processing was performed using the R programming language. The two batches of the RNA-seq data (EUCLIDS and PERFORM) were pre-processed and then merged using genes present in both datasets. Pre-processing included removal of ribosomal RNA (rRNA) and globin RNA using genes from the depletion kit used in the RNA-seq protocol *(HBB, MT-RNR2, MT-RNR1, HBA2, HBG2, HBG1, HBA1)*. Genes with counts of ≤ 10 in at least three samples were also removed. After merging of the two datasets, PCA was performed to assess the effect of disease group, age, sex, plate, sequencing batch as well as identification and removal of outliers. Counts were normalised using the DESeq2 package, employing the median of ratio method. This normalisation method takes into account both sequencing depth and RNA composition of samples, enabling meaningful comparisons of gene expression levels between different samples. Genes with counts of ≤ 20 in at least three samples were removed from the normalised dataset.

8.2.6.2 Targeted analyses

The normalised RNA-seq dataset was used to perform targeted analyses on genes related to IFNγ, IL2, T cell inhibition, exhaustion, and apoptosis. This was done to further explore the hypothesis of dysregulated T cell function in MIS-C and to provide insights into the findings from QuantiFERON and mass cytometry experiments. The T cell exhaustion and apoptosis genes related to expression markers used in mass cytometry were selected for analysis (Table 8-1). Gene counts were compared across disease groups using Wilcoxon pairwise comparisons with BH adjustment.

Table 8-1 Names and function of genes selected for RNA-seq analysis[451].

Gene	Function
Interferon gamma (IFNγ)	Encodes a soluble cytokine that is produced primarily by activated T cells and NK cells. IFNγ plays an important role in host defence and immune regulation. **Excluded from analysis - gene counts <20**
Interferon gamma receptor 1 (IFNγR1)	Encodes the IFNγR1 protein, a transmembrane protein expressed on numerous immune cells. It forms a heterodimer complex with the IFNγ receptor 2 protein, which allows cells to respond to IFNγ.
Interferon gamma receptor 2 (IFNγR2)	Encodes the IFNγR2 protein, a transmembrane protein expressed on numerous immune cells. It forms a heterodimer complex with the IFNγ receptor 1 protein, which allows cells to respond to IFNγ.
Interleukin 2 (IL2)	Encodes a protein that is secreted by activated T cells. IL2 promotes activation, proliferation and survival of T cells and plays a role in immune tolerance through development and maintenance of Tregs. **Excluded from analysis - gene counts < 20**
CD25/Interleukin 2 receptor alpha subunit (IL2RA)	Encodes the IL2RA subunit, a cell surface receptor, primarily expressed by activated T cells, B cells and Tregs. Binding of IL2 initiates a signalling cascade that promotes T cell activation and proliferation.
CD122/Interleukin 2 receptor beta subunit (IL2RB)	Encodes the IL2RB subunit, a cell surface receptor expressed on various immune cells. It forms a heterodimer with IL2RA/IL15 receptor alpha subunit to form functioning receptors for IL2 and IL15.
Interleukin 2 receptor gamma subunit (IL2RG)	Encodes the IL2RG subunit, which is an important component of many interleukin receptors including IL2, IL4, IL7, IL9, IL15 and IL21.
CD95/Fas cell surface death receptor (FAS)	Encodes a cell surface receptor protein which plays a critical role in regulating programmed cell death (PCD)/apoptosis. It is expressed on various cell types, including T cells.
CD172/Fas cell surface death receptor ligand (FASL)	Encodes a cell surface protein which is primarily expressed on activated T cells and NK cells. Fas-FasL interaction leads to apoptosis of target cells and can also eliminate self-reactive T cells.
Fas associated via death domain (FADD)	Encodes an adaptor molecule which recruits Caspase 8 or Caspase 10 to the activated CD95 (FAS) receptors; it is vital for the induction of apoptosis.
Cysteine-aspartic acid protease eight (CASP8)	Encodes the proenzyme Caspase 8 which plays a key role in PCD.
CD152/ Cytotoxic T lymphocyte antigen 4 (CTLA4)	Encodes an inhibitory protein receptor that is found primarily on the surface of T cells.

Table 8-1 continued.

Gene	Function
CD223/Lymphocyte activating gene 3 (LAG3)	Encodes a cell surface protein that is primarily expressed on immune cells including T cells, Tregs, B cells and NK cells. LAG3 inhibits T cell activation through interaction with Major Histocompatibility complex class II (MHC II) molecules on APCs.
CD279/ Programmed cell death protein 1 (PD-1)	Encodes a cell surface receptor that is primarily expressed on T cells, B cells and NK cells. The interaction of PD-1 with its ligands sends inhibitory signals to T cells.
CD274/ Programmed cell death ligand 1 (PDL1)	Encodes a cell surface protein that is a ligand for PD-1. Expressed on various cells including tumour cells, APCs and some normal tissue. Expression can be induced by inflammatory signals.
CD273/Programmed cell death ligand 2 (PDL2)	Encodes a cell surface protein that is a ligand for PD-1. Primarily expressed on APCs.

8.3 Results

8.3.1 Demographic and clinical characteristics

A total of 136 individuals were included, comprised of children with MIS-C (n = 55), Severe Bacterial Illness (SBI) (n = 17), Severe Viral Illness (SVI) (n = 8), Kawasaki disease KD (n = 5), other Inflammatory disease (n = 9), healthy paediatric controls (HPC) (n = 15) and healthy adult controls (HAC) (n = 27).

The clinical and demographic characteristics of the paediatric cohort are shown in Table 8-2 and details of the HAC can be found in Appendix 7, Table A7-1. The median ages of children with MIS-C (9 years, IQR 6-12 years), SBI (11 years, IQR 9-13 years), SVI (12 years, IQR 8-12 years) and Inflammatory (10 years, IQR 5-12 years) were comparable (Table 8-2). However, the median ages of children with KD (1 year, IQR 1-4 years) and HPC (6 years, IQR 5-10 years) were lower than the other disease groups. A male preponderance was seen in MIS-C (66% males), KD (80% males) and Inflammatory disease (67% males) (Table 8-2). Among the disease group, MIS-C had the highest proportion of patients from African/Caribbean and mixed ethnicities (21% vs 0-13%) (Table 8-2). The highest proportions of patients with comorbidities were seen in SBI (47%) and SVI (63%), the overall burden of comorbidities was 20% for the whole cohort. Further details regarding the reported comorbidities in each disease group are shown in Appendix 7, Table A7-2.

The median maximum CRP was highest in MIS-C (220 mg/L, IQR 150-260 mg/L) and SBI (100 mg/L, IQR 170-340 mg/L). The median maximum neutrophil count was highest in SBI (17 x 10^9/L, IQR 12-20 x 10^9/L) and Inflammatory disease (13 x 10^9/L, IQR 9-19 x 10^9/L). Although lymphopenia was observed in most disease groups, it was most notable in MIS-C (median 0.5 x 10^9/L, IQR 0.4-1.0 x 10^9/L) (Table 8-2). SARS-CoV-2 PCR was positive in 4 (7.3%) patients with MIS-C, 2 (11.8%) patients with SBI and 5 (62.5%) patients with SVI. SARS-CoV-2 seropositivity ranged between 11-84% with the highest proportion of seropositivity found in the MIS-C disease group (Table 8-2).

Across all disease groups, 29 patients received IVIG (27%), 64 received corticosteroids (59%) and 21 received monoclonal antibodies (Mab) (19%) (Table 8-2). Due to the clinical severity, need for initiation of prompt therapy, and significant number of routine blood tests already being conducted as part of their clinical care, it was not possible to get pre-treatment blood samples in majority of cases (57%). The proportion of patients who received immunomodulatory treatment prior to research blood sampling in each disease group is shown in Table 8-2.

This cohort is representative of children with severe febrile illness, as such, 37 (67%) children with MIS-C, 12 (71%) children with SBI, 7 (88%) children with SVI, 0 children with KD and 3 (33%) children with Inflammatory disease required admission to intensive care. The mortality rate was low, at 0.9%, with one patient death in the SBI disease group.

The RNA-seq dataset, which was used for corroboration of findings from the QuantiFERON assay and mass cytometry analyses, comprised of children with MIS-C (n = 38), bacterial illness (n = 188), viral illness (n = 138) and KD (n = 136). The clinical characteristics of the RNA-seq cohort are shown in Appendix 7, Table A7-3.

Table 8-2 Demographic and clinical characteristics of the cohorts included in the study.

MIS-C = multisystem inflammatory syndrome in children, SBI = Severe bacterial illness, SVI = Severe Viral illness, KD = Kawasaki disease, Inflammatory = non-SARS-CoV-2 associated inflammatory disease, HPC = healthy paediatric controls, TP1 = timepoint 1, n = count, IQR = interquartile range, % = percentage

	MIS-C (n = 55)	**SBI (n = 17)**	**SVI (n = 8)**	**KD (n = 5)**	**Inflammatory (n = 9)**	**HPC (n = 15)**	**Overall (n = 109)**
Age, median (IQR), [years]	9.0 (6.0 - 12)	11 (9.0 - 13)	12 (8.0 - 12)	1.0 (1.0 - 4.0)	10 (5.0 - 12)	6.0 (5.0 - 10)	9.0 (5.0 - 12)
Male, n (%)	36 (65.5%)	8 (47.1%)	4 (50.0%)	4 (80.0%)	6 (66.7%)	8 (57.1%)	66 (61.1%)
Self-reported ethnicity, n (%)							
African/Caribbean	12 (21.8%)	2 (11.8%)	1 (12.5%)	0 (0%)	0 (0%)	3 (21.4%)	18 (16.7%)
Asian	8 (14.5%)	4 (23.5%)	4 (50.0%)	2 (40.0%)	2 (22.2%)	0 (0%)	20 (18.5%)
Caucasian	21 (38.2%)	10 (58.8%)	3 (37.5%)	2 (40.0%)	5 (55.6%)	9 (64.3%)	50 (46.3%)
Mixed	9 (16.4%)	1 (5.9%)	0 (0%)	0 (0%)	0 (0%)	2 (14.3%)	12 (11.1%)
Other/Not known	5 (9.1%)	0 (0%)	0 (0%)	1 (20.0%)	2 (22.2%)	0 (0%)	8 (7.4%)
Comorbidities	6 (10.9%)	8 (47.1%)	5 (62.5%)	0 (0%)	1 (11.1%)	2 (14.3%)	22 (20.4%)
Maximum CRP, median (IQR) [mg/L]	220 (150 - 260)	200 (170 - 340)	38 (17 - 120)	120 (120 - 150)	43 (11 - 120)	-	170 (61 - 250)
Maximum neutrophils, median (IQR) [x 10^9/L]	12 (7.8 - 15)	17 (12 - 20)	8.0 (7.0 - 11)	9.7 (7.9 - 13)	13 (9.0 - 19)	-	11 (6.2 - 16)
Minimum lymphocytes, median (IQR) [x 10^9/L]	0.50 (0.4 – 1.0)	0.80 (0.5 – 1.0)	0.70 (0.7 – 1.0)	2.8 (2.1 - 3.7)	0.90 (0.6 - 1.0)	-	8.0 (4.0 - 12)
SARS-CoV-2 PCR Positive, n (%)							
Positive	4 (7.3%)	2 (11.8%)	5 (62.5%)	0 (0%)	0 (0%)	0 (0%)	11 (10.2%)
Negative	46 (83.6%)	10 (58.8%)	3 (37.5%)	5 (100%)	6 (66.7%)	10 (66.7%)	80 (74.1%)
Not done	5 (9.1%)	5 (29.4%)	0 (0%)	0 (0%)	3 (33.3%)	5 (33.3)	17 (15.7%)
SARS-CoV-2 serology, n (%)							
Positive	48 (87.3%)	3 (17.6%)	2 (28.6%)	1 (20%)	1 (11.1%)	0 (0%)	55 (50.9%)
Negative	1 (1.8%)	1 (5.9%)	0 (0%)	4 (80%)	2 (22.2%)	0 (0%)	8 (7.4%)
Not done	6 (10.9%)	13 (76.5%)	5 (71.4%)	0 (0%)	6 (66.7%)	15 (100%)	45 (41.7%)

Table 8-2 continued.

	MIS-C (n = 55)	SBI (n = 17)	SVI (n = 8)	KD (n = 5)	Inflammatory (n = 9)	HPC (n = 15)	Overall (n = 109)
Treatments received, n (%)							
IVIG	21 (38.2%)	3 (17.6%)	0 (0%)	3 (60.0%)	2 (22.2%)	-	29 (26.9%)
IVIG prior to TP1 sampling	14 (25.5%)	3 (17.6%)	0 (0%)	2 (40.0%)	2 (22.2%)	-	21 (19.4%)
Corticosteroids	48 (87.3%)	5 (29.4%)	5 (62.5%)	1 (20.0%)	5 (55.6%)	-	64 (59.3%)
Corticosteroids prior to TP1 sampling	41 (74.5%)	4 (23.5%)	5 (62.5%)	1 (20.0%)	3 (33.3%)	-	54 (50.0%)
Monoclonal antibodies	16 (29.1%)	0 (0%)	2 (25.0%)	1 (20.0%)	2 (22.2%)	-	21 (19.4%)
Mab prior to TP1 sampling	6 (10.9%)	0 (0%)	1 (12.5%)	0 (0%)	0 (0%)	-	7 (6.5%)
ICU admission, n (%)	37 (67.3%)	12 (70.6%)	7 (87.5%)	0 (0%)	3 (33.3%)	-	59 (54.6%)
Shock, n (%)	22 (40.0%)	7 (41.2%)	1 (12.5%)	0 (0%)	0 (0%)	-	30 (27.8%)
Inotropic support, n (%)	30 (54.5%)	8 (47.1%)	2 (25.0%)	0 (0%)	1 (11.1%)	-	41 (38.0%)
Invasive ventilation, n (%)	2 (3.6%)	8 (47.1%)	7 (87.5%)	0 (0%)	2 (22.2%)	-	19 (17.6%)
Renal replacement therapy, n (%)	0 (0%)	1 (5.9%)	0 (0%)	0 (0%)	1 (11.1%)	-	2 (1.9%)
ECMO, n (%)	0 (0%)	1 (5.9%)	0 (0%)	0 (0%)	0 (0%)	-	1 (0.9%)
Death, n (%)	0 (0%)	1 (5.9%)	0 (0%)	0 (0%)	0 (0%)	-	1 (0.9%)
Length of admission, median (IQR), [days]	6.0 (5.0 - 8.0)	8.0 (6.0 - 33)	24 (15 - 38)	5.0 (4.0 - 10)	9.0 (8.0 - 23)	-	6.0 (5.0 - 9.0)

8.3.2 Supernatant cytokine multiplex assay results

To evaluate the response to stimulation with SARS-CoV-2 antigen and mitogen, cytokines were measured in supernatant harvested following the QuantiFERON assay. The 13-plex cytokine assay was performed on a total of 234 (3 samples per patient: nil, ag1, mitogen) acute (TP1) and convalescent (TP3) samples collected from 131 individuals (Table 8-3). Some patients had samples taken at both TP1 and TP3. The 4-plex cytokine assay was conducted on a smaller subset due to limited sample availability (Table 8-3). The PCAs did not show any batch effects in the 13-plex and 4-plex datasets (Appendix 7, Figure A7-1 and Figure A7-2).

Table 8-3 Summary of the number of participants and samples at timepoint 1 (acute) and timepoint 3 (convalescence) for the 13-plex and 4-plex cytokine panel.

	All	MIS-C	SBI	SVI	KD	Inflammatory	HPC	HAC
13-plex cytokine panel								
Number of individuals	131	55	17	8	5	9	15	27
Timepoint one samples, Number of samples	123	42	21	6	27	-	-	123
Timepoint three samples, Number of samples	51	9	3	9	0	45	81	51
4-plex cytokine panel								
Number of individuals	47	19	9	5	4	0	5	47
Timepoint one samples, Number of samples	30	15	15	3	0	-	-	30
Timepoint three samples, Number of samples	30	12	0	9	0	15	15	30

Raw data has been presented for the unstimulated (nil) samples, while the percentage change from unstimulated samples has been reported for results following stimulation with ag1 and mitogen. Boxplots of cytokines of interest with statistically significant results are presented in this chapter, while results of the remaining cytokines are shown in Appendix 7, Figure A7-3, Figure A7-4 and Figure A7-5. A summary of the cytokine results is displayed at the of end this section, with a gradient table for visualisation of trends across disease groups and controls (Table 8-4).

8.3.2.1 Cytokine results: Unstimulated samples (nil)

Most of the cytokines tested showed no statistical differences in concentrations between disease groups in acute (TP1) or convalescent (TP3) unstimulated samples, except for IP10 (Figure 8-1), IL17A (Figure 8-2), IL8 and IL10 (Appendix 7 Figure A7-3). IP10 levels were increased in acute MIS-C and acute SVI compared to the acute Inflammatory cohort and HPC (all $p < 0.01$). IL17A levels were raised in acute MIS-C and acute SBI compared to acute SVI and HPC (all $p < 0.05$). IL8 levels were reduced in acute MIS-C compared to acute SBI and acute Inflammatory (all $p < 0.01$). IL10 levels were increased in acute MIS-C, acute SBI and acute SVI compared to HPC (all $p < 0.01$). The differences in IP10, IL17A, IL8 and IL10 across disease groups and controls were not present in the convalescent samples (Figure 8-1, Figure 8-2, Appendix 7 Figure A7-3).

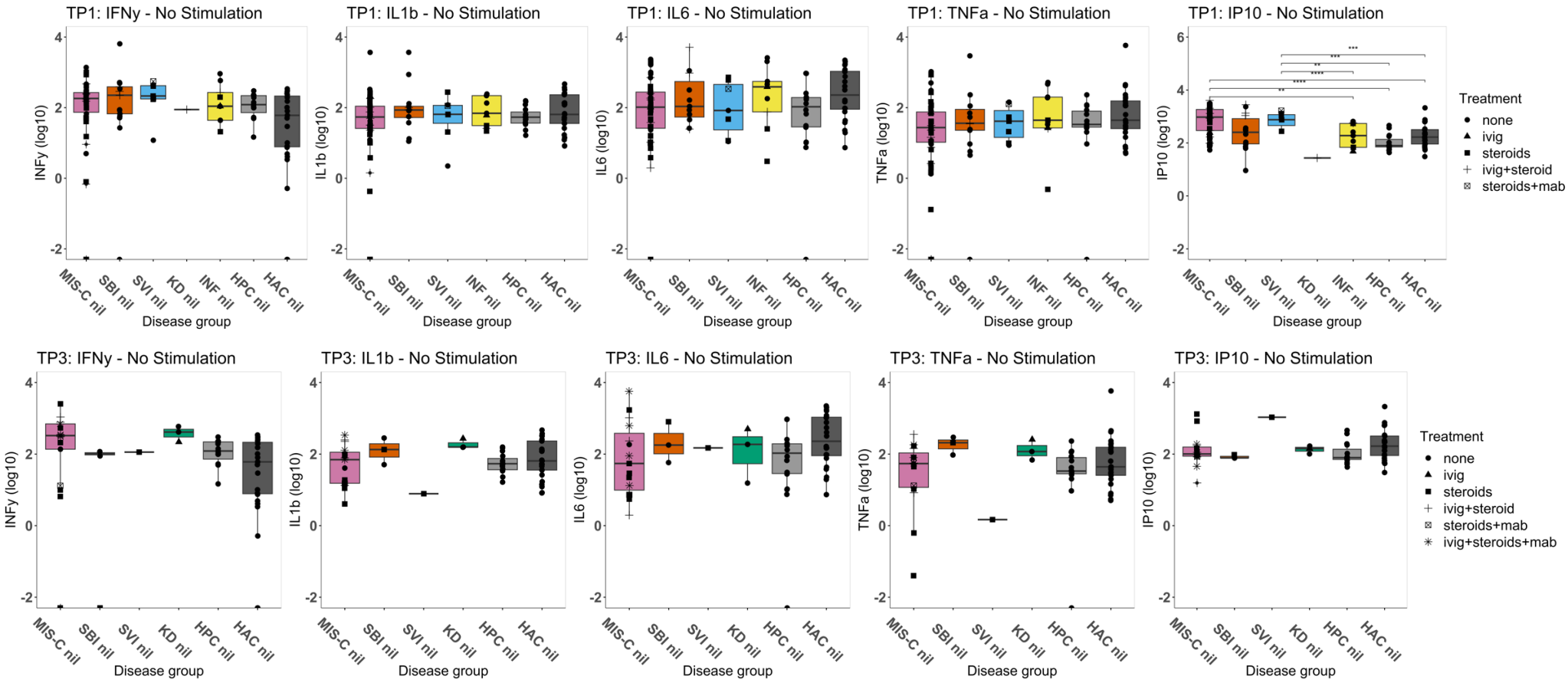

Figure 8-1 Boxplots showing the levels of IFNγ, IL1β, IL6, TNFα and IP10 in acute (TP1) and convalescent (TP3) unstimulated (nil) samples.

Log10 transformed data are shown. Each point represents a participant for the following groups: MIS-C, severe bacterial illness (SBI), severe viral illness (SVI), Kawasaki disease (KD), other Inflammatory disease (INF). The shape of the point corresponds to the treatment received prior to blood sampling: ivig = intravenous immunoglobulin, steroid = corticosteroids, mab = monoclonal antibody. Wilcoxon pairwise comparisons with Benjamini Hochberg correction were performed; only significant p values are displayed.

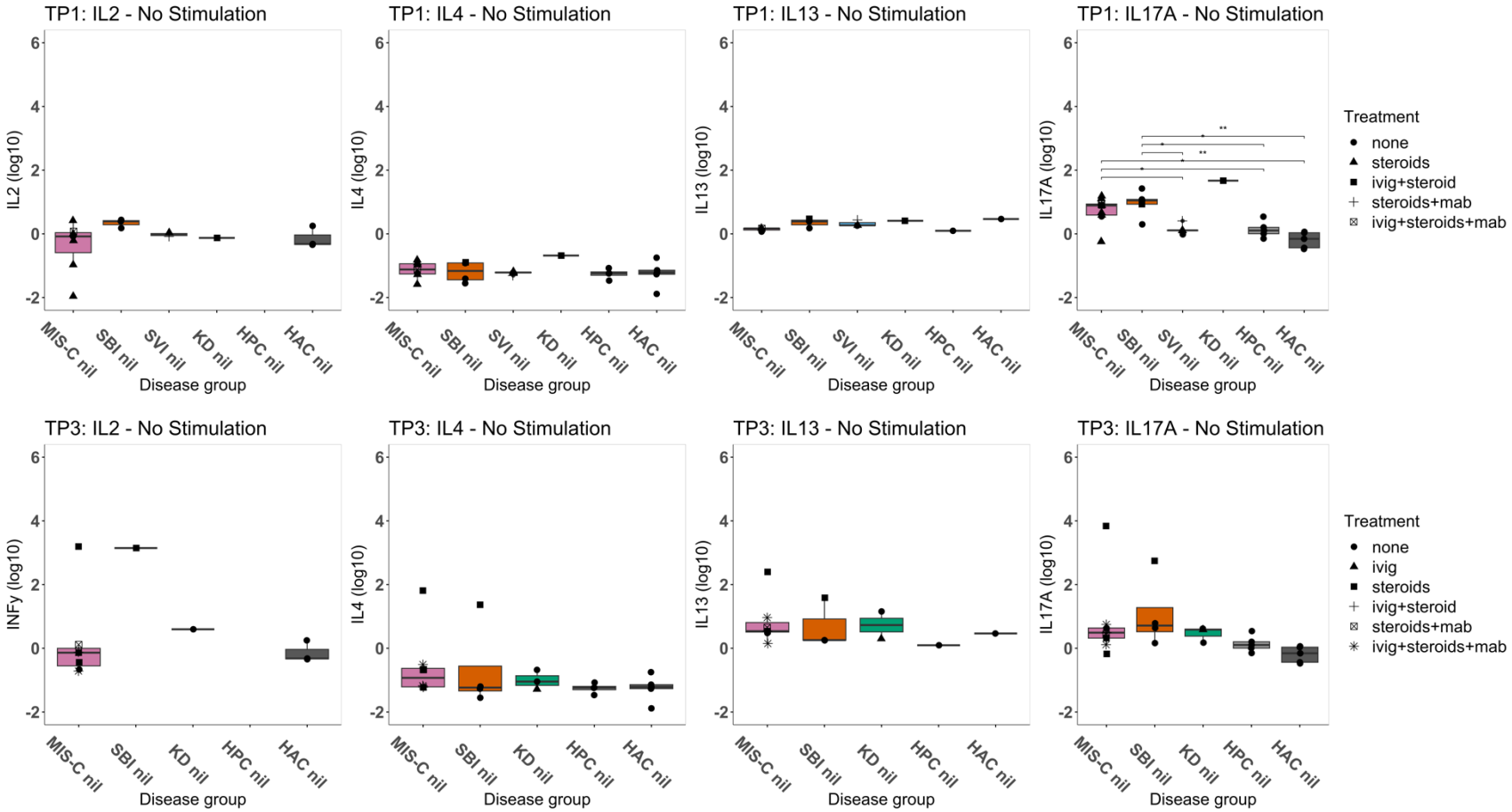

Figure 8-2 Boxplots showing the levels of IL2, IL4, IL13 and IL17A in acute (TP1) and convalescent (TP3) unstimulated (nil) samples.

Log10 transformed data are shown. Each point represents a participant for the following groups: MIS-C, severe bacterial illness (SBI), severe viral illness (SVI), Kawasaki disease (KD), other Inflammatory disease (INF). The shape of the point corresponds to the treatment received prior to blood sampling: ivig = intravenous immunoglobulin, steroid = corticosteroids, mab = monoclonal antibody. Wilcoxon pairwise comparisons with Benjamini Hochberg correction were performed; only significant p values are displayed.

8.3.2.2 Cytokine results: Stimulation with SARS-CoV-2 antigen

Stimulation with SARS-CoV-2 antigen (ag1) assesses activation of specific T cells in individuals with prior exposure to SARS-CoV-2. The percentage increase in IFNγ (Figure 8-3), IL6 (Figure 8-3), IP10 (Figure 8-3) and IL10 (Appendix 7 Figure A7-4) was significantly lower in acute MIS-C compared to HAC (all $p < 0.001$), with incomplete recovery seen in convalescent MIS-C in all three cytokines (Figure 8-3, Appendix 7 Figure A7-4). There was reduced upregulation of IFNγ and IP10 in acute SBI compared to HAC ($p = 0.0001$), with recovery in convalescence (Figure 8-3). No differences were observed between MIS-C and HAC in all other cytokines measured, including the type one and three interferons. No significant differences in the cytokine response following ag1 stimulation were observed in the febrile controls and HPC, which was expected as the majority of these children did not have previous exposure to SARS-CoV-2.

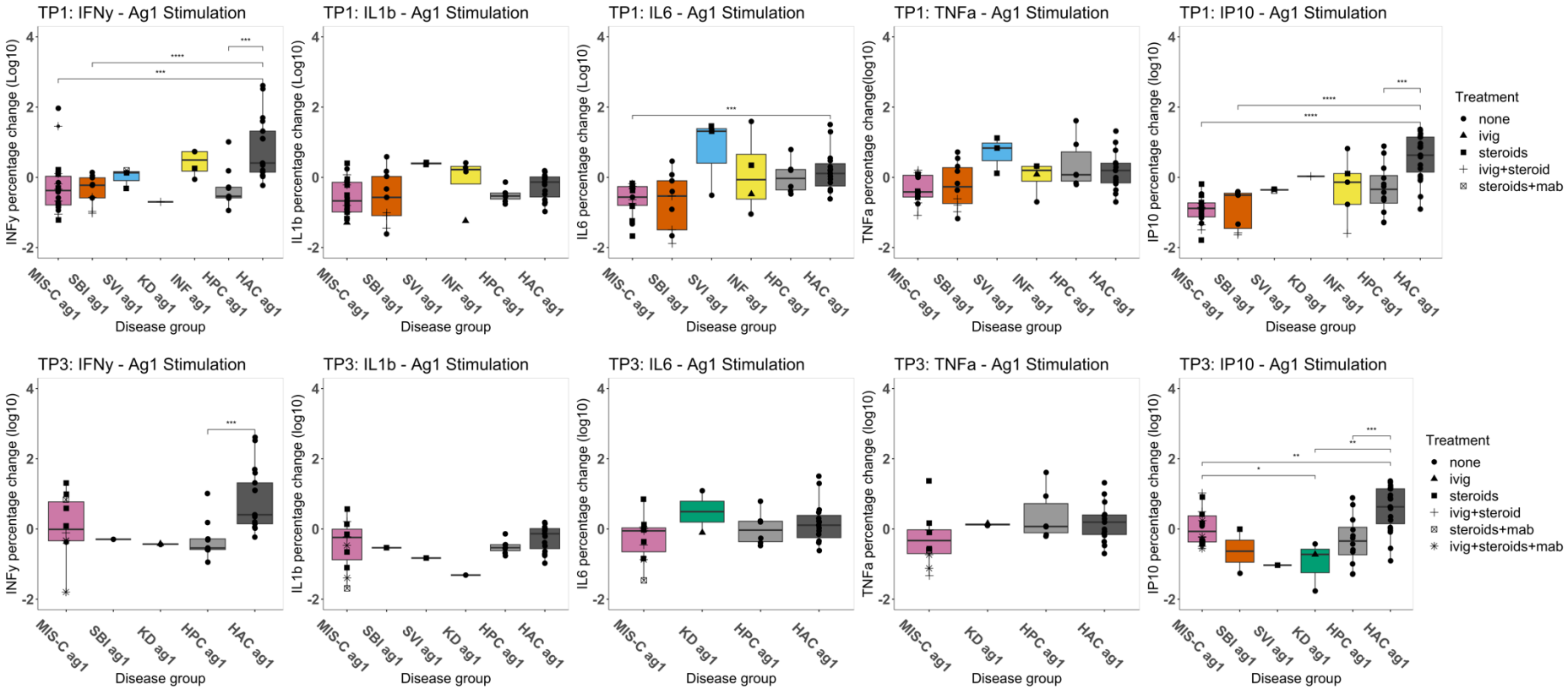

Figure 8-3 Boxplots showing the percentage change from unstimulated samples in levels of IFNγ, IL1β, IL6, TNFα and IP10 in acute (TP1) and convalescent (TP3) samples stimulated with SARS-CoV-2 antigen (ag1).

Log10 transformed data are shown. Each point represents a participant for the following groups: MIS-C, severe bacterial illness (SBI), severe viral illness (SVI), Kawasaki disease (KD), other Inflammatory disease (INF). The shape of the point corresponds to the treatment received prior to blood sampling: ivig = intravenous immunoglobulin, steroid = corticosteroids, mab = monoclonal antibody. Wilcoxon pairwise comparisons with Benjamini Hochberg correction were performed; only significant p values are displayed.

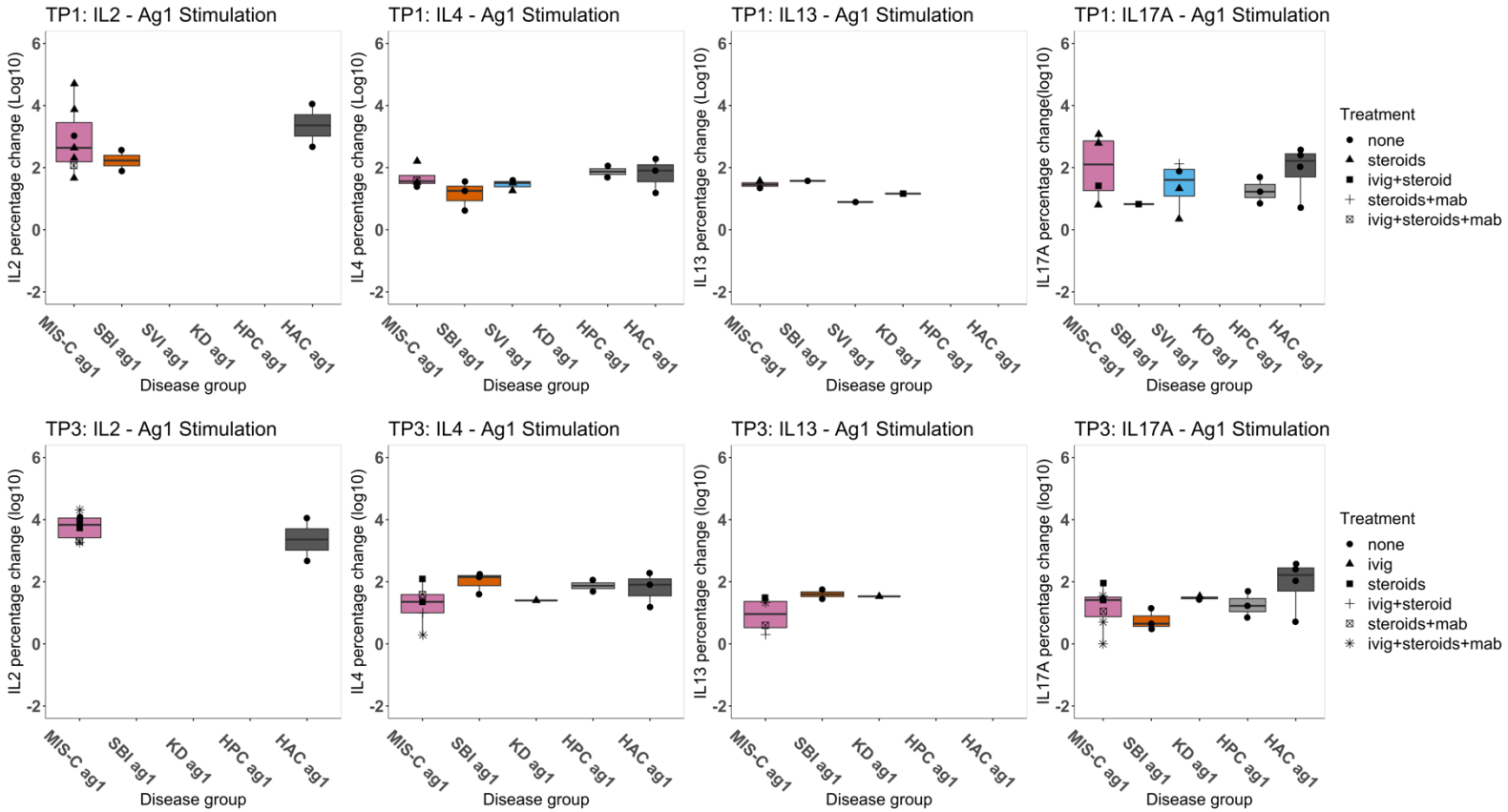

Figure 8-4 Boxplots showing the percentage change from unstimulated samples in levels of IL2, IL4, IL13 and IL17A in acute (TP1) and convalescent (TP3) samples stimulated with SARS-CoV-2 antigen (ag1).

Log10 transformed data are shown. Each point representations a participant for the following groups: MIS-C, severe bacterial illness (SBI), severe viral illness (SVI), Kawasaki disease (KD), other Inflammatory disease (INF). The shape of the point corresponds to the treatment received prior to blood sampling: ivig = intravenous immunoglobulin, steroid = corticosteroids, mab = monoclonal antibody. Wilcoxon pairwise comparison with Benjamini Hochberg correction were performed; only significant p values are displayed.

8.3.2.3 Cytokine results: Stimulation with mitogen

Following stimulation with mitogen there was reduced upregulation of multiple cytokines in acute MIS-C, acute SBI and acute SVI compared to HPC, with evidence of recovery in convalescence. IFNγ, IP10, IL17A, IL10 and GM-CSF were reduced in acute MIS-C, acute SBI and acute SVI (all $p < 0.01$) (Figure 8-5, Figure 8-6, Appendix 7 Figure A7-5). IL1β and IL6 were reduced in acute MIS-C and acute SBI compared to HPC (all $p < 0.01$) (Figure 8-5, Appendix 7 Figure A7-5). IFNα2, IFNβ and IL12p70 (all $p < 0.01$) were exclusively reduced in acute SBI (Appendix 7 Figure A7-5). TNFα, IL4, and IFNλ1 were exclusively reduced in MIS-C compared to HPC (all $p < 0.01$) (Figure 8-5, Figure 8-6, Appendix 7 Figure A7-5).

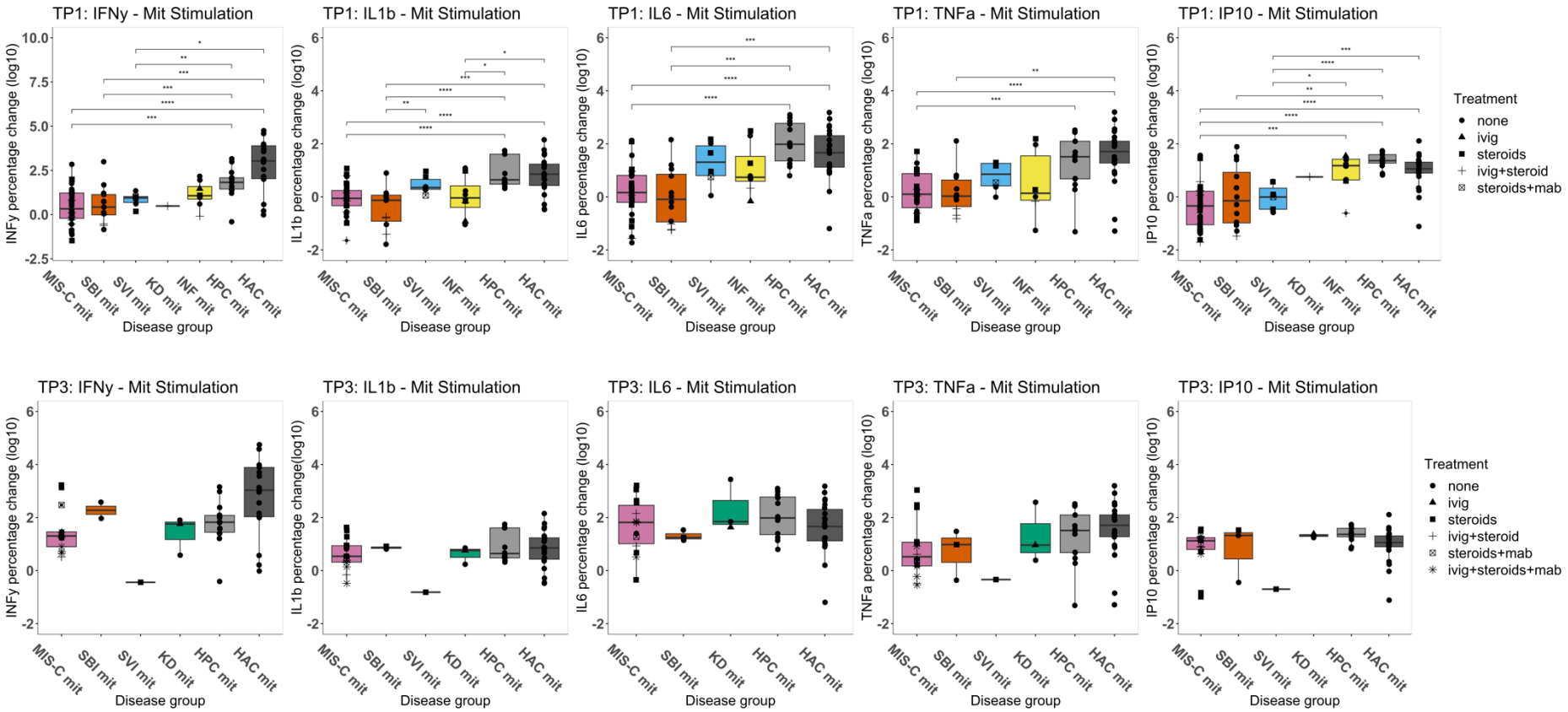

Figure 8-5 Boxplots showing the percentage change from unstimulated samples in levels of IFNγ, IL1β, IL6, TNFα and IP10 in acute (TP1) and convalescent (TP3) samples stimulated with mitogen (mit).

Log10 transformed data are shown. Each point representations a participant for the following groups: MIS-C, severe bacterial illness (SBI), severe viral illness (SVI), Kawasaki disease (KD), other Inflammatory disease (INF). The shape of the point corresponds to the treatment received prior to blood sampling: ivig = intravenous immunoglobulin, steroid = corticosteroids, mab = monoclonal antibody. Wilcoxon pairwise comparison with Benjamini Hochberg correction were performed; only significant P values are displayed.

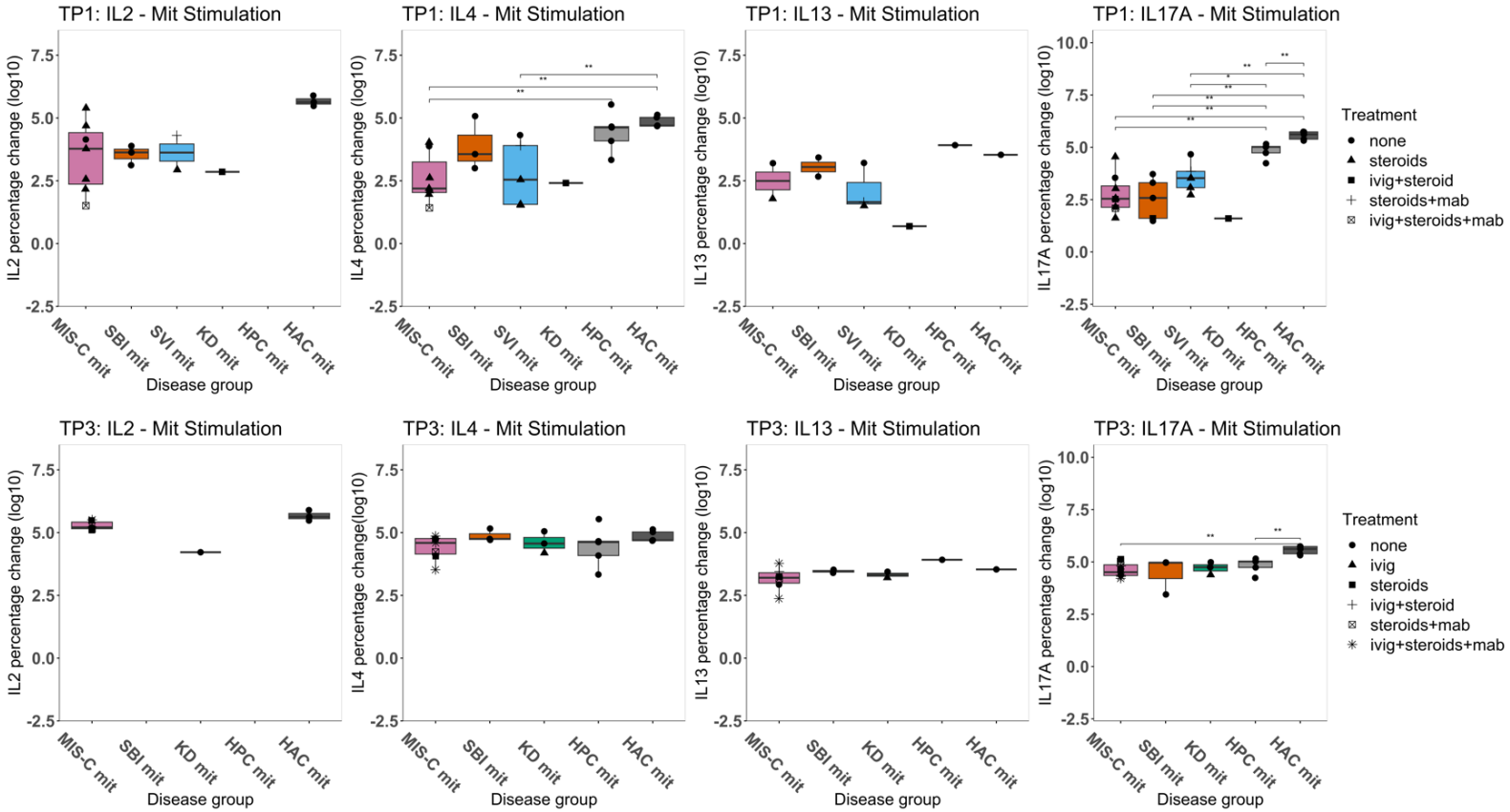

Figure 8-6 Boxplots showing the percentage change from unstimulated samples in levels of IL2, IL4, IL13 and IL17A in acute (TP1) and convalescent (TP3) samples stimulated with mitogen (mit).

Log10 transformed data are shown. Each point representations a participant for the following groups: MIS-C, severe bacterial illness (SBI), severe viral illness (SVI), Kawasaki disease (KD), other Inflammatory disease (INF). The shape of the point corresponds to the treatment received prior to blood sampling: ivig = intravenous immunoglobulin, steroid = corticosteroids, mab = monoclonal antibody. Wilcoxon pairwise comparison with Benjamini Hochberg correction were performed; only significant P values are displayed.

8.3.2.4 Summary of cytokine results

Table 8-4 is a summary gradient table of the cytokine data, which provides a visual representation of the overall trends. Unstimulated TP1 results from all disease groups show low levels of cytokines with recovery of cytokine levels at TP3, resembling the cytokine levels found in HPC. Following ag1 stimulation, HAC had the greatest percentage increase in cytokine levels. The cytokine response to ag1 is reduced in MIS-C TP1, with evidence of incomplete recovery at TP3. Of note, the response to ag1 in KD patients is high at TP1 and TP3. Finally, there is a reduced cytokine response following mitogen stimulation in all disease groups at TP1 and while there is recovery at TP3, it is incomplete, as the percentage increase in all disease groups at TP3 is lower than HPC.

Table 8-4 Summary of supernatant cytokine results from the SARS-CoV-2 QuantiFERON assay.

Median values by cohort and timepoint for unstimulated samples and percentage change from unstimulated samples following stimulation with SARS-CoV-2 antigen (ag1) and are shown. Patients with MIS-C, severe bacterial illness (SBI), Kawasaki disease (KD), severe viral illness (SVI) and other Inflammatory conditions at acute (TP1) and convalescence (TP3), as well as healthy paediatric controls (HPC) and healthy COVID-19 vaccinated adults (HAC) were included. The number of samples are indicated in the table for each result.

	Highest value
	50th Percentile
	Lowest value

	BASELINE - median results for each cohort/timepoint										
Disease group and timepoint	MIS-C - TP1	MIS-C - TP3	SBI - TP1	SBI - TP3	KD - TP1	KD - TP3	SVI - TP1	SVI - TP3	Inflammatory - TP1	HPC	HAC
IL1b	42	70	86	134	NA	158	65	8	69	54	64
IL6	103	55	164	179	NA	187	83	149	389	86	319
TNFα	24	54	35	208	NA	118	41	1	44	33	44
IP10	948	101	256	78	27	143	757	1071	190	79	167
IFNλ1	82	170	123	97	1000000	240	229	10	264	119	80
IL8	541	2384	3314	3365	7386	3359	1494	210	5469	1769	4512
IL12p70	2	8	4	4	4	4	2	0	3	3	2
IFNα2	9	16	14	14	23	34	11	4	14	11	3
IFNλ2/3	232	175	292	130	215	385	252	60	226	213	210
GMCSF	6	35	20	24	18	9	12	0	10	8	0
IFNβ	14	0	27	10	0	43	7	3	14	0	0
IL20	32	11	23	7	28	6	31	157	14	11	5
IFNγ	169	307	156	89	88	413	215	114	110	122	29
Number of samples	41	15	13	3	1	3	7	1	9	15	25
SARS-CoV-2 AG1 STIMULATION - median percentage change from baseline for each cohort/timepoint											
Disease group and timepoint	MIS-C - TP1	MIS-C - TP3	SBI - TP1	SBI - TP3	KD - TP1	KD - TP3	SVI - TP1	SVI - TP3	Inflammatory - TP1	HPC	HAC
IL1b	8%	22%	8%	-22%	NA	-9%	-22%	15%	-2%	2%	28%
IL6	-4%	35%	3%	-43%	NA	79%	5%	-25%	0%	-2%	45%
TNFα	-16%	19%	25%	-18%	NA	125%	49%	-42%	-12%	-26%	66%
IP10	0%	60%	1%	5%	107%	19%	-7%	9%	3%	26%	427%
IFNλ1	1%	-6%	5%	633305%	-100%	29%	-51%	-100%	-22%	6%	7%
IL8	51%	36%	40%	68%	97%	37%	67%	89%	21%	67%	78%
IL12p70	6%	3%	14%	6%	14%	-1%	-10%	-24%	-14%	-2%	9%
IFNα2	7%	4%	6%	-7%	14%	12%	-1%	-50%	-24%	9%	15%
IFNλ2/3	-2%	15%	6%	-25%	24%	26%	-40%	-33%	-32%	18%	10%
GMCSF	-10%	6%	14%	-31%	22%	44%	-7%	-100%	-32%	2%	32%
IFNβ	-10%	12%	-12%	28%	3771%	89%	-87%	-100%	-61%	-41%	141%
IL20	-2%	27%	7%	-23%	3%	24%	12%	-22%	-7%	-11%	56%
IFNγ	8%	47%	26%	4%	20%	36%	2%	-68%	-13%	25%	246%
Number of samples	35	15	13	3	1	3	6	1	9	14	22
MITOGEN STIMULATION - median percentage change from baseline for each cohort/timepoint											
Disease group and timepoint	MIS-C - TP1	MIS-C - TP3	SBI - TP1	SBI - TP3	KD - TP1	KD - TP3	SVI - TP1	SVI - TP3	Inflammatory - TP1	HPC	HAC
IL1b	85%	346%	17%	649%	NA	573%	210%	96%	15%	402%	692%
IL6	114%	6492%	64%	1772%	NA	7063%	911%	554%	-1%	8673%	3102%
TNFα	107%	268%	87%	959%	NA	920%	349%	85%	46%	3266%	2924%
IP10	18%	1331%	38%	2116%	568%	2172%	99%	1510%	20%	2178%	1125%
IFNλ1	7%	18%	7%	52%	-100%	220%	14%	15%	70%	83%	24%
IL8	495%	419%	142%	450%	249%	144%	620%	230%	17%	757%	355%
IL12p70	15%	27%	8%	32%	65%	145%	32%	54%	-35%	51%	211%
IFNα2	3%	36%	10%	-19%	54%	31%	20%	61%	-15%	43%	47%
IFNλ2/3	-7%	29%	1%	-10%	57%	44%	11%	9%	22%	20%	36%
GMCSF	32%	183%	24%	1561%	98%	566%	98%	122%	33%	1591%	16706%
IFNβ	13%	59%	7%	130%	9047%	1626%	360%	187%	-31%	101%	289%
IL20	24%	1342%	41%	5137%	24%	3122%	242%	104%	2%	2464%	10328%
IFNγ	139%	2025%	265%	23720%	306%	5776%	803%	1168%	36%	6683%	91444%
Number of samples	35	15	13	3	1	3	6	1	9	14	22

8.3.2.5 Cytokine results: effects of immunomodulatory treatment

Of the acute (TP1) samples, 50% were from patients who had received corticosteroids, 19% were from patients who had received IVIG and 6.5% were from patients who had received monoclonal antibodies prior to research blood sampling (Table 8-2). The results of the K-means clustering analysis of the supernatant cytokine dataset revealed 3 distinct clusters for unstimulated samples and ag1 stimulated samples and 4 clusters for mitogen stimulated samples (Figure 8-7). There were no discernible effects of immunomodulatory treatment on cytokine levels. The formed clusters were not related to treatment received, indicating that factors other than treatments received are likely to be influencing the clustering patterns observed (Figure 8-7).

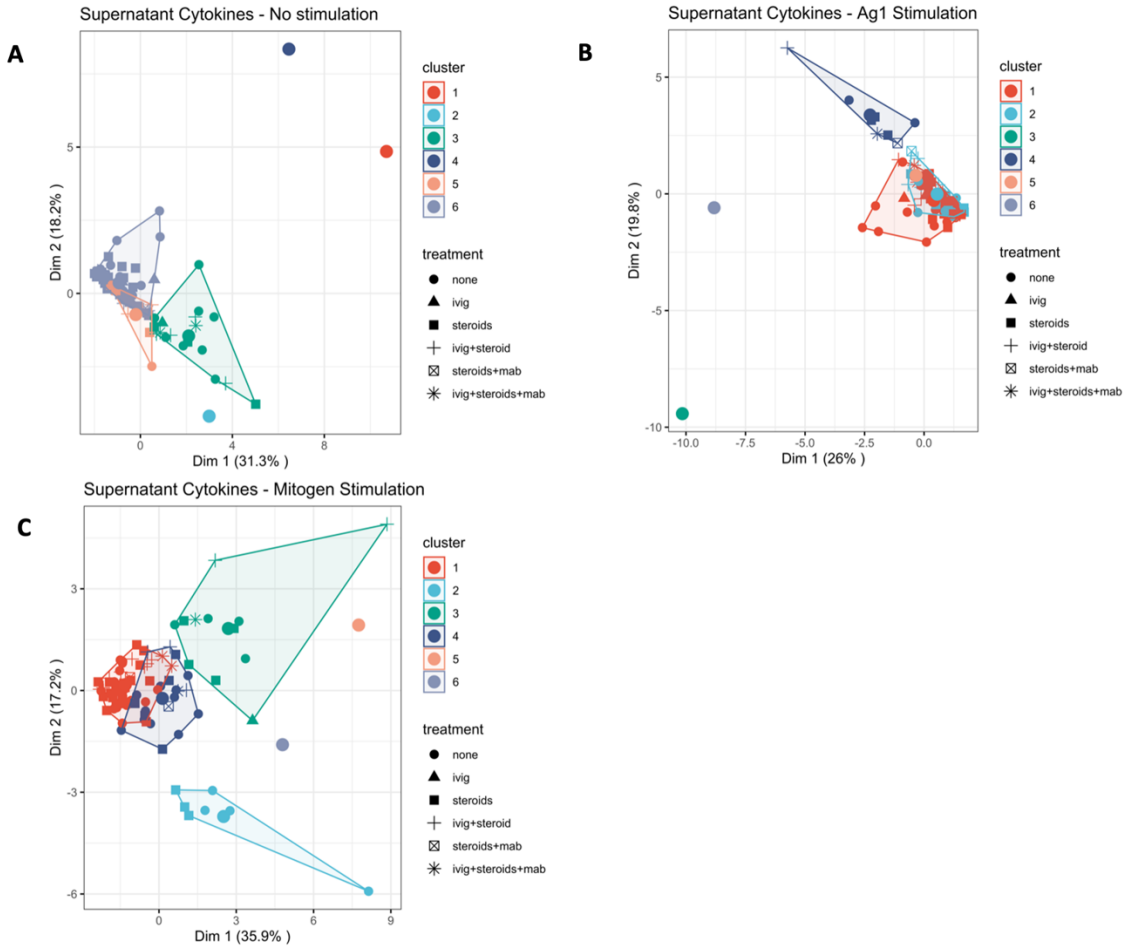

Figure 8-7 K-means clustering plot for supernatant cytokines samples with no stimulation (A), stimulation with SARS-CoV-2 antigen (Ag1) (B) and stimulation with mitogen (C).

The clusters and their respective centre points are represented by different colours. The shape of the point corresponds to the treatment received prior to blood sampling: ivig = intravenous immunoglobulin, steroid = corticosteroids, mab = monoclonal antibody.

8.3.3 Mass cytometry results

To gain further insight into the functional immunology in MIS-C, a subset of the QuantiFERON samples (nil, ag1, mit) were selected for mass cytometry, this included 42 samples from 12 children with MIS-C (TP1:24, TP3:18) and 9 samples from 3 HPC. Patients with both TP1 and TP3 samples were prioritised for selection. First, an unsupervised hierarchical analysis was conducted on variables relating to T cell immunity to provide an overview of the trends in the unstimulated (nil) and stimulated (ag1 and mit) samples. As this was an exploratory analysis, the initial results offer a descriptive characterisation of the observed trends. Next, a secondary unsupervised hierarchical analysis was conducted for assessment of the trends in fold change from unstimulated samples following stimulation with ag1 and mitogen. Subsequently, statistical comparisons of the raw data were conducted.

Unsupervised hierarchical analysis of the raw data revealed three distinct clusters: a) MIS-C TP1 nil, MIS-C TP1 ag1 and MIS-C TP1 mit b) MIS-C TP3 nil, MIS-C TP3 ag1, HPC nil and HPC ag1 c) MIS-C TP3 mit and HPC mit (Figure 8-8). Meanwhile, the analysis of the foldchange from unstimulated samples following stimulation revealed two distinct clusters: a) MIS-C TP3 mit and HPC mit b) MIS-C TP1 ag1, MIS-C TP3 ag1, HPC ag1 and MIS-C TP1 mit.

8.3.3.1 Mass cytometry results: unstimulated samples

Unstimulated MIS-C TP1 samples exhibited lower proportions of naïve effector $CD4^+$ T cells, naïve effector $CD8^+$ T cells, memory $CD4^+$ T cells and γδT cells compared to MIS-C TP3 and HPC (Figure 8-8). The proportions of T cells expressing CD279 (PD1) were comparable across the groups, except for MIS-C TP1 exhibiting increased proportions of memory $CD8^+$ T cells expressing CD279. MIS-C TP1 also displayed increased proportions of memory $CD8^+$ T cells, memory Tregs and γδT cells expressing CD95, compared to MIS-C TP3 and HPC. The proportions of T cells expressing CD152 (CTLA4) and IL6 were greatest in HPC (Figure 8-8). IL2 expressing T cells and TNFα expressing memory $CD8^+$ T cells were increased in MIS-C TP1 compared to MIS-C TP3 and HPC. Conversely, IFNγ expressing T cells were greatest in MIS-C TP3, followed by MIS-C TP1 and HPC - with the exception of proportions of IFNγ expressing memory $CD8^+$ T cells, which were highest in MIS-C TP1 (Figure 8-8).

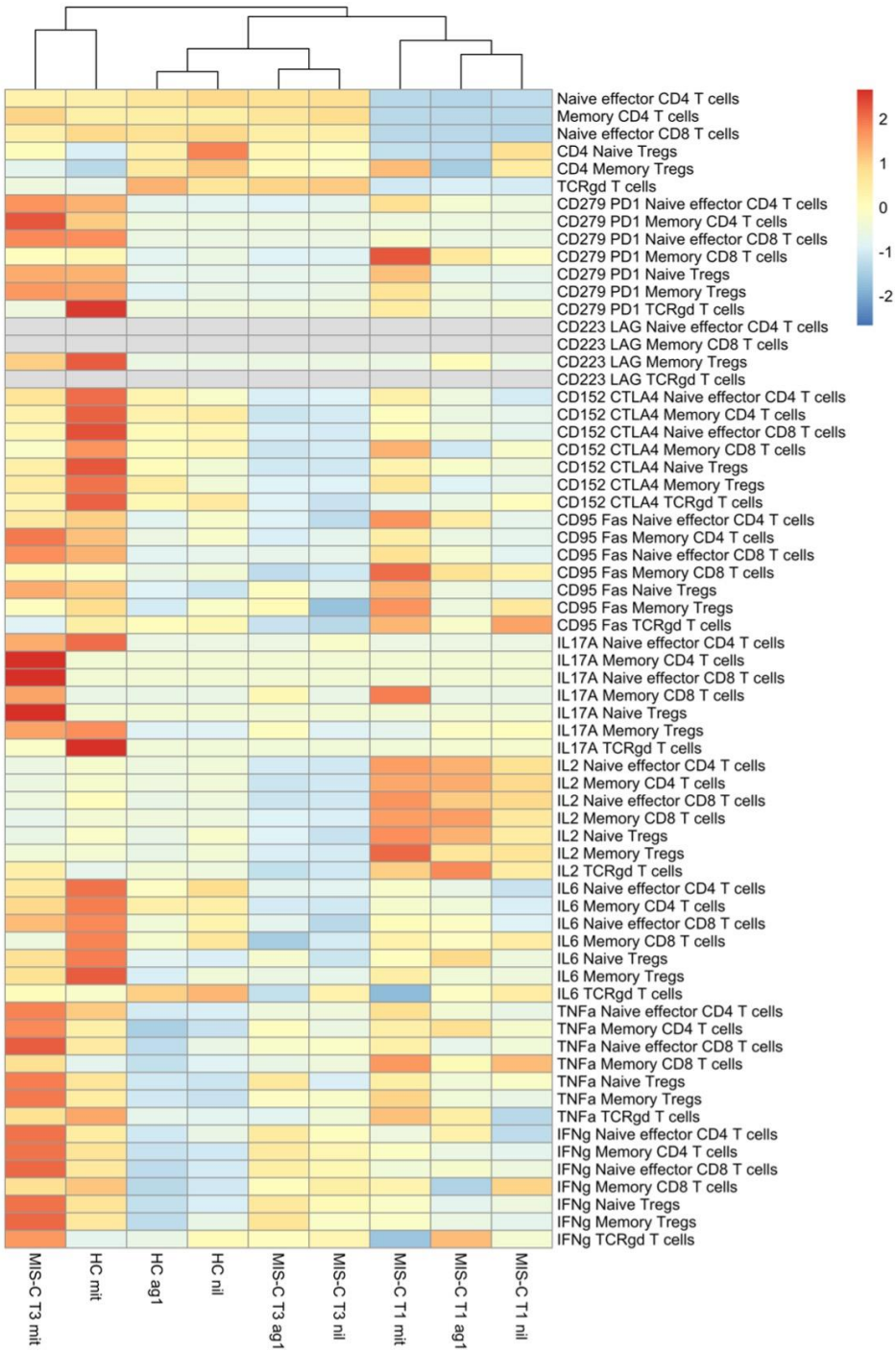

Figure 8-8 Heatmap of the mass cytometry results for QuantiFERON samples – median raw data by group has been displayed.

Variables associated with T cell immunity are summarised using an unsupervised hierarchical clustering model with group (disease group, timepoint, stimulation) plotted on the x axis. Patients with MIS-C at timepoints 1 and 3 (MIS-C TP1 n = 8, MIS-C TP3, n = 6) and healthy paediatric controls (HC, n = 3) were included. Three stimulation states are shown, no stimulation = "nil", stimulation with SARS-CoV-2 antigen = "ag1" and stimulation with mitogen (phytohemagglutinin) = "mit".

8.3.3.2 Mass cytometry results: stimulation with SARS-CoV-2 antigen

Evaluation of the fold change from unstimulated samples for samples stimulated with ag1 (Figure 8-9), showed a greater upregulation in proportions of T cells in MIS-C TP1 and MIS-C TP3 compared to HPC (Figure 8-9). The increase in CD152 and CD95 expressing naïve effector $CD4^+$ T cells, naïve effector $CD8^+$ T cells and $CD4^+$ memory T cells was highest in MIS-C TP1 compared to MIS-C TP3 and HPC. There was a trend of increased proportion of T cells expressing IL2 and reduced proportion of T cells expressing IL6 and TNFα in MIS-C TP1, compared to MIS-C TP3 and HPC (Figure 8-9).

8.3.3.3 Mass cytometry results: stimulation with mitogen

Evaluation of the fold change from unstimulated samples for samples stimulated with mitogen showed an overall greater response in HPC and MIS-C TP3, compared to MIS-C TP1 (Figure 8-9). MIS-C TP3 showed a greater increase in proportions of T cells compared to MIS-C TP1 and HPC (Figure 8-9). T cells expressing CD279, CD152, CD95 and intracellular cytokine expression (IFNγ, IL6, TNFα) on T cells, was highest in HPC, followed by MIS-C TP3 and MIS-C TP1 (Figure 8-9).

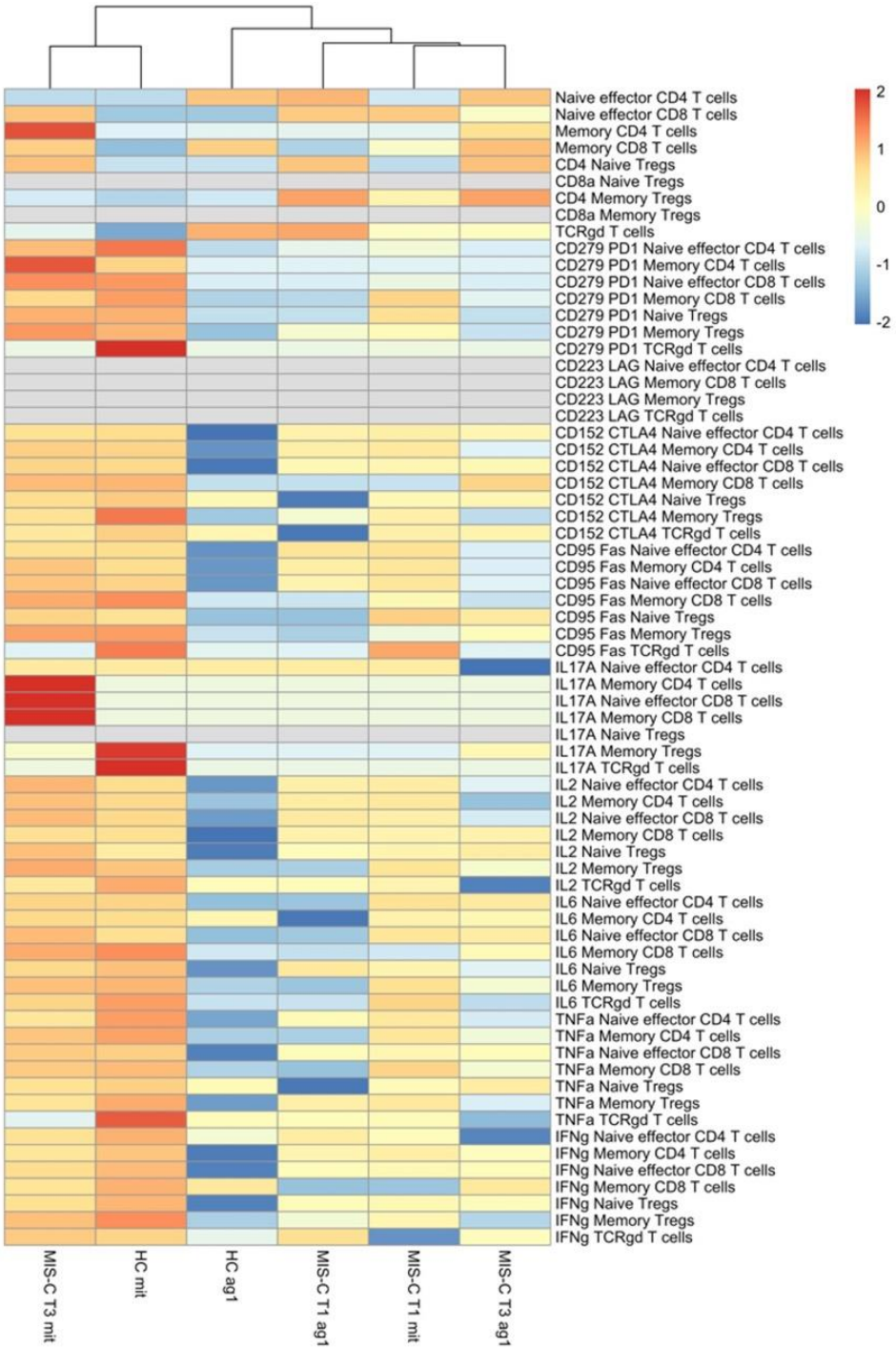

Figure 8-9 Heatmap of the mass cytometry results for QuantiFERON samples – median foldchange by group has been displayed.

Variables associated with T cell immunity are summarised using an unsupervised hierarchical clustering model with group (disease group, timepoint, stimulation) plotted on the x axis. Patients with MIS-C at timepoints 1 and 3 (MIS-C TP1 n = 8, MIS-C TP3, n = 6) and healthy paediatric controls (HC, n = 3) were included. Two stimulation states are shown, stimulation with SARS-CoV-2 antigen = "ag1" and stimulation with mitogen (phytohemagglutinin) = "mit".

8.3.3.4 Mass cytometry results: pairwise comparisons

A small number of significant results were found following pairwise comparisons of variables related to T cell immunity (Table 8-5). The majority of the findings pertain to trends in the unstimulated samples described above, with significantly reduced naïve effector $CD4^+$ T cells, naïve effector $CD8^+$ T cells and memory $CD4^+$ T cells in MIS-C TP1 compared to MIS-C TP3 and HPC (all adjusted p values < 0.05). Following ag1 stimulation, there were significantly reduced TNFα expressing naïve Tregs in MIS-C TP1 compared to MIS-C TP3 (p = 0.01). After mitogen stimulation, the proportions of naïve effector $CD4^+$ T cells were significantly lower in MIS-C TP1 compared to HPC (p = 0.04).

Table 8-5 Targeted analyses of mass cytometry results of samples following SARS-CoV-2 QuantiFERON assay.

Significant results from Wilcoxon pairwise comparisons for variables relating to T cell immune response are shown with unadjusted and Benjamini Hochberg adjusted p values. Patients with MIS-C at timepoints 1 and 3 (MIS-C TP1 n = 8, MIS-C TP3, n = 6) and healthy paediatric controls (HPC, n = 3) were included in the analyses. Three stimulation states are shown, Nil = no stimulation, Ag1 = stimulation with SARS-CoV-2 antigens and Mit = stimulation with mitogen. Cells have been highlighted by direction of change.

Stimulation status	Variable	Group 1	Group 2	Direction	P value	Adjusted P value
Nil	Naïve effector $CD4^+$ T cells	HPC	MIS-C TP1	↑ Group 1	0.016	0.024
Nil	Naïve effector $CD4^+$ T cells	MIS-C TP1	MIS-C TP3	↓ Group 1	0.006	0.017
Nil	Memory $CD4^+$ T cells	HPC	MIS-C TP1	↑ Group 1	0.009	0.014
Nil	Memory $CD4^+$ T cells	MIS-C TP1	MIS-C TP3	↓ Group 1	0.008	0.014
Nil	Naïve effector $CD8^+$ T cells	HPC	MIS-C TP1	↑ Group 1	0.009	0.014
Nil	Naïve effector $CD8^+$ T cells	MIS-C TP1	MIS-C TP3	↓ Group 1	0.003	0.008
Ag1	TNFα Naïve Tregs	MIS-C TP1	MIS-C TP3	↓ Group 1	0.005	0.014
Mit	Naïve effector $CD4^+$ T cells	HPC	MIS-C TP1	↑ Group 1	0.012	0.036

8.3.3.5 Mass cytometry results: effects of immunomodulatory treatment

PCA was conducted to evaluate the effect of immunomodulatory treatment on the mass cytometry results. Of the TP1 samples, 62.5% (15/24) were from patients who had received corticosteroids, 12.5% (3/24) were from patients who had received IVIG and 12.5% (3/24) were from patients who had received monoclonal antibodies prior to blood sampling. The PCA did not reveal any discernible treatment effects in this dataset as evidenced by absence of differentiation by treatment groups (Figure 8-10).

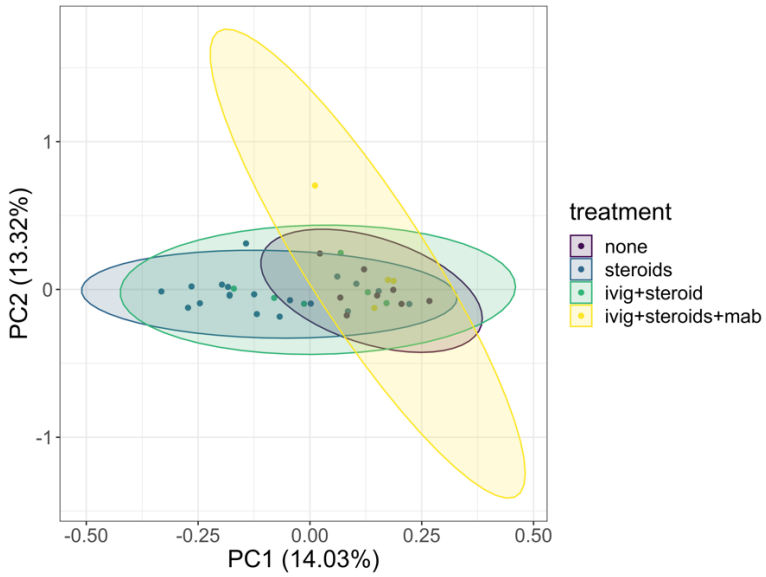

Figure 8-10 Principal component analysis of the mass cytometry samples from the unstimulated SARS-CoV-2 QuantiFERON assay showing principal components one (PC1) and principal components two (PC2).

The data points have been coloured by treatment received prior to research blood sampling. IVIG = intravenous immunoglobulin, mab = monoclonal antibody.

8.3.3.6 Mass cytometry results: effects of incubation

To assess the effect of incubation on mass cytometry results, PCA was conducted on mass cytometry results from the unstimulated (nil) samples from SARS-CoV-2 QuantiFERON assay and blood samples from the same individuals which were not subjected to incubation. The PCA revealed distinct separation between incubated and unincubated samples (Figure 8-11). Unsupervised hierarchical clustering provided further insights into the differences between the incubated and unincubated mass cytometry samples. The heatmap in Figure 8-12 displays the general trend of reduced cell proportion and expression markers in the incubated samples compared to the unincubated samples, with a few exceptions. The statistically significant results from the pairwise comparisons are shown in Table 8-6. There were reduced proportions of naïve and memory $CD4^+$ T

regs, IL6 expressing memory $CD4^+$ T cells and memory Tregs and CD95 expressing T cells in the MIS-C TP1 incubated samples compared to the unincubated samples (all $p < 0.05$) (Table 8-6). Similarly, the MIS-C TP3 incubated samples exhibited reduced proportions of naïve and memory $CD4^+$ T regs along with reduced CD95 expressing T cells (all $p \leq 0.02$) (Table 8-6). Conversely, the proportions of IFNγ expressing naïve effector $CD4^+$ and $CD8^+$ T cells were higher in the MIS-C TP3 incubated samples compared to unincubated samples. No significant differences were seen in the incubated and unincubated healthy control samples (Table 8-6).

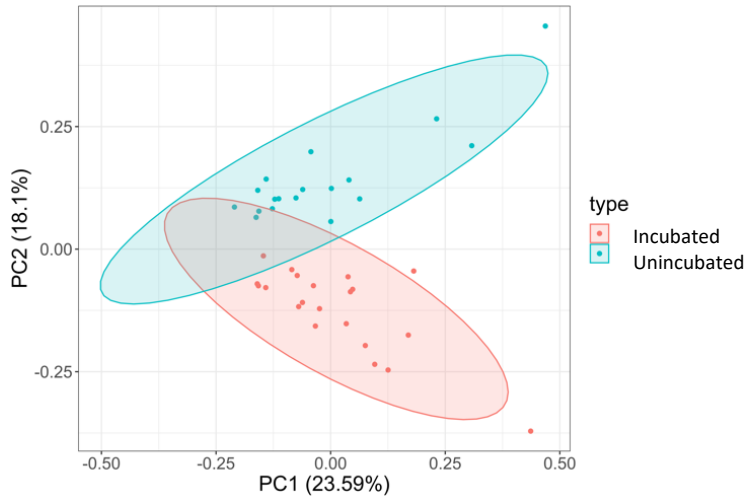

Figure 8-11 Principal component analysis showing principal component one (PC1) and principal component two (PC2) of the mass cytometry results from the unstimulated SARS-CoV-2 QuantiFERON assay (incubated samples) and mass cytometry results from whole blood samples (unincubated samples) from the same individuals.

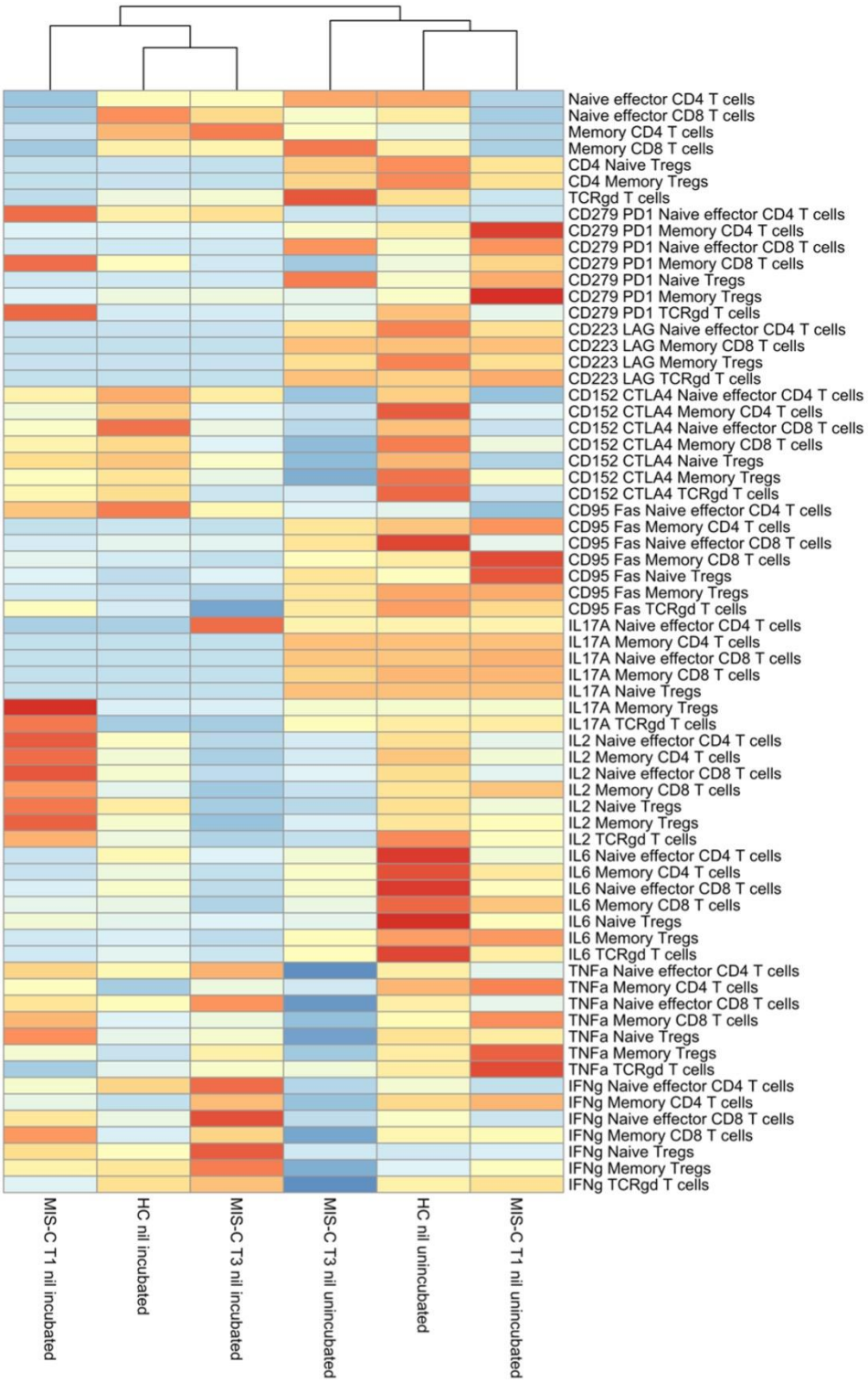

Figure 8-12 Heatmap of mass cytometry results from incubated and unincubated samples.

The heat map summarises variables associated with T cell immunity using an unsupervised hierarchical clustering model with cohort (disease group, timepoint, incubation status) plotted on the x axis. Raw median values for each cohort are displayed. HC = healthy paediatric controls, nil = no stimulation.

Variable	Direction	Adjusted P value
MIS-C TP1		
CD152/CTLA4 Naïve effector CD4 T cells	↑ incubated vs unincubated	0.04
CD4 Naïve Tregs	↓ incubated vs unincubated	0.02
CD4 Memory Tregs	↓ incubated vs unincubated	<0.001
CD279/PD1 Naïve effector CD4 T cells	↓ incubated vs unincubated	0.01
CD95/Fas Naïve effector CD4 T cells	↓ incubated vs unincubated	0.02
CD95/Fas Memory CD4 T cells	↓ incubated vs unincubated	<0.001
CD95/Fas Naïve Tregs	↓ incubated vs unincubated	0.02
CD95/Fas Memory Tregs	↓ incubated vs unincubated	0.02
IL6 Memory CD4 T cells	↓ incubated vs unincubated	<0.01
IL6 Memory Tregs	↓ incubated vs unincubated	0.04
MIS-C TP3		
CD279/PD1 Naïve effector CD4 T cells	↑ incubated vs unincubated	0.03
IFNγ Naïve effector CD4 T cells	↑ incubated vs unincubated	0.02
IFNγ Naïve effector CD8 T cells	↑ incubated vs unincubated	0.05
CD4 Naïve Tregs	↓ incubated vs unincubated	0.02
CD4 Memory Tregs	↓ incubated vs unincubated	0.01
CD95/Fas Memory CD4 T cells	↓ incubated vs unincubated	0.01
CD95/Fas Naïve Tregs	↓ incubated vs unincubated	0.02
CD95/Fas Memory Tregs	↓ incubated vs unincubated	0.02
HC		
Nil significant		

Table 8-6 Wilcoxon pairwise comparisons of mass cytometry results from incubated and unincubated unstimulated samples.

Only significant results following Benjamini Hochberg correction are shown. HC = healthy paediatric controls. Cells have been highlighted by direction of change.

8.3.4 RNA-seq results

Targeted analyses of genes relating to IFNγ, IL2 and T cell inhibition, exhaustion, and apoptosis, were conducted to further explore the role of dysregulated T cell immunity in MIS-C. The results of the whole blood RNA-seq analyses are shown in Figure 8-13 and Figure 8-14. It was not possible to analyse the IFNγ and IL2 genes due to insufficient gene counts, therefore only their associated receptors were analysed. Children with MIS-C and bacterial illness had significantly higher expression of IFNγ receptor 1 (IFNGR1) and IFNγ receptor 2 (IFNGR2) genes, compared to children with viral illness, KD and HPC (all $p < 0.05$) (Figure 8-13). The expression of IL2 receptor alpha (IL2RA) and IL2 receptor gamma (IL2RG) genes were significantly higher in MIS-C compared to bacterial illness, viral illness, KD and HPC (all $p < 0.02$) (Figure 8-13). On the contrary, the expression of IL2 receptor beta (IL2RB) was significantly lower in MIS-C and bacterial illness compared to viral illness, KD and HPC (all $p < 0.02$) (Figure 8-13).

In general, there was increased expression of T cell apoptosis, exhaustion, and inhibition related genes in MIS-C compared to other febrile disease and healthy controls (Figure 8-14). Interaction of CD95 (FAS) with CD172 (FASL), along with the presence of FADD (which mediates apoptotic signals) and activation of Caspase 8, is necessary for the induction of apoptosis[452]. The expression of CD95 (FAS) was raised in MIS-C compared to viral illness and HC, while CD172 (FASL) expression was reduced in MIS-C compared to viral illness and HC (all $p < 0.01$) (Figure 8-14). Additionally, the expression of FADD and CASP8 was increased in MIS-C compared to febrile controls and HC (all $p < 0.05$) (Figure 8-14). Children with MIS-C had significantly higher expression of the CD152 (CTLA4) (all $p < 0.05$) (Figure 8-14), which encodes a protein that has inhibitory effects on T cells, compared to children with bacterial illness, KD, and HC. Intriguingly, CD223 (LAG3), a marker of T cell exhaustion, was found to be reduced in MIS-C compared to viral illness ($p = 0.0009$) (Figure 8-14). The interaction of CD279 (PD-1) with its ligands (CD274 and CD273) can suppress T cell activity while chronic expression of CD279 (PD-1) on T cells is associated with T cell exhaustion[453]. The expression of CD279 (PD-1) was raised in MIS-C compared to bacterial illness and KD, and CD274 (PDL1) expression was higher in MIS-C compared to viral illness and HC (all $p < 0.01$) (Figure 8-14). Additionally, CD273 (PDL2) expression was raised in MIS-C compared to bacterial illness, viral illness, and HC (all $p < 0.01$) (Figure 8-14).

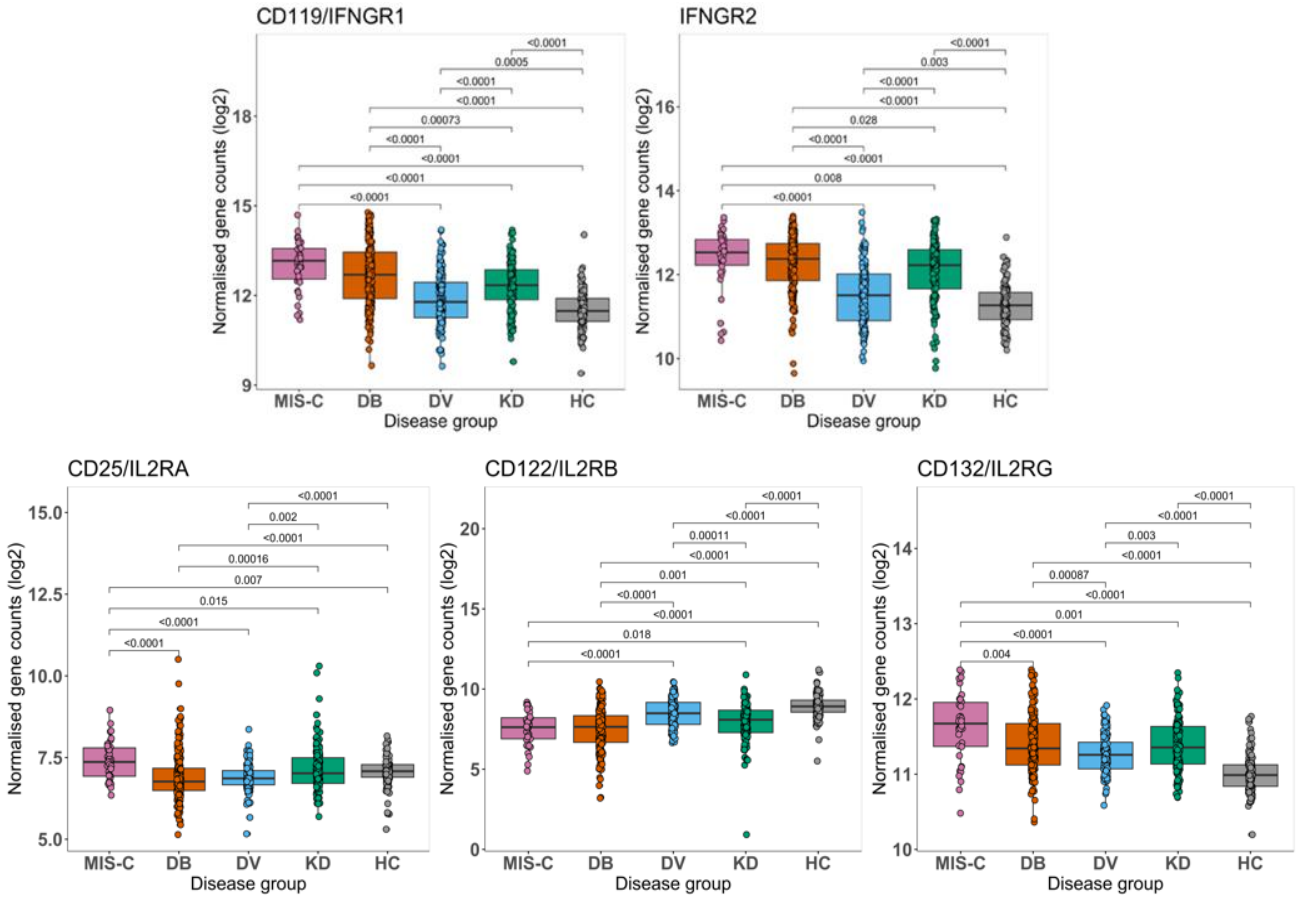

Figure 8-13 Boxplots showing normalised gene counts (log2) for IFNγ and IL2 receptors by disease groups

Wilcoxon pairwise comparisons with Benjamini Hochberg correction were conducted; only significant P values are displayed. IFNGR1/2 = interferon gamma receptor one/two, IL2RA/B/G = interleukin receptor alpha/beta/gamma. DB = definite bacterial, DV = definite viral, KD = Kawasaki disease, HC = healthy paediatric controls.

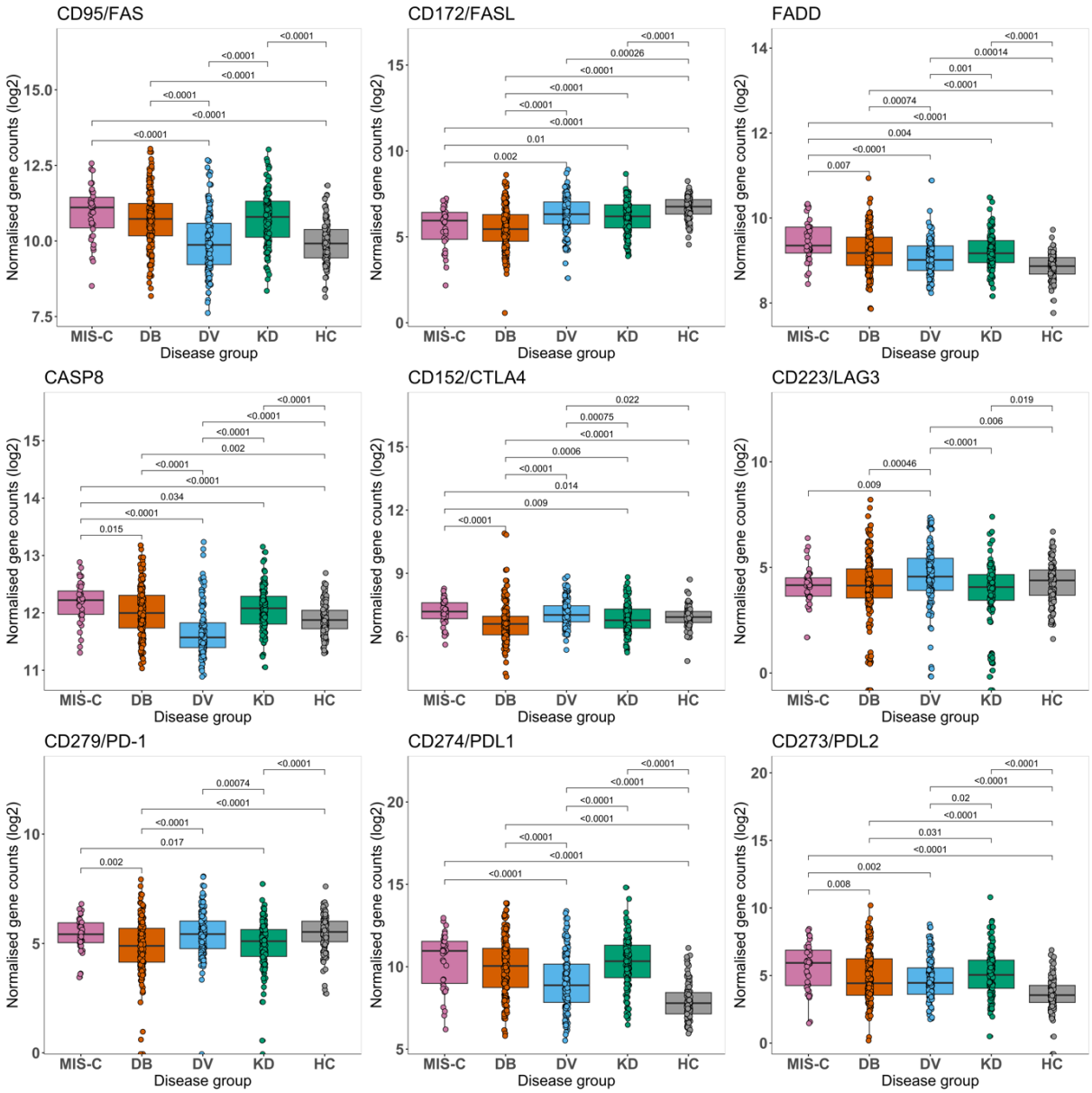

Figure 8-14 Boxplots showing normalised gene counts (log2) by disease groups for genes associated with T cell exhaustion: Cluster of Differentiation (CD)152, CD95, CD172, CD279, CD274, CD273 and CD223.

Wilcoxon pairwise comparisons with Benjamini Hochberg correction were performed; only significant p values are displayed. MIS-C = Multisystem inflammatory syndrome in children, DB = definite bacterial, DV = definite viral, KD = Kawasaki disease, HC = healthy paediatric controls.

8.4 Discussion

The work presented in this chapter used multiple methodologies including *ex vivo* whole blood stimulation experiment and cytokine measurement, mass cytometry and RNA-seq data to gain further insights into the role of T cell-mediated immunopathology in MIS-C. Additionally, comparison of MIS-C with other febrile conditions including bacterial illness, viral illness, KD, other Inflammatory diseases, and healthy controls enabled identification of immunopathological features that are specific to MIS-C and those that are common among paediatric febrile illness. The ensuing discussion will cover the following key themes that have emerged from the results including: a dysregulated cytokine response in acute MIS-C, a dysregulated T cell response in acute MIS-C, reduced SARS-CoV-2 antigen specific response in acute MIS-C, evidence for T cell exhaustion in acute MIS-C and evidence supporting the molecular "off-switch" hypothesis in acute paediatric febrile illness.

The analysis of the unstimulated supernatant cytokine response showed a distinct cytokine profile in acute MIS-C, with elevated levels of IL17A, IL10 and IP10 which have been previously reported[163,280,281,283,287,288,454–456]. IL17A is proinflammatory cytokine secreted by lymphocytes and innate immune cells, which promotes local production of chemokines. This in turn leads to recruitment of myeloid cells to sites of inflammation[457–459], potentially contributing to the tissue damage and inflammation in MIS-C. Elevated levels of IL10, on the other hand, suggest a compensatory mechanism to counterbalance the pro-inflammatory response in acute MIS-C. IP10 is a chemoattractant for activated T cells[460] and its elevated levels suggest increased T cell migration and inflammation in acute MIS-C. Moreover, the production of IP10 is induced by raised IFNγ levels which suggests that acute MIS-C is associated with an upregulated IFNγ response. Although elevated levels of IFNγ were not seen in this acute MIS-C cohort, previous studies have reported high levels of IFNγ along with other proinflammatory cytokines including, IL6, IL8 and TNFα in acute MIS-C[280,281,283,455]. The discrepancy in these cytokine results (IFNγ, IL6, IL8 and TNFα) could be due to degradation of cytokines during incubation for the QuantiFERON assay prior to cytokine measurement. Moreover, considering that 50% of samples were obtained from patients treated with corticosteroids prior to blood sampling, it could be construed that the cytokine results were affected by immunomodulatory treatment. However, the results of the K-means clustering analyses indicated that treatment effects are unlikely to be the sole explanation (Figure 8-7). In addition, correcting for age and sex in the data analysis could enhance the interpretation and reliability of the results, as these factors are known to influence the immune response[427,461–463]. It is also important to acknowledge that inconsistencies exist in the reported cytokine profiles of MIS-C across published studies. This may be due to the small

numbers of patients with MIS-C, inclusion of different comparator groups and differences in timing of sample collection in these studies. Therefore, multi-centre studies with larger numbers and inclusion of paediatric COVID-19, febrile paediatric controls and healthy paediatric controls, are needed to enhance the understanding of the cytokine response in MIS-C.

The RNA-seq analysis offered additional insights into the IFNγ response in MIS-C. Although it was not possible to analyse the expression levels of the IFNγ gene due to low gene counts, analysis of the IFNγ receptor genes (IFNGR1 and IFNGR2) revealed increased expression in MIS-C and bacterial illness compared to viral illness, KD and healthy paediatric controls. As well as inducing anti-viral genes[15], IFNγ also influences genes which modulate the innate and adaptive immune response and has been shown to play a vital role in the host response to bacterial illness[464]. Therefore, in the context of MIS-C and bacterial illness, increased expression of IFNγ receptor genes could be suggestive of an intensified, dysregulated or prolonged IFNγ response resulting in excessive inflammation associated with severe MIS-C and bacterial illness. Further research is necessary to fully understand the mechanisms underlying the observed dysregulated IFNγ response.

Lymphopenia is a prominent feature of MIS-C and has been widely reported in clinical[196,197,202,405] and immunophenotyping studies[252,295,465]. The mass cytometry data provides further support for this observation with reduced proportions of naïve effector $CD4^+$ T cells, naïve effector $CD8^+$ T cells, memory $CD4^+$ cells and γδT cells observed in MIS-C TP1 compared to HPC and MIS-C TP3 unstimulated samples. The mechanisms contributing to T cell lymphopenia in MIS-C are yet to be determined and possible explanations include excessive lymphocyte activation and migration to affected tissues and increased lymphocyte apoptosis or cell death[283].

Despite the overall low number of T cells in MIS-C TP1, there were increased proportions of IL2 expressing T cells (involved in T cell activation and proliferation) compared to MIS-C TP3 and HPC, indicating a higher degree of T cell activation and potential proliferation in acute MIS-C. The combination of lymphopenia and activated T cells is not uncommon and has been described in other viral infections[466], autoimmune and immunodeficiency disorders[467,468]. This indicates that the immune system that is actively engaged, leading to T cell activation, despite overall low proportions of T cells in the circulation.

The findings of lymphopenia and increased T cell activation on mass cytometry are consistent with the results of the RNA-seq analysis showing increased expression of IL2 receptor genes (IL2RA and IL2RG),

suggesting enhanced IL2 signalling. The mass cytometry findings also displayed reduced proportions of CD152 (CTLA4, a negative regulatory of T cell activation) expressing T cells in MIS-C TP1 compared to HPC, however, the RNA-seq data showed increased expression of the CD152 gene in MIS-C compared to HPC. This could be due to several reasons including: expression of CD152 in other cells other than T lymphocytes, a possible dysregulation in the pathway, a compensatory mechanism or complex regulatory mechanism involving factors beyond the expression of CD152 e.g., post-transcriptional modifications. Collectively, these findings illustrate an altered T cell response in MIS-C, which is characterised by lymphopenia, enhanced T cell activation and potential dysregulation of negative regulatory pathways.

Evaluation of cytokines following SARS-CoV-2 antigen stimulation showed reduced upregulation of IFNγ, IP10 and IL10 levels in acute MIS-C compared to healthy COVID-19 vaccinated adults with prior exposure to SARS-CoV-2. This was restored in convalescent MIS-C, where cytokine levels were similar to that of healthy COVID-19 vaccinated adults. While the impact of lymphopenia on the results was not formally adjusted for, additional analysis (Appendix 7, Figure A7-6) revealed no correlation between lymphocyte count and cytokine levels following antigen stimulation. This suggests that lymphopenia alone is not influencing the reduced cytokine response observed in acute MIS-C. Consequently, exploration of factors such as T cell exhaustion and apoptosis in the pathophysiology of MIS-C became crucial for understanding the impaired SARS-CoV-2 antigen specific immune response in acute MIS-C, despite prior exposure to the virus. T cell exhaustion has been observed in chronic infections[469], cancer[470] and sepsis[471], and is characterised by loss of effector functions due to prolonged exposure to inflammatory signals and persistent antigen stimulation[472]. T cell apoptosis, or programmed cell death, is an important regulatory mechanism to maintain immune homeostasis which can also occur following T cell exhaustion[473]. The mass cytometry findings did not provide strong evidence for T cell exhaustion and apoptosis, however, there were a few notable observations suggesting potential involvement, including increased proportion of CD95 (FAS) expressing memory $CD8^+$ T cells, memory Tregs and memory γδT cells in MIS-C TP1 unstimulated samples. Moreover, there were increased proportions of CD279 (PD-1) expressing memory $CD8^+$ T cells in MIS-C TP1 unstimulated samples. The RNA-seq data provided complimentary evidence with increased expression of markers associated with T cell inhibition (CD152/CTLA4), T cell apoptosis (FAS, FADD, CASP8) and T cell exhaustion (PD-1) in MIS-C compared to paediatric febrile and healthy controls. These findings support the involvement of T cell exhaustion and apoptosis in the immunopathology of MIS-C. Furthermore, the persistence of SARS-CoV-2 antigens in the GI tract, as demonstrated by Yonker et al.[474], provides a potential mechanism for chronic antigen stimulation driving T cell dysfunction and

exhaustion in MIS-C. The role of T cell exhaustion and possible mechanisms requires further investigation as it holds implications for the management of MIS-C. If T cell exhaustion is indeed driving the inflammation in MIS-C, there is potential for the use of PD-1 inhibitors, as evidenced in certain infections[475] and cancers[476]. Alternatively, it is important to consider whether T cell exhaustion is a consequence of the MIS-C disease process, presenting limited intervention opportunities, or if it precedes the onset of MIS-C, offering potential reversibility.

Ex vivo stimulation of whole blood with mitogen (phytohemagglutinin, a non-specific T cell stimulant) failed to result in an upregulation of pro-inflammatory cytokines (IFNγ, IL1β, IL6, TNFα, IP10, GM-CSF) in acute MIS-C, bacterial illness, and viral illness, with recovery in convalescence. These findings are congruent with similar studies in paediatric sepsis, showing failure of innate cells and adaptive cells to produce cytokines following *ex vivo* stimulation[477]. The hypo-responsiveness of immune cells to further stimulation has been hypothesised to represent a counter-regulatory mechanism, a molecular "off-switch", against high levels of systemic inflammation. This appears to be shared response in acute MIS-C, bacterial illness and viral illness and requires further rigorous investigation.

This work has some limitations. MIS-C encompasses a spectrum of disease severity and clinical presentations, which could introduce variability in the immune dysregulation trends observed. To limit this variation, only children with severe MIS-C were included. However, inclusion of different MIS-C clinical phenotypes and analysis of results stratified by phenotype may provide a more complete understanding. Furthermore, children were only recruited from two central London hospitals, which may limit the generalisability of the findings to populations from other cities and countries. Therefore, further studies involving diverse cohorts from multiple countries are needed to validate findings and draw more comprehensive conclusions.

The QuantiFERON assay offers several advantages, including an optimised and standardised protocol that is user-friendly and efficient. These characteristics were especially valuable when there was an urgent need to understand a new disease. However, it's essential to acknowledge the limitations. The QuantiFERON assay, with its emphasis on IFNγ production, does not provide a comprehensive assessment of the entire spectrum of T cell functions. For a more detailed analysis, alternative techniques such as PBMC isolation coupled with immunophenotyping, which allows the study of specific T cell subsets and their functional characteristics or ELISPOT assays which provide a direct measure of cytokine-secreting cells, offering a functional perspective on T cell responses, may be more suitable. Recognising the need for a more detailed analysis, mass cytometry was conducted in

conjunction with the QuantiFERON assay. This integrated approach facilitated a broader and more comprehensive exploration of T cell phenotypes and functions, enhancing the overall understanding of the immunopathology associated with MIS-C.

The QuantiFERON assay was also limited by the availability of samples from children with viral illness, KD and other Inflammatory diseases. Furthermore, children with KD and other Inflammatory diseases were less severely unwell compared to the other disease groups, which potentially confounds the interpretation of the findings. Nonetheless, some important differences and similarities in the immune response across the cohorts were recognised.

The mass cytometry on samples following the QuantiFERON assay was only carried out on samples from 5 acute MIS-C, 5 convalescent MIS-C and 3 HPC; other febrile controls and healthy vaccinated adults were not included. The small sample size and lack of febrile controls and vaccinated adults reduced the ability to draw comprehensive conclusions. Additionally, while these analyses were exploratory, p-values were corrected for multiple comparisons. However, it's crucial to note that despite corrections, issues related to multiple comparisons may persist (e.g., increased risk of Type I errors, overestimation of significance), warranting consideration. Including a larger and more diverse cohort would provide a more comprehensive insight and enhance the accuracy and reliability of the findings.

As many of the recruited children were acutely unwell and were having multiple blood tests for their clinical management, it was challenging to take the relatively large volume of blood (4 ml) required for the QuantiFERON assay, prior to the patient receiving any immunomodulatory treatment. As such, around half of the cohort had received immunomodulatory treatment, primarily corticosteroids, prior to blood sampling. However, a clustering analysis showed no significant effect of immunomodulatory treatment on the cytokine results and a PCA showed no distinct separation of samples by treatment groups for the mass cytometry results. Additionally, while TP1 samples were taken as soon as possible after hospital admission, there was an inherent limitation of variation in the timing of blood sampling in relation to the disease course of MIS-C, as this was dependent on when individuals presented to hospital.

Cytokines have been measured on unstimulated samples which undergo incubation at 37°C, which could alter the levels of some cytokines. Future work would involve comparing the supernatant cytokine results with cytokines measured from the plasma or serum of the same patients. Evaluation

of the effect of incubation on the mass cytometry results revealed an attenuated response in incubated samples, nonetheless the overall trends remained consistent. Furthermore, the foldchange calculations were made between incubated unstimulated samples and incubated stimulated samples from the same patients. The use of unstimulated samples subjected to the same conditions as the stimulated samples and within patient comparisons helped to control potential confounding factors. Future studies could incorporate multiple functional assays to provide complementary information to help strengthen overall conclusions, for instance, assessment of proliferation of T cells in response to antigenic stimulation and assessment of T cell-mediated cytotoxicity activity against target cells expressing specific antigens.

Finally, whole blood RNA-seq data was used for corroborating the cytokine and mass cytometry findings, however the use of single cell RNA-seq could provide more detailed insights. Single cell RNA-seq allows examination of gene expression at the individual cell level and therefore could help explain the heterogeneity of the MIS-C immune response, as well as providing a deeper understanding of the underlying mechanisms.

8.5 Conclusion

The work in this chapter uses multiple approaches to provide novel insights into the immunopathology of MIS-C, with a specific focus on the role of a dysregulated T cell response in the development of MIS-C. The findings highlight the complexity of the immunopathological mechanisms involved in MIS-C, including a dysregulated cytokine response, reduced SARS-CoV-2 antigen specific response, a dysregulated T cell response with evidence of T cell exhaustion/apoptosis and a molecular “off switch” mechanism which is shared with other febrile illnesses. These findings not only offer valuable guidance for future research studies aimed at unravelling underlying mechanisms, but also establish a foundational basis for shaping therapeutic strategies in MIS-C. The identification of T cell exhaustion prompts exploration into therapeutic interventions, such as PD-1 inhibitors, to enhance T cell function. Additionally, the recognition of shared molecular mechanisms with other febrile illnesses opens a promising avenue for the development of broad-spectrum therapeutics. In conclusion, this work enhances our understanding of MIS-C and offers a step forward in developing more effective and targeted approaches to address its complex immunopathological features, to ultimately improve patient outcomes.

Chapter 9: Discussion

9.1 Summary

The emergence of SARS-CoV-2 and rapid spread of COVID-19, along with the subsequent development of MIS-C and COVID-19 vaccine-induced myocarditis, presented unparalleled challenges at a global scale. There was an urgent need to rapidly establish research studies and generate data to improve the understanding of the novel virus and its associated conditions. There was a huge interdisciplinary collaborative effort worldwide, which accelerated the progress of research and accumulation of knowledge to combat the impact of these conditions through improved prevention, diagnosis, and management strategies. My PhD research has contributed to this endeavour by using several different approaches to advance the understanding of multiple aspects of SARS-CoV-2 associated diseases in children.

My involvement in DIAMONDS and its preceding studies gave me access to large clinical databases and pre-COVID-19 pandemic samples. Although DIAMONDS was established prior to the COVID-19 pandemic, a timely amendment allowed incorporation of SARS-CoV-2 research. This allowed me to use the infrastructure established within DIAMONDS, to rapidly recruit patients and controls, and collect valuable samples during the pandemic for my research. This highlighted the importance of utilising existing infrastructures and mobilising resources to effectively respond in times of emergency, a lesson that extends beyond the immediate context to potential future emergencies.

In the early stages of the pandemic, increased antibody levels were observed in severe cases of adult COVID-19[477], which prompted investigation of antibody dependent enhancement (ADE). ADE was an important hypothesis to address as it can result in increased viral replication, delayed immune response and can potentially impact vaccination strategies and clinical management - as seen in other viruses (e.g. dengue[156]). My investigations of the role of cross-reactive and SARS-CoV-2 specific antibodies did not find evidence for ADE driving the age-related differences observed in COVID-19 disease severity. Although a study by Hoepel et al.[181] offered *in vitro* evidence for a potential ADE mechanism in COVID-19, and others have reported elevated levels of SARS-CoV-2 IgG afucosylation among individuals with severe COVID-19, which is associated with ADCC[182,183], the overall body of evidence supporting ADE remains limited. My findings are in line with the majority of other studies which have not identified evidence for the harmful effects of SARS-CoV-2 specific antibodies or cross-

reactive antibodies[177,179,180]. Moreover, the overall favourable tolerance of COVID-19 vaccinations[478], the safe administration of convalescent plasma for COVID-19 treatment (although it proved ineffective)[479], and instances of individuals experiencing repeated infections without developing severe illness[480] collectively suggest that ADE is improbable as a contributing factor in COVID-19. Notably, in contrast to studies showing a relationship between SARS-CoV-2 antibody titres and severity of adult COVID-19[69,157,159,160], I did not identify this trend in the paediatric COVID-19 cohort, which suggests that the humoral response to SARS-CoV-2 may be different in children compared to adults. It is important to acknowledge some of the limitations of this work. Cross-reactive antibody testing was not performed for all the seasonal coronaviruses and antibody functionality was not assessed. Also, due to the rarity of paediatric COVID-19 cases requiring hospitalisation, the sample size of this cohort was relatively small (n = 30), which may result in increased type 2 error and false negative findings. In summary, while the question of whether antibodies mediate severe COVID-19 remains unanswered, the current scientific understanding is that antibodies play a protective role in COVID-19.

Due to the spectrum of clinical presentations and severity of MIS-C, and presence of overlapping features with other infectious and inflammatory diseases[196,202], it was important to identify methods of reducing the diagnostic uncertainty. The DIAMONDS dataset allowed comparisons of clinical and laboratory features in a large cohort of children with MIS-C, Bacterial illness, Viral illness, and KD. This led to the development of a diagnostic score which could accurately distinguish MIS-C from other conditions with similar features. Although the score requires external validation, it shows promise for use as a decision-making tool (AUC 0.90), which can aid timely diagnosis and prompt initiation of treatment. While researchers have also developed similar scores with good performance[246,247,249,250], this score offers a simple and reliable alternative. Furthermore, the use of sophisticated machine learning algorithms for feature selection and weighting (e.g. Least Absolute Shrinkage and Selection Operator[248] or Forward Selection Partial Least Squares[481]) can potentially help refine the diagnostic score and improve its accuracy and performance.

My analyses revealed that the majority of patients with MIS-C tested positive for SARS-CoV-2 IgG, with higher antibody titres compared to the febrile controls. This is consistent with findings from other studies demonstrating higher SARS-CoV-2 IgG titres in MIS-C compared to severe paediatric COVID-19[392] and hospitalised paediatric controls[397]. Interestingly, there was no significant relationship between SARS-CoV-2 antibody titres and MIS-C disease severity. This is a novel contribution to the field that challenges the initial hypothesis of an antibody-mediated pathology driving MIS-C. In

addition, the longitudinal analyses revealed a trend of increasing SARS-CoV-2 seropositivity over time in patients with MIS-C and febrile controls. These findings suggest the need for re-evaluation of the WHO and CDC case definitions of MIS-C, which include seropositivity as evidence of exposure to SARS-CoV-2. Furthermore, these results highlight the urgent need for the development of more specific diagnostic markers for MIS-C.

During my PhD, I had the privilege of contributing to the establishment of the BATS consortium and study. BATS is an unfunded observational study, which was made possible due to the remarkable goodwill of healthcare professionals from around the world who generously contributed valuable data. This experience was an important reminder of the immense value of teamwork and collaborative efforts in answering urgent research questions. I utilised the BATS dataset for conducting descriptive analyses of MIS-C in a large, international cohort. These findings were consistent with previous reports[199,209,210], reinforcing the existing evidence base for MIS-C. I subsequently identified variables associated with disease severity and developed a severity score using baseline physiological and laboratory parameters, to predict disease severity at both baseline and 48 hours post hospital admission. Following external validation, the severity score has the potential to be translated into a user-friendly mobile phone application for use in the emergency department. The application could facilitate risk stratification and a tailored management approach, ultimately leading to improved patient care and outcomes.

The primary aim of BATS, to identify the most effective treatment for MIS-C, and the voluntary nature of the study, introduces potential selection and ascertainment bias. The presence of missing laboratory values required imputation for use in the severity score analyses, which can introduce its own biases and should be considered when interpreting the results. Considering the significance of cardiac involvement as a major complication in MIS-C, another valuable clinical risk score would possess the capability to predict patients at risk of cardiac complications, such as inotrope requirement within the next 12 hours or development of CAA. However, it is important to note that the current severity score did not demonstrate optimal performance in predicting cardiac outcomes, despite my attempts to explore this aspect. Therefore, refining the score and adopting a more targeted approach specifically tailored toward assessing cardiac outcomes would be imperative for its further enhancement and clinical utility. Finally, as with the diagnostic score, integration of machine learning algorithms may enhance the accuracy and performance of the severity score.

At the beginning of my PhD, there were limited studies on the immunology of SARS-CoV-2 associated diseases that included comparisons between adults, children, febrile controls, and healthy controls. I recognised the importance of recruiting appropriate patients and controls, as well as collecting the right sample types at relevant timepoints to obtain meaningful results. Therefore, adults and children with COVID-19, children with MIS-C, children with COVID-19 vaccine-induced myocarditis, paediatric febrile controls, healthy paediatric controls, and healthy COVID-19 vaccinated adults were included in my research. I also collected samples from patients during acute illness and convalescence to explore the dynamic changes in immune responses. This comprehensive approach provided valuable insights into the immunopathology of SARS-CoV-2 associated diseases, specifically the antibody and T cell responses.

The results of the antibody mechanistic studies represent the first investigation of its kind. Notably, anti-cardiac antibodies were not identified in the serum of patients with MIS-C and COVID-19 vaccine-induced myocarditis, and there was no evidence of antibodies from patient sera binding to donor cardiac tissue. Collectively, these results suggest that it is unlikely that antibodies alone are mediating the cardiac pathology in MIS-C and COVID-19 vaccine-induced myocarditis. It is possible that the presence of both viral antigens and antibodies is required, as suggested by the findings from Yonker et al. showing viral antigenaemia in MIS-C and COVID-19 vaccine-induced myocarditis[293,352], which warrants further investigation. Of note, this study had some limitations, including the small sample size and use of adult cardiac donors and adult positive controls, which may have contributed to the absence of positive findings.

In a parallel narrative, the intriguing observation of a low incidence of severe COVID-19[482] and MIS-C[199,209,397] in children with immune deficiencies challenges established assumptions about the immunopathology of these conditions. Traditionally, it was assumed that compromised immune function would lead to increased susceptibility and severity of viral infections. However, the contrasting observation suggests that factors beyond immune deficiency alone may contribute to the development of severe disease. It opens the possibility of alternative protective mechanisms or compensatory pathways in these populations and raises questions about the role of an overactive immune response in driving severe disease.

While several studies have characterised the T cell populations in MIS-C and reported distinct immunological profiles[280,287,295,306], my research stands out as the first to assess the functional T cell response in both acute and convalescent MIS-C, compared to paediatric febrile and healthy controls.

The results reveal a diminished specific T cell response to stimulation with SARS-CoV-2 antigen in acute MIS-C, with partial recovery in convalescence. This suggests the possibility of transient T cell exhaustion or apoptosis, which is supported by the mass cytometry and RNA-seq results. It is important that further research is carried out to better understand the underlying mechanisms, because if T cell exhaustion is indeed a critical driver of MIS-C pathogenesis, targeted interventions to reverse T cell exhaustion hold promise for improving patient outcomes.

Furthermore, all acutely unwell febrile children had a reduced response to mitogen stimulation, which was restored in convalescence. This shared immunological response likely represents the "molecular off-switch", which has been proposed as a potential regulatory mechanism for preventing excessive or prolonged inflammation[477]. The limitations of this work include a small number of febrile controls and convalescent samples and the potential influence of the laboratory methodology (e.g. incubation) on the results.

Many researchers have performed comprehensive studies evaluating the immunology of MIS-C and COVID-19 vaccine-induced myocarditis, however, the exact mechanisms underlying the immunopathogenesis and immunopathology of these conditions are not fully understood. The results of my functional antibody and T cell studies are novel findings which not only provide valuable contributions to current understanding but also offer direction for future work.

9.2 Future work

Although the incidence of SARS-CoV-2 associated diseases in children is decreasing and very few cases are now being reported, it is vital to continue research in this field. Unravelling the mechanisms underlying SARS-CoV-2 associated diseases can advance the understanding of the host-immune responses to viruses, as well as offer insights into the mechanisms driving similar conditions, such as KD. Additionally, knowledge from ongoing research and established networks and infrastructures will ensure an effective and rapid response to any future emerging infectious diseases.

To build upon my findings, future research should address the following key areas. Validation and refinement of the MIS-C diagnostic and severity scores using data from a comprehensive multi-centred cohort will enhance their utility in clinical practice, and will be invaluable in the event of subsequent waves of MIS-C. Further interrogation of the antibody response in COVID-19 and MIS-C through additional functional assays, such as measurement of neutralising ability or antibody-mediated effector functions, is warranted. In addition, the presence of SARS-CoV-2 antigens may be required for antibody-mediated damage, therefore experiments using cardiomyocytes expressing SARS-CoV-2 antigens or infected tissues for functional studies may provide further insights into the cardiac pathology seen in MIS-C and COVID-19 vaccine-induced myocarditis. An alternative mechanism worth exploring for the cardiac pathology in MIS-C is the effect of raised IL6, which has been shown to suppress cardiac function in other conditions, through *in vitro* assessment of cardiac contractility or electromyography. The hypothesis of T cell exhaustion also warrants further investigation. This could include multiple approaches, including single cell RNA-seq or functional studies assessing the impact of anti-PD1 treatment on the restoration of exhausted T cells following antigen stimulation. This could help identify potential diagnostic and therapeutic targets. An essential area of future research is the assessment of long-term outcomes of SARS-CoV-2 associated diseases, including the impact on physical health, immunology, mental health and risk of other health problems. Outside the context of SARS-CoV-2, the lack of response to mitogen in acute paediatric febrile illnesses and the “molecular off-switch” phenomenon presents an intriguing and important area of research that deserves further exploration. Understanding the molecular mechanisms involved can shed light on the dysregulated immune response observed in severe childhood infections. This has significant implications including development of tools to identify at risk individuals and targeted therapies for improved patient outcomes.

9.3 Concluding remarks

The research carried out during my PhD has provided a comprehensive understanding of the clinical and immunological aspects of paediatric SARS-CoV-2 associated diseases, in particular MIS-C. The findings have important implications for the diagnosis, prognosis and management of MIS-C, and also provide valuable directions for future research. Embarking on a clinical academic career amidst a global pandemic has presented significant challenges as well as remarkable opportunities for growth. This experience has highlighted the importance of adopting proactive approaches to foster interdisciplinary collaboration and enable rapid implementation of evidence-based strategies to mitigate the impact of emerging diseases. Moving forward, integrating the lessons learnt from the COVID-19 pandemic will contribute to enhanced global health preparedness and improved patient outcomes.

References

1. Chappell, J. D. & Dermody, T. S. Biology of Viruses and Viral Diseases. *Mandell, Douglas, and Bennett's Principles and Practice of Infectious Diseases* 1681 (2015) doi:10.1016/B978-1-4557-4801-3.00134-X.
2. Louten, J. Virus Structure and Classification. *Essential Human Virology* 19–29 (2016) doi:10.1016/B978-0-12-800947-5.00002-8.
3. López-García, P. & Moreira, D. Viruses in Biology. *Evo Edu Outreach* **5**, 389–398 (2012).
4. Ryu, W.-S. Virus Life Cycle. *Molecular Virology of Human Pathogenic Viruses* 31–45 (2017) doi:10.1016/B978-0-12-800838-6.00003-5.
5. Mueller, S. N. & Rouse, B. T. Immune responses to viruses. *Clinical Immunology* 421–431 (2008) doi:10.1016/B978-0-323-04404-2.10027-2.
6. Thompson, M. R., Kaminski, J. J., Kurt-Jones, E. A. & Fitzgerald, K. A. Pattern Recognition Receptors and the Innate Immune Response to Viral Infection. *Viruses* **3**, 920–940 (2011).
7. Brennan, K. & Bowie, A. G. Activation of host pattern recognition receptors by viruses. *Curr Opin Microbiol* **13**, 503–507 (2010).
8. Iwanaszko, M. & Kimmel, M. NF-κB and IRF pathways: cross-regulation on target genes promoter level. *BMC Genomics* **16**, 307 (2015).
9. Kawai, T. & Akira, S. Innate immune recognition of viral infection. *Nat Immunol* **7**, 131–137 (2006).
10. Sun, S.-C. The non-canonical NF-κB pathway in immunity and inflammation. *Nat Rev Immunol* **17**, 545–558 (2017).
11. Liu, T., Zhang, L., Joo, D. & Sun, S.-C. NF-κB signaling in inflammation. *Sig Transduct Target Ther* **2**, 1–9 (2017).
12. Santoro, M. G., Rossi, A. & Amici, C. NF-κB and virus infection: who controls whom. *The EMBO Journal* **22**, 2552–2560 (2003).

13. Iwasaki, A. A Virological View of Innate Immune Recognition. *Annu Rev Microbiol* **66**, 177–196 (2012).
14. Grandvaux, N., tenOever, B. R., Servant, M. J. & Hiscott, J. The interferon antiviral response: from viral invasion to evasion. *Curr Opin Infect Dis* **15**, 259–267 (2002).
15. Katze, M. G., He, Y. & Gale, M. Viruses and interferon: a fight for supremacy. *Nat Rev Immunol* **2**, 675–687 (2002).
16. Harvey, A. G. *et al.* Dendritic cell-natural killer cell cross-talk modulates T cell activation in response to influenza A viral infection. *Front Immunol* **13**, 1006998 (2022).
17. Björkström, N. K., Strunz, B. & Ljunggren, H.-G. Natural killer cells in antiviral immunity. *Nat Rev Immunol* **22**, 112–123 (2022).
18. Newton, A. H., Cardani, A. & Braciale, T. J. The host immune response in respiratory virus infection: balancing virus clearance and immunopathology. *Semin Immunopathol* **38**, 471–482 (2016).
19. Luckheeram, R. V., Zhou, R., Verma, A. D. & Xia, B. CD4+T Cells: Differentiation and Functions. *Clin Dev Immunol* **2012**, 925135 (2012).
20. Charles A Janeway, J., Travers, P., Walport, M. & Shlomchik, M. J. T cell-mediated cytotoxicity. in *Immunobiology: The Immune System in Health and Disease. 5th edition* (Garland Science, 2001).
21. Marshall, J. S., Warrington, R., Watson, W. & Kim, H. L. An introduction to immunology and immunopathology. *Allergy, Asthma & Clinical Immunology* **14**, 49 (2018).
22. Biggs, A. T. & Littlejohn, L. F. Vaccination and natural immunity: Advantages and risks as a matter of public health policy. *The Lancet Regional Health – Americas* **8**, (2022).
23. Rouse, B. T. & Sehrawat, S. Immunity and immunopathology to viruses: what decides the outcome? *Nat Rev Immunol* **10**, 514–526 (2010).
24. Fajgenbaum, D. C. & June, C. H. Cytokine Storm. *New England Journal of Medicine* **383**, 2255–2273 (2020).
25. Choutka, J., Jansari, V., Hornig, M. & Iwasaki, A. Unexplained post-acute infection syndromes. *Nat Med* **28**, 911–923 (2022).

26. Kahn, J. S. & McIntosh, K. History and Recent Advances in Coronavirus Discovery. *The Pediatric Infectious Disease Journal* **24**, S223 (2005).

27. Park, S., Lee, Y., Michelow, I. C. & Choe, Y. J. Global Seasonality of Human Coronaviruses: A Systematic Review. *Open Forum Infectious Diseases* **7**, ofaa443 (2020).

28. Liu, D. X., Liang, J. Q. & Fung, T. S. Human Coronavirus-229E, -OC43, -NL63, and -HKU1 (Coronaviridae). *Encyclopedia of Virology* 428–440 (2021) doi:10.1016/B978-0-12-809633-8.21501-X.

29. Ljubin-Sternak, S., Meštrović, T., Lukšić, I., Mijač, M. & Vraneš, J. Seasonal Coronaviruses and Other Neglected Respiratory Viruses: A Global Perspective and a Local Snapshot. *Frontiers in Public Health* **9**, (2021).

30. Drosten, C. *et al.* Identification of a Novel Coronavirus in Patients with Severe Acute Respiratory Syndrome. *New England Journal of Medicine* **348**, 1967–1976 (2003).

31. Peiris, J. S. M. *et al.* Coronavirus as a possible cause of severe acute respiratory syndrome. *The Lancet* **361**, 1319–1325 (2003).

32. Li, W. *et al.* Bats Are Natural Reservoirs of SARS-Like Coronaviruses. *Science* **310**, 676–679 (2005).

33. Wang, L. F. & Eaton, B. T. Bats, civets and the emergence of SARS. *Curr Top Microbiol Immunol* **315**, 325–344 (2007).

34. Hui, D. S. C. Severe acute respiratory syndrome (SARS): epidemiology and clinical features. *Postgraduate Medical Journal* **80**, 373–381 (2004).

35. Summary of probable SARS cases with onset of illness from 1 November 2002 to 31 July 2003. https://www.who.int/publications/m/item/summary-of-probable-sars-cases-with-onset-of-illness-from-1-november-2002-to-31-july-2003.

36. Iannarella, R. *et al.* Coronavirus infections in children: from SARS and MERS to COVID-19, a narrative review of epidemiological and clinical features. *Acta Biomed* **91**, e2020032 (2020).

37. Fehr, A. R., Channappanavar, R. & Perlman, S. Middle East Respiratory Syndrome: Emergence of a Pathogenic Human Coronavirus. *Annu. Rev. Med.* **68**, 387–399 (2017).

38. Zaki, A. M., van Boheemen, S., Bestebroer, T. M., Osterhaus, A. D. M. E. & Fouchier, R. A. M. Isolation of a novel coronavirus from a man with pneumonia in Saudi Arabia. *N Engl J Med* **367**, 1814–1820 (2012).

39. Hui, D. S., Perlman, S. & Zumla, A. Spread of MERS to South Korea and China. *Lancet Respir Med* **3**, 509–510 (2015).

40. Middle East respiratory syndrome coronavirus (MERS-CoV). https://www.who.int/health-topics/middle-east-respiratory-syndrome-coronavirus-mers.

41. Oh, M. *et al.* Middle East respiratory syndrome: what we learned from the 2015 outbreak in the Republic of Korea. *Korean J Intern Med* **33**, 233–246 (2018).

42. CSR. MERS outbreaks. *World Health Organization - Regional Office for the Eastern Mediterranean* http://www.emro.who.int/health-topics/mers-cov/mers-outbreaks.html.

43. Zhu, N. *et al.* A Novel Coronavirus from Patients with Pneumonia in China, 2019. *N Engl J Med* **382**, 727–733 (2020).

44. Wu, F. *et al.* A new coronavirus associated with human respiratory disease in China. *Nature* **579**, 265–269 (2020).

45. Hu, B., Guo, H., Zhou, P. & Shi, Z.-L. Characteristics of SARS-CoV-2 and COVID-19. *Nature Reviews Microbiology* **19**, 141–154 (2021).

46. Wang, M.-Y. *et al.* SARS-CoV-2: Structure, Biology, and Structure-Based Therapeutics Development. *Front Cell Infect Microbiol* **10**, (2020).

47. Lamers, M. M. & Haagmans, B. L. SARS-CoV-2 pathogenesis. *Nat Rev Microbiol* **20**, 270–284 (2022).

48. Hoffmann, M. *et al.* SARS-CoV-2 Cell Entry Depends on ACE2 and TMPRSS2 and Is Blocked by a Clinically Proven Protease Inhibitor. *Cell* **181**, 271-280.e8 (2020).

49. Heurich, A. *et al.* TMPRSS2 and ADAM17 Cleave ACE2 Differentially and Only Proteolysis by TMPRSS2 Augments Entry Driven by the Severe Acute Respiratory Syndrome Coronavirus Spike Protein. *J Virol* **88**, 1293–1307 (2014).

50. Diamond, M. S. & Kanneganti, T.-D. Innate immunity: the first line of defense against SARS-CoV-2. *Nat Immunol* **23**, 165–176 (2022).
51. Timeline: WHO's COVID-19 response. https://www.who.int/emergencies/diseases/novel-coronavirus-2019/interactive-timeline.
52. Ea, M., A, R., Rt, G. & Pe, S. Transmission of SARS-CoV-2: A Review of Viral, Host, and Environmental Factors. *Annals of internal medicine* **174**, (2021).
53. Transmission of SARS-CoV-2: implications for infection prevention precautions. https://www.who.int/news-room/commentaries/detail/transmission-of-sars-cov-2-implications-for-infection-prevention-precautions.
54. WHO Coronavirus (COVID-19) Dashboard. https://covid19.who.int.
55. Shen, J. *et al.* Innate and adaptive immunity to SARS-CoV-2 and predisposing factors. *Frontiers in Immunology* **14**, (2023).
56. Boechat, J. L., Chora, I., Morais, A. & Delgado, L. The immune response to SARS-CoV-2 and COVID-19 immunopathology – Current perspectives. *Pulmonology* **27**, 423–437 (2021).
57. Gu, W. *et al.* The molecular mechanism of SARS-CoV-2 evading host antiviral innate immunity. *Virol J* **19**, 49 (2022).
58. Xia, H. *et al.* Evasion of Type I Interferon by SARS-CoV-2. *Cell Rep* **33**, 108234 (2020).
59. Lei, X. *et al.* Activation and evasion of type I interferon responses by SARS-CoV-2. *Nature Communications* **11**, 3810 (2020).
60. Kaklamanos, A. *et al.* COVID-19 Immunobiology: Lessons Learned, New Questions Arise. *Frontiers in Immunology* **12**, (2021).
61. Tian, W. *et al.* Immune suppression in the early stage of COVID-19 disease. *Nature Communications* **11**, 5859 (2020).
62. Carvalho, T., Krammer, F. & Iwasaki, A. The first 12 months of COVID-19: a timeline of immunological insights. *Nat Rev Immunol* **21**, 245–256 (2021).

63. Blanco-Melo, D. *et al.* Imbalanced Host Response to SARS-CoV-2 Drives Development of COVID-19. *Cell* **181**, 1036-1045.e9 (2020).

64. Hou, H. *et al.* Detection of IgM and IgG antibodies in patients with coronavirus disease 2019. *Clin Transl Immunology* **9**, (2020).

65. Mou, D. *et al.* Profile of specific antibodies to the SARS-CoV-2. *J Med Microbiol* **70**, 001335 (2021).

66. Long, Q.-X. *et al.* Antibody responses to SARS-CoV-2 in patients with COVID-19. *Nature Medicine* **26**, 845–848 (2020).

67. Tan, W. *et al.* Viral Kinetics and Antibody Responses in Patients with COVID-19. *medRxiv* 2020.03.24.20042382 (2020) doi:10.1101/2020.03.24.20042382.

68. Wang, Y. *et al.* Kinetics of viral load and antibody response in relation to COVID-19 severity. *J Clin Invest* **130**, 5235–5244 (2020).

69. Zhao, J. *et al.* Antibody Responses to SARS-CoV-2 in Patients With Novel Coronavirus Disease 2019. *Clin Infect Dis* **71**, 2027–2034 (2020).

70. Bernardes, J. P. *et al.* Longitudinal Multi-omics Analyses Identify Responses of Megakaryocytes, Erythroid Cells, and Plasmablasts as Hallmarks of Severe COVID-19. *Immunity* **53**, 1296 (2020).

71. Wilk, A. J. *et al.* A single-cell atlas of the peripheral immune response in patients with severe COVID-19. *Nat Med* **26**, 1070–1076 (2020).

72. Kuri-Cervantes, L. *et al.* Comprehensive mapping of immune perturbations associated with severe COVID-19. *Science Immunology* **5**, eabd7114 (2020).

73. Liu, K. *et al.* Clinical characteristics of novel coronavirus cases in tertiary hospitals in Hubei Province. *Chin Med J (Engl)* **133**, 1025–1031 (2020).

74. Huang, C. *et al.* Clinical features of patients infected with 2019 novel coronavirus in Wuhan, China. *The Lancet* **395**, 497–506 (2020).

75. Huang, I. & Pranata, R. Lymphopenia in severe coronavirus disease-2019 (COVID-19): systematic review and meta-analysis. *Journal of Intensive Care* **8**, 36 (2020).

76. Chen, G. *et al.* Clinical and immunological features of severe and moderate coronavirus disease 2019. *J Clin Invest* **130**, 2620–2629 (2020).

77. Zhao, Q. *et al.* Lymphopenia is associated with severe coronavirus disease 2019 (COVID-19) infections: A systemic review and meta-analysis. *Int J Infect Dis* **96**, 131–135 (2020).

78. Helal, M. A. *et al.* Molecular basis of the potential interaction of SARS-CoV-2 spike protein to CD147 in COVID-19 associated-lymphopenia. *J Biomol Struct Dyn* 1–11 doi:10.1080/07391102.2020.1822208.

79. Moon, C. Fighting COVID-19 exhausts T cells. *Nat Rev Immunol* 1 (2020) doi:10.1038/s41577-020-0304-7.

80. Diao, B. *et al.* Reduction and Functional Exhaustion of T Cells in Patients With Coronavirus Disease 2019 (COVID-19). *Front. Immunol.* **11**, (2020).

81. Bradley, B. T. *et al.* Histopathology and ultrastructural findings of fatal COVID-19 infections in Washington State: a case series. *The Lancet* **396**, 320–332 (2020).

82. Liu, Q. *et al.* Pathological changes in the lungs and lymphatic organs of 12 COVID-19 autopsy cases. *National Science Review* **7**, 1868–1878 (2020).

83. Nienhold, R. *et al.* Two distinct immunopathological profiles in autopsy lungs of COVID-19. *Nature Communications* **11**, 5086 (2020).

84. Siddiqi, H. K. & Mehra, M. R. COVID-19 illness in native and immunosuppressed states: A clinical–therapeutic staging proposal. *J Heart Lung Transplant* **39**, 405–407 (2020).

85. Mangalmurti, N. & Hunter, C. A. Cytokine Storms: Understanding COVID-19. *Immunity* **53**, 19–25 (2020).

86. Feng, Y. *et al.* COVID-19 with Different Severities: A Multicenter Study of Clinical Features. *Am J Respir Crit Care Med* **201**, 1380–1388 (2020).

87. Wang, W. *et al.* Definition and Risks of Cytokine Release Syndrome in 11 Critically Ill COVID-19 Patients With Pneumonia: Analysis of Disease Characteristics. *The Journal of Infectious Diseases* **222**, 1444–1451 (2020).

88. Channappanavar, R. & Perlman, S. Pathogenic human coronavirus infections: causes and consequences of cytokine storm and immunopathology. *Semin Immunopathol* **39**, 529–539 (2017).

89. Collange, O. *et al.* Coronavirus Disease 2019: Associated Multiple Organ Damage. *Open Forum Infect Dis* **7**, (2020).

90. Silva, M. J. A. *et al.* Hyperinflammatory Response in COVID-19: A Systematic Review. *Viruses* **15**, 553 (2023).

91. Ricklin, D., Hajishengallis, G., Yang, K. & Lambris, J. D. Complement: a key system for immune surveillance and homeostasis. *Nature Immunology* **11**, 785–797 (2010).

92. Noris, M., Benigni, A. & Remuzzi, G. The case of complement activation in COVID-19 multiorgan impact. *Kidney Int* **98**, 314–322 (2020).

93. Perico, L. *et al.* Immunity, endothelial injury and complement-induced coagulopathy in COVID-19. *Nature Reviews Nephrology* **17**, 46–64 (2021).

94. Del Turco, S., Vianello, A., Ragusa, R., Caselli, C. & Basta, G. COVID-19 and cardiovascular consequences: Is the endothelial dysfunction the hardest challenge? *Thromb Res* **196**, 143–151 (2020).

95. Gao, Y. *et al.* Diagnostic utility of clinical laboratory data determinations for patients with the severe COVID-19. *J Med Virol* **92**, 791–796 (2020).

96. Del Valle, D. M. *et al.* An inflammatory cytokine signature predicts COVID-19 severity and survival. *Nature Medicine* **26**, 1636–1643 (2020).

97. Ruan, Q., Yang, K., Wang, W., Jiang, L. & Song, J. Clinical predictors of mortality due to COVID-19 based on an analysis of data of 150 patients from Wuhan, China. *Intensive Care Med* **46**, 846–848 (2020).

98. Mandel, M., Harari, G., Gurevich, M. & Achiron, A. Cytokine prediction of mortality in COVID19 patients. *Cytokine* **134**, 155190 (2020).

99. Tan, L. Y., Komarasamy, T. V. & RMT Balasubramaniam, V. Hyperinflammatory Immune Response and COVID-19: A Double Edged Sword. *Frontiers in Immunology* **12**, (2021).

100. Wang, L. G. & Wang, L. Current Strategies in Treating Cytokine Release Syndrome Triggered by Coronavirus SARS-CoV-2. *Immunotargets Ther* **11**, 23–35 (2022).

101. Montazersaheb, S. *et al.* COVID-19 infection: an overview on cytokine storm and related interventions. *Virology Journal* **19**, 92 (2022).

102. Abani, O. *et al.* Tocilizumab in patients admitted to hospital with COVID-19 (RECOVERY): a randomised, controlled, open-label, platform trial. *The Lancet* **397**, 1637–1645 (2021).

103. Irfan, O. *et al.* Clinical characteristics, treatment and outcomes of paediatric COVID-19: a systematic review and meta-analysis. *Archives of Disease in Childhood* **106**, 440–448 (2021).

104. Swann, O. V. *et al.* Clinical characteristics of children and young people admitted to hospital with covid-19 in United Kingdom: prospective multicentre observational cohort study. *BMJ* **370**, m3249 (2020).

105. Wu, Z. & McGoogan, J. M. Characteristics of and Important Lessons From the Coronavirus Disease 2019 (COVID-19) Outbreak in China: Summary of a Report of 72 314 Cases From the Chinese Center for Disease Control and Prevention. *JAMA* **323**, 1239–1242 (2020).

106. McAloon, C. *et al.* Incubation period of COVID-19: a rapid systematic review and meta-analysis of observational research. *BMJ Open* **10**, e039652 (2020).

107. Lauer, S. A. *et al.* The Incubation Period of Coronavirus Disease 2019 (COVID-19) From Publicly Reported Confirmed Cases: Estimation and Application. *Ann Intern Med* M20-0504 (2020) doi:10.7326/M20-0504.

108. Wu, Y. *et al.* Incubation Period of COVID-19 Caused by Unique SARS-CoV-2 Strains: A Systematic Review and Meta-analysis. *JAMA Netw Open* **5**, e2228008 (2022).

109. Byambasuren, O., Bell, K., McLaws, L. & Glasziou, P. Estimating the extent of asymptomatic COVID-19 and its potential for community transmission: systematic review and meta-analysis. 14.

110. Nishiura, H. *et al.* Estimation of the asymptomatic ratio of novel coronavirus infections (COVID-19). *International Journal of Infectious Diseases* **94**, 154–155 (2020).

111. Oran, D. P. & Topol, E. J. Prevalence of Asymptomatic SARS-CoV-2 Infection. *Ann Intern Med* **173**, 362–367 (2020).

112. Viner, R. M. *et al.* Systematic review of reviews of symptoms and signs of COVID-19 in children and adolescents. *Arch Dis Child* **106**, 802–807 (2020).

113. Giacomelli, A. *et al.* Self-reported Olfactory and Taste Disorders in Patients With Severe Acute Respiratory Coronavirus 2 Infection: A Cross-sectional Study. *Clin Infect Dis* **71**, 889–890 (2020).

114. Wang, D. *et al.* Clinical Characteristics of 138 Hospitalized Patients With 2019 Novel Coronavirus–Infected Pneumonia in Wuhan, China. *JAMA* **323**, 1061–1069 (2020).

115. Zaim, S., Chong, J. H., Sankaranarayanan, V. & Harky, A. COVID-19 and Multiorgan Response. *Curr Probl Cardiol* **45**, 100618 (2020).

116. Clinical management of COVID-19: Living guideline, 13 January 2023. https://www.who.int/publications-detail-redirect/WHO-2019-nCoV-clinical-2023.1.

117. Vosoughi, F. *et al.* A systematic review and meta-analysis of the epidemiological characteristics of COVID-19 in children. *BMC Pediatrics* **22**, 613 (2022).

118. Liguoro, I. *et al.* SARS-COV-2 infection in children and newborns: a systematic review. *Eur J Pediatr* **179**, 1029–1046 (2020).

119. Forrest, C. B. *et al.* Severity of Acute COVID-19 in Children <18 Years Old March 2020 to December 2021. *Pediatrics* **149**, e2021055765 (2022).

120. Pijls, B. G. *et al.* Demographic risk factors for COVID-19 infection, severity, ICU admission and death: a meta-analysis of 59 studies. *BMJ Open* **11**, e044640 (2021).

121. Jordan, R. E., Adab, P. & Cheng, K. K. Covid-19: risk factors for severe disease and death. *BMJ* **368**, m1198 (2020).

122. Mackey, K. *et al.* Racial and Ethnic Disparities in COVID-19–Related Infections, Hospitalizations, and Deaths. *Ann Intern Med* **174**, 362–373 (2020).

123. Liu, H., Chen, S., Liu, M., Nie, H. & Lu, H. Comorbid Chronic Diseases are Strongly Correlated with Disease Severity among COVID-19 Patients: A Systematic Review and Meta-Analysis. *Aging Dis* **11**, 668–678 (2020).

124. Beaney, T. *et al.* Trends and associated factors for Covid-19 hospitalisation and fatality risk in 2.3 million adults in England. *Nat Commun* **13**, 2356 (2022).

125. Gao, Y. *et al.* Risk factors for severe and critically ill COVID-19 patients: A review. *Allergy* **76**, 428–455 (2021).

126. Woodruff, R. C. *et al.* Risk Factors for Severe COVID-19 in Children. *Pediatrics* **149**, e2021053418 (2021).

127. Graff, K. *et al.* Risk Factors for Severe COVID-19 in Children. *The Pediatric Infectious Disease Journal* **40**, e137 (2021).

128. Choi, J. H., Choi, S.-H. & Yun, K. W. Risk Factors for Severe COVID-19 in Children: A Systematic Review and Meta-Analysis. *J Korean Med Sci* **37**, (2022).

129. Niemi, M. E. K., Daly, M. J. & Ganna, A. The human genetic epidemiology of COVID-19. *Nat Rev Genet* **23**, 533–546 (2022).

130. WHO COVID-19 Case definition. https://www.who.int/publications-detail-redirect/WHO-2019-nCoV-Surveillance_Case_Definition-2022.1.

131. Coronavirus Disease 2019 (COVID-19) 2021 Case Definition | CDC. https://ndc.services.cdc.gov/case-definitions/coronavirus-disease-2019-2021/ (2021).

132. Guan, W. *et al.* Clinical Characteristics of Coronavirus Disease 2019 in China. *N Engl J Med* **382**, 1708–1720 (2020).

133. Cascella, M., Rajnik, M., Aleem, A., Dulebohn, S. C. & Di Napoli, R. Features, Evaluation, and Treatment of Coronavirus (COVID-19). in *StatPearls* (StatPearls Publishing, Treasure Island (FL), 2023).

134. Beigel, J. H. *et al.* Remdesivir for the Treatment of Covid-19 — Final Report. *N Engl J Med* **383**, 1813–1826 (2020).

135. Gupta, A. *et al.* Early Treatment for Covid-19 with SARS-CoV-2 Neutralizing Antibody Sotrovimab. *New England Journal of Medicine* **385**, 1941–1950 (2021).

136. RECOVERY Collaborative Group *et al.* Dexamethasone in Hospitalized Patients with Covid-19. *N Engl J Med* **384**, 693–704 (2021).

137. Therapeutics and COVID-19: living guideline. https://www.who.int/publications-detail-redirect/WHO-2019-nCoV-therapeutics-2022.4.

138. Li, Y. *et al.* A Comprehensive Review of the Global Efforts on COVID-19 Vaccine Development. *ACS Cent. Sci.* **7**, 512–533 (2021).

139. The Oxford/AstraZeneca (ChAdOx1-S [recombinant] vaccine) COVID-19 vaccine: what you need to know. https://www.who.int/news-room/feature-stories/detail/the-oxford-astrazeneca-covid-19-vaccine-what-you-need-to-know.

140. Livingston, E. H., Malani, P. N. & Creech, C. B. The Johnson & Johnson Vaccine for COVID-19. *JAMA* **325**, 1575 (2021).

141. Jackson, L. A. *et al.* An mRNA Vaccine against SARS-CoV-2 — Preliminary Report. *N Engl J Med* **383**, 1920–1931 (2020).

142. Walsh, E. E. *et al.* Safety and Immunogenicity of Two RNA-Based Covid-19 Vaccine Candidates. *New England Journal of Medicine* **383**, 2439–2450 (2020).

143. Liu, B. *et al.* Whole of population-based cohort study of recovery time from COVID-19 in New South Wales Australia. *The Lancet Regional Health – Western Pacific* **12**, (2021).

144. Thygesen, J. H. *et al.* COVID-19 trajectories among 57 million adults in England: a cohort study using electronic health records. *The Lancet Digital Health* **4**, e542–e557 (2022).

145. Ballouz, T. *et al.* Recovery and symptom trajectories up to two years after SARS-CoV-2 infection: population based, longitudinal cohort study. *BMJ* **381**, e074425 (2023).

146. Zhou, F. *et al.* Clinical course and risk factors for mortality of adult inpatients with COVID-19 in Wuhan, China: a retrospective cohort study. *The Lancet* **395**, 1054–1062 (2020).

147. Zou, L. *et al.* SARS-CoV-2 Viral Load in Upper Respiratory Specimens of Infected Patients. *New England Journal of Medicine* **382**, 1177–1179 (2020).

148. To, K. K.-W. *et al.* Temporal profiles of viral load in posterior oropharyngeal saliva samples and serum antibody responses during infection by SARS-CoV-2: an observational cohort study. *The Lancet Infectious Diseases* **20**, 565–574 (2020).

149. Viner, R. M. *et al.* Susceptibility to SARS-CoV-2 Infection Among Children and Adolescents Compared With Adults: A Systematic Review and Meta-analysis. *JAMA Pediatrics* **175**, 143–156 (2021).

150. Mandell, L., Woodhead, M., Ewig, S. & Torres, A. *Respiratory Infections*. (CRC Press, 2006).

151. Ben-Yehuda, A. & Weksler, M. E. Host Resistance and The Immune System. *Clinics in Geriatric Medicine* **8**, 701–712 (1992).

152. Rodriguez-Morales, A. J. *et al.* Clinical, laboratory and imaging features of COVID-19: A systematic review and meta-analysis. *Travel Medicine and Infectious Disease* 101623 (2020) doi:10.1016/j.tmaid.2020.101623.

153. Zimmermann, P. & Curtis, N. Coronavirus Infections in Children Including COVID-19: An Overview of the Epidemiology, Clinical Features, Diagnosis, Treatment and Prevention Options in Children. *The Pediatric Infectious Disease Journal* **Online First**, (2020).

154. Park, J.-E., Jung, S., Kim, A. & Park, J.-E. MERS transmission and risk factors: a systematic review. *BMC Public Health* **18**, 574 (2018).

155. Iwasaki, A. & Yang, Y. The potential danger of suboptimal antibody responses in COVID-19. *Nature Reviews Immunology* **20**, 339–341 (2020).

156. Xu, L., Ma, Z., Li, Y., Pang, Z. & Xiao, S. Antibody dependent enhancement: Unavoidable problems in vaccine development. *Adv Immunol* **151**, 99–133 (2021).

157. Zhang, L. *et al.* Antibody responses against SARS coronavirus are correlated with disease outcome of infected individuals. *J Med Virol* **78**, 1–8 (2006).

158. Liu, L. *et al.* Anti–spike IgG causes severe acute lung injury by skewing macrophage responses during acute SARS-CoV infection. *JCI Insight* **4**, (2019).

159. Hendriks, J. *et al.* High Titers of Low Affinity Antibodies in COVID-19 Patients Are Associated With Disease Severity. *Frontiers in Immunology* **13**, (2022).

160. Guo, Y. *et al.* Different Profiles of Antibodies and Cytokines Were Found Between Severe and Moderate COVID-19 Patients. *Front Immunol* **12**, 723585 (2021).

161. Shrock, E. *et al.* Viral epitope profiling of COVID-19 patients reveals cross-reactivity and correlates of severity. *Science* **370**, eabd4250 (2020).

162. Weisberg, S. P. *et al.* Distinct antibody responses to SARS-CoV-2 in children and adults across the COVID-19 clinical spectrum. *Nat Immunol* **22**, 25–31 (2021).

163. Pierce, C. A. *et al.* Immune responses to SARS-CoV-2 infection in hospitalized pediatric and adult patients. *Sci Transl Med* **12**, eabd5487 (2020).

164. Zohar, T. *et al.* Compromised Humoral Functional Evolution Tracks with SARS-CoV-2 Mortality. *Cell* **183**, 1508-1519.e12 (2020).

165. Takita, M. *et al.* Low SARS-CoV-2 antibody titers may be associated with poor clinical outcomes for patients with severe COVID-19. *Sci Rep* **12**, 9147 (2022).

166. De Vito, D. *et al.* Reduced COVID-19 mortality linked with early antibodies against SARS-CoV-2, irrespective of age. *Eur J Intern Med* **98**, 77–82 (2022).

167. Mathew, D. *et al.* Deep immune profiling of COVID-19 patients reveals distinct immunotypes with therapeutic implications. *Science* **369**, eabc8511 (2020).

168. Lucas, C. *et al.* Delayed production of neutralizing antibodies correlates with fatal COVID-19. *Nat Med* **27**, 1178–1186 (2021).

169. Luo, H. *et al.* The Characterization of Disease Severity Associated IgG Subclasses Response in COVID-19 Patients. *Frontiers in Immunology* **12**, (2021).

170. Ma, H. *et al.* Serum IgA, IgM, and IgG responses in COVID-19. *Cell Mol Immunol* **17**, 773–775 (2020).

171. Sananez, I. *et al.* A poor and delayed anti-SARS-CoV2 IgG response is associated to severe COVID-19 in children. *eBioMedicine* **72**, (2021).

172. Anderson, E. M. *et al.* SARS-CoV-2 antibody responses in children with MIS-C and mild and severe COVID-19. *medRxiv* 2020.08.17.20176552 (2020) doi:10.1101/2020.08.17.20176552.

173. Hachim, A. *et al.* The SARS-CoV-2 antibody landscape is lower in magnitude for structural proteins, diversified for accessory proteins and stable long-term in children. *medRxiv* 2021.01.03.21249180 (2021) doi:10.1101/2021.01.03.21249180.

174. Toh, Z. Q. *et al.* Comparison of Seroconversion in Children and Adults With Mild COVID-19. *JAMA Network Open* **5**, e221313 (2022).

175. Huang, A. T. *et al.* A systematic review of antibody mediated immunity to coronaviruses: kinetics, correlates of protection, and association with severity. *Nat Commun* **11**, 4704 (2020).

176. Fraley, E. *et al.* Cross-reactive antibody immunity against SARS-CoV-2 in children and adults. *Cell Mol Immunol* **18**, 1826–1828 (2021).

177. Lv, H. *et al.* Cross-reactive antibody response between SARS-CoV-2 and SARS-CoV infections. *bioRxiv* 2020.03.15.993097 (2020) doi:10.1101/2020.03.15.993097.

178. Guo, L. *et al.* Cross-reactive antibody against human coronavirus OC43 spike protein correlates with disease severity in COVID-19 patients: a retrospective study. *Emerg Microbes Infect* **10**, 664–676 (2021).

179. Sagar, M. *et al.* Recent endemic coronavirus infection is associated with less-severe COVID-19. *J Clin Invest* **131**, (2021).

180. Ng, K. W. *et al.* Preexisting and de novo humoral immunity to SARS-CoV-2 in humans. *Science* **370**, 1339–1343 (2020).

181. Hoepel, W. *et al.* Anti-SARS-CoV-2 IgG from severely ill COVID-19 patients promotes macrophage hyper-inflammatory responses. *bioRxiv* 2020.07.13.190140 (2020) doi:10.1101/2020.07.13.190140.

182. Larsen, M. D. *et al.* Afucosylated IgG characterizes enveloped viral responses and correlates with COVID-19 severity. *Science* **371**, eabc8378 (2021).

183. Chakraborty, S. *et al.* Proinflammatory IgG Fc structures in patients with severe COVID-19. *Nat Immunol* **22**, 67–73 (2021).

184. Oosterhoff, J. J., Larsen, M. D., Schoot, C. E. van der & Vidarsson, G. Afucosylated IgG responses in humans – structural clues to the regulation of humoral immunity. *Trends in Immunology* **43**, 800–814 (2022).

185. Simonovich, V. A. *et al.* A Randomized Trial of Convalescent Plasma in Covid-19 Severe Pneumonia. *N Engl J Med* **384**, 619–629 (2021).

186. Duan, K. *et al.* Effectiveness of convalescent plasma therapy in severe COVID-19 patients. *Proc Natl Acad Sci U S A* **117**, 9490–9496 (2020).

187. Joyner, M. J. *et al.* Early safety indicators of COVID-19 convalescent plasma in 5000 patients. *J Clin Invest* **130**, 4791–4797.

188. Agarwal, A. *et al.* Convalescent plasma in the management of moderate covid-19 in adults in India: open label phase II multicentre randomised controlled trial (PLACID Trial). *BMJ* **371**, m3939 (2020).

189. Pierce, C. A. *et al.* Natural mucosal barriers and COVID-19 in children. *JCI Insight* **6**, (2021).

190. Dowell, A. C. *et al.* Children develop robust and sustained cross-reactive spike-specific immune responses to SARS-CoV-2 infection. *Nat Immunol* **23**, 40–49 (2022).

191. Zimmermann, P. & Curtis, N. Why is COVID-19 less severe in children? A review of the proposed mechanisms underlying the age-related difference in severity of SARS-CoV-2 infections. *Archives of Disease in Childhood* **106**, 429–439 (2021).

192. Bastard, P. *et al.* Autoantibodies against type I IFNs in patients with life-threatening COVID-19. *Science* **370**, (2020).

193. Velavan, T. P. *et al.* Host genetic factors determining COVID-19 susceptibility and severity. *eBioMedicine* **72**, (2021).

194. Paediatric multisystem inflammatory syndrome temporally associated with COVID-19 (PIMS) - guidance for clinicians. *RCPCH* https://www.rcpch.ac.uk/resources/paediatric-multisystem-inflammatory-syndrome-temporally-associated-covid-19-pims-guidance.

195. Li, W., Tang, Y., Shi, Y., Chen, Y. & Liu, E. Why multisystem inflammatory syndrome in children has been less commonly described in Asia? *Transl Pediatr* **9**, 873–875 (2020).

196. Whittaker, E. *et al.* Clinical Characteristics of 58 Children With a Pediatric Inflammatory Multisystem Syndrome Temporally Associated With SARS-CoV-2. *JAMA* **324**, 259–269 (2020).

197. Feldstein, L. R. *et al.* Multisystem Inflammatory Syndrome in U.S. Children and Adolescents. *New England Journal of Medicine* **383**, 334–346 (2020).

198. Dufort, E. M. *et al.* Multisystem Inflammatory Syndrome in Children in New York State. *New England Journal of Medicine* **383**, 347–358 (2020).

199. Ahmed, M. *et al.* Multisystem inflammatory syndrome in children: A systematic review. *EClinicalMedicine* **26**, 100527 (2020).

200. Godfred-Cato, S. *et al.* COVID-19-Associated Multisystem Inflammatory Syndrome in Children - United States, March-July 2020. *MMWR Morb Mortal Wkly Rep* **69**, 1074–1080 (2020).

201. Vella, L. A. & Rowley, A. H. Current Insights Into the Pathophysiology of Multisystem Inflammatory Syndrome in Children. *Curr Pediatr Rep* **9**, 83–92 (2021).

202. Riphagen, S., Gomez, X., Gonzalez-Martinez, C., Wilkinson, N. & Theocharis, P. Hyperinflammatory shock in children during COVID-19 pandemic. *The Lancet* **395**, 1607–1608 (2020).

203. CDC. Multisystem Inflammatory Syndrome (MIS). *Centers for Disease Control and Prevention* https://www.cdc.gov/mis/mis-c/hcp/index.html (2020).

204. Multisystem inflammatory syndrome in children and adolescents temporally related to COVID-19. https://www.who.int/news-room/commentaries/detail/multisystem-inflammatory-syndrome-in-children-and-adolescents-with-covid-19.

205. Payne, A. B. *et al.* Incidence of Multisystem Inflammatory Syndrome in Children Among US Persons Infected With SARS-CoV-2. *JAMA Network Open* **4**, e2116420 (2021).

206. Holm, M. *et al.* Multisystem inflammatory syndrome in children occurred in one of four thousand children with severe acute respiratory syndrome coronavirus 2. *Acta Paediatrica* **110**, 2581–2583 (2021).

207. Belot, A. *et al.* SARS-CoV-2-related paediatric inflammatory multisystem syndrome, an epidemiological study, France, 1 March to 17 May 2020. *Euro surveillance : bulletin Europeen sur les maladies transmissibles = European communicable disease bulletin* **25**, (2020).

208. Flood, J. *et al.* Paediatric multisystem inflammatory syndrome temporally associated with SARS-CoV-2 (PIMS-TS): Prospective, national surveillance, United Kingdom and Ireland, 2020. *The Lancet Regional Health – Europe* **3**, (2021).

209. Radia, T. *et al.* Multi-system inflammatory syndrome in children & adolescents (MIS-C): A systematic review of clinical features and presentation. *Paediatric Respiratory Reviews* **38**, 51–57 (2021).

210. Santos, M. O. *et al.* Multisystem inflammatory syndrome (MIS-C): a systematic review and meta-analysis of clinical characteristics, treatment, and outcomes. *J Pediatr (Rio J)* **98**, 338–349 (2022).

211. Belhadjer, Z. *et al.* Acute Heart Failure in Multisystem Inflammatory Syndrome in Children in the Context of Global SARS-CoV-2 Pandemic. *Circulation* **142**, 429–436 (2020).

212. Alsaied, T. *et al.* Review of Cardiac Involvement in Multisystem Inflammatory Syndrome in Children. *Circulation* **143**, 78–88 (2021).

213. LaRovere, K. L. *et al.* Neurologic Involvement in Children and Adolescents Hospitalized in the United States for COVID-19 or Multisystem Inflammatory Syndrome. *JAMA Neurology* (2021) doi:10.1001/jamaneurol.2021.0504.

214. Rapid risk assessment: Paediatric inflammatory multisystem syndrome and SARS -CoV-2 infection in children. *European Centre for Disease Prevention and Control*

https://www.ecdc.europa.eu/en/publications-data/paediatric-inflammatory-multisystem-syndrome-and-sars-cov-2-rapid-risk-assessment (2020).

215. Davies, P. *et al.* Intensive care admissions of children with paediatric inflammatory multisystem syndrome temporally associated with SARS-CoV-2 (PIMS-TS) in the UK: a multicentre observational study. *The Lancet Child & Adolescent Health* **4**, 669–677 (2020).
216. Henderson, L. A. *et al.* American College of Rheumatology Clinical Guidance for Multisystem Inflammatory Syndrome in Children Associated With SARS–CoV-2 and Hyperinflammation in Pediatric COVID-19: Version 2. *Arthritis & Rheumatology* **73**, e13–e29 (2021).
217. Brumfiel, C. M., DiLorenzo, A. M. & Petronic-Rosic, V. M. Dermatologic manifestations of COVID-19-associated multisystem inflammatory syndrome in children. *Clin Dermatol* **39**, 329–333 (2021).
218. Naka, F., Melnick, L., Gorelik, M. & Morel, K. D. A dermatologic perspective on multisystem inflammatory syndrome in children. *Clin Dermatol* **39**, 163–168 (2021).
219. Blatz, A. M. *et al.* Cutaneous Findings in SARS-CoV-2-Associated Multisystem Inflammatory Disease in Children. *Open Forum Infectious Diseases* **8**, ofab074 (2021).
220. Lo Vecchio, A. *et al.* Factors Associated With Severe Gastrointestinal Diagnoses in Children With SARS-CoV-2 Infection or Multisystem Inflammatory Syndrome. *JAMA Network Open* **4**, e2139974 (2021).
221. Manz, N. *et al.* MIS-C-Implications for the Pediatric Surgeon: An Algorithm for Differential Diagnostic Considerations. *Children (Basel)* **8**, 712 (2021).
222. Wu, E. Y. & Campbell, M. J. Cardiac Manifestations of Multisystem Inflammatory Syndrome in Children (MIS-C) Following COVID-19. *Curr Cardiol Rep* **23**, 168 (2021).
223. Bentes, A. A. *et al.* Neuro-COVID-19 With or Without the Multisystem Inflammatory Syndrome (MIS-C): A Single-Center Study. *J Mol Neurosci* **73**, 250–258 (2023).

224. Schupper, A. J., Yaeger, K. A. & Morgenstern, P. F. Neurological manifestations of pediatric multisystem inflammatory syndrome potentially associated with COVID-19. *Childs Nerv Syst* **36**, 1579–1580 (2020).

225. Bova, S. M. *et al.* Neurological Involvement in Multisystem Inflammatory Syndrome in Children: Clinical, Electroencephalographic and Magnetic Resonance Imaging Peculiarities and Therapeutic Implications. An Italian Single-Center Experience. *Frontiers in Pediatrics* **10**, (2022).

226. O'Loughlin, L., Alvarez Toledo, N., Budrie, L., Waechter, R. & Rayner, J. A Systematic Review of Severe Neurological Manifestations in Pediatric Patients with Coexisting SARS-CoV-2 Infection. *Neurology International* **13**, 410–427 (2021).

227. More, K. *et al.* Multisystem inflammatory syndrome in neonates (MIS-N) associated with SARS-CoV2 infection: a case series. *Eur J Pediatr* **181**, 1883–1898 (2022).

228. Krishnan, P. & Susan George, G. Neonatal MIS-C. in *StatPearls* (StatPearls Publishing, Treasure Island (FL), 2023).

229. Pawar, R. *et al.* Neonatal Multisystem Inflammatory Syndrome (MIS-N) Associated with Prenatal Maternal SARS-CoV-2: A Case Series. *Children (Basel)* **8**, 572 (2021).

230. Shaiba, L. A. *et al.* Multisystemic Inflammatory Syndrome in Neonates: A Systematic Review. *Neonatology* **119**, 405–417 (2022).

231. Morris, S. B. *et al.* Case Series of Multisystem Inflammatory Syndrome in Adults Associated with SARS-CoV-2 Infection - United Kingdom and United States, March-August 2020. *MMWR Morb Mortal Wkly Rep* **69**, 1450–1456 (2020).

232. Yao, Q., Waley, L. & Liou, N. Adult presentation of multisystem inflammatory syndrome (MIS) associated with recent COVID-19 infection: lessons learnt in timely diagnosis and management. *BMJ Case Rep* **14**, e243114 (2021).

233. Kunal, S., Ish, P., Sakthivel, P., Malhotra, N. & Gupta, K. The emerging threat of multisystem inflammatory syndrome in adults (MIS-A) in COVID-19: A systematic review. *Heart & Lung* **54**, 7–18 (2022).

234. Patel, P. *et al.* Clinical Characteristics of Multisystem Inflammatory Syndrome in Adults: A Systematic Review. *JAMA Network Open* **4**, e2126456 (2021).

235. Rhedin, S. *et al.* Risk factors for multisystem inflammatory syndrome in children – A population-based cohort study of over 2 million children. *Lancet Reg Health Eur* **19**, 100443 (2022).

236. Auger, N. *et al.* Multisystem inflammatory syndrome in 1.2 million children: longitudinal cohort study of risk factors. *Pediatr Res* 1–9 (2023) doi:10.1038/s41390-023-02633-y.

237. Martin, B., Rao, S. & Bennett, T. D. Disparities in Multisystem Inflammatory Syndrome in Children and COVID-19 Across the Organ Dysfunction Continuum. *JAMA Network Open* **6**, e2249552 (2023).

238. Kompaniyets, L. Body Mass Index and Risk for COVID-19–Related Hospitalization, Intensive Care Unit Admission, Invasive Mechanical Ventilation, and Death — United States, March–December 2020. *MMWR Morb Mortal Wkly Rep* **70**, (2021).

239. Javalkar, K. *et al.* Socioeconomic and Racial and/or Ethnic Disparities in Multisystem Inflammatory Syndrome. *Pediatrics* **147**, e2020039933 (2021).

240. Broad, J. *et al.* Post-COVID-19 paediatric inflammatory multisystem syndrome: association of ethnicity, key worker and socioeconomic status with risk and severity. *Archives of Disease in Childhood* **106**, 1218–1225 (2021).

241. Abuhammour, W. *et al.* Genetic and Clinical Characteristics of Patients in the Middle East With Multisystem Inflammatory Syndrome in Children. *JAMA Network Open* **5**, e2214985 (2022).

242. Lee, P. Y. *et al.* Immune dysregulation and multisystem inflammatory syndrome in children (MIS-C) in individuals with haploinsufficiency of SOCS1. *J Allergy Clin Immunol* **146**, 1194-1200.e1 (2020).

243. Chou, J. *et al.* Mechanisms underlying genetic susceptibility to multisystem inflammatory syndrome in children (MIS-C). *Journal of Allergy and Clinical Immunology* **148**, 732-738.e1 (2021).

244. Lee, D. *et al.* Inborn errors of OAS–RNase L in SARS-CoV-2–related multisystem inflammatory syndrome in children. *Science* **379**, eabo3627 (2022).

245. Sobh, A. *et al.* How multisystem inflammatory syndrome in children discriminated from Kawasaki disease: a differentiating score based on an inception cohort study. *Clin Rheumatol* **42**, 1151–1161 (2023).

246. Kostik, M. M. *et al.* Distinguishing Between Multisystem Inflammatory Syndrome, Associated With COVID-19 in Children and the Kawasaki Disease: Development of Preliminary Criteria Based on the Data of the Retrospective Multicenter Cohort Study. *Frontiers in Pediatrics* **9**, (2021).

247. Clark, M. T. *et al.* A Diagnostic Prediction Model to Distinguish Multisystem Inflammatory Syndrome in Children. *ACR Open Rheumatology* **4**, 1050–1059 (2022).

248. Tibshirani, R. Regression Shrinkage and Selection via the Lasso. *Journal of the Royal Statistical Society. Series B (Methodological)* **58**, 267–288 (1996).

249. Godfred-Cato, S. *et al.* Distinguishing Multisystem Inflammatory Syndrome in Children From COVID-19, Kawasaki Disease and Toxic Shock Syndrome. *Pediatr Infect Dis J* **41**, 315–323 (2022).

250. Lam, J. Y. *et al.* A machine-learning algorithm for diagnosis of multisystem inflammatory syndrome in children and Kawasaki disease in the USA: a retrospective model development and validation study. *The Lancet Digital Health* **4**, e717–e726 (2022).

251. Lam, J. Y. *et al.* Implementation of KIDMATCH: A Clinical Decision Support Tool for Diagnosing Pediatric Patients with Multisystem Inflammatory Syndrome and Kawasaki Disease. *AMIA Annual Symposium Proceedings* **2022**, 653 (2022).

252. Rey-Jurado, E. *et al.* Deep immunophenotyping reveals biomarkers of multisystemic inflammatory syndrome in children in a Latin American cohort. *Journal of Allergy and Clinical Immunology* **150**, 1074-1085.e11 (2022).

253. Gonçalves, G. S. *et al.* Circulating sTREM-1 as a predictive biomarker of pediatric multisystemic inflammatory syndrome (MIS-C). *Cytokine* **161**, 156084 (2023).

254. Rajamanickam, A. *et al.* Unique cellular immune signatures of multisystem inflammatory syndrome in children. *PLOS Pathogens* **18**, e1010915 (2022).

255. Karagol, C. *et al.* Delta neutrophil index and C-reactive protein: a potential diagnostic marker of multisystem inflammatory syndrome in children (MIS-C) with COVID-19. *Eur J Pediatr* **181**, 775–781 (2022).

256. Loy, C. J. *et al.* Nucleic acid biomarkers of immune response and cell and tissue damage in children with COVID-19 and MIS-C. *CR Med* **4**, (2023).

257. Jackson, H. R. *et al.* Diagnosis of Multisystem Inflammatory Syndrome in Children by a Whole-Blood Transcriptional Signature. *Journal of the Pediatric Infectious Diseases Society* piad035 (2023) doi:10.1093/jpids/piad035.

258. Maltz-Matyschsyk, M. *et al.* Development of a biomarker signature using grating-coupled fluorescence plasmonic microarray for diagnosis of MIS-C. *Frontiers in Bioengineering and Biotechnology* **11**, (2023).

259. Zhao, Y., Yin, L., Patel, J., Tang, L. & Huang, Y. The inflammatory markers of multisystem inflammatory syndrome in children (MIS-C) and adolescents associated with COVID-19: A meta-analysis. *Journal of Medical Virology* **93**, 4358–4369 (2021).

260. Karunakar, P. *et al.* Clinical profile and outcomes of multisystem inflammatory syndrome in children (MIS-C): Hospital-based prospective observational study from a tertiary care hospital in South India. *J Paediatr Child Health* **58**, 1964–1971 (2022).

261. Cetin, B. S. *et al.* Evaluation of Baseline Characteristics and Prognostic Factors in Multisystemic Inflammatory Syndrome in Children: Is It Possible to Foresee the Prognosis in the First Step? *Journal of Clinical Medicine* **11**, 4615 (2022).

262. Merckx, J. *et al.* Predictors of severe illness in children with multisystem inflammatory syndrome after SARS-CoV-2 infection: a multicentre cohort study. *CMAJ* **194**, E513–E523 (2022).

263. Brizuela, M. *et al.* Influence of sex on disease severity in children with COVID-19 and Multisystem Inflammatory Syndrome in Latin America. 2021.02.07.21251212 Preprint at https://doi.org/10.1101/2021.02.07.21251212 (2021).

264. Niño Taravilla, C., Lara Aguilera, N., Zuleta Morales, Y. & Ortiz Fritz, P. PP031 [Infections » Covid-19 / Sars-CoV-2]: OBSERVATIONAL STUDY OF MULTISYSTEM INFLAMMATORY SYNDROME IN CHILDREN (MIS-C) IN A PEDIATRIC INTENSIVE CARE UNIT IN CHILE. ANALYSIS OF PREDICTIVE FACTORS OF SEVERITY. *Pediatric Critical Care Medicine* **23**, (2022).

265. Abrams, J. Y. *et al.* Factors linked to severe outcomes in multisystem inflammatory syndrome in children (MIS-C) in the USA: a retrospective surveillance study. *Lancet Child Adolesc Health* **5**, 323–331 (2021).

266. Varga, P. *et al.* Multicolored MIS-C, a single-centre cohort study. *BMC Pediatrics* **23**, 190 (2023).

267. Zengin, N. *et al.* Serum Vitamin D Levels in Relation to Development of Multisystem Inflammatory Syndrome in Pediatric COVID-19. *J Pediatr Infect Dis* **17**, 308–316 (2022).

268. McAree, D. *et al.* Clinical Predictors of Subacute Myocardial Dysfunction in Multisystem Inflammatory Syndrome in Children (MIS-C) Associated with COVID-19. *Pediatr Cardiol* 1–12 (2022) doi:10.1007/s00246-022-03021-9.

269. Fernandes, D. M. *et al.* Severe Acute Respiratory Syndrome Coronavirus 2 Clinical Syndromes and Predictors of Disease Severity in Hospitalized Children and Youth. *J Pediatr* **230**, 23-31.e10 (2021).

270. Snipaitiene, A., Sirataviciene, A., Varoneckaite, L., Sileikiene, R. & Jankauskaite, L. Platelet role in the prediction of MIS-C severity. *Front Pediatr* **11**, 1153623 (2023).

271. Sık, G. *et al.* Mortality risk factors among critically ill children with MIS-C in PICUs: a multicenter study. *Pediatr Res* 1–8 (2023) doi:10.1038/s41390-023-02518-0.

272. Kaidar, K. *et al.* Risk factors for haemodynamic compromise in multisystem inflammatory syndrome in children-a multicentre retrospective study. *Rheumatology (Oxford)* keac692 (2022) doi:10.1093/rheumatology/keac692.

273. Tibi, R. *et al.* Emergency department levels of NT-proBNP and inotropic/vasoactive support in multi-inflammatory syndrome in children (MIS-C). *Am J Emerg Med* **56**, 296–297 (2022).

274. Abraham, A. *et al.* OP039 [Combined Organ Systems » Other]: PREDICTIVE FACTORS FOR PICU ADMISSION IN PATIENTS WITH MIS-C. *Pediatric Critical Care Medicine* **23**, (2022).

275. Mamishi, S. *et al.* Multisystem inflammatory syndrome associated with SARS-CoV-2 infection in children: update and new insights from the second report of an Iranian referral hospital. *Epidemiology & Infection* **150**, e179 (2022).

276. Savorgnan, F. *et al.* Physiologic profile associated with severe multisystem inflammatory syndrome in children: a retrospective study. *Pediatr Res* **93**, 102–109 (2023).

277. Güllü, U. U., İpek, S., Güngör, Ş., Yurttutan, S. & Demiray, Ş. Haematological parameters predicting cardiac involvement in children with COVID-19 infection. *Journal of Paediatrics and Child Health* **58**, 2236–2242 (2022).

278. de Cevins, C. *et al.* A monocyte/dendritic cell molecular signature of SARS-CoV-2-related multisystem inflammatory syndrome in children with severe myocarditis. *Med (N Y)* **2**, 1072-1092.e7 (2021).

279. Levin, M. Childhood Multisystem Inflammatory Syndrome — A New Challenge in the Pandemic. *New England Journal of Medicine* **383**, 393–395 (2020).

280. Carter, M. J. *et al.* Peripheral immunophenotypes in children with multisystem inflammatory syndrome associated with SARS-CoV-2 infection. *Nature Medicine* **26**, 1701–1707 (2020).

281. Diorio, C. *et al.* Multisystem inflammatory syndrome in children and COVID-19 are distinct presentations of SARS–CoV-2. *J Clin Invest* **130**, 5967–5975 (2020).

282. Jiang, L. *et al.* COVID-19 and multisystem inflammatory syndrome in children and adolescents. *The Lancet Infectious Diseases* **20**, e276–e288 (2020).

283. Gruber, C. N. *et al.* Mapping Systemic Inflammation and Antibody Responses in Multisystem Inflammatory Syndrome in Children (MIS-C). *Cell* **183**, 982-995.e14 (2020).

284. Ramaswamy, A. *et al.* Immune dysregulation and autoreactivity correlate with disease severity in SARS-CoV-2-associated multisystem inflammatory syndrome in children. *Immunity* **54**, 1083-1095.e7 (2021).

285. Boribong, B. P. *et al.* Neutrophil profiles of pediatric COVID-19 and multisystem inflammatory syndrome in children. *CR Med* **3**, (2022).

286. Patel, H., McArdle, A., Seaby, E., Levin, M. & Whittaker, E. The immunopathogenesis of SARS-CoV-2 infection in children: diagnostics, treatment and prevention. *Clinical & Translational Immunology* **11**, e1405 (2022).

287. Consiglio, C. R. *et al.* The Immunology of Multisystem Inflammatory Syndrome in Children with COVID-19. *Cell* **183**, 968-981.e7 (2020).

288. Esteve-Sole, A. *et al.* Similarities and differences between the immunopathogenesis of COVID-19–related pediatric multisystem inflammatory syndrome and Kawasaki disease. *J Clin Invest* **131**, (2021).

289. Venkataraman, A. *et al.* Plasma biomarker profiling of PIMS-TS, COVID-19 and SARS-CoV2 seropositive children – a cross-sectional observational study from southern India. *EBioMedicine* **66**, (2021).

290. Diaz, F. *et al.* Comparison of Interleukin-6 Plasma Concentration in Multisystem Inflammatory Syndrome in Children Associated With SARS-CoV-2 and Pediatric Sepsis. *Front Pediatr* **9**, 756083 (2021).

291. Pathan, N., Sandiford, C., Harding, S. E. & Levin, M. Characterization of a myocardial depressant factor in meningococcal septicemia. *Crit Care Med* **30**, 2191–2198 (2002).

292. Pathan, N. *et al.* Myocardial depressant effects of interleukin 6 in meningococcal sepsis are regulated by p38 mitogen-activated protein kinase*. *Critical Care Medicine* **39**, 1692 (2011).

293. Yonker, L. M. *et al.* Multisystem inflammatory syndrome in children is driven by zonulin-dependent loss of gut mucosal barrier. *J Clin Invest* **131**, (2021).

294. Bartsch, Y. C. *et al.* Humoral signatures of protective and pathological SARS-CoV-2 infection in children. *Nat Med* **27**, 454–462 (2021).

295. Vella, L. A. *et al.* Deep immune profiling of MIS-C demonstrates marked but transient immune activation compared to adult and pediatric COVID-19. *Sci Immunol* **6**, eabf7570 (2021).

296. Myles, A., Gearhart, P. J. & Cancro, M. P. Signals that drive T-bet expression in B cells. *Cell Immunol* **321**, 3–7 (2017).

297. Barnett, B. E. *et al.* Cutting Edge: B Cell–Intrinsic T-bet Expression Is Required To Control Chronic Viral Infection. *The Journal of Immunology* **197**, 1017–1022 (2016).

298. Rubtsova, K. *et al.* B cells expressing the transcription factor T-bet drive lupus-like autoimmunity. *J Clin Invest* **127**, 1392–1404 (2017).

299. Pfeifer, J. *et al.* Autoantibodies against interleukin-1 receptor antagonist in multisystem inflammatory syndrome in children: a multicentre, retrospective, cohort study. *Lancet Rheumatol* **4**, e329–e337 (2022).

300. Menikou, S., Langford, P. R. & Levin, M. Kawasaki Disease: The Role of Immune Complexes Revisited. *Front. Immunol.* **10**, (2019).

301. Mason, W. H., Jordan, S. C., Sakai, R., Takahashi, M. & Bernstein, B. Circulating immune complexes in Kawasaki syndrome. *The Pediatric Infectious Disease Journal* **4**, 48–51 (1985).

302. Ono, S., Onimaru, T., Kawakami, K., Hokonohara, M. & Miyata, K. Impaired granulocyte chemotaxis and increased circulating immune complexes in Kawasaki disease. *J Pediatr* **106**, 567–570 (1985).

303. Levin, M. *et al.* Platelet immune complex interaction in pathogenesis of Kawasaki disease and childhood polyarteritis. *Br Med J (Clin Res Ed)* **290**, 1456–1460 (1985).

304. Onouchi, Y. The genetics of Kawasaki disease. *Int J Rheum Dis* **21**, 26–30 (2018).

305. Jafarzadeh, A., Jafarzadeh, S., Nozari, P., Mokhtari, P. & Nemati, M. Lymphopenia an important immunological abnormality in patients with COVID-19: Possible mechanisms. *Scandinavian Journal of Immunology* **93**, e12967 (2021).

306. Cotugno, N. *et al.* Virological and immunological features of SARS-CoV-2-infected children who develop neutralizing antibodies. *Cell Rep* **34**, 108852 (2021).

307. McCormick, J. K., Yarwood, J. M. & Schlievert, P. M. Toxic Shock Syndrome and Bacterial Superantigens: An Update. *Annual Review of Microbiology* **55**, 77–104 (2001).

308. Deacy, A. M., Gan, S. K.-E. & Derrick, J. P. Superantigen Recognition and Interactions: Functions, Mechanisms and Applications. *Frontiers in Immunology* **12**, (2021).

309. Cheng, M. H. *et al.* Superantigenic character of an insert unique to SARS-CoV-2 spike supported by skewed TCR repertoire in patients with hyperinflammation. *Proc Natl Acad Sci U S A* **117**, 25254–25262 (2020).

310. Porritt, R. A. *et al.* Identification of a unique TCR repertoire, consistent with a superantigen selection process in Children with Multi-system Inflammatory Syndrome. *bioRxiv* 2020.11.09.372169 (2020) doi:10.1101/2020.11.09.372169.

311. Porritt, R. A. *et al.* HLA class I-associated expansion of TRBV11-2 T cells in multisystem inflammatory syndrome in children. *J Clin Invest* **131**, 146614 (2021).

312. Amormino, C. *et al.* SARS-CoV-2 Spike Does Not Possess Intrinsic Superantigen-like Inflammatory Activity. *Cells* **11**, 2526 (2022).

313. Burns, J. C. MIS-C: myths have been debunked, but mysteries remain. *Nat Rev Rheumatol* **19**, 70–71 (2023).

314. Moreews, M. *et al.* Polyclonal expansion of TCR Vbeta 21.3+ CD4+ and CD8+ T cells is a hallmark of Multisystem Inflammatory Syndrome in Children. *Sci Immunol* **6**, eabh1516 (2021).

315. Swank, Z. *et al.* Persistent Circulating Severe Acute Respiratory Syndrome Coronavirus 2 Spike Is Associated With Post-acute Coronavirus Disease 2019 Sequelae. *Clinical Infectious Diseases* **76**, e487–e490 (2023).

316. Wang, W., Uzzau, S., Goldblum, S. E. & Fasano, A. Human zonulin, a potential modulator of intestinal tight junctions. *Journal of Cell Science* **113**, 4435–4440 (2000).

317. Sigal, G. B. *et al.* Measurement of Severe Acute Respiratory Syndrome Coronavirus 2 Antigens in Plasma of Pediatric Patients With Acute Coronavirus Disease 2019 or Multisystem Inflammatory Syndrome in Children Using an Ultrasensitive and Quantitative Immunoassay. *Clin Infect Dis* **75**, 1351–1358 (2022).

318. Harwood, R. *et al.* A national consensus management pathway for paediatric inflammatory multisystem syndrome temporally associated with COVID-19 (PIMS-TS): results of a national Delphi process. *The Lancet Child & Adolescent Health* **5**, 133–141 (2021).

319. Son, M. B. F. *et al.* Multisystem Inflammatory Syndrome in Children — Initial Therapy and Outcomes. *New England Journal of Medicine* **385**, 23–34 (2021).

320. McArdle, A. J. *et al.* Treatment of Multisystem Inflammatory Syndrome in Children. *New England Journal of Medicine* **385**, 11–22 (2021).

321. Channon-Wells, S. *et al.* Immunoglobulin, glucocorticoid, or combination therapy for multisystem inflammatory syndrome in children: a propensity-weighted cohort study. *The Lancet Rheumatology* **5**, e184–e199 (2023).

322. Ouldali, N. *et al.* Association of Intravenous Immunoglobulins Plus Methylprednisolone vs Immunoglobulins Alone With Course of Fever in Multisystem Inflammatory Syndrome in Children. *JAMA* **325**, 855 (2021).

323. Welzel, T. *et al.* Methylprednisolone versus intravenous immunoglobulins in children with paediatric inflammatory multisystem syndrome temporally associated with SARS-CoV-2 (PIMS-TS): an open-label, multicentre, randomised trial. *Lancet Child Adolesc Health* **7**, 238–248 (2023).

324. Welcome — RECOVERY Trial. https://www.recoverytrial.net/.

325. Faust, S. N. *et al.* Immunomodulatory therapy in children with paediatric inflammatory multisystem syndrome temporally associated with SARS-CoV-2 (PIMS-TS, MIS-C; RECOVERY): a randomised, controlled, open-label, platform trial. *The Lancet Child & Adolescent Health* **8**, 190–200 (2024).

326. Jain, S., He, F., Brown, K., Burns, J. C. & Tremoulet, A. H. Multisystem Inflammatory Syndrome therapies in children (MISTIC): A randomized trial. *Contemporary Clinical Trials Communications* **32**, 101060 (2023).

327. Davies, P., du Pré, P., Lillie, J. & Kanthimathinathan, H. K. One-Year Outcomes of Critical Care Patients Post–COVID-19 Multisystem Inflammatory Syndrome in Children. *JAMA Pediatrics* **175**, 1281–1283 (2021).

328. Farooqi, K. M. *et al.* Longitudinal Outcomes for Multisystem Inflammatory Syndrome in Children. *Pediatrics* **148**, e2021051155 (2021).

329. Penner, J. *et al.* 6-month multidisciplinary follow-up and outcomes of patients with paediatric inflammatory multisystem syndrome (PIMS-TS) at a UK tertiary paediatric hospital: a retrospective cohort study. *The Lancet Child & Adolescent Health* **5**, 473–482 (2021).

330. Capone, C. A. *et al.* Six Month Follow-up of Patients With Multi-System Inflammatory Syndrome in Children. *Pediatrics* **148**, e2021050973 (2021).

331. Cantarutti, N. *et al.* Long-Term Cardiovascular Outcome in Children with MIS-C Linked to SARS-CoV-2 Infection—An Italian Multicenter Experience. *Biology (Basel)* **11**, 1474 (2022).

332. Chakraborty, A. *et al.* Long-Term Cardiovascular Outcomes of Multisystem Inflammatory Syndrome in Children Associated with COVID-19 Using an Institution Based Algorithm. *Pediatr Cardiol* **44**, 367–380 (2023).

333. Marshall, M. *et al.* Symptomatic Acute Myocarditis in 7 Adolescents After Pfizer-BioNTech COVID-19 Vaccination. *Pediatrics* **148**, e2021052478 (2021).

334. Barda, N. *et al.* Safety of the BNT162b2 mRNA Covid-19 Vaccine in a Nationwide Setting. *N Engl J Med* **385**, 1078–1090 (2021).

335. Ammirati, E. *et al.* Temporal relation between second dose BNT162b2 mRNA Covid-19 vaccine and cardiac involvement in a patient with previous SARS-COV-2 infection. *Int J Cardiol Heart Vasc* **34**, 100774 (2021).

336. Abu Mouch, S. *et al.* Myocarditis following COVID-19 mRNA vaccination. *Vaccine* **39**, 3790–3793 (2021).

337. Klein, N. P. *et al.* Surveillance for Adverse Events After COVID-19 mRNA Vaccination. *JAMA* **326**, 1390–1399 (2021).

338. de Meester, A., Luwaert, R. & Chaudron, J. M. Symptomatic pericarditis after influenza vaccination: report of two cases. *Chest* **117**, 1803–1805 (2000).

339. Keinath, K., Church, T., Kurth, B. & Hulten, E. Myocarditis secondary to smallpox vaccination. *BMJ Case Rep* **2018**, bcr2017223523 (2018).

340. Oster, M. E. *et al.* Myocarditis Cases Reported After mRNA-Based COVID-19 Vaccination in the US From December 2020 to August 2021. *JAMA* **327**, 331–340 (2022).

341. Husby, A. *et al.* SARS-CoV-2 vaccination and myocarditis or myopericarditis: population based cohort study. *BMJ* **375**, e068665 (2021).

342. Gao, J. *et al.* A Systematic Review and Meta-analysis of the Association Between SARS-CoV-2 Vaccination and Myocarditis or Pericarditis. *Am J Prev Med* **64**, 275–284 (2023).

343. Pillay, J. *et al.* Incidence, risk factors, natural history, and hypothesised mechanisms of myocarditis and pericarditis following covid-19 vaccination: living evidence syntheses and review. *BMJ* **378**, e069445 (2022).

344. Ahmed, S. K. *et al.* Global reports of myocarditis following COVID-19 vaccination: A systematic review and meta-analysis. *Diabetes Metab Syndr* **16**, 102513 (2022).

345. Fatima, M. *et al.* Development of myocarditis and pericarditis after COVID-19 vaccination in adult population: A systematic review. *Annals of Medicine and Surgery* **76**, 103486 (2022).

346. Lee, A. S. Y. *et al.* Myocarditis Following COVID-19 Vaccination: A Systematic Review (October 2020–October 2021). *Heart, Lung and Circulation* **31**, 757–765 (2022).

347. Hadley, S. M. *et al.* Follow-up cardiac magnetic resonance in children with vaccine-associated myocarditis. *Eur J Pediatr* **181**, 2879–2883 (2022).

348. Vojdani, A. & Kharrazian, D. Potential antigenic cross-reactivity between SARS-CoV-2 and human tissue with a possible link to an increase in autoimmune diseases. *Clinical Immunology* **217**, 108480 (2020).

349. Heymans, S. & Cooper, L. T. Myocarditis after COVID-19 mRNA vaccination: clinical observations and potential mechanisms. *Nat Rev Cardiol* **19**, 75–77 (2022).

350. Switzer, C. & Loeb, M. Evaluating the relationship between myocarditis and mRNA vaccination. *Expert Rev Vaccines* **21**, 83–89 (2022).

351. Bozkurt, B., Kamat, I. & Hotez, P. J. Myocarditis With COVID-19 mRNA Vaccines. *Circulation* **144**, 471–484 (2021).

352. Yonker, L. M. *et al.* Circulating Spike Protein Detected in Post–COVID-19 mRNA Vaccine Myocarditis. *Circulation* **0**,.

353. Frustaci, A. *et al.* Hypersensitivity Myocarditis after COVID-19 mRNA Vaccination. *J Clin Med* **11**, 1660 (2022).

354. Kimura, M. *et al.* Fulminant necrotizing eosinophilic myocarditis after COVID-19 vaccination survived with mechanical circulatory support. *ESC Heart Fail* **9**, 2732–2737 (2022).

355. Kounis, N. G., Koniari, I., Mplani, V., Plotas, P. & Velissaris, D. Hypersensitivity Myocarditis and the Pathogenetic Conundrum of COVID-19 Vaccine-Related Myocarditis. *Cardiology* 1–3 (2022) doi:10.1159/000524224.

356. Salciccia, S. *et al.* Testosterone target therapy: focus on immune response, controversies and clinical implications in patients with COVID-19 infection. *Ther Adv Endocrinol Metab* **12**, 20420188211010105 (2021).

357. Voleti, N., Reddy, S. P. & Ssentongo, P. Myocarditis in SARS-CoV-2 infection vs. COVID-19 vaccination: A systematic review and meta-analysis. *Frontiers in Cardiovascular Medicine* **9**, (2022).

358. Abraham, N. *et al.* Myocarditis and/or pericarditis risk after mRNA COVID-19 vaccination: A Canadian head to head comparison of BNT162b2 and mRNA-1273 vaccines. *Vaccine* **40**, 4663 (2022).

359. Mahase, E. Covid-19: Vulnerable children aged 12-15 will be offered Pfizer vaccine, UK announces. *BMJ* **374**, n1841 (2021).

360. Gellad, W. F. Myocarditis after vaccination against covid-19. *BMJ* **375**, n3090 (2021).

361. Worku, D. Multisystem Inflammatory Syndrome in Adults (MIS-A) and SARS-CoV2: An Evolving Relationship. *BioMed* **3**, 195–201 (2023).

362. Yousaf, A. R. *et al.* Reported cases of multisystem inflammatory syndrome in children aged 12–20 years in the USA who received a COVID-19 vaccine, December, 2020, through August, 2021: a surveillance investigation. *The Lancet Child & Adolescent Health* **6**, 303–312 (2022).

363. Ouldali, N. *et al.* Hyper inflammatory syndrome following COVID-19 mRNA vaccine in children: A national post-authorization pharmacovigilance study. *The Lancet Regional Health – Europe* **17**, (2022).

364. Levy, M. *et al.* Multisystem Inflammatory Syndrome in Children by COVID-19 Vaccination Status of Adolescents in France. *JAMA* **327**, 281–283 (2022).

365. Zambrano, L. D. Effectiveness of BNT162b2 (Pfizer-BioNTech) mRNA Vaccination Against Multisystem Inflammatory Syndrome in Children Among Persons Aged 12–18 Years — United States, July–December 2021. *MMWR Morb Mortal Wkly Rep* **71**, (2022).

366. Davis, H. E., McCorkell, L., Vogel, J. M. & Topol, E. J. Long COVID: major findings, mechanisms and recommendations. *Nat Rev Microbiol* **21**, 133–146 (2023).

367. Michelen, M. *et al.* Characterising long COVID: a living systematic review. *BMJ Global Health* **6**, e005427 (2021).

368. Coronavirus » Post-COVID syndrome (long COVID). https://www.england.nhs.uk/coronavirus/post-covid-syndrome-long-covid/.

369. DIAMONDS: Personalised Molecular Testing For Serious Illness. *DIAMONDS* https://www.diamonds2020.eu/.

370. Diagnosis, Treatment, and Long-Term Management of Kawasaki Disease: A Scientific Statement for Health Professionals From the American Heart Association | Circulation. https://www.ahajournals.org/doi/10.1161/CIR.0000000000000484.

371. Nijman, R. G. *et al.* A Novel Framework for Phenotyping Children With Suspected or Confirmed Infection for Future Biomarker Studies. *Front Pediatr* **9**, 688272 (2021).

372. https://bestavailabletreatmentstudy.co.uk/. https://bestavailabletreatmentstudy.co.uk/.

373. Harris, P. A. *et al.* Research electronic data capture (REDCap)—A metadata-driven methodology and workflow process for providing translational research informatics support. *Journal of Biomedical Informatics* **42**, 377–381 (2009).

374. Davis, D. *et al.* The delirium and population health informatics cohort study protocol: ascertaining the determinants and outcomes from delirium in a whole population. *BMC Geriatrics* **18**, 45 (2018).

375. Delirium and Population Health Informatics Cohort (DELPHIC) Study. *Health Research Authority* https://www.hra.nhs.uk/planning-and-improving-research/application-summaries/research-summaries/delirium-and-population-health-informatics-cohort-delphic-study/.

376. About | Perform. https://www.perform2020.org/about.

377. Home | EUCLIDS. https://www.euclids-project.eu/.

378. World Health Organization. Diagnostic Imaging and Laboratory Technology. *Use of Anticoagulants in Diagnostic Laboratory Investigations*. https://apps.who.int/iris/handle/10665/65957 (2002).

379. McKinnon, K. M. Flow Cytometry: An Overview. *Curr Protoc Immunol* **120**, 5.1.1-5.1.11 (2018).

380. Flow cytometry introduction | Abcam. https://www.abcam.com/protocols/introduction-to-flow-cytometry#measurement%20of%20scsattered%20light%20and%20fluorescence.

381. Fact Sheets | Testing & Diagnosis | Fact Sheet - Recommendations for Human Immunodeficiency... Clinics | TB | CDC. https://www.cdc.gov/tb/publications/factsheets/testing/igra.htm (2022).
382. QuantiFERON SARS-CoV-2 Starter Set Blood Collection Tubes Instructions for Use (Handbook) - QIAGEN. https://www.qiagen.com/gb/resources/resourcedetail?id=2a36a234-bfde-45f4-ae08-7c28ef95df7b&lang=en.
383. Kay, A. W., Strauss-Albee, D. M. & Blish, C. A. Application of Mass Cytometry (CyTOF) for Functional and Phenotypic Analysis of Natural Killer Cells. *Methods Mol Biol* **1441**, 13–26 (2016).
384. Iyer, A., Hamers, A. A. J. & Pillai, A. B. CyTOF® for the Masses. *Frontiers in Immunology* **13**, (2022).
385. Fish, M. *et al.* Utilising mass cytometry with CD45 barcoding and standardised leucocyte phenotyping for immune trajectory assessment in critically ill patients. *Br J Anaesth* **126**, e149–e152 (2021).
386. Schuyler, R. P. *et al.* Minimizing Batch Effects in Mass Cytometry Data. *Frontiers in Immunology* **10**, (2019).
387. Kukurba, K. R. & Montgomery, S. B. RNA Sequencing and Analysis. *Cold Spring Harb Protoc* **2015**, 951–969 (2015).
388. R Core Team. R: A Language and Environment for Statistical Computing. R Foundation for Statistical Computing (2022).
389. Posit. *Posit* https://www.posit.co/.
390. Home - GraphPad. https://www.graphpad.com/.
391. Docherty, A. B. *et al.* Features of 20 133 UK patients in hospital with covid-19 using the ISARIC WHO Clinical Characterisation Protocol: prospective observational cohort study. *BMJ* **369**, m1985 (2020).
392. Götzinger, F. *et al.* COVID-19 in children and adolescents in Europe: a multinational, multicentre cohort study. *The Lancet Child & Adolescent Health* **4**, 653–661 (2020).

393. Benjamini, Y. & Hochberg, Y. Controlling the False Discovery Rate: A Practical and Powerful Approach to Multiple Testing. *Journal of the Royal Statistical Society. Series B (Methodological)* **57**, 289–300 (1995).

394. A minimal common outcome measure set for COVID-19 clinical research. *Lancet Infect Dis* **20**, e192–e197 (2020).

395. Wiersinga, W. J., Rhodes, A., Cheng, A. C., Peacock, S. J. & Prescott, H. C. Pathophysiology, Transmission, Diagnosis, and Treatment of Coronavirus Disease 2019 (COVID-19): A Review. *JAMA* **324**, 782–793 (2020).

396. Arvin, A. M. *et al.* A perspective on potential antibody-dependent enhancement of SARS-CoV-2. *Nature* **584**, 353–363 (2020).

397. Hoste, L., Van Paemel, R. & Haerynck, F. Multisystem inflammatory syndrome in children related to COVID-19: a systematic review. *Eur J Pediatr* 1–16 (2021) doi:10.1007/s00431-021-03993-5.

398. Seery, V. *et al.* Blood neutrophils from children with COVID-19 exhibit both inflammatory and anti-inflammatory markers. *EBioMedicine* **67**, 103357 (2021).

399. Guzman, M. G. & Vazquez, S. The Complexity of Antibody-Dependent Enhancement of Dengue Virus Infection. *Viruses* **2**, 2649–2662 (2010).

400. Teo, A., Tan, H. D., Loy, T., Chia, P. Y. & Chua, C. L. L. Understanding antibody-dependent enhancement in dengue: Are afucosylated IgG1s a concern? *PLoS Pathog* **19**, e1011223 (2023).

401. Bournazos, S., Gupta, A. & Ravetch, J. V. The role of IgG Fc receptors in antibody-dependent enhancement. *Nat Rev Immunol* **20**, 633–643 (2020).

402. Gruber, C. N. Mapping Systemic Inflammation and Antibody Responses in Multisystem Inflammatory Syndrome in Children (MIS-C). 29.

403. Anderson, E. M. *et al.* SARS-CoV-2 antibody responses in children with MIS-C and mild and severe COVID-19. *J Pediatric Infect Dis Soc* piaa161 (2020) doi:10.1093/jpids/piaa161.

404. Licciardi, F. *et al.* SARS-CoV-2-Induced Kawasaki-Like Hyperinflammatory Syndrome: A Novel COVID Phenotype in Children. *Pediatrics* **146**, e20201711 (2020).

405. Verdoni, L. *et al.* An outbreak of severe Kawasaki-like disease at the Italian epicentre of the SARS-CoV-2 epidemic: an observational cohort study. *The Lancet* **395**, 1771–1778 (2020).

406. Cheung, E. W. *et al.* Multisystem Inflammatory Syndrome Related to COVID-19 in Previously Healthy Children and Adolescents in New York City. *JAMA* **324**, 294–296 (2020).

407. Youden, W. J. Index for rating diagnostic tests. *Cancer* **3**, 32–35 (1950).

408. Antibody testing for SARS-CoV-2: key information. *GOV.UK* https://www.gov.uk/government/publications/antibody-testing-for-sars-cov-2-key-information/antibody-testing-for-sars-cov-2-information-for-general-practitioners.

409. Rostad, C. A. *et al.* Serology in Children with Multisystem Inflammatory Syndrome (MIS-C) associated with COVID-19. 2020.07.10.20150755 Preprint at https://doi.org/10.1101/2020.07.10.20150755 (2020).

410. Feldstein, L. R. *et al.* Characteristics and Outcomes of US Children and Adolescents With Multisystem Inflammatory Syndrome in Children (MIS-C) Compared With Severe Acute COVID-19. *JAMA* **325**, 1074 (2021).

411. Kay, J. & Upchurch, K. S. ACR/EULAR 2010 rheumatoid arthritis classification criteria. *Rheumatology* **51**, vi5–vi9 (2012).

412. Fine, A. M., Nizet, V. & Mandl, K. D. Large-scale validation of the Centor and McIsaac scores to predict group A streptococcal pharyngitis. *Arch Intern Med* **172**, 847–852 (2012).

413. Dhaliwal, M. *et al.* Severity and Cardiac Involvement in Multisystem Inflammatory Syndrome in Children. *Indian J Pediatr* **89**, 1040–1044 (2022).

414. Sperotto, F. *et al.* Cardiac manifestations in SARS-CoV-2-associated multisystem inflammatory syndrome in children: a comprehensive review and proposed clinical approach. *Eur J Pediatr* 1–16 (2020) doi:10.1007/s00431-020-03766-6.

415. de Graeff, N. *et al.* European consensus-based recommendations for the diagnosis and treatment of Kawasaki disease - the SHARE initiative. *Rheumatology (Oxford)* **58**, 672–682 (2019).

416. Eleftheriou, D. *et al.* Management of Kawasaki disease. *Arch Dis Child* **99**, 74–83 (2014).

417. McCrindle, B. W. *et al.* Diagnosis, Treatment, and Long-Term Management of Kawasaki Disease: A Scientific Statement for Health Professionals From the American Heart Association. *Circulation* **135**, e927–e999 (2017).

418. Zachariah, P. Severity predictors in pediatric SARS-CoV-2 and MIS-C. *The Journal of Pediatrics* **232**, 307–310 (2021).

419. Brisca, G. *et al.* Timely Recognition and Early Multi-Step Antinflammatory Therapy May Prevent ICU Admission of Patients With MIS-C: Proposal for a Severity Score. *Frontiers in Pediatrics* **9**, (2021).

420. World Bank Country and Lending Groups – World Bank Data Help Desk. https://datahelpdesk.worldbank.org/knowledgebase/articles/906519-world-bank-country-and-lending-groups.

421. Lopez, L. *et al.* Pediatric Heart Network Echocardiographic Z-Scores: Comparison to Other Published Models. *J Am Soc Echocardiogr* **34**, 185–192 (2021).

422. Levin, M. *et al.* Effects of saline or albumin fluid bolus in resuscitation: evidence from re-analysis of the FEAST trial. *The Lancet Respiratory Medicine* **7**, 581–593 (2019).

423. Romanelli, D. & Farrell, M. W. AVPU Score. in *StatPearls* (StatPearls Publishing, Treasure Island (FL), 2023).

424. Reference Ranges | MCQ writing for the MRCPCH. https://www.rcpch.ac.uk/sites/default/files/rcpch/HTWQ/reference_ranges.html.

425. Yasuhara, J., Watanabe, K., Takagi, H., Sumitomo, N. & Kuno, T. COVID-19 and multisystem inflammatory syndrome in children: A systematic review and meta-analysis. *Pediatr Pulmonol* **56**, 837–848 (2021).

426. Ingersoll, M. A. Sex differences shape the response to infectious diseases. *PLoS Pathog* **13**, e1006688 (2017).

427. Jacobsen, H. & Klein, S. L. Sex Differences in Immunity to Viral Infections. *Front Immunol* **12**, 720952 (2021).

428. Mauvais-Jarvis, F. *et al.* Sex and gender: modifiers of health, disease, and medicine. *Lancet* **396**, 565–582 (2020).

429. McCombe, P. A., Hardy, T. A., Nona, R. J. & Greer, J. M. Sex differences in Guillain Barré syndrome, chronic inflammatory demyelinating polyradiculoneuropathy and experimental autoimmune neuritis. *Front Immunol* **13**, 1038411 (2022).

430. Vázquez-Martínez, E. R., García-Gómez, E., Camacho-Arroyo, I. & González-Pedrajo, B. Sexual dimorphism in bacterial infections. *Biology of Sex Differences* **9**, 27 (2018).

431. Lakshminrusimha, S., Hudak, M. L., Dimitriades, V. R. & Higgins, R. D. Multisystem Inflammatory Syndrome in Neonates following Maternal SARS-CoV-2 COVID-19 Infection. *Am J Perinatol* 1166–1171 (2021) doi:10.1055/a-1682-3075.

432. Sil, A., Das, A. & Datta, D. Mucocutaneous manifestations of COVID-19-related multisystem inflammatory syndrome in adults: an update. *Clin Exp Dermatol* **47**, 1774–1780 (2022).

433. McCrindle, B. W. *et al.* SARS-CoV-2 Variants and Multisystem Inflammatory Syndrome in Children. *N Engl J Med* **388**, 1624–1626 (2023).

434. Stierman, B. *et al.* Racial and Ethnic Disparities in Multisystem Inflammatory Syndrome in Children in the United States, March 2020 to February 2021. *The Pediatric Infectious Disease Journal* **40**, e400 (2021).

435. Acevedo, L. *et al.* Mortality and clinical characteristics of multisystem inflammatory syndrome in children (MIS-C) associated with covid-19 in critically ill patients: an observational multicenter study (MISCO study). *BMC Pediatrics* **21**, 516 (2021).

436. Naylor-Wardle, J., Rowland, B. & Kunadian, V. Socioeconomic status and cardiovascular health in the COVID-19 pandemic. *Heart* **107**, 358–365 (2021).

437. Schultz, W. M. *et al.* Socioeconomic Status and Cardiovascular Outcomes. *Circulation* **137**, 2166–2178 (2018).

438. Zhang, Y.-B. *et al.* Associations of healthy lifestyle and socioeconomic status with mortality and incident cardiovascular disease: two prospective cohort studies. *BMJ* **373**, n604 (2021).

439. Turner, D. *et al.* Development, validation, and evaluation of a pediatric ulcerative colitis activity index: a prospective multicenter study. *Gastroenterology* **133**, 423–432 (2007).

440. Straney, L. *et al.* Paediatric index of mortality 3: an updated model for predicting mortality in pediatric intensive care*. *Pediatr Crit Care Med* **14**, 673–681 (2013).

441. Shann, F., Pearson, G., Slater, A. & Wilkinson, K. Paediatric index of mortality (PIM): a mortality prediction model for children in intensive care. *Intensive Care Med* **23**, 201–207 (1997).

442. Kang Heechan *et al.* Abstract 17354: Clinical Outcomes for Children With Paediatric Inflammatory Multisystem Syndrome Temporally Associated With SARS-CoV-2 (PIMS-TS). *Circulation* **142**, A17354–A17354 (2020).

443. Davies, P. *et al.* Association Between Treatments and Short-Term Biochemical Improvements and Clinical Outcomes in Post-Severe Acute Respiratory Syndrome Coronavirus-2 Inflammatory Syndrome. *Pediatric Critical Care Medicine* **22**, e285 (2021).

444. Patel, H. *et al.* Evaluation of Autoantibody Binding to Cardiac Tissue in Multisystem Inflammatory Syndrome in Children and COVID-19 Vaccination–Induced Myocarditis. *JAMA Network Open* **6**, e2314291 (2023).

445. Taweevisit, M., Chindamporn, A., Sujjavorakul, K., Samransamruajkit, R. & Thorner, P. S. Multisystem inflammatory syndrome in children (MIS-C) showing disseminated aspergillosis, cytomegalovirus reactivation and persistent SARS-COV-2: Case report with autopsy review. *Pathology - Research and Practice* **238**, 154106 (2022).

446. Dolhnikoff, M. *et al.* SARS-CoV-2 in cardiac tissue of a child with COVID-19-related multisystem inflammatory syndrome. *The Lancet Child & Adolescent Health* **4**, 790–794 (2020).

447. Duarte-Neto, A. N. *et al.* An autopsy study of the spectrum of severe COVID-19 in children: From SARS to different phenotypes of MIS-C. *eClinicalMedicine* **35**, (2021).

448. Noval Rivas, M., Porritt, R. A., Cheng, M. H., Bahar, I. & Arditi, M. COVID-19-associated multisystem inflammatory syndrome in children (MIS-C): A novel disease that mimics toxic shock syndrome-the superantigen hypothesis. *J Allergy Clin Immunol* **147**, 57–59 (2021).

449. Hsieh, L.-E. *et al.* T Cells in Multisystem Inflammatory Syndrome in Children (MIS-C) Have a Predominant CD4+ T Helper Response to SARS-CoV-2 Peptides and Numerous Virus-Specific CD4- CD8- Double-Negative T Cells. *Int J Mol Sci* **23**, 7219 (2022).

450. Rybkina, K. *et al.* SARS-CoV-2 infection and recovery in children: Distinct T cell responses in MIS-C compared to COVID-19. *J Exp Med* **220**, e20221518 (2023).

451. GeneCards - Human Genes | Gene Database | Gene Search. https://www.genecards.org/.

452. Yamada, A., Arakaki, R., Saito, M., Kudo, Y. & Ishimaru, N. Dual Role of Fas/FasL-Mediated Signal in Peripheral Immune Tolerance. *Frontiers in Immunology* **8**, (2017).

453. Jubel, J. M., Barbati, Z. R., Burger, C., Wirtz, D. C. & Schildberg, F. A. The Role of PD-1 in Acute and Chronic Infection. *Frontiers in Immunology* **11**, (2020).

454. Gurlevik, S. L. *et al.* The difference of the inflammatory milieu in MIS-C and severe COVID-19. *Pediatr Res* **92**, 1805–1814 (2022).

455. Peart Akindele, N. *et al.* Distinct Cytokine and Chemokine Dysregulation in Hospitalized Children With Acute Coronavirus Disease 2019 and Multisystem Inflammatory Syndrome With Similar Levels of Nasopharyngeal Severe Acute Respiratory Syndrome Coronavirus 2 Shedding. *J Infect Dis* **224**, 606–615 (2021).

456. Syrimi, E. *et al.* The immune landscape of SARS-CoV-2-associated Multisystem Inflammatory Syndrome in Children (MIS-C) from acute disease to recovery. *iScience* **24**, 103215 (2021).

457. Jin, W. & Dong, C. IL-17 cytokines in immunity and inflammation. *Emerg Microbes Infect* **2**, e60 (2013).

458. Gaffen, S. L. Structure and signalling in the IL-17 receptor family. *Nat Rev Immunol* **9**, 556–567 (2009).

459. Fossiez, F. *et al.* Interleukin-17. *International Reviews of Immunology* **16**, 541–551 (1998).

460. Neville, L. F., Mathiak, G. & Bagasra, O. The immunobiology of interferon-gamma inducible protein 10 kD (IP-10): A novel, pleiotropic member of the C-X-C chemokine superfamily. *Cytokine & Growth Factor Reviews* **8**, 207–219 (1997).

461. Valiathan, R., Ashman, M. & Asthana, D. Effects of Ageing on the Immune System: Infants to Elderly. *Scandinavian Journal of Immunology* **83**, 255–266 (2016).

462. Bernstein, E. D. & Murasko, D. M. Effect of age on cytokine production in humans. *Age (Omaha)* **21**, 137–151 (1998).

463. Wegner, A. *et al.* Sex differences in the pro-inflammatory cytokine response to endotoxin unfold in vivo but not ex vivo in healthy humans. *Innate Immun* **23**, 432–439 (2017).

464. Boxx, G. M. & Cheng, G. The Roles of Type I Interferon in Bacterial Infection. *Cell Host Microbe* **19**, 760–769 (2016).

465. Carter, M. J., Shankar-Hari, M. & Tibby, S. M. Paediatric Inflammatory Multisystem Syndrome Temporally-Associated with SARS-CoV-2 Infection: An Overview. *Intensive Care Med* **47**, 90–93 (2021).

466. Santos-Oliveira, J. R. *et al.* High levels of T lymphocyte activation in Leishmania-HIV-1 co-infected individuals despite low HIV viral load. *BMC Infectious Diseases* **10**, 358 (2010).

467. Khoruts, A. & Fraser, J. M. A causal link between lymphopenia and autoimmunity. *Immunol Lett* **98**, 23–31 (2005).

468. Sheu, T.-T. & Chiang, B.-L. Lymphopenia, Lymphopenia-Induced Proliferation, and Autoimmunity. *Int J Mol Sci* **22**, 4152 (2021).

469. Kahan, S. M., Wherry, E. J. & Zajac, A. J. T cell exhaustion during persistent viral infections. *Virology* **479–480**, 180–193 (2015).

470. Gumber, D. & Wang, L. D. Improving CAR-T immunotherapy: Overcoming the challenges of T cell exhaustion. *eBioMedicine* **77**, (2022).

471. Jensen, I. J., Sjaastad, F. V., Griffith, T. S. & Badovinac, V. P. Sepsis induced T cell immunoparalysis: the ins and outs of impaired T cell immunity. *J Immunol* **200**, 1543–1553 (2018).

472. Blank, C. U. *et al.* Defining 'T cell exhaustion'. *Nat Rev Immunol* **19**, 665–674 (2019).

473. Saeidi, A. *et al.* T-Cell Exhaustion in Chronic Infections: Reversing the State of Exhaustion and Reinvigorating Optimal Protective Immune Responses. *Front Immunol* **9**, 2569 (2018).

474. Yonker, L. M. *et al.* Multisystem inflammatory syndrome in children is driven by zonulin-dependent loss of gut mucosal barrier. *J Clin Invest* **131**, 149633 (2021).

475. Wykes, M. N. & Lewin, S. R. Immune checkpoint blockade in infectious diseases. *Nat Rev Immunol* **18**, 91–104 (2018).

476. Ai, L. *et al.* Research Status and Outlook of PD-1/PD-L1 Inhibitors for Cancer Therapy. *Drug Des Devel Ther* **14**, 3625–3649 (2020).

477. Hall, M. W. Immune Modulation in Pediatric Sepsis. *J Pediatr Intensive Care* **8**, 42–50 (2019).

478. Chirico, F., da Silva, J. A. T., Tsigaris, P. & Sharun, K. Safety & effectiveness of COVID-19 vaccines: A narrative review. *Indian J Med Res* **155**, 91–104 (2022).

479. Iannizzi, C. *et al.* Convalescent plasma for people with COVID-19: a living systematic review. *Cochrane Database of Systematic Reviews* (2023) doi:10.1002/14651858.CD013600.pub6.

480. Gan, L., Chen, Y., Tan, J., Wang, X. & Zhang, D. Does potential antibody-dependent enhancement occur during SARS-CoV-2 infection after natural infection or vaccination? A meta-analysis. *BMC Infectious Diseases* **22**, 742 (2022).

481. lachlancoin. lachlancoin/fspls: Minimal TB biomarkers. Zenodo https://doi.org/10.5281/zenodo.1488409 (2018).

482. Kwak, B. O. & Eun, B. W. COVID-19 in immunocompromised children and adolescents. *Clin Exp Pediatr* **66**, 182–189 (2023).

Appendix – 1

Table A1-1 Case definitions of MIS-C by the World Health Organisation[204], Centers for Disease Control and Prevention[203] and the Royal College of Paediatrics and Child Health[189].

WHO	Children and adolescents 0 – 19 years of age with fever > 3 days AND two of the following: (a) rash or bilateral non-purulent conjunctivitis or muco-cutaneous inflammation signs; (b) hypotension or shock; (c) features of myocardial dysfunction, pericarditis, valvulitis or coronary abnormalities; (d) evidence of coagulopathy; (e) acute gastrointestinal problems (diarrhoea, vomiting or abdominal pain) AND Elevated markers of inflammation such as ESR, CRP or procalcitonin AND No other obvious microbial cause of inflammation, including bacterial sepsis, staphylococcal or streptococcal shock syndromes AND Evidence of COVID-19 (RT-PCR, antigen test or serology positive) or likely contact with patients with COVID-19
US (CDC)	An individual aged < 21 years presenting with fever, laboratory evidence of inflammation and evidence of clinically severe illness so requiring hospitalisation, with multisystem (≥2) organ involvement AND No alternative plausible diagnoses AND Positive for current or recent SARS-CoV-2 infection by RT-PCR, serology or antigen test; or COVID-19 exposure within the 4 weeks prior to the onset of symptoms
UK (RCPCH)	A child presenting with persistent fever, inflammation (neutrophilia, elevated CRP and lymphopenia) and evidence of single or multi-organ dysfunction (shock, cardiac, respiratory, renal, gastrointestinal or neurological disorder) with additional features. This may include children fulfilling full or partial criteria for Kawasaki disease Exclusion of any other microbial cause, including bacterial sepsis, staphylococcal or streptococcal shock syndromes, infections associated with myocarditis such as enterovirus (waiting for results of these investigations should not delay seeking expert advice) SARS-CoV-2 PCR testing may be positive or negative

Appendix – 2

2.1. IHC optimisation experiments

Optimisation experiments were performed to determine the ideal primary antibody (patient/control serum) and secondary antibody dilutions.

Dilution ratio of secondary antibodies – IgG

Two dilutions of FITC conjugated anti-human IgG (Agilent Technologies, UK) were tested, 1 in 250 and 1 in 400. Due to limited availability of healthy paediatric serum, only serum from healthy vaccinated adults was used for these experiments. One in 100 dilution was used for the primary antibody. On comparison of the FITC signal intensity, no significant differences were observed with the different dilutions of secondary antibody for the PBS control and healthy vaccinated adults (Figure A2-1). The IHC images taken at 20x magnification, however, showed better quality at 1 in 250 dilution of FITC conjugated anti-human IgG (Figure A2-2), therefore this was used in subsequent experiments.

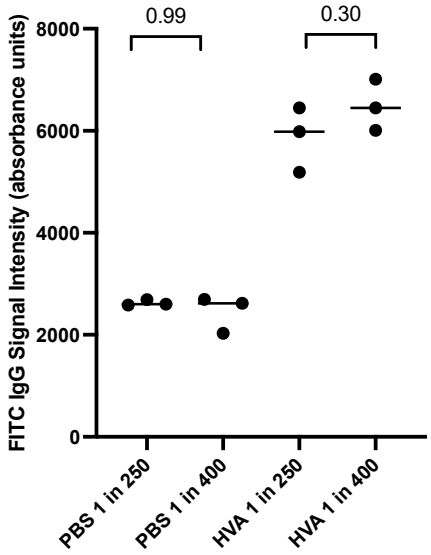

Figure A2-1 FITC IgG signal intensity in cardiac tissue treated with serum (1 in 100) from healthy vaccinated adults (HVA) and phosphate buffered saline (PBS) control with 1 in 250 and 1 in 400 dilutions of FITC conjugated anti-human IgG.

P values for Mann-Whitney comparisons have been displayed.

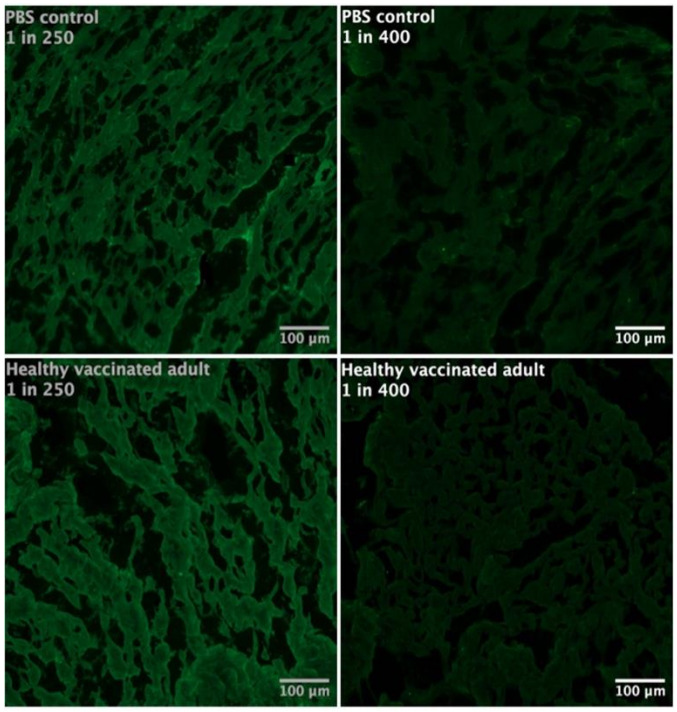

Figure A2-2 IHC images of IgG staining of healthy donor cardiac tissue treated with serum (1 in 100) from healthy vaccinated adult and phosphate buffered saline (PBS) control with 1 in 250 and 1 in 400 dilutions of FITC conjugated anti-human IgG.

Images were taken on a wide-field microscope at 20x magnification.

Dilution ratio of secondary antibodies – IgM

For ease of comparison the same dilution, 1 in 250 (same concentration), was tested for FITC conjugated anti-human IgM (Agilent Technologies, UK). Figure A2-3 displays the images from a PBS control and an healthy vaccinated adult, which showed acceptable visualisation of the tissue.

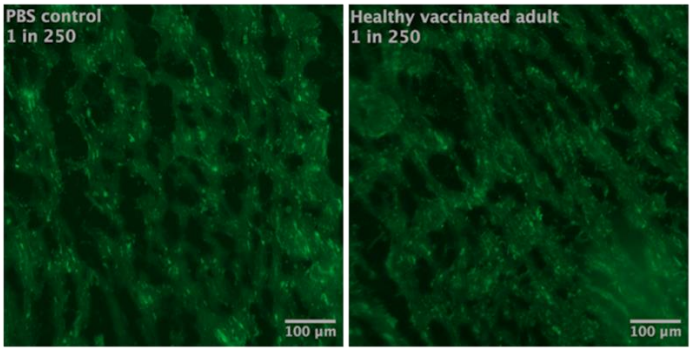

Figure A2-3 IHC images of IgM staining of healthy donor cardiac tissue treated with serum (1 in 100) from healthy vaccinated adults and phosphate buffered saline (PBS) control with 1 in 250 FITC conjugated anti-human IgM.

Images were taken on a wide-field microscope at 20x magnification.

Dilution ratio of secondary antibodies – IgA

The IHC images for IgA staining with PBS control and healthy vaccinated adults using FITC conjugated anti-human IgA antibody (Agilent Technologies, UK) at 1 in 250 dilution, were not adequate for qualitative assessment as the FITC staining was not bright enough. Therefore, further dilutions of 1 in 150 and 1 in 50 were tested and ultimately 1 in 50 dilution was used in the final protocol (Figure A2-4).

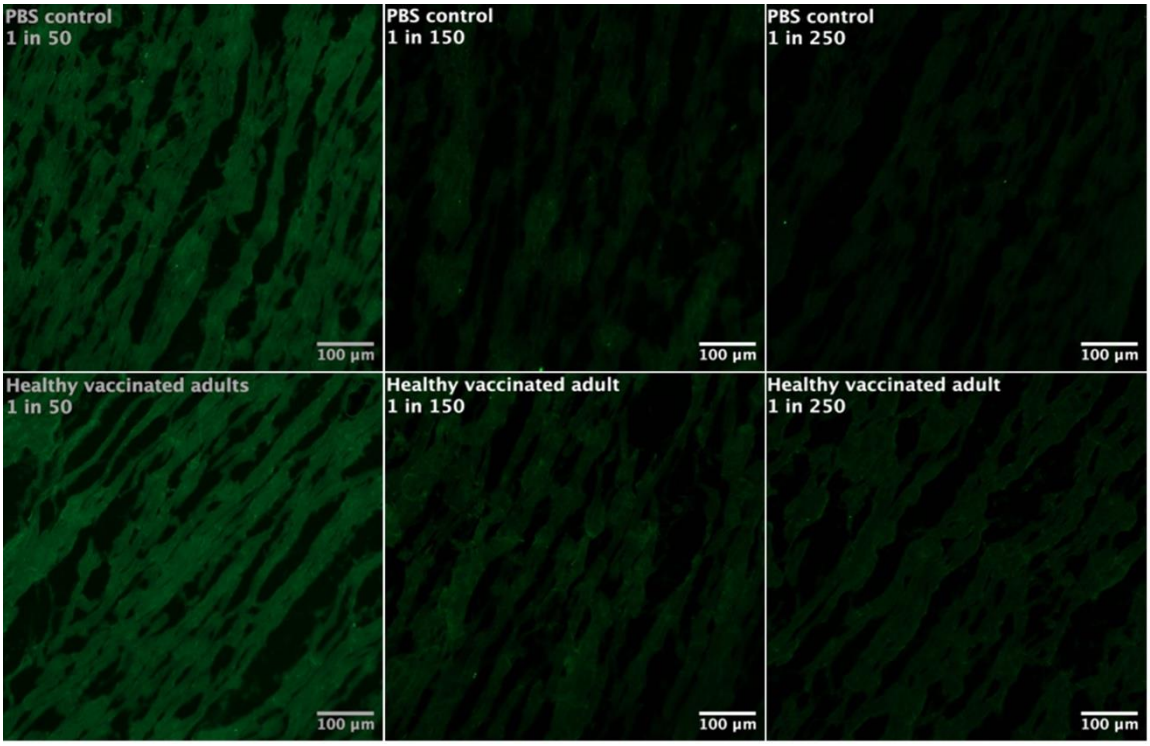

Figure A2-4 IHC images of IgA staining of healthy donor cardiac tissue treated with serum (1 in 100) from healthy vaccinated adults and phosphate buffered saline (PBS) control with 1 in 50, 1 in 150 and 1 in 250 dilutions of FITC conjugated anti-human IgA.

Images were taken on a wide-field microscope at 20x magnification.

Dilution ratio of patient/control serum

Optimisation experiments were carried out to determine the serum dilution which would show differences in FITC signal intensity between serum samples and PBS, and between healthy vaccinated controlled and patients with MIS-C. Experiments with serum dilutions of 1 in 25, 1 in 50 and 1 in 100 were performed for IgG. The greatest difference in signal intensity, between healthy vaccinated adults and MIS-C patients, was observed at 1 in 50 and 1 in 100 serum dilutions (p = 0.1) (Figure A2-5). Moreover, there was a significant difference in the signal intensity between both healthy vaccinated adults and MIS-C patients compared to PBS control (p = 0.02) at the 1 in 50 dilution (Figure A2-5). Therefore, 1 in 50 serum dilution was used for the IHC experiments. The same serum dilution was used for IgM and IgA.

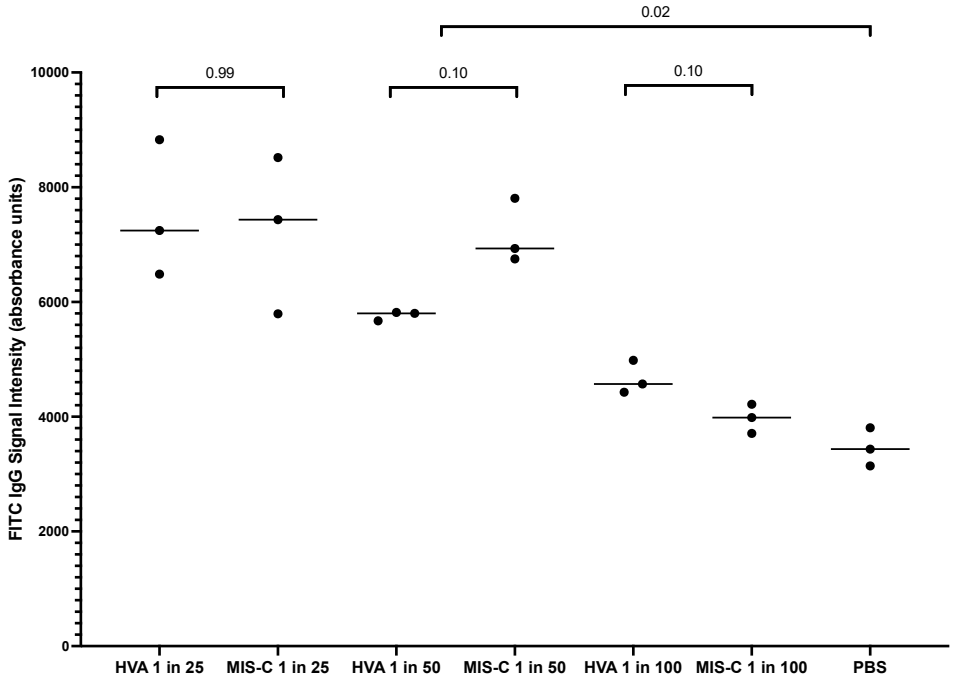

Figure A2-5 FITC IgG signal intensity in cardiac tissue treated with different concentrations of serum (1 in 25, 1 in 50 and 1 in 100) from healthy vaccinated adults (HVA), patients with multisystem inflammatory syndrome in children (MIS-C) and phosphate buffered saline (PBS) control.

2.2. ELISA optimisation experiments

Optimisation experiments were carried out to determine the ideal dilutions of the antigens (whole heart lysate, myosin and troponin), primary antibody (patient/control serum), secondary antibody (HRP-conjugated anti-human IgG) and HRP-TMB reaction duration. Samples from two positive controls and two healthy vaccinated adults were used for these experiments.

Whole heart lysate assay

Multiple experimental conditions were trialled including different whole heart lysate concentrations (1 in 2000, 1 in 4000 and 1 in 6000), serum concentrations (1 in 100, 1 in 1000 and 1 in 10000), HRP-conjugated anti-human IgG concentrations (1 in 3000 and 1 in 6000). Following the addition of TMB, the plate was covered in foil and checked every minute for progressive colour change as the HRP-TMB reaction took place. A progressive colour change was observed from 1 minute to 6 minutes, indicating ongoing reaction (Figure A2-6). At 7 minutes, there appeared to be no further colour change, suggesting a plateau had been reached and therefore the reaction was stopped. The optical density results for the various experimental conditions were reviewed to determine the best experimental conditions (Figure A2-7). This included balancing conditions where the greatest difference was seen between the positive controls and healthy controls with optical density readings that were not too high, as this can result in saturation of the detection system and increased background reading. The final conditions for the whole heart lysate ELISA were determined as follows: whole heart lysate dilution of 1 in 4000, HRP conjugated anti-IgG dilution 1 in 6000, serum dilution 1 in 100 and HRP-TMB reaction time 7 minutes.

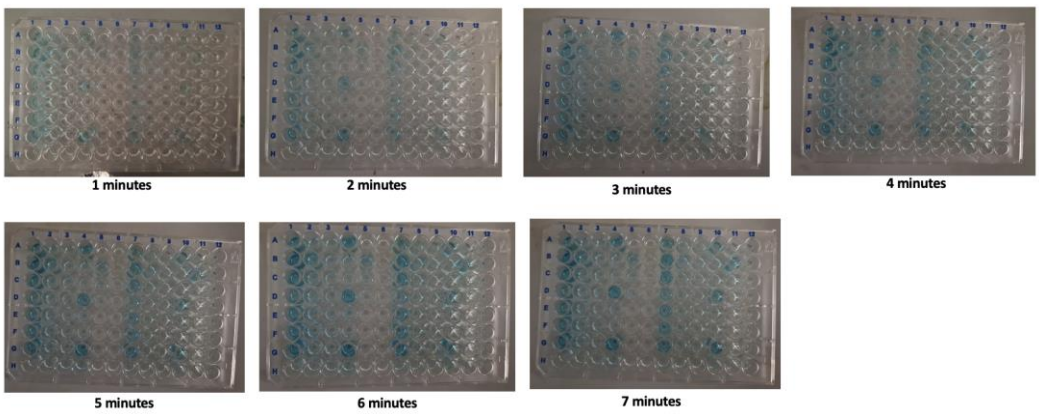

Figure A2-6 Photographs of the whole heart lysate ELISA microplate from the optimisation experiment.

Photographs were taken at 1-minute intervals following the addition of TBM to visualise the colour change taking place due to the HRP-TMB reaction and determine the optimal reaction time.

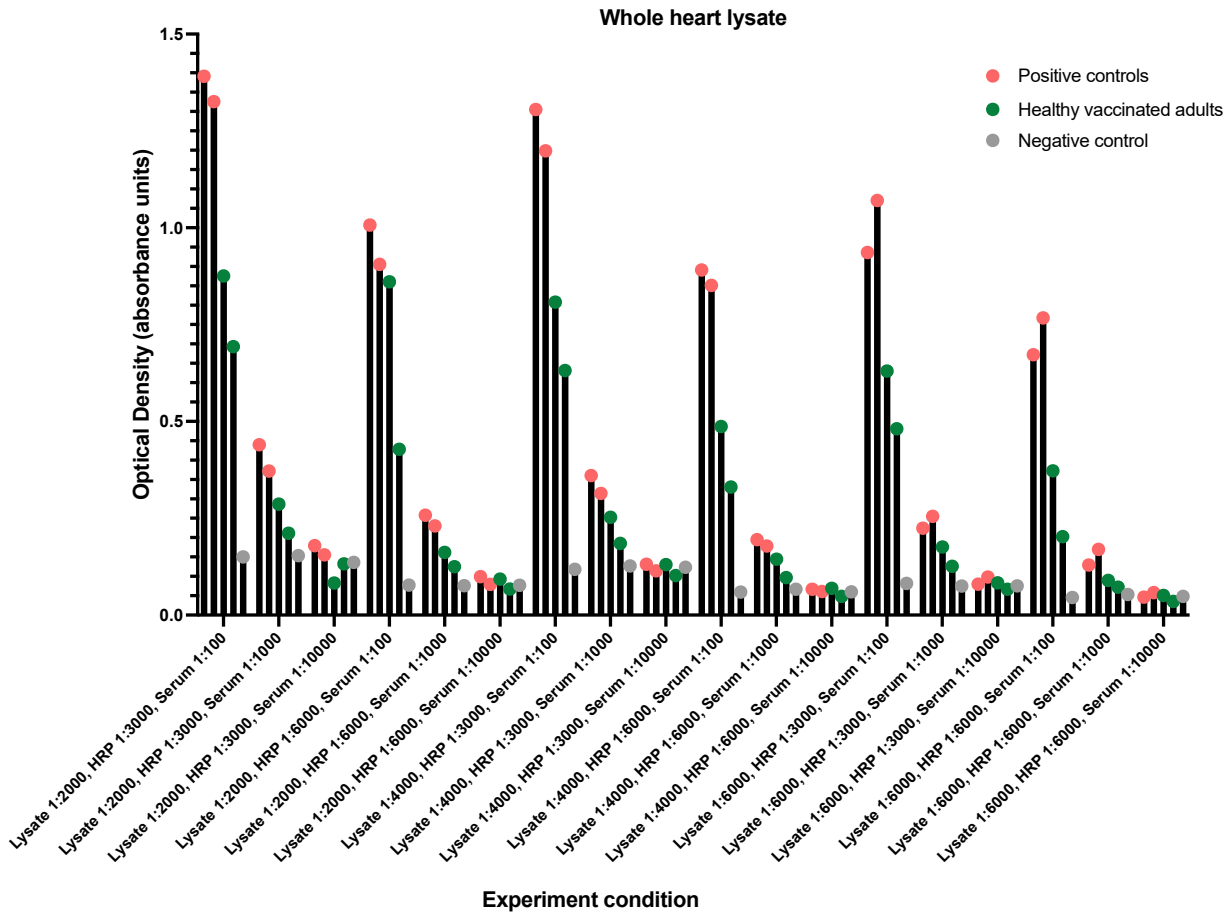

Figure A2-7 Whole heart lysate IgG ELISA results from the optimisation experiments.

The optical density with different concentrations of whole heart lysate (lysate 1 in 2000, 1 in 4000, 1 in 6000), in combination with different HRP conjugated anti-human IgG concentrations (HRP 1 in 3000, 1 in 6000) and different patient/control serum concentrations (serum 1 in 100, 1 in 1000, 1 in 10000) is shown. Serum from two positive controls and two healthy adult COVID-19 vaccinated controls was used. ELISA diluent was used as negative control.

Myosin

The same process as described for the whole heart lysate ELISA was followed for the myosin ELISA optimisation experiments. Multiple experimental conditions were trialled including different myosin concentrations (1 in 20000, 1 in 40000 and 1 in 60000), serum concentrations (1 in 100, 1 in 1000 and 1 in 10000) and HRP-conjugated anti-human IgG concentrations (1 in 3000 and 1 in 6000). Figure A2-8 shows the optical density results for the different experimental conditions. The final conditions for the myosin ELISA were determined as follows: myosin dilution of 1 in 40000, HRP dilution of 1 in 3000, serum dilution of 1 in 100 and HRP-TMB reaction time of 8 minutes.

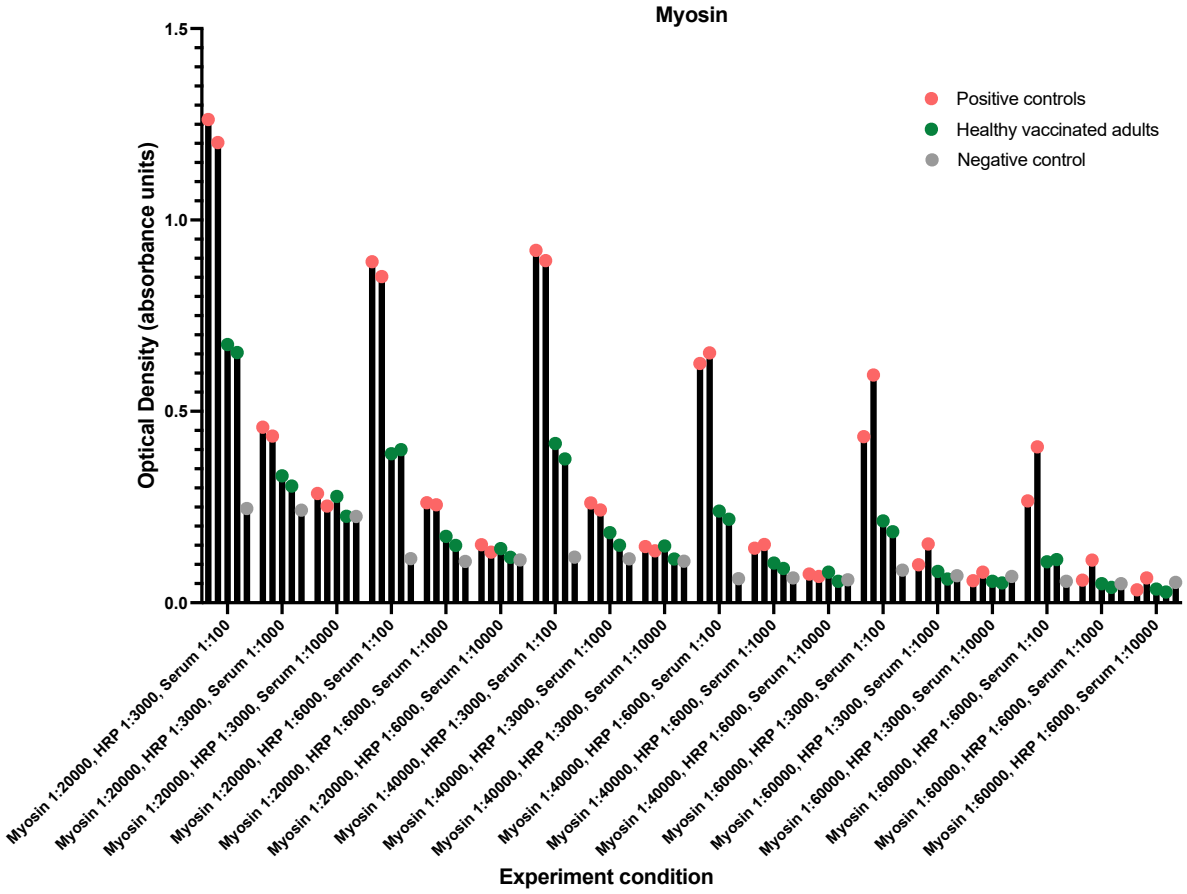

Figure A2-8 Myosin IgG ELISA results from the optimisation experiments.

The optical density with different concentrations of whole heart lysate (myosin 1 in 20000, 1 in 40000, 1 in 60000), in combination with different HRP conjugated anti-human IgG concentrations (HRP 1 in 3000, 1 in 6000) and different patient/control serum concentrations (serum 1 in 100, 1 in 1000, 1 in 10000) is shown. Serum from two positive controls and two healthy adult COVID-19 vaccinated controls was used. ELISA diluent was used as negative control.

Troponin

The same process as described for the whole heart lysate ELISA was followed for the troponin ELISA optimisation experiments. Multiple experimental conditions were trialled including different troponin concentrations (1 in 1250, 1 in 2500 and 1 in 5000), serum concentrations (1 in 100, 1 in 1000 and 1 in 10000) and HRP-conjugated anti-human IgG concentrations (1 in 2000 and 1 in 3000). Figure A2-9 shows the optical density results for the different experimental conditions. The final conditions for the troponin ELISA were determined as follows: myosin dilution of 1 in 2500, HRP dilution of 1 in 3000, serum dilution of 1 in 100 and HRP-TMB reaction time of 9 minutes.

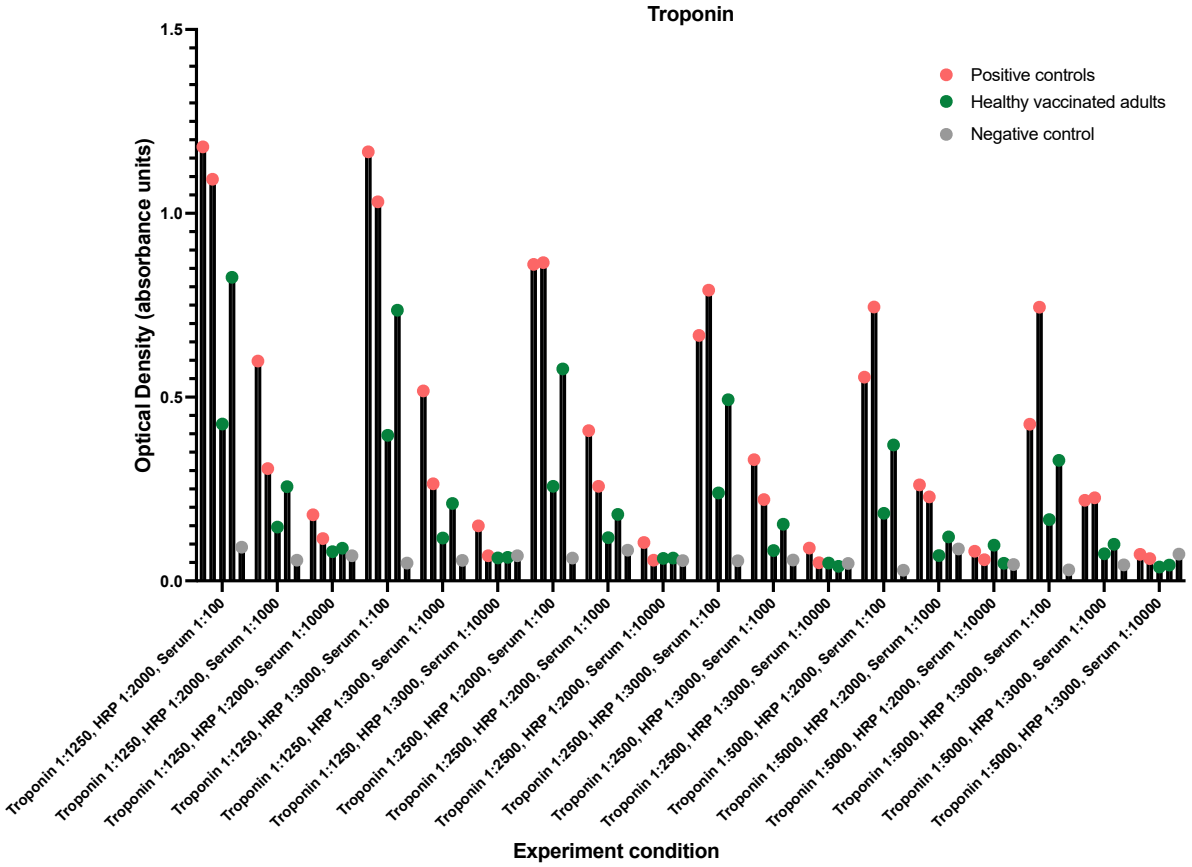

Figure A2-9 Troponin anti-IgG ELISA results from the optimisation experiments.

The optical density with different concentrations of whole heart lysate (lysate 1 in 1250, 1 in 2500, 1 in 5000), in combination with different HRP conjugated anti-human IgG concentrations (HRP 1 in 2000, 1 in 3000) and different patient/control serum concentrations (serum 1 in 100, 1 in 1000, 1 in 10000) is shown. Serum from two positive controls and two healthy adult COVID-19 vaccinated controls was used. ELISA diluent was used as negative control.

Appendix – 3

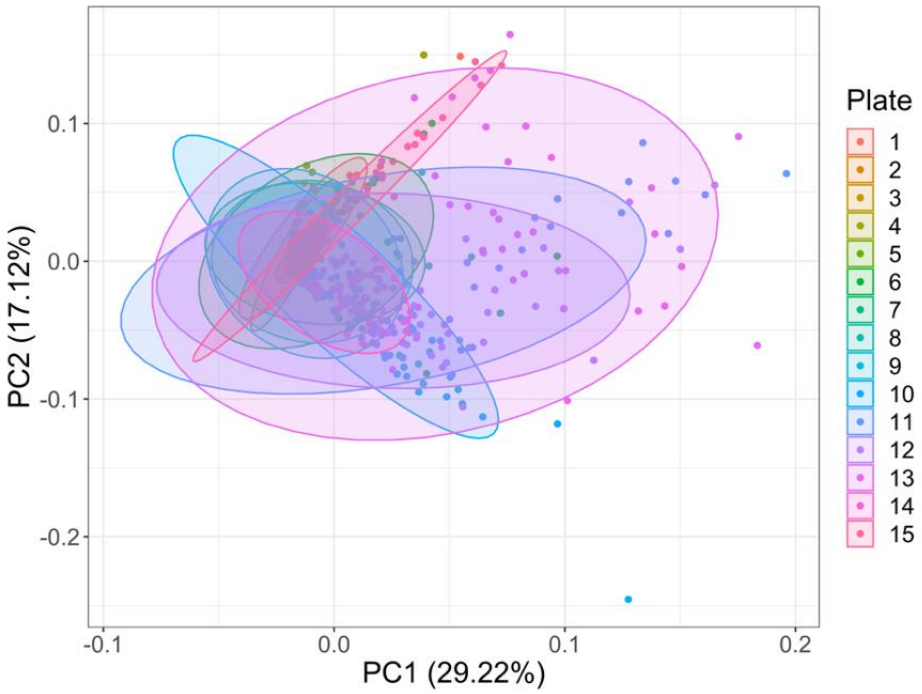

Figure A3-1 Principal component analysis for the coronavirus antibody dataset showing principal components one (PC1) and two (PC2).

The data points have been coloured and framed by plate number.

Appendix – 4

Table A4-1 Demographic and clinical features for cohort in Chapter 5.

	MIS-C (n = 170)	**Incomplete MIS-C (n = 33)**	**Bacterial (n = 208)**	**Viral (n = 142)**	**Inflammatory (n = 64)**	**KD (n = 21)**
Age (years) Median, [IQR]	9.0 [6.3 – 12]	10 [6.0 – 13]	8.0 [3.0 – 13]	2.5 [1.0 – 10]	11 [5.0 – 14]	1.0 [1.0 – 4.0]
Female sex, n (%)	62 (36.5%)	11 (33.3%)	84 (40.4%)	55 (38.7%)	30 (46.9%)	7 (33.3%)
Self-reported ethnicity, n (%)						
Asian	38 (22.4%)	5 (15.2%)	32 (15.4%)	28 (19.7%)	10 (15.6%)	8 (38.1%)
Black	20 (11.8%)	3 (9.1%)	22 (10.6%)	17 (12.0%)	2 (3.1%)	1 (4.8%)
Caucasian	59 (34.7%)	12 (36.4%)	109 (52.4%)	73 (51.4%)	34 (53.1%)	6 (28.6%)
Middle Eastern	1 (0.6%)	3 (9.1%)	8 (3.8%)	6 (4.2%)	6 (9.4%)	1 (4.8%)
Mixed	18 (10.6%)	1 (3.0%)	5 (2.4%)	5 (3.5%)	0 (0%)	1 (4.8%)
Unknown	34 (20.0%)	9 (27.3%)	32 (15.4%)	13 (9.2%)	12 (18.8%)	4 (19.0%)
Maximum CRP (mg/L), Median [IQR]	220 [170 - 300]	170 [60 - 270]	150 [99 - 230]	16 [6.0 - 29]	52 [19 - 130]	120 [67 - 210]
Maximum neutrophil count (x10^9/L), Median [IQR]	11 [7.7 - 16]	9.5 [5.0 - 15]	9.8 [4.9 - 14]	5.4 [2.8 - 8.5]	7.8 [5.2 - 13]	11 [9.4 - 13]
Minimum Lymphocyte count (x10^9/L), Median [IQR]	0.70 [0.44 - 1.2]	0.70 [0.40 - 1.4]	1.0 [0.50 - 1.7]	1.6 [0.70 - 2.9]	1.4 [0.68 - 1.9]	2.1 [1.8 - 3.7]
ICU admission, n (%)	119 (70.0%)	16 (48.5%)	58 (27.9%)	47 (33.1%)	15 (23.4%)	6 (28.6%)
Invasive ventilation, n (%)	14 (8.2%)	7 (21.2%)	36 (17.3%)	41 (28.9%)	6 (9.4%)	0 (0%)
Inotrope requirement, n (%)	102 (60.0%)	11 (33.3%)	32 (15.4%)	7 (4.9%)	9 (14.1%)	3 (14.3%)
Renal replacement therapy, n (%)	1 (0.6%)	3 (9.1%)	4 (1.9%)	0 (0%)	2 (3.1%)	0 (0%)
ECMO, n (%)	1 (0.6%)	0 (0%)	1 (0.5%)	2 (1.4%)	1 (1.6%)	0 (0%)
Patient died, n (%)	1 (0.6%)	1 (3.0%)	4 (1.9%)	2 (1.4%)	1 (1.6%)	0 (0%)

Appendix – 5

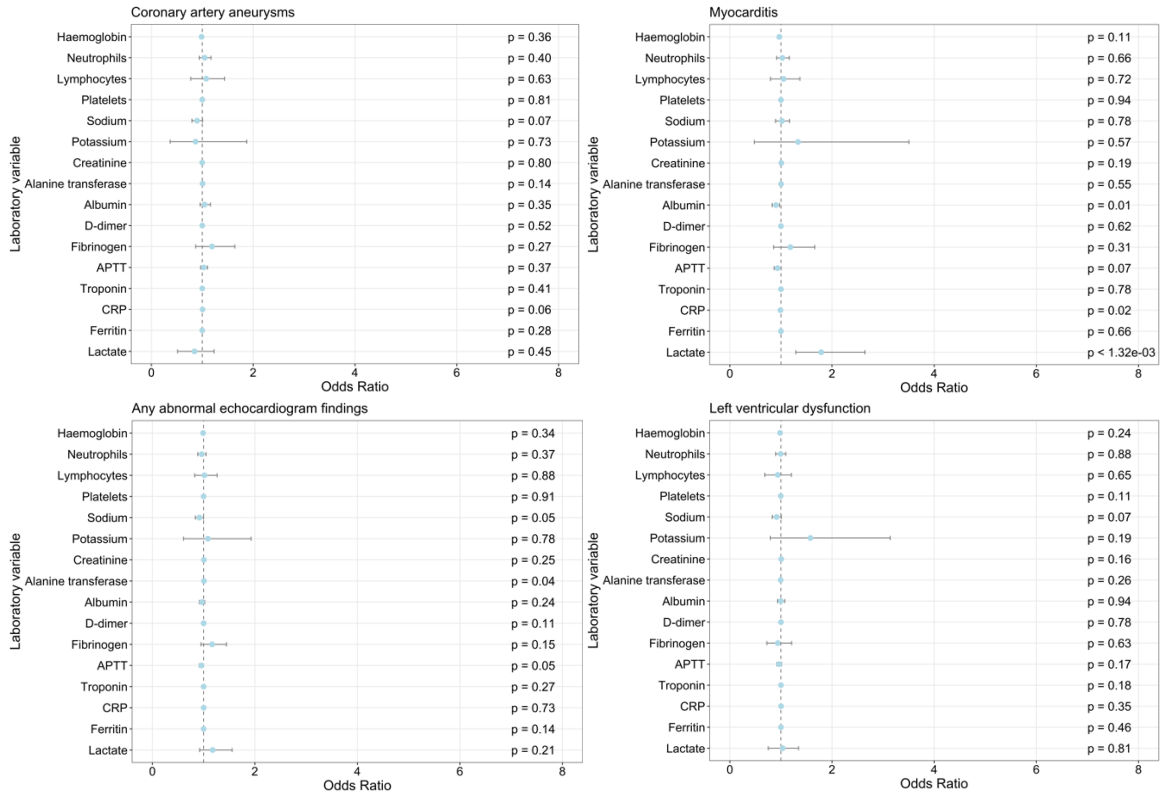

Figure A5-1 Odds Ratio plot for comparison of laboratory variables as risk factors for Severe/Very Severe Disease for the Best Available Treatment Study MIS-C cohort.

Odds ratios are derived from multivariable logistic regression analysis. Reference variables: Sex = Female, Ethnicity = Caucasian, Resource setting = High-Income settings. Adjusted p values are shown. N = 1230.

Table A5-1 Demographic features of the Best Available Treatment Study MIS-C cohort stratified by disease severity.

n = counts, % = percentages, IQR = interquartile range. Chi-squared tests (categorical data) and Wilcoxon pairwise comparisons (continuous data) were performed to compare the results of the Mild + Moderate group with the Severe + Very Severe group. Significant p values (< 0.05) have been highlighted.

	Mild (n = 476)	**Moderate (n = 452)**	**Severe (n = 264)**	**Very Severe (n = 93)**	**Mild + Moderate (n=928)**	**Severe + Very Severe (n=357)**	**P value (Mild Moderate vs Severe/V Severe)**
Age (years), median [IQR]	5.8 [2.7 - 9.8]	7.8 [4.2 - 11]	8.3 [5.8 - 12]	8.1 [4.0 - 12]	6.9 [3.7-10.7]	8.1 [4.0-12]	< 0.01
Sex							
Female	179 (37.6%)	186 (41.2%)	116 (43.9%)	49 (52.7%)	365 (39.4%)	165 (46.3%)	0.03
Male	297 (62.4%)	266 (58.8%)	148 (56.1%)	44 (47.3%)	563 (60.6%)	192 (53.7%)	0.03
Ethnicity							
Asian	27 (5.7%)	16 (3.5%)	14 (5.3%)	4 (4.3%)	43 (4.6%)	18 (5.0%)	0.51
Black	25 (5.3%)	45 (10.0%)	30 (11.4%)	11 (11.8%)	70 (7.5%)	41 (11.5%)	0.06
Caucasian	242 (50.8%)	175 (38.7%)	85 (32.2%)	20 (21.5%)	417 (45.0%)	105 (29.4%)	< 0.0001
Hispanic	146 (30.7%)	128 (28.3%)	83 (31.4%)	43 (46.2%)	274 (29.6%)	126 (35.3%)	< 0.0001
Other or not known	36 (7.6%)	88 (19.5%)	52 (19.7%)	15 (16.1%)	124 (13.4%)	67 (18.8%)	< 0.0001
Significant Comorbidity	20 (4.2%)	35 (7.7%)	10 (3.8%)	10 (10.8%)	55 (5.9%)	20 (5.6%)	0.93
Weight z-score, median [IQR]	0.40 [-0.34 - 1.2]	0.46 [-0.33 - 1.5]	0.69 [-0.092 - 1.5]	0.46 [-0.51 - 1.6]	0.43 [-0.34 - 1.36]	0.46 [-0.51 - 1.6]	0.07
Resource setting							
Low and Lower Middle-Income Economies	34 (7.1%)	44 (9.7%)	21 (8.0%)	3 (3.2%)	78 (8.4%)	24 (6.7%)	0.64
Upper Middle-Income Economies	176 (37.0%)	209 (46.2%)	126 (47.7%)	57 (61.3%)	385 (41.5%)	183 (51.3%)	< 0.01
High-Income Economies	266 (55.9%)	199 (44.0%)	117 (44.3%)	33 (35.5%)	465 (50.1%)	150 (42.0%)	< 0.01

Table A5-2 Clinical features of the Best Available Treatment Study MIS-C cohort stratified by baseline disease severity.

Chi squared tests and Wilcoxon pairwise comparisons were performed to compare the results of the Mild + Moderate groups with the Severe + Very Severe groups. Significant p values (< 0.05) have been highlighted. n = Counts, % = percentages, IQR = interquartile range, BCG = Bacillus Calmette–Guérin, KD = Kawasaki disease, PCR = polymerase chain reaction, IVIG = intravenous immunoglobulin, IL= interleukin, TNFα = tumour necrosis factor alpha.

	Mild (n = 476)	**Moderate (n = 452)**	**Severe (n = 264)**	**Very Severe (n = 93)**	**P value (Mild/Moderate vs Severe/V Severe)**
Days of fever, median [IQR]	5.0 [3.0 - 7.0]	4.0 [3.0 - 6.0]	5.0 [3.0 - 6.0]	5.0 [3.0 - 6.0]	0.09
Sore throat	105 (22.1%)	117 (25.9%)	73 (27.7%)	22 (23.7%)	0.69
Cough	83 (17.4%)	106 (23.5%)	56 (21.2%)	25 (26.9%)	0.50
Respiratory distress	11 (2.3%)	55 (12.2%)	35 (13.3%)	31 (33.3%)	< 0.0001
Abdominal pain	239 (50.2%)	283 (62.6%)	178 (67.4%)	61 (65.6%)	< 0.001
Diarrhoea	184 (38.7%)	172 (38.1%)	139 (52.7%)	50 (53.8%)	< 0.0001
Vomiting	205 (43.1%)	240 (53.1%)	174 (65.9%)	64 (68.8%)	< 0.0001
Headache	112 (23.5%)	161 (35.6%)	92 (34.8%)	22 (23.7%)	0.53
Seizures	8 (1.7%)	6 (1.3%)	2 (0.8%)	5 (5.4%)	0.39
Encephalopathy	6 (1.3%)	12 (2.7%)	19 (7.2%)	10 (10.8%)	< 0.001
Irritable	101 (21.2%)	89 (19.7%)	40 (15.2%)	23 (24.7%)	0.91
Lethargy	110 (23.1%)	167 (36.9%)	98 (37.1%)	48 (51.6%)	< 0.001
Joint pain	40 (8.4%)	47 (10.4%)	20 (7.6%)	12 (12.9%)	0.41
Rash	282 (59.2%)	264 (58.4%)	154 (58.3%)	51 (54.8%)	0.02
Conjunctivitis	257 (54.0%)	240 (53.1%)	140 (53.0%)	45 (48.4%)	0.08
Oedema	112 (23.5%)	131 (29.0%)	65 (24.6%)	25 (26.9%)	0.08
Mucous membrane changes	231 (48.5%)	232 (51.3%)	127 (48.1%)	37 (39.8%)	1.0
Skin peeling	21 (4.4%)	23 (5.1%)	18 (6.8%)	6 (6.5%)	0.01
Lymphadenopathy	139 (29.2%)	133 (29.4%)	60 (22.7%)	26 (28.0%)	< 0.001
BCG reactivation	2 (0.4%)	3 (0.7%)	4 (1.5%)	1 (1.1%)	< 0.001
Full KD criteria met	127 (26.7%)	136 (30.1%)	53 (20.1%)	22 (23.7%)	0.04

Table A5-2 continued

	Mild (n = 476)	Moderate (n = 452)	Severe (n = 264)	Very Severe (n = 93)	P value (Mild/Moderate vs Severe/V Severe)
SARS-CoV-2 PCR Positive	98 (20.6%)	92 (20.4%)	54 (20.5%)	41 (44.1%)	0.02
SARS-CoV-2 Serology Positive	277 (58.2%)	327 (72.3%)	198 (75.0%)	69 (74.2%)	0.09
Treatment					
Corticosteroids	319 (67.0%)	364 (80.5%)	248 (93.9%)	85 (91.4%)	0.10
IVIG	396 (83.2%)	372 (82.3%)	229 (86.7%)	84 (90.3%)	0.17
Anti-IL1	18 (3.8%)	22 (4.8%)	16 (6.1%)	13 (13.9%)	1.00
Anti-IL6	2 (0.4%)	7 (1.5%)	13 (4.9%)	21 (22.6%)	1.00
Anti-TNFα	6 (1.2%)	2 (0.44%)	3 (1.1%)	0 (0%)	1.00
Other	2 (0.4%)	3 (0.66%)	1 (0.38%)	4 (4.3%)	1.00
Echocardiogram findings					
Left ventricular dysfunction	48 (10.1%)	70 (15.5%)	105 (39.8%)	37 (39.8%)	< 0.0001
Myocarditis	19 (4.0%)	27 (6.0%)	41 (15.5%)	20 (21.5%)	< 0.0001
Coronary artery aneurysm	62 (13%)	42 (9.3%)	35 (13.3%)	13 (14.0%)	0.59
Persistent coronary artery aneurysm	23 (4.8%)	14 (3.1%)	6 (2.3%)	5 (5.4%)	0.86
Any abnormal findings	196 (41.2%)	187 (41.4%)	185 (70%)	68 (73.1%)	< 0.0001
Inotropes	NA	NA	NA	NA	-
Invasive ventilation	NA	NA	NA	NA	-
Renal Replacement therapy	NA	NA	NA	NA	-
ECMO	NA	NA	NA	NA	-
Death	NA	NA	NA	NA	-
Length of admission, median [IQR]	8.0 [5.0 - 11]	9.0 [6.0 - 14]	10 [7.0 - 14]	14 [10 - 18]	< 0.0001

Table A5-3 Baseline laboratory markers of the Best Available Treatment Study MIS-C cohort stratified by baseline disease severity.

Wilcoxon pairwise tests were conducted to compare the laboratory results, while Chi-squared tests were performed to compare the occurrence of missing results between the Mild/Moderate group and the Severe/Very Severe group. Significant p values (< 0.05) have been highlighted. n = counts, % = percentages, IQR = interquartile range.

	Mild (n = 476)	**Moderate (n = 452)**	**Severe (n = 264)**	**Very Severe (n = 93)**	**P values (Mild/Moderate vs Severe/V Severe)**
	(n = 476)	(n = 452)	(n = 264)	(n = 93)	
Haemoglobin (g/l), median [IQR]	120 [110 - 130]	120 [110 - 130]	120 [110 - 130]	110 [97 - 120]	< 0.0001
Missing, n (%)	16 (3.4%)	23 (5.1%)	10 (3.8%)	2 (2.2%)	0.07
White Blood Count (x10^9/L), median [IQR]	11 [7.5 - 15]	9.7 [6.7 - 13]	11 [7.7 - 15]	13 [7.4 - 18]	< 0.0001
Missing, n (%)	17 (3.6%)	24 (5.3%)	10 (3.8%)	1 (1.1%)	0.03
Neutrophils (x10^9/L), median [IQR]	7.8 [5.0 - 11]	7.2 [5.0 - 10]	8.8 [6.1 - 12]	9.9 [5.8 - 15]	< 0.0001
Missing, n (%)	31 (6.5%)	70 (15.5%)	37 (14.0%)	5 (5.4%)	< 0.01
Lymphocytes (x10^9/L), median [IQR]	1.5 [0.96 - 2.7]	1.2 [0.70 - 1.9]	1.0 [0.60 - 1.5]	0.95 [0.68 - 1.5]	< 0.0001
Missing, n (%)	28 (5.9%)	54 (11.9%)	23 (8.7%)	2 (2.2%)	0.2
Platelets (x10^9/L), median [IQR]	230 [150 - 330]	180 [120 - 250]	150 [110 - 210]	140 [94 - 200]	< 0.0001
Missing, n (%)	20 (4.2%)	31 (6.9%)	11 (4.2%)	3 (3.2%)	< 0.01
Sodium (mmol/L), median [IQR]	140 [130 - 140]	130 [130 - 140]	130 [130 - 140]	130 [130 - 140]	< 0.0001
Missing, n (%)	79 (16.6%)	98 (21.7%)	37 (14.0%)	7 (7.5%)	< 0.0001
Potassium (mmol/L), median [IQR]	4.1 [3.8 - 4.4]	4.0 [3.7 - 4.4]	3.9 [3.6 - 4.3]	3.9 [3.4 - 4.5]	< 0.01
Missing, n (%)	84 (17.6%)	104 (23.0%)	41 (15.5%)	9 (9.7%)	< 0.0001
Phosphate (mmol/L), median [IQR]	1.2 [1.0 - 1.4]	1.1 [0.94 - 1.4]	1.1 [0.91 - 1.3]	1.2 [0.90 - 1.5]	0.46
Missing, n (%)	328 (68.9%)	343 (75.9%)	180 (68.2%)	40 (43.0%)	< 0.0001

Table A5-3 continued.

	Mild (n = 476)	Moderate (n = 452)	Severe (n = 264)	Very Severe (n = 93)	P values (Mild/Moderate vs Severe/V Severe)
Creatinine (µmol/L), median [IQR]	41 [28 - 52]	47 [35 - 62]	56 [44 - 77]	71 [47 - 130]	< 0.0001
Missing, n (%)	74 (15.5%)	86 (19.0%)	37 (14.0%)	9 (9.7%)	< 0.0001
ALT (U/L), median [IQR]	28 [16 - 51]	33 [19 - 63]	37 [22 - 58]	42 [28 - 84]	< 0.001
Missing, n (%)	81 (17.0%)	102 (22.6%)	58 (22.0%)	15 (16.1%)	< 0.0001
Albumin (g/L), median [IQR]	36 [32 - 40]	35 [30 - 38]	31 [27 - 36]	29 [24 - 32]	< 0.0001
Missing, n (%)	138 (29.0%)	143 (31.6%)	80 (30.3%)	22 (23.7%)	< 0.0001
D-dimer (ng/mL), median [IQR]	1800 [980 - 3400]	2400 [1300 - 4100]	3000 [1600 - 5000]	4300 [2500 - 8400]	< 0.0001
Missing, n (%)	173 (36.3%)	196 (43.4%)	102 (38.6%)	36 (38.7%)	< 0.0001
Fibrinogen (g/L), median [IQR]	5.4 [4.4 - 6.5]	5.3 [4.0 - 6.2]	5.6 [4.4 - 6.9]	5.3 [3.5 - 6.5]	0.52
Missing, n (%)	156 (32.8%)	198 (43.8%)	96 (36.4%)	30 (32.3%)	< 0.0001
APTT (s), median [IQR]	32 [28 - 37]	33 [28 - 38]	33 [29 - 39]	34 [29 - 43]	0.30
Missing, n (%)	153 (32.1%)	179 (39.6%)	94 (35.6%)	23 (24.7%)	< 0.0001
Troponin (ng/L), median [IQR]	11 [4.0 - 40]	17 [5.5 - 50]	40 [10 - 110]	50 [20 - 120]	< 0.0001
Missing, n (%)	197 (41.4%)	229 (50.7%)	129 (48.9%)	42 (45.2%)	< 0.01
BNP (pg/ml), median [IQR]	120 [30 - 380]	83 [19 - 260]	450 [94 - 990]	920 [240 - 2300]	< 0.0001
Missing, n (%)	382 (80.3%)	390 (86.3%)	220 (83.3%)	74 (79.6%)	0.02
CRP (mg/L), median [IQR]	120 [67 - 190]	140 [85 - 200]	170 [110 - 250]	230 [93 - 300]	< 0.0001
Missing, n (%)	49 (10.3%)	96 (21.2%)	34 (12.9%)	15 (16.1%)	<0.01
Ferritin (ng/mL), median [IQR]	270 [160 - 520]	380 [230 - 660]	530 [280 - 920]	850 [430 - 1700]	< 0.0001
Missing, n (%)	193 (40.5%)	226 (50.0%)	120 (45.5%)	33 (35.5%)	< 0.0001
Lactate (mmol/L), median [IQR]	1.6 [1.2 - 2.1]	1.6 [1.1 - 2.1]	2.0 [1.5 - 2.8]	2.1 [1.7 - 3.2]	< 0.0001
Missing, n (%)	366 (76.9%)	275 (60.8%)	135 (51.1%)	32 (34.4%)	< 0.0001
Vitamin D (nmol/L), median [IQR]	42 [28 - 69]	37 [27 - 44]	24 [16 - 31]	21 [21 - 21]	NA
Missing, n (%)	455 (95.6%)	432 (95.6%)	244 (92.4%)	92 (98.9%)	NA

Appendix – 6

Table A6-1 Clinical and demographic details of seven adult myocarditis/inflammatory cardiomyopathy patients included in Chapter 7.

	Patient - 1	**Patient - 2**	**Patient - 3**	**Patient - 4**	**Patient - 5**	**Patient - 6**	**Patient - 7**
Age (years)	61	48	68	76	48	61	27
Sex	Female	Male	Female	Male	Male	Male	Male
Self-reported ethnicity	Caucasian	Caucasian	Caucasian	Caucasian	Caucasian	Caucasian	Caucasian
Maximum CRP (mg/L) [normal range < 3 mg/L]	136	4	14.3	270.5	3	31.4	56.6
Maximum cardiac Troponin (ng/L) [normal range: < 14 ng/L]	353	48	610	34	20	318	2179
Maximum NT-proBNP (ng/L) [normal range < 50 ng/L]	38744	256	824	9004	8131	208886	266
Ejection fraction on echocardiogram [normal range 50-70%]	19%	40%	59%	20%	15%	33%	56%
Significant Cardiac Magnetic Resonance Imaging findings	Not done	late gadolinium enhancement	No significant abnormality	late gadolinium enhancement, perimyocarditis	late gadolinium enhancement	No significant abnormality	late gadolinium enhancement, oedema, myocarditis
Cardiac biopsy diagnosis	inflammatory cardiomyopathy	inflammatory cardiomyopathy	acute myocarditis	inflammatory cardiomyopathy	inflammatory cardiomyopathy	inflammatory cardiomyopathy	inflammatory cardiomyopathy
Final diagnosis	terminal inflammatory cardiomyopathy	inflammatory cardiomyopathy	Immune Checkpoint Inhibitors-induced myocarditis	inflammatory cardiomyopathy	inflammatory cardiomyopathy	inflammatory cardiomyopathy	recurrent myocarditis

Appendix – 7

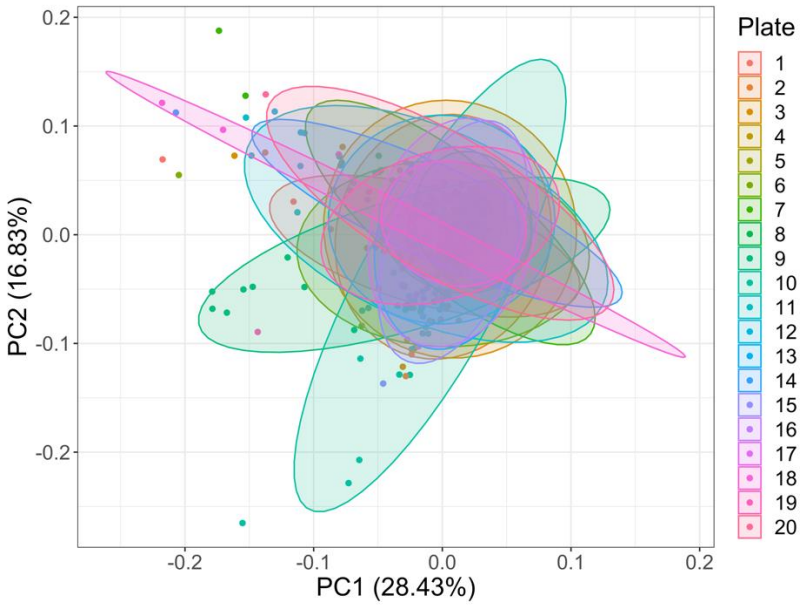

Figure A7-1 Principal component analysis for the 13-plex cytokine dataset showing principal components one (PC1) and two (PC2).

The data points have been coloured and framed by plate number.

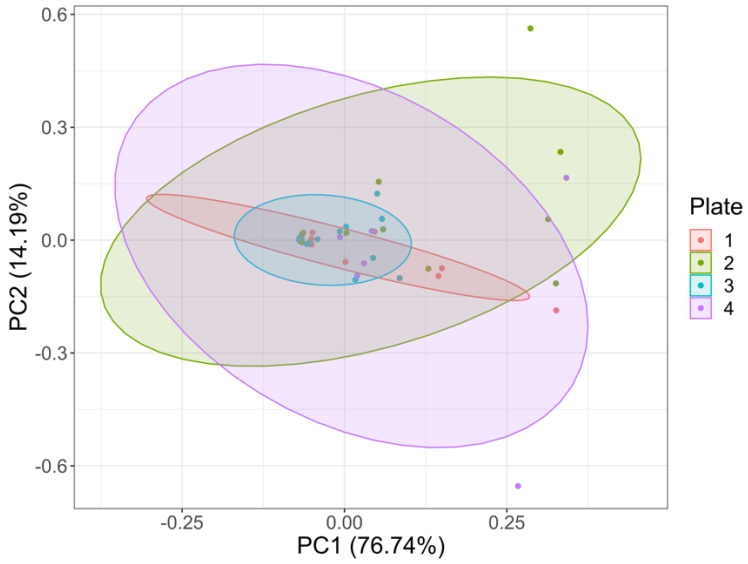

Figure A7-2 Principal component analysis for the 4-plex cytokine dataset showing principal components one (PC1) and two (PC2).

The data points have been coloured and framed by plate number.

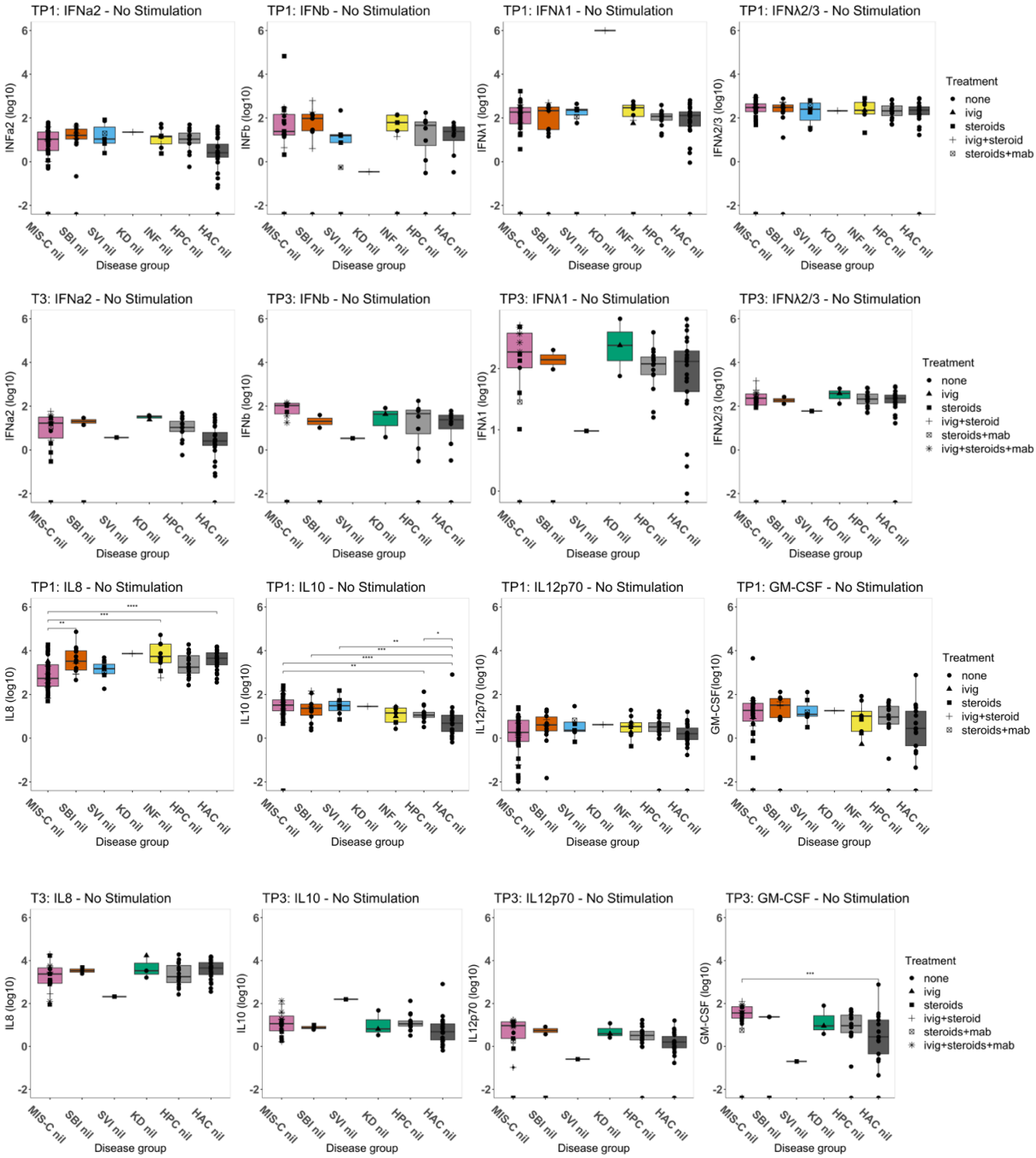

Figure A7-3 Boxplots showing the levels of IFNα2, IFNβ, IFNλ1, IFNλ2/3, IL8, IL10, IL12p70, and GM-CSF in acute (TP1) and convalescent (TP3) unstimulated (nil) samples.

Log10 transformed data are shown. Each point represents a participant for the following groups: MIS-C, severe bacterial illness (SBI), severe viral illness (SVI), Kawasaki disease (KD), other Inflammatory disease (INF). The shape of the point corresponds to the treatment received prior to blood sampling: ivig = intravenous immunoglobulin, steroid = corticosteroids, mab = monoclonal antibody. Wilcoxon pairwise comparisons with Benjamini Hochberg correction were performed; only significant p values are displayed.

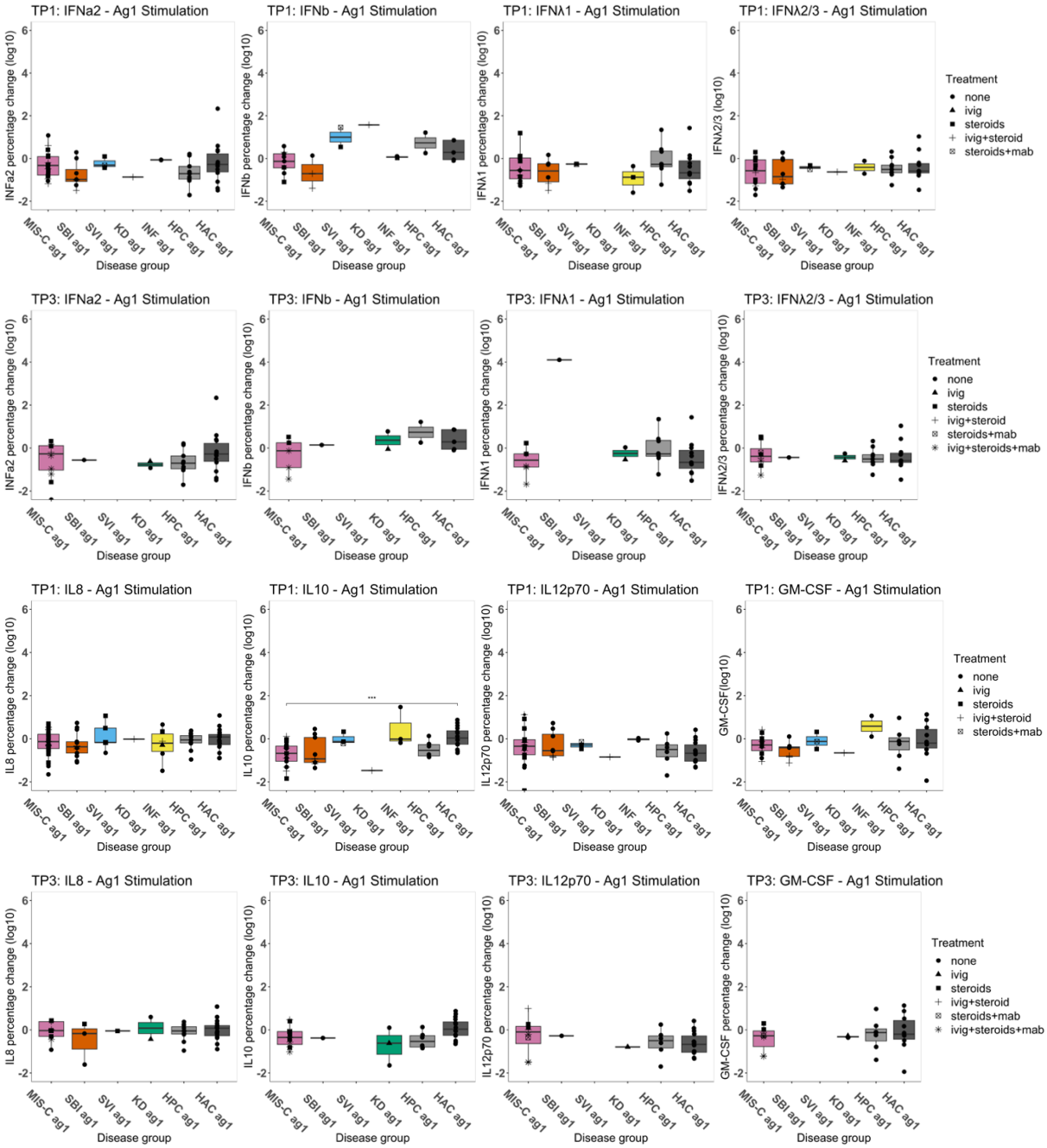

Figure A7-4 Boxplots showing the percentage change from unstimulated samples in levels of IFNα2, IFNβ, IFNλ1, IFNλ2/3, IL8, IL10, IL12p70, and GM-CSF in acute (TP1) and convalescent (TP3) samples stimulated with SARS-CoV-2 antigen (ag1).

Log10 transformed data are shown. Each point represents a participant for the following groups: MIS-C, severe bacterial illness (SBI), severe viral illness (SVI), Kawasaki disease (KD), other Inflammatory disease (INF). The shape of the point corresponds to the treatment received prior to blood sampling: ivig = intravenous immunoglobulin, steroid = corticosteroids, mab = monoclonal antibody. Wilcoxon pairwise comparisons with Benjamini Hochberg correction were performed; only significant p values are displayed.

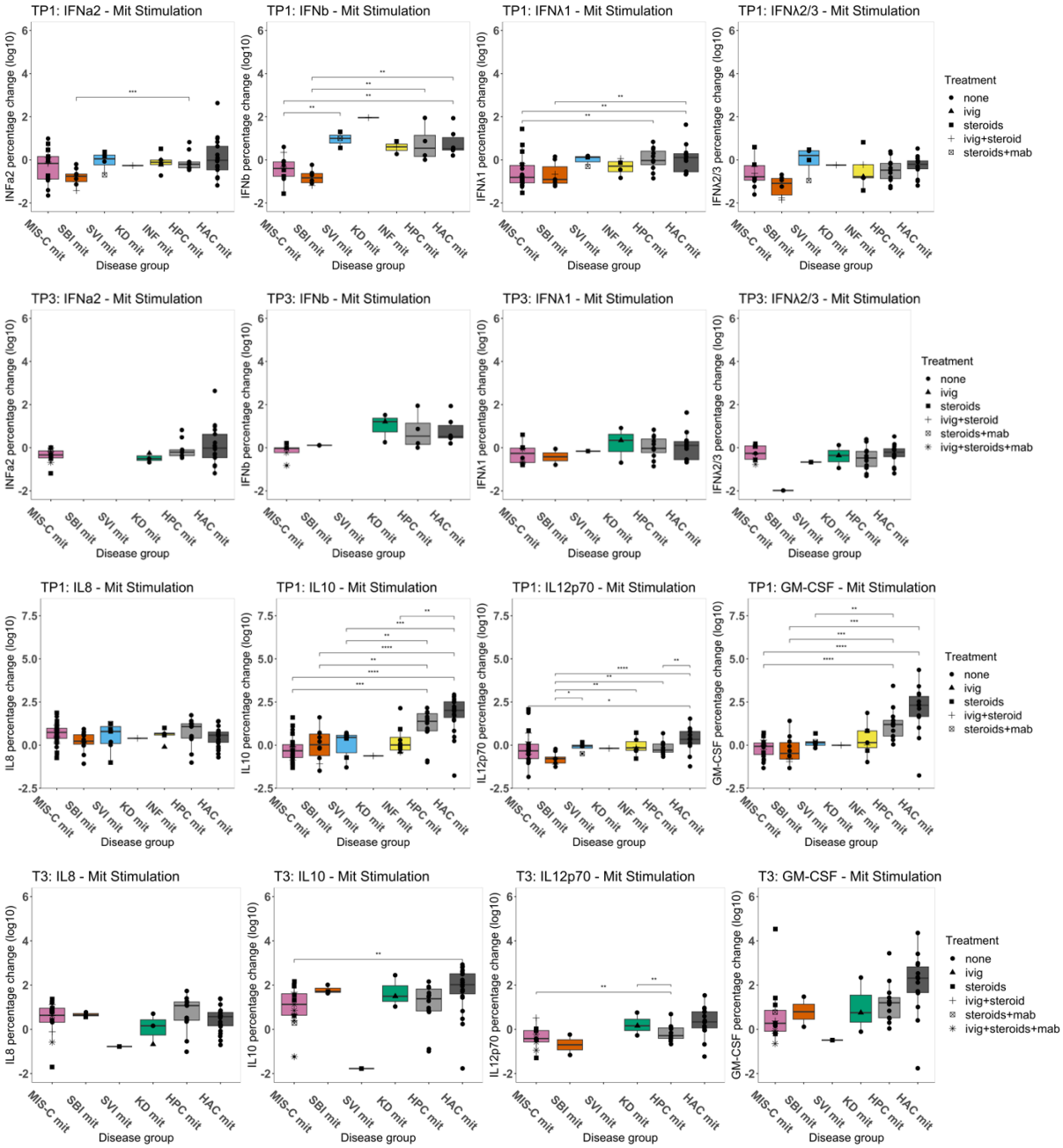

Figure A7-5 Boxplots showing the percentage change from unstimulated samples in levels of IFNα2, IFNβ, IFNλ1, IFNλ2/3, IL8, IL10, IL12p70, and GM-CSF in acute (TP1) and convalescent (TP3) samples stimulated with mitogen (mit).

Log10 transformed data are shown. Each point represents a participant for the following groups: MIS-C, severe bacterial illness (SBI), severe viral illness (SVI), Kawasaki disease (KD), other Inflammatory disease (INF). The shape of the point corresponds to the treatment received prior to blood sampling: ivig = intravenous immunoglobulin, steroid = corticosteroids, mab = monoclonal antibody. Wilcoxon pairwise comparisons with Benjamini Hochberg correction were performed; only significant p values are displayed.

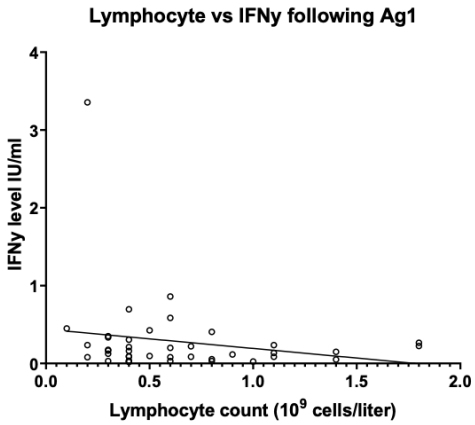

Spearman R: -0.17
P: 0.31

Figure A7-6 Scatterplot showing the relationship between lymphocyte count and IFNγ levels in acute MIS-C samples following stimulation with SARS-CoV-2 antigen stimulation. N=38.

Spearman's correlation coefficient (R) and p value have been displayed.

Table A7-1 Demographic features of the healthy adult controls (HAC) included in Chapter 8.

Participant ID	Sex	Age (years)	Self-reported ethnicity	Date of sample	COVID-19 vaccine received	Date of vaccination	Dose of last vaccine prior to sampling
Healthy adult control 1	Male	> 21	North/Mid/East European	06/07/2021	mRNA Vaccine BNT162b2	10/03/2021	Second
Healthy adult control 2	Female	> 21	North/Mid/East European	06/07/2021	mRNA Vaccine BNT162b3	21/04/2021	Second
Healthy adult control 3	Female	> 21	North/Mid/East European	06/07/2021	mRNA Vaccine BNT162b4	04/03/2021	Second
Healthy adult control 4	Female	> 21	South Asian	06/07/2021	mRNA Vaccine BNT162b5	07/04/2021	Second
Healthy adult control 5	Female	> 21	North/Mid/East European	13/07/2021	mRNA Vaccine BNT162b6	13/04/2021	Second
Healthy adult control 6	Male	> 21	North/Mid/East European	13/07/2021	mRNA Vaccine BNT162b7	16/03/2021	Second
Healthy adult control 7	Male	> 21	North/Mid/East European	13/07/2021	Non-replicating viral vector vaccine AZD1222 (ChAdOx1)	20/05/2021	Second
Healthy adult control 8	Male	> 21	African - other	13/07/2021	mRNA Vaccine BNT162b4	31/03/2021	Second
Healthy adult control 9	Female	> 21	North/Mid/East European	13/07/2021	mRNA Vaccine BNT162b4	01/07/2021	Second
Healthy adult control 10	Female	> 21	North/Mid/East European	14/07/2021	mRNA Vaccine BNT162b4	20/03/2021	Second
Healthy adult control 11	Male	> 21	South American - other	14/07/2021	mRNA Vaccine BNT162b4	12/05/2021	Second
Healthy adult control 12	Male	> 21	North/Mid/East European	15/07/2021	mRNA Vaccine BNT162b4	> 14 days prior to sampling	Second
Healthy adult control 13	Male	> 21	North/Mid/East European	22/07/2021	mRNA Vaccine BNT162b4	10/03/2021	Second
Healthy adult control 14	Male	> 21	North/Mid/East European	22/07/2021	Non-replicating viral vector vaccine AZD1222 (ChAdOx1)	24/06/2021	Second
Healthy adult control 15	Female	> 21	North/Mid/East European	03/02/2021	mRNA Vaccine BNT162b4	04/01/2021	First
Healthy adult control 16	Female	> 21	North/Mid/East European	05/02/2021	mRNA Vaccine BNT162b4	01/01/2021	First
Healthy adult control 17	Female	> 21	East Asian	06/10/2021	mRNA Vaccine BNT162b4	19/03/2021	Second

Table A7-1 continued.

Participant ID	Sex	Age (years)	Self-reported ethnicity	Date of sample	COVID-19 vaccine received	Date of vaccination	Dose of last vaccine prior to sampling
Healthy adult control 18	Female	> 21	North/Mid/East European	06/10/2021	mRNA Vaccine BNT162b4	22/03/2021	Second
Healthy adult control 19	Male	> 21	South American - other	06/10/2021	mRNA Vaccine BNT162b4	26/08/2021	Second
Healthy adult control 20	Female	> 21	North/Mid/East European	06/10/2021	mRNA Vaccine BNT162b4	10/04/2021	Second
Healthy adult control 21	Female	> 21	North/Mid/East European	26/11/2021	mRNA Vaccine BNT162b4	07/10/2021	Booster
Healthy adult control 22	Male	> 21	North/Mid/East European	26/11/2021	mRNA Vaccine BNT162b4	02/10/2021	Booster
Healthy adult control 23	Male	> 21	South Asian	26/11/2021	mRNA Vaccine BNT162b4	04/05/2021	Second
Healthy adult control 24	Female	> 21	East Asian	01/12/2021	mRNA Vaccine BNT162b4	17/11/2021	Booster
Healthy adult control 25	Male	> 21	North/Mid/East European	01/12/2021	mRNA Vaccine BNT162b4	03/04/2021	First
Healthy adult control 26	Male	> 21	Middle Eastern - Arab	01/12/2021	mRNA Vaccine BNT162b4	11/07/2021	Second
Healthy adult control 27	Male	> 21	North/Mid/East European	01/12/2021	mRNA Vaccine BNT162b4	> 14 days prior to sampling	Second

Table A7-2 Details of reported comorbidities in the paediatric cohorts included in Chapter 8.

SBI = Severe bacterial illness, SVI = Severe Viral illness, HPC = healthy paediatric control

MIS-C, n = 6/55	
Attention deficit hyperactivity disorder	1
Asthma	2
Eczema	1
Autism	1
Inflammatory bowel disease	1
SBI, n = 8/17	
Anxiety	1
Asthma	1
Autism	1
Global developmental delay	3
Genetic disorder	1
Grave's disease	1
Prematurity	3
Severe food allergy	1
Seizures	2
SVI, n = 5/8	
Cerebral palsy	2
Global developmental delay	2
Growth hormone deficiency	1
Diabetes Mellitus	1
Eczema	1
Genetic disorder	1
Prematurity	1
Sickle cell disease	1
HPC, n = 2/15	
Seizures	1
Ventricular septal defect	1

Table A7-3 Clinical, demographic and laboratory features of children included in the RNA-seq analysis in Chapter 8.

Healthy controls were used for normalisation of the data. This table is adapted from Jackson et al.[257]*.*

n = counts, % = percentage

	MIS-C (n = 38)	**KD (n = 136)**	**Viral (n = 138)**	**Bacterial (n = 188)**	**Healthy controls (n = 134)**
Age in months	126 (65-151)	30 (16-52)	7 (2-20)	38 (11-96)	92 (29 – 154)
Sex at birth (female, %)	13 (39%)	59 (43%)	45 (33%)	85 (45%)	63 (47%)
Days since symptom onset	6 (5-7)	6 (5-8)	5 (2-6)	2 (1-4)	-
Required inotropic support (n, %)	20 (52.6%)	2 (1.4%)	3 (2%)	50 (26.6%)	-
Required non-invasive ventilation (n, %)	5 (13.2%)	2 (1.4%)	6 (4.3%)	46 (24%)	-
Required invasive ventilation (n, %)	4 (10.5%)	0	7 (5.1%)	16 (8.5%)	-
Admitted to PICU (n, %)	23 (60.6%)	1 (0.7%)	25 (18%)	84 (44.7%)	-
White blood cells ($x10^9$/L)	9.7 (8.1-11.5)	13.2 (10.4-18)	9.9 (6-14)	2 (1-4)	-
Neutrophils ($x10^9$/L)	8.1 (4.5-11.0)	9.2 (6.3-11.5)	3.6 (1.8-6.5)	50 (26.6%)	-
Lymphocytes ($x10^9$/L)	1.2 (0.8-1.8)	2.8 (1.7-4.9)	4.7 (2.8-6.7)	46 (24%)	-
Monocytes ($x10^9$/L)	0.3 (0.2-0.4)	0.7 (0.5-1.1)	0.8 (0.5-1.4)	1.6 (0.7-4.8)	-
Platelets ($x10^9$/L)	209 (144-300.5)	343 (257-426)	365 (245-509)	243 (157-329)	-
CRP (mg/L)	173 (99-250)	73 (43-162)	13.2 (4.1-38)	116.8 (40.3-212)	-